Damping Mechanisms and Their Effects on the Whipping Response of a Submerged Submarine Subjected to an Underwater Explosion

by

Jeffrey W. Stettler

B.S., Chemical Engineering
Lehigh University, 1983

Submitted to the Department of Ocean Engineering and the Department of Mechanical Engineering in Partial Fulfillment of the Requirements for the Degrees of

Naval Engineer
and
Master of Science in Mechanical Engineering

at the
Massachusetts Institute of Technology
May 1995

N00123-89-G-0580

Signature of Author _____ 5/9/95
Department of Ocean Engineering, May 1995

Certified by _____ 5/12/95
Professor Alan J. Brown, Department of Ocean Engineering
Thesis Supervisor

Certified by _____
Professor James H. Williams, Jr., Department of Mechanical Engineering
Thesis Reader

Accepted by _____
Professor A. Douglas Carmichael, Department of Ocean Engineering
Chairman Department Graduate Committee

Accepted by _____
Professor Ain A. Sonin, Department of Mechanical Engineering
Chairman Department Graduate Committee

DAMPING MECHANISMS AND THEIR EFFECTS ON THE WHIPPING RESPONSE OF A SUBMERGED SUBMARINE SUBJECTED TO AN UNDERWATER EXPLOSION

by

JEFFREY W. STETTLER

Submitted to the Department of Ocean Engineering and the Department of Mechanical Engineering on May 12, 1995 in partial fulfillment of the requirements for the Degrees of Naval Engineer and Master of Science in Mechanical Engineering

ABSTRACT

An analytical approach to the solution of the whipping response of a submerged submarine to the pulsation of a nearby explosion bubble is presented. Particular aspects of energy dissipation (damping) are addressed in regards to their effects on the overall loading forces and dynamic response of the submarine. Particular damping mechanisms discussed include hull damping (hull material and structural), internal damping (internal structures and sloshing liquids), and external damping (hydrodynamic damping including wave radiation and viscous fluid effects).

A flexible analytic model is developed, using the fundamentals of vibration and hydro-mechanics. A finite-element beam model is used to represent the flexural structure of the hull. Internal structures are modeled as separate dynamic systems, using both discrete and modal superposition approaches. Onboard liquids are modeled using a mechanical-equivalent system based upon a potential flow solution of the liquid free-surface. External hydrodynamic forces are modeled using a modified Morison formulation, with fluid velocities and accelerations calculated based upon a popular explosion bubble model. The equations of motion for the composite dynamic systems are solved in the time-domain using a modified Newmark direct time integration scheme, with iterations at each time step accomplished using a modified Newton-Raphson method.

The analytic model is implemented on a personal computer, and used to numerically investigate various damping mechanisms associated with dissipation of whipping energy. Additionally, the analytic model is compared to explosion-induced whipping tests conducted on the U.S. Navy test platform "Red Snapper". The analytic model compared well to the experimental data for early-time response (through the 2nd bubble period), but tended to over predict response for later times.

Potential weaknesses with the analytic model are discussed in light of the comparisons with experimental data, and recommendations for future analytic work in the area are made.

Thesis Supervisor: Professor Alan Brown, Department of Ocean Engineering

ACKNOWLEDGMENTS

Above all else, the author would like to thank his wife Lisa for her unfailing love and patience throughout the time of this work, for without her support, this document ... would probably have been much shorter.

Second, the author wishes to document an incredible debt of gratitude to his son Ricky. Throughout his first year of life, his refreshingly spirited company made even the most frustrating days seem wonderful.

The author would like to also thank his thesis advisor, Professor (Captain, USN) Alan Brown for his encouragement, support, and guidance over the past three years.

Finally, the author would like to thank a very large number of true professionals (too large to list here), both in uniform and out, who have provided guidance, support, encouragement, even comedy over the past three years.

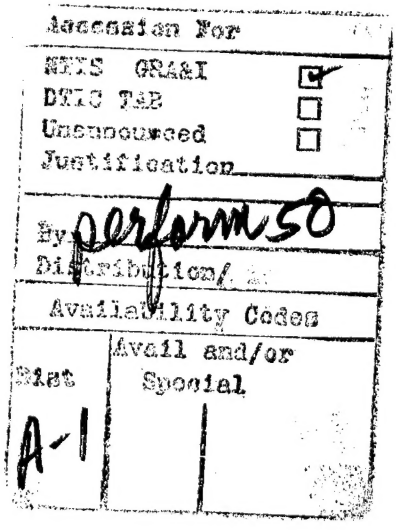

TABLE OF CONTENTS

NOMENCLATURE

∇	vector gradient operator
$\forall$	volume
Φ	matrix of mode shape vectors, velocity potential function
α	Rayleigh coefficient, non-dimensional bubble radius
β	Rayleigh coefficient, viscous-frequency parameter, coefficient for Newmark algorithm, control variable for free surface effect
δ	logarithmic decrement
ε	strain, control variable for bubble migration
γ	coefficient for Newmark algorithm, adiabatic constant for explosive
η	free surface elevation
ϕ	mode shape vector, velocity potential
λ	non-dimensional rate of change of bubble depth
μ	coefficient of friction
ν	kinematic viscosity
θ	rotation angle, angular orientation
ρ	density
σ	stress, non-dimensional rate of change of bubble radius
τ	non-dimensional time
ω	radial frequency
ζ	non-dimensional bubble depth
ζ_n	modal viscous damping ratio
A	amplitude, area
C	damping matrix
C_A	added mass coefficient
C_D	drag coefficient for explosion bubble
C_d, C_d^l	drag coefficient
C_m	inertia coefficient
C_n	modal damping
D	specific damping energy, diameter
D_0	initial head on bubble
E	Young's modulus
F	force vector
G	Green function, shear modulus
I	2nd moment of area, moment of inertia
J	polar moment of inertia
K	stiffness matrix
KC	Keulegan-Carpenter number
K_n	modal stiffness
L	length
M	mass matrix

M_l	mass of liquid in a tank
M_n	modal mass
N	number of cycles, number of modes
P	pressure
Q_n	modal force
Rn	peak Reynolds' number
S	surface
T	period
U_0	amplitude of relative velocity
V	velocity
W	energy/work, explosive charge weight
$X, \dot{X}, \ddot{X}$	displacement vector
a	tank width, bubble radius
c	damping
d	bubble depth
e_1, e_2	strengths of sources, dipoles
f	force
g	acceleration due to gravity
h	hysteresis damping constant, tank depth
k	stiffness, constant for explosive
m	mass, applied moment
n	mode number, normal vector
q	vector of modal coordinates
r	radial distance
t	time
$u, \dot{u}$	fluid velocity, acceleration
v	velocity
v_m	bubble migration velocity
$x, \dot{x}, \ddot{x}$	displacement, velocity, acceleration

1. INTRODUCTION

1.1 Underwater explosions and ship whipping.

Designers of naval ships have long been concerned with the effects of underwater explosions. Historically, most attention has been paid to the effects of contact charges and charges of near to intermediate standoff. Protection methods to these effects have typically included heavy side-protective systems to minimize possibility of hull rupture and shock-mounting of vital machinery and equipment to minimize damage caused by the high frequency shock wave resulting from the explosion.

While hull rupture and internal shock wave effects are still considered of major importance to ship survivability, increasing attention has been paid in recent years to the *whipping* of ship hulls caused by charges of near to intermediate standoff. Whipping can be defined as the transient, flexing motion of the whole hull of a ship in its vibrational modes corresponding to the lowest natural frequencies[1]. Such motion, if of sufficient magnitude, can cause hull girder buckling, tearing, or other loss of hull girder strength.

Numerous examples of catastrophic or near-catastrophic whipping can be cited throughout naval history. As recently as 1991, the U.S. Navy Guided Missile Cruiser USS Princeton (CG-59) struck a floating contact mine in the Persian Gulf. Although the local hull rupture caused by the mine explosion (near the bow) was not a threat to the survival of the ship, the subsequent whipping of the hull caused near-catastrophic hull girder damage near the stern of the ship.

When an underwater explosive detonates, the solid explosive material suddenly reacts, leaving behind gaseous products at very high temperature and pressure. Almost immediately, the *shock wave*, produced due to the sudden discontinuity in pressure, propagates radially, approximately with the speed of sound in water. This shock wave carries with it approximately one-third of the energy released during the reaction[2]. It is this shock wave that is typically responsible for localized hull rupture and damage to internal equipment.

Left behind as the shock wave propagates through the fluid medium is a cavity of gaseous reaction products at high pressure. This cavity subsequently expands (as a bubble) to relieve the difference in pressure, accelerating the surrounding fluid. The bubble continues to expand beyond the point of hydrostatic equilibrium (due to the inertia of the surrounding fluid) until a point of dynamic equilibrium is reached. The bubble then

---

[1]Hicks, A.N., "Explosion Induced Hull Whipping", *Advances in Marine Structures*, Admiralty Research Establishment, Dunfermline, Scotland, UK, 1986, p. 390.
[2]*Ibid.*, p. 392.

reverses, continuing to contract until dynamic equilibrium is again reached, where it quickly rebounds and again begins to expand. This bubble expansion and contraction continues until the energy of the reaction is fully dissipated. As the bubble rebounds, it greatly accelerates the surrounding water, generating a substantial pressure pulse (commonly known as the *bubble pulse*). This bubble pulse can impart significant loads on structures in the vicinity.

Thus, for certain underwater explosions, a ship can experience loading, not only from the radiating shock wave, but also from the quasi-periodic bubble pulse. Although the whipping motion of a ship hull is characterized by *free vibration* of the hull in the water, it is this quasi-periodic loading which can reinforce the free vibration and magnify the response of the hull to whipping, particularly when the period of the bubble pulse is in the vicinity of the natural periods of hull flexure.

1.2 The importance of damping in ship whipping.

The first, most easily observed effect of damping on structural vibration is in the decrease in amplitude during free vibration. Figure 1-1 illustrates the effect of damping on the free vibration of a cantilever beam. If the cantilever with *some* damping is deformed and then released, it will oscillate with a regular period, but the amplitude of the oscillation will decrease with time. Without damping, the cantilever would continue to vibrate without the decrease in amplitude. In fact, the free vibrations of damped structures will normally be reduced at a rate that may be used as a measure of the amount of damping in the system. A well known measure of damping, known as the *logarithmic decrement*, δ, is related to the ratio of the nth to the $(n+N)$th cycle amplitudes by:

$$\delta = \frac{1}{N} \ln\left(\frac{A_n}{A_{n+N}}\right) \qquad (1\text{-}1)$$

where A_n is the amplitude of the nth cycle and A_{n+N} is the amplitude of the $(n+N)$th cycle. Similarly to a cantilever, the amplitude of free vibration of a whipping ship will decrease with time due to the presence of damping.

A second, and perhaps more important effect of damping is on the steady state amplitude attained when a structure is excited by a harmonically oscillating force. As discussed in any text on mechanical vibrations, the maximum magnitude of the response of any structure subjected to harmonic excitation (or periodic excitation that can be represented as a Fourier series of harmonic terms) is determined by the relation of the frequency of excitation to the natural frequencies of the structure, as well as the stiffness,

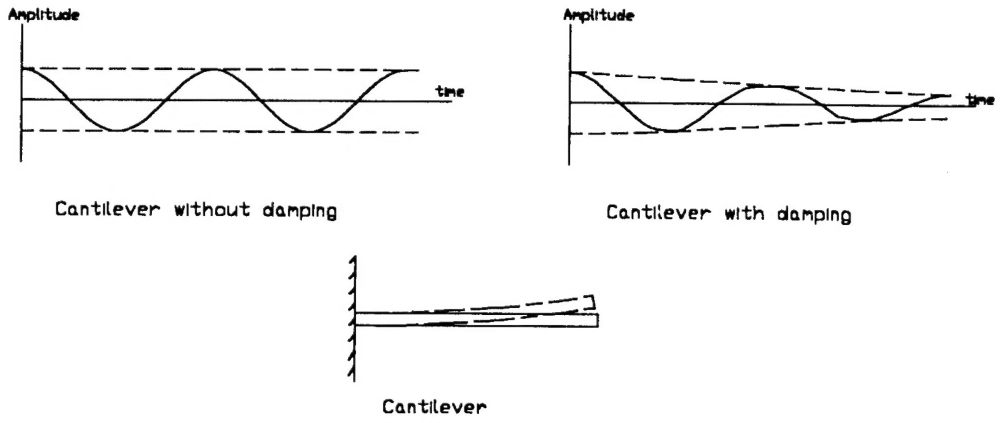

Figure 1-1. Effect of damping (with time) on the free vibration of a cantilever.

damping and mass of the structure (and, of course, the magnitude of the excitation). As shown in figure 1-2 (illustrated for a single degree of freedom system subjected to harmonic excitation), the response is predominantly controlled by stiffness when the excitation frequency (ω) is much less than the natural frequency (ω_n) of the structure (elastic forces dominate the equations of motion due to the small acceleration and inertia forces). When the excitation frequency is much greater than the natural frequency, the response is predominantly controlled by mass (inertia forces dominate the equations of motion). When the excitation frequency is close to the natural frequency (near resonance), however, the elastic and inertia forces approximately balance, and the major demand on the excitation forces is to overcome system damping, implying that the amount of system damping controls the dynamic response. In this region, when damping is low, the response magnitude is high, and when damping is high, the response amplitude is low. Thus, the response near resonance can be very much greater than the static response (ω approaching zero), particularly if the damping is very low.

As discussed previously, the bubble pulse can generate low frequency, quasi-periodic loading on the ship. For certain underwater explosive combinations (explosive charge weight and standoff), the frequency of this loading can be on the order of the natural frequencies of the ship's low frequency flexural modes. Thus, hull flexural vibrations, excited by the quasi-periodic bubble pulse loading, can approach a resonant response in the low frequency modes. It is clear then that damping can have a significant influence on the magnitude of the whipping response of the hull to the bubble pulse.

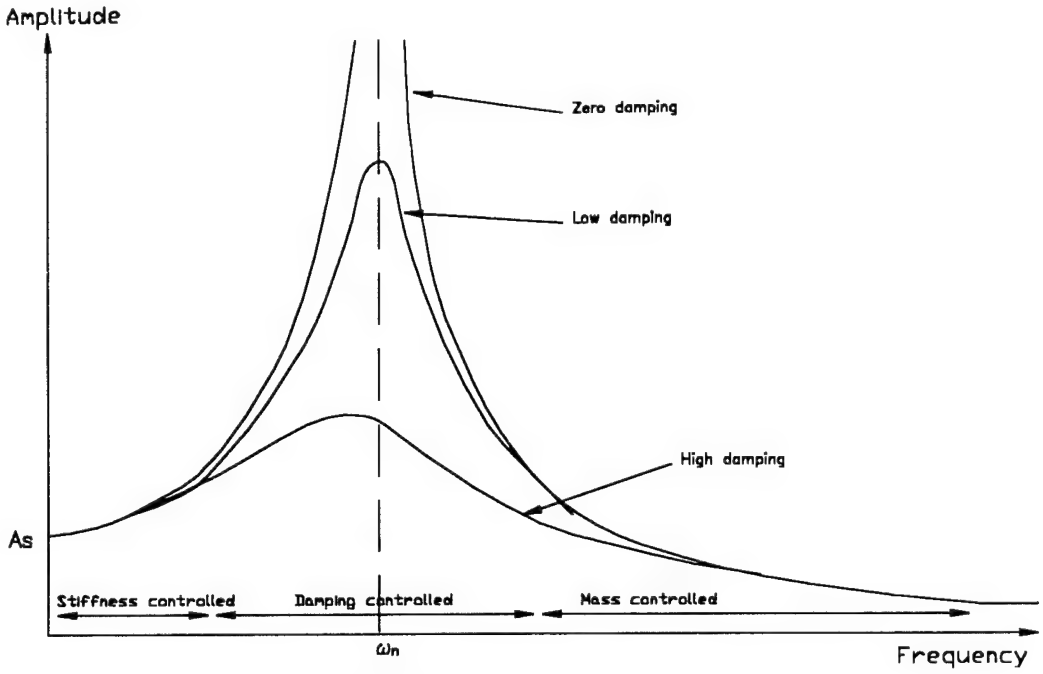

Figure 1-2. Effect of damping (with frequency) on the steady state vibration of a single degree of freedom system.

2. DAMPING MECHANISMS IMPORTANT IN SHIP WHIPPING

2.1 Introduction.

In dynamics, the word *damping* generally refers to the dissipation of energy during the motion of a body or structure. This energy eventually is converted to heat by friction or generates waves in the surrounding medium. When a structure, such as a ship, vibrates or moves in on ocean environment, energy can be dissipated within the structure itself, through internal components, or externally into the surrounding fluid. Specific mechanisms of damping, which can be expected to be important in ship and submarine whipping, are discussed here and then incorporated into a model for submarine whipping in chapter 3.

2.2 Hull damping.

The loss of vibrational energy within a complex structure can be accomplished through several possible mechanisms, depending on the frequency of the vibration and geometry of the structure. In general, low frequency energy (consistent with ship whipping) is lost within a structure through friction, which in turn generates heat which is conducted, convected and radiated away. This friction can occur among the material particles or crystals (within the structural elements) as they move relative to one another during material deformation. This damping mechanism is referred to as *material* or *hysteresis damping*. Friction can also occur at the interface between structural elements as they slide relative to one another (i.e. at joints). This damping mechanism is often referred to as *structural* or *dry friction damping*.

As will be discussed in greater detail subsequently, it is useful to define the hull damping in terms of equivalent viscous damping. By doing this, the damping forces associated with material and structure can be represented as being proportional to the velocity. The resulting equations of motion for the vibration of the *hull* could then be written in the form

$$\mathbf{M}\ddot{\mathbf{x}} + \mathbf{C}\dot{\mathbf{x}} + \mathbf{K}\mathbf{x} = \mathbf{f} \qquad (2\text{-}1)$$

where **M** is the mass matrix of the hull, **C** is the equivalent viscous damping matrix, **K** is the stiffness matrix, **x** is the displacement vector, **f** is the external load vector, and superposed dots refer to time derivatives ($\dot{x}$ is velocity and $\ddot{x}$ is acceleration). Although material damping is more representative of the energy dissipation within the material, and structural damping more representative of losses in joints, it will be noted that an equivalent viscous damping is assumed for most *real* structural dynamic analyses. The

precise nature of the damping is less important than modeling the correct energy loss per cycle.

2.2.1 Material (hysteresis) damping.

When materials are deformed, energy is absorbed and dissipated by the material due to friction during internal reconstruction of the micro and/or macro structure as the material deforms. This reconstruction ranges from crystal lattice to molecular scale effects. This process, referred to as *material damping* or *hysteresis damping*, is discussed in great detail by Lazan[3] and Nashif[4].

All *real* materials dissipate energy during cyclic deformation. Regardless of the precise physical mechanisms involved, energy dissipation can be highly nonlinear, and therefore detailed analysis can be very difficult. One approach toward quantifying the internal damping behavior of real materials is through the *hysteresis loop*, figure 2-1. The loop plots strain vs. stress during cyclic deformation of a material volume and is obtained from experimental measurements. Typically, hysteresis loops representative of construction metals such as steel are extremely thin, deviating little from a single line (unless the metal is strained well into the plastic range). Thus, for elastic ship hull whipping of a steel hull, the damping provided by material hysteresis would be expected to be small compared to other damping mechanisms discussed subsequently.

The area inside the hysteresis loop is the *specific damping energy*, D, and is equal to the energy dissipated per unit volume of material per cycle

$$D = \oint \sigma \cdot d\varepsilon = \int_0^{2\pi/\omega} \sigma \cdot \left(\frac{d\varepsilon}{dt} \right) \cdot dt \qquad (2\text{-}2)$$

where σ is stress and ε is strain. Equation (2-2) implies that the *rate* of energy dissipation (dD/dt) is proportional to the strain rate. This is equivalent to the hysteresis damping being proportional to the strain rate.

The specific damping energy is very small for most conventional structural materials, such as steel, for typical elastic stress-strain levels. High-damping alloys and viscoelastic materials have higher specific damping energies, and therefore are much better at dissipating energy.

---

[3]Lazan, B.J., *Damping of Materials and Members in Structural Mechanics*, Pergamon Press, New York, 1968.

[4]Nashif, A.D., Jones, D.I.G., and Henderson, J.P., *Vibration Damping*, John Wiley and Sons, New York, 1985.

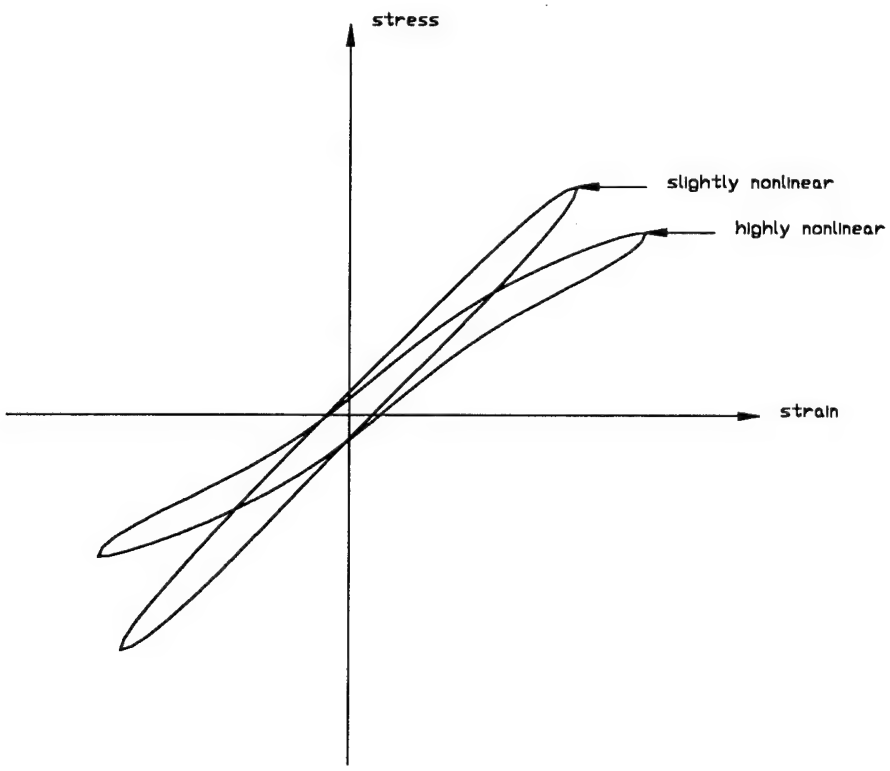

Figure 2-1. Typical hysteresis loops.

As discussed in the previous section, it is useful to represent hysteresis damping in terms of an equivalent viscous damping. An equivalent viscous damping coefficient for hysteresis damping can be found by considering the harmonic motion of an equivalent spring-viscous damper system (figure 2-2). For this system, the force F(t) necessary to cause a displacement x(t) is given by

$$F(t) = kx(t) + c\dot{x}(t) \tag{2-3}$$

where k is the spring constant, c is the viscous damping constant, and $\dot{x}$ is the velocity (dx/dt). For harmonic motion of frequency ω and amplitude X, the displacement can be written in the form

$$x(t) = X\sin(\omega t) \tag{2-4}$$

Inserting equation (2-4) into equation (2-3) gives

$$F(t) = kX\sin(\omega t) + cX\omega\cos(\omega t) \tag{2-5a}$$

$$F(t) = kx \pm c\omega\sqrt{X^2 - (X\sin\omega t)^2} \tag{2-5b}$$

$$F(t) = kx \pm c\omega\sqrt{X^2 - x^2} \tag{2-5c}$$

When F(t) is plotted against x(t), equation (2-5c) represents a closed loop similar to a hysteresis loop (figure 2-3). The energy dissipated by the damper in one cycle of motion is found by substituting equation (2-5a) into equation (2-2):

$$\Delta W = \oint \sigma d\varepsilon = \int F dx = \int F\left(\frac{dx}{dt}\right)dt = \int_0^{2\pi/\omega} (kX\sin\omega t + cX\omega\cos\omega t)(\omega X\cos\omega t)dt = \pi\omega cX^2 \tag{2-6}$$

where ΔW is the energy loss in the damper in one cycle, which is the equivalent to the specific damping energy, D, for hysteretic damping.

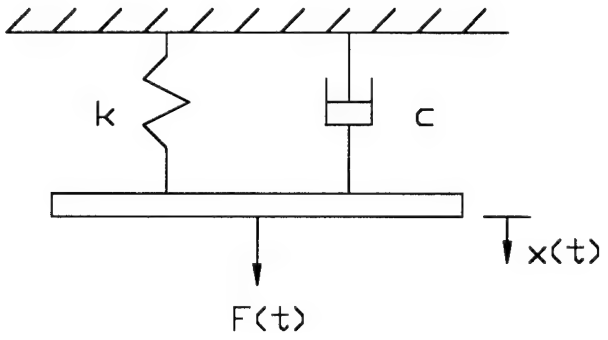

Figure 2-2. Equivalent spring-viscous damper system.

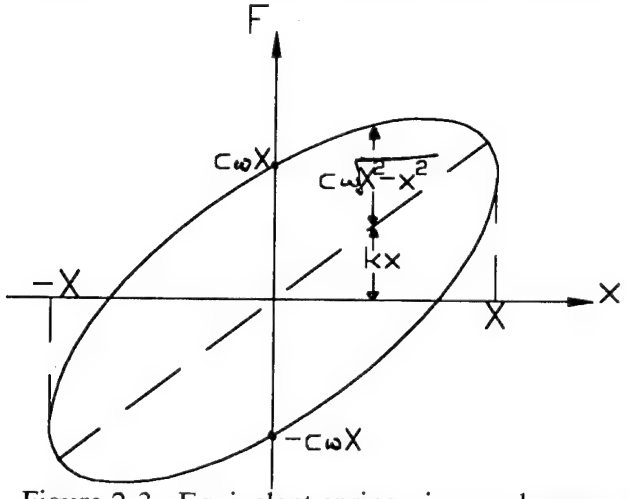

Figure 2-3. Equivalent spring-viscous damper system.

For real hysteresis damping, however, it has been found experimentally that the specific damping energy, D, is *independent* of frequency, but approximately proportional to the square of the amplitude of the strain[5]. Thus, the equivalent viscous damping coefficient, c_{eq}, must be inversely proportional to the frequency, which can be represented by

$$c_{eq} = \frac{h}{\omega} \tag{2-7}$$

[5]Rao, S., *Mechanical Vibrations*, Addison-Wellesley Publishing Co., Reading, MA, 1990, p. 102.

where h is called the *hysteresis damping constant*. As discussed subsequently, the idea that the equivalent viscous damping constant for material hysteresis damping is inversely proportional to frequency is made use of in the practical modeling of material damping in real structures.

2.2.2 Structural (dry friction) damping.

In addition to damping within the material of a structure, damping also occurs at the interface between structural elements as they slide relative to one another. This type of damping is usually referred to as *structural damping, slip damping, Coulomb damping*, or simply *dry friction damping* (it amounts to Coulomb or "dry" friction forces). This type of damping is considered important when structural elements are joined non-rigidly by riveting, clamping, or bolting, where a moderate amount of clamping pressure allows for some slip between elements. As for material damping, structural damping is discussed in great detail by Lazan[6], and Nashif[7].

Because of the potential geometric complexities, quantitative evaluation of structural damping in complex structures is impractical even when numerical techniques such as finite element analysis are used. However, most structurally significant joints making up a ship hull are *rigidly welded* rather than bolted or riveted. Thus, for elastic ship hull whipping, it would be expected that damping provided by structural dry friction forces would be very small compared to other damping forces discussed subsequently. It should be noted, however, that for certain ship designs (particularly many submarines and submersibles), internal decking is often connected to the main structure of the hull through various types of sliding deck joints or suspension mechanisms. Thus, in some ship applications, it is necessary to account for *some* degree of dry friction damping, particularly when considering potentially large amplitude hull flexural motions.

In general, *Coulomb's Law of Dry Friction* states that when two bodies are in contact, the tangential force required to produce sliding is proportional to the normal force acting in the plane of contact. Once sliding has begun, the force remains constant. The dry friction force is given by

$$f_D = \mu N \tag{2-8}$$

where N is the normal force and μ is the coefficient of friction which is characteristic for the interface of the two surfaces. Thus, the structural dry friction damping force at the interface of two sliding surfaces is in a direction opposite to the direction of the relative

---

[6]Lazan, *op. cit.*
[7]Nashif, *op. cit.*

velocities of the two surfaces but is *independent* of the displacement or velocity; it depends only on the normal force between the two surfaces.

The fact that the dry friction forces remain constant as long as sliding motion exists between two surfaces (and are not dependent on displacement or velocity) leads to the conclusion that, in each successive cycle (or oscillation) of a structure, the amplitude of the motion is reduced by an amount proportional only to the friction forces resulting from the sliding within the structure. For a simple one dimensional case, the reduction in amplitude with each successive oscillation will remain constant as long as relative motion exists.

2.2.3 Modeling material and structural damping in complex structures.

If the material and structural damping properties of a structure could be quantitatively determined throughout the structure, a finite element procedure could be used to include the distributed damping properties (as element damping matrices) in the complete dynamic solution of the structural motions. In practice, however, direct evaluation of distributed structural damping properties in complex structures does not lend itself well to the numerical solutions for structural dynamics (although distributed damping has been included in some simple finite element applications[8]). Material and structural damping (as previously defined) are typically expressed in terms of damping ratios established from experiments, rather than by means of an explicit damping matrix. In fact, for many applications, there is no need to express the damping explicitly by means of a damping matrix, but rather only in terms of the modal damping ratios (ζ_n) which can be applied through the principle of modal superposition. This concept is often called *modal damping*. An extension of modal damping in which an explicit damping matrix is defined through a linear combination of the mass and stiffness matrices is called *Rayleigh damping*.

Modal damping and modal superposition. The method of dynamic analysis using modal superposition is discussed in numerous texts (Clough and Penzien[9], Smith[10], for example) and is discussed briefly here only for continuity. Fundamentally, the original set of *N coupled* equations of motion (for an *N* degree of freedom system) are *transformed* to a set of *N independent* normal (modal) coordinate equations. The

---

[8]Kaliske, M., Jagusch, J., Gebbeken, N., and Rothert, H., "Damping models in finite element computations", *Structural Dynamics-Proceedings of the 2nd European Conference on Structural Dynamics (Vol. I)*, Rotterdam, 1993, pp. 585-591.

[9]Clough, R.W. and Penzien, J., *Dynamics of Structures* (second edition), McGraw-Hill, New York, 1993.

[10]Smith, J.W., *Vibration of Structures - Applications in Civil Engineering Design*, Chapman and Hall, London, 1988.

dynamic response can be obtained by solving separately for the response of each normal (modal) coordinate and then superposing these to obtain the response in the original coordinate system.

The equations of motion for a multiple degree of freedom dynamic systems can be written in matrix form:

$$M\ddot{x} + C\dot{x} + Kx = f \tag{2-9}$$

where, in general, matrices **M**, **C**, and **K** all have non-diagonal terms (i.e. the equations of motion are coupled). The modal equations of motion are obtained from equations (2-9) by applying a modal transformation,

$$x = \Phi q \tag{2-10}$$

where Φ is the matrix whose columns are the mode shape vectors

$$\Phi = \left[\phi_1 \phi_2 \ldots \phi_N\right] \tag{2-11}$$

(ϕ_i is the vector representing the shape of the *i*th mode), and **q** is a vector of normal or modal coordinates. Pre-multiplying each term by the transform of the *n*th mode shape vector, yields an equation of motion for each mode (uncoupled from other modes) of the form:

$$M_n\ddot{q}_n + C_n\dot{q}_n + K_n q_n = Q_n \tag{2-12}$$

where:

$$\begin{aligned} M_n &= \phi_n^T M \phi_n \equiv \text{modal mass coefficient} \\ C_n &= \phi_n^T C \phi_n \equiv \text{modal viscous damping coefficient} \\ K_n &= \phi_n^T K \phi_n \equiv \text{modal stiffness coefficient} \\ Q_n &= \phi_n^T f \equiv \text{modal force} \end{aligned} \tag{2-13}$$

Equations (2-13) for modal mass and modal stiffness come about because of the orthogonality property of the normal mode shapes, which can be extended to modal viscous damping if the orthogonality condition is also assumed to apply to the damping matrix (as will be discussed subsequently). If equation (2-12) is divided by the modal mass coefficient, the modal equations of motion may be written in an alternate form:

$$\ddot{q}_n + 2\zeta_n\omega_n\dot{q}_n + \omega_n^2 q_n = \frac{Q_n}{M_n} \tag{2-14}$$

where ω_n is the (modal) natural frequency, and ζ_n is defined as the modal viscous damping ratio

$$\zeta_n = \frac{C_n}{2\omega_n M_n} \tag{2-15}$$

The (modal) natural frequencies (ω_n) and mode shape vectors (ϕ_n) are found by solving the generalized eigenproblem for the undamped free vibration of the dynamic system:

$$K\phi_n = \omega_n^2 M\phi_n \tag{2-16}$$

As discussed previously, it is often more convenient (and physically reasonable) to define the damping of a complex multiple degree of freedom system using a viscous damping ratio for each mode, rather than to try to explicitly evaluate coefficients of the damping matrix **C**, because the modal damping ratios can be determined experimentally (or estimated with adequate precision in many cases).

With the (uncoupled) modal equations of motion defined, the modal displacements can be found, and the total displacement can be found by summing the modal contributions using equation (2-10):

$$x = \sum_{n=1}^{N} \phi_n q_n \tag{2-17}$$

Thus, the total response of a system modeled using modal superposition can be thought of as a sum of the responses of *N independent* single degree of freedom systems.

Rayleigh (proportional) damping. Under some circumstances, it is desirable or practicable to use modal superposition to uncouple the equations of motion in solving for the dynamic response of a system. In other circumstances, it may be desirable to use the basic concept of modal superposition, but develop an explicit damping matrix (**C**) which may be used to solve the complete equations of motion in the time domain. This can be done by applying what has become known as *Rayleigh damping* or *proportional damping* (named after Lord Rayleigh, who first suggested its use). Rayleigh or proportional damping is discussed in varying detail in numerous sources (Clough and Penzien[11], Bathe[12], for example).

Under Rayleigh or proportional damping, it is assumed that the damping matrix can be adequately represented by making it a linear superposition of the mass matrix (mass proportional damping), the stiffness matrix (stiffness proportional damping), or both. By applying a linear superposition, the orthogonality condition which applies to the mass and stiffness matrices (as discussed previously) would also apply to the damping matrix. Thus, the damping matrix could be written in the form:

$$C = \alpha M + \beta K \tag{2-18}$$

---

[11]Clough and Penzien, *op. cit.*

[12]Bathe, K.J., *Finite Element Procedures in Engineering Analysis*, Prentice-Hall, Englewood Cliffs, NJ, 1982.

where α and β are proportionality constants. The damping associated with equation (2-18) may be recognized by evaluating the generalized modal damping associated with it by combining it with equations (2-13) and (2-15), and solving for the modal damping ratio:

$$C_n = \phi_n^T C \phi_n = \phi_n^T [\alpha M + \beta K] \phi_n = \alpha M_n + \beta K_n \tag{2-19}$$

$$\zeta_n = \frac{C_n}{2\omega_n M_n} = \frac{\alpha}{2\omega_n} + \frac{\beta \omega_n}{2} \tag{2-20}$$

Thus, the damping associated with any particular mode can be thought of as a linear combination of a factor which is *inversely* proportional to frequency (the mass proportional term), and a factor which is *directly* proportional to frequency (the stiffness proportional term). An important point to note is that the Rayleigh damping model is consistent with the discussion of material (hysteresis) and structural damping presented earlier. Thus, Rayleigh damping can be thought of as providing a good model to account for material and structural damping (for elastic whipping, as discussed in the previous sections).

The relationship between damping ratio and frequency for Rayleigh damping can be illustrated as shown in figure 2-4. The cases of purely mass proportional damping ($\beta = 0$) and purely stiffness proportional damping ($\alpha = 0$) are shown separately from the combined or general case.

As illustrated in figure 2-4, the two Rayleigh damping proportionality constants, α and β, can be evaluated by solving two simultaneous equations if the (modal) damping ratios, ζ_a and ζ_b, associated with two specific (modal) frequencies, ω_a and ω_b, are known (i.e. from experiment). Substitution of the two damping ratios and frequencies into equation (2-20), combining the resulting equations into matrix form, and carrying out a matrix inversion gives the solution of the two damping proportionality constants:

$$\begin{Bmatrix} \zeta_a \\ \zeta_b \end{Bmatrix} = \frac{1}{2} \begin{bmatrix} 1/\omega_a & \omega_a \\ 1/\omega_b & \omega_b \end{bmatrix} \begin{Bmatrix} \alpha \\ \beta \end{Bmatrix} \tag{2-21}$$

$$\begin{Bmatrix} \alpha \\ \beta \end{Bmatrix} = 2 \frac{\omega_a \omega_b}{\omega_b^2 - \omega_a^2} \begin{bmatrix} \omega_b & -\omega_a \\ -1/\omega_b & 1/\omega_a \end{bmatrix} \begin{Bmatrix} \zeta_a \\ \zeta_b \end{Bmatrix} \tag{2-22}$$

It is apparent from figure 2-4 that the use of Rayleigh damping provides for very high damping ratios for modes of very high frequencies (ω much greater than ω_b). The end result is that the *responses* of very high frequency modes are effectively eliminated by the high damping imposed by the Rayleigh damping. In the case of elastic ship whipping, where only the lower few modes are of concern (as discussed previously), this limitation

can be considered acceptable as long as the higher frequency used for evaluation of the Rayleigh proportionality constants (ω_b) is set among the higher modes expected to contribute significantly to the whipping response.

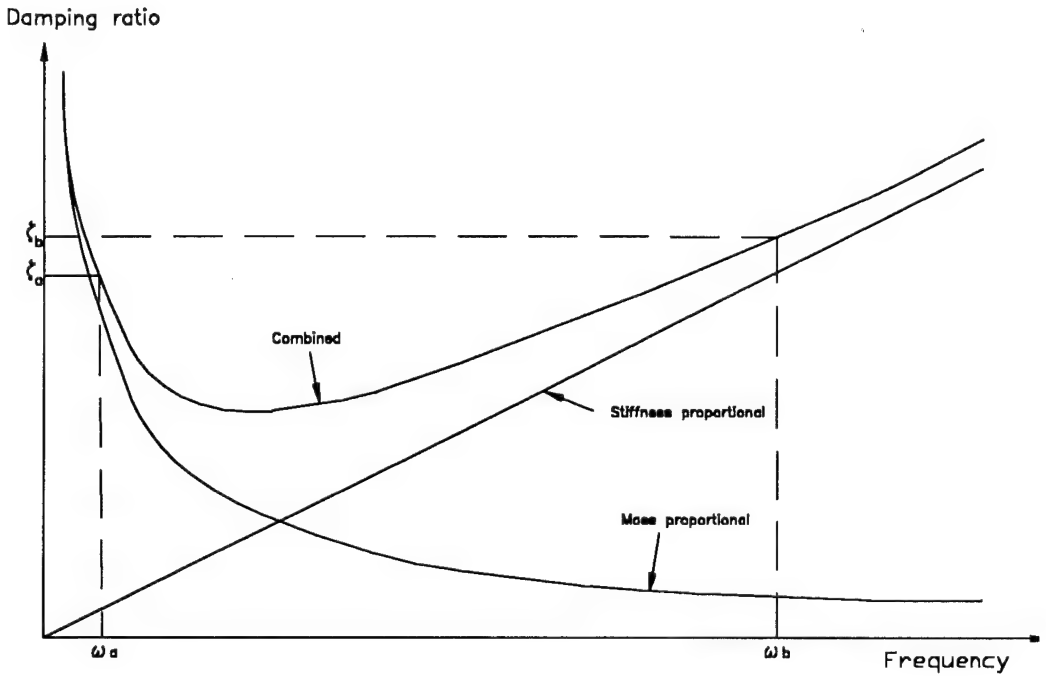

Figure 2-4. Relationship between damping ratio and frequency for Rayleigh damping.

2.3 Internal damping.

Within any complex structure, such as a ship, energy can be lost (or simply transferred) to "separate" dynamic systems which are in some form "attached" to the main structure. For ships, two broad categories could be considered under this category. *Discrete internal masses or structures* such as machinery and equipment connected indirectly to the hull through decking, machinery foundations, and shock or sound mounts, can act as dynamic subsystems, redistributing and absorbing dynamic energy transferred from the hull. Additionally, onboard *liquids* which have free surface can act as dynamic subsystems, redistributing and absorbing dynamic energy by *sloshing*. Because of the large number of discrete internal structures and liquid storage tanks found onboard most ships, it is important to consider the mechanisms through which energy can be transferred and absorbed into these internal damping devices.

2.3.1 Damping through discrete internal structures.

Heavy machinery, electronic equipment, and other discrete masses onboard a ship can be considered to have a significant potential for dissipating hull whipping energy.

Figure 2-5 illustrates notional discrete masses, connected to the hull via mounts, internal decking, foundations, etc. As will be discussed subsequently, the dynamic response of more complex internal structures could be modeled as easily as individual masses by applying the principle of modal superposition (under the assumption of linear response). For purposes of this analysis, the term "discrete internal structure" will be used to refer to any mass or discrete structure that may be modeled as a discrete internal dynamic system in terms of transfer and absorption of hull whipping energy. While it is certainly not desired that heavy machinery or electronic equipment absorb large amounts of energy, it must be assumed that their ultimate connection to the hull provides the potential for the transfer of energy from the whipping hull.

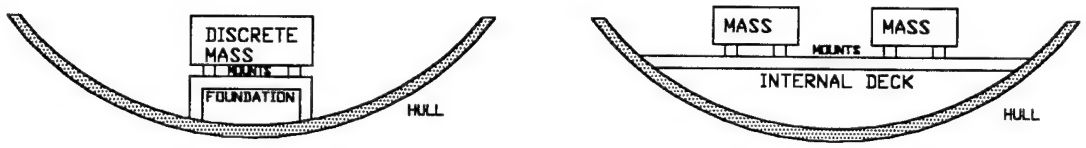

Figure 2-5. Discrete masses connected to the hull via mounts, internal decking, foundations, etc.

Whether or not discrete internal structures connected to a hull provide damping to hull whipping depends upon the sizes of the masses, the dynamic properties of the mechanisms through which they are connected to the hull (decking, foundations, mounts, etc.), the dynamic properties of the hull, and the frequency of hull whipping (frequency of excitation). In section 1.2, it was stated that the controlling mechanism in the response of a system to excitation (stiffness, damping, or mass) is determined by the relation of the excitation frequency (or frequencies) to the natural frequency (or frequencies) of the system. The maximum amount of energy is transferred when the frequency of excitation is equal to a natural frequency (at resonance). In the case of discrete internal structures connected to a whipping hull, it is evident that maximum energy would be transferred when the frequency of hull whipping is equal to a natural frequency of the system composed of the hull, the discrete internal structure, and the connection mechanisms. An understanding of the dynamic effects of discrete internal structures connected to a whipping ship can be made by first considering the effects of a single mass connected to a (rigid) vibrating structure, where the structure and mass are free to vibrate in only one direction (a two degree of freedom system), and then, using the principle of modal superposition, extending this to more complex arrangements of multiple masses connected

to a vibrating structure, such as a whipping ship hull (i.e. multiple degree of freedom systems).

The two degree of freedom system (dynamic vibration absorber). A single mass connected to a much larger vibrating structure can be used to dissipate or absorb vibrational energy of the larger structure. In machinery and structural dynamics, this concept has gained practical significance in the application of the *dynamic vibration absorber*. The concept of the dynamic vibration absorber is presented by Den Hartog[13], and their design and application is discussed in detail in numerous other sources (Korenev[14], Hunt[15], for example). A small auxiliary mass is connected to a harmonically vibrating structure by a spring of specified stiffness (the location of the mass is selected to have the maximum effect on the significant resonant mode of the vibrating structure). In the case where damping is provided by the connecting mechanism (e.g. by a dashpot), the auxiliary mass is called a *damped dynamic vibration absorber* or *tuned mass damper*. Treating the main structure and vibration absorber as a two degree of freedom dynamic system (figure 2-6), Den Hartog showed that the amplitude of harmonic vibration of the main structure could be reduced to zero at a specified excitation frequency (or reduced over a *range* of frequencies). This could be accomplished by "tuning" the properties of the vibration absorber (adjusting the mass, stiffness of the spring, and damping in the dashpot). The downside in the application of dynamic vibration absorbers appears in the potentially large amplitude response (displacement and acceleration) of the absorber masses. In the case of heavy machinery and electronic equipment onboard a whipping ship, this could translate to high displacements and accelerations on the delicate equipment, and large forces on the mounts and decking.

For the simple dynamic vibration absorber attached to a large vibrating structure, the equations of motion for this simple two degree of freedom system can be derived by considering dynamic equilibrium of each of the masses separately. Figure 2-7 illustrates each of the masses and the dynamic forces acting upon them. From equilibrium, the equations of motion may be written:

$$M\ddot{X} + KX = F_{ext} + c(\dot{x} - \dot{X}) + k(x - X) \quad \text{(for the main mass)} \qquad (2\text{-}23)$$

$$m\ddot{x} + c(\dot{x} - \dot{X}) + k(x - X) = 0 \quad \text{(for the absorber mass)} \qquad (2\text{-}24)$$

where capital letters refer to the main structure and lower case letters refer to the absorber, as shown in figure 2-6. These equations of motion could be written in an alternate form by defining the *force exerted on the main structure by the absorber*:

---

[13]Den Hartog, J.P., *Mechanical Vibrations*, (4th edition), McGraw-Hill, New York, 1956.
[14]Korenev and Reznikov, *Dynamic Vibration Absorbers*, John Wiley and Sons, New York, 1993.
[15]Hunt, J.B., *Dynamic Vibration Absorbers*, Mechanical Engineering Publications, London, 1979.

$$F_{absorber} = k(x - X) + c(\dot{x} - \dot{X}) \tag{2-25}$$

which, of course is the negative of the force exerted on the absorber by the main structure. Thus, the equations of motion could be written:

$$M\ddot{X} + C\dot{X} + KX = F_{ext} + F_{abs} \quad \text{(for the main mass)} \tag{2-26}$$

$$F_{absorber} = c(\dot{x} - \dot{X}) + k(x - X) = -m\ddot{x} \quad \text{(for the absorber mass)} \tag{2-27}$$

Equations (2-26) and (2-27) form a set of 2 simultaneous differential equations (coupled) which may be solved under various conditions for displacements, velocities and accelerations.

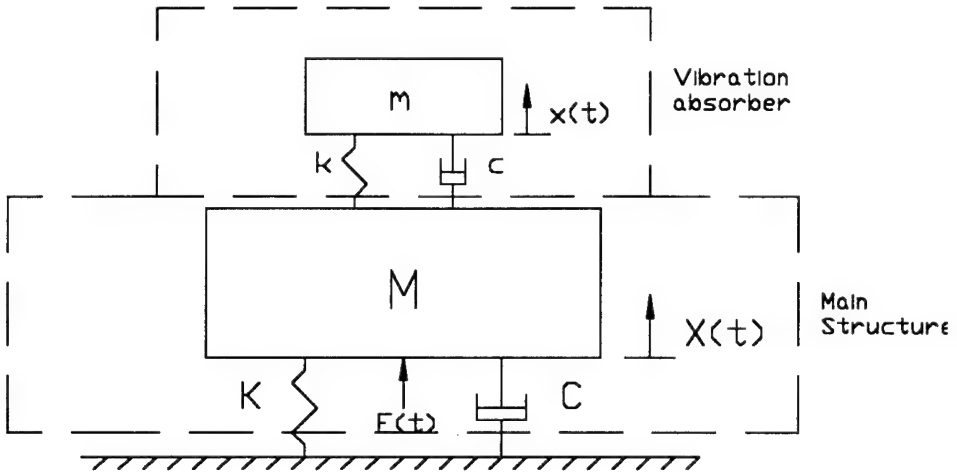

Figure 2-6. Dynamic vibration absorber.

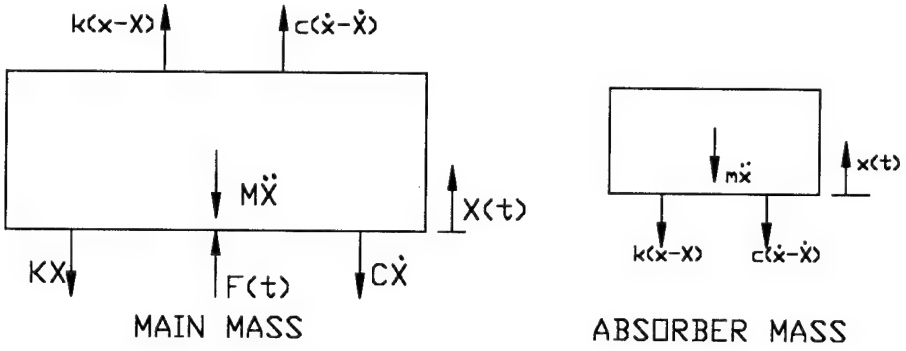

Figure 2-7. Dynamic forces on each mass of a dynamic vibration absorber.

Multiple degree of freedom systems. For more complex arrangements of internal structure, where many degrees of freedom would be required to properly model the dynamic response, the displacements, accelerations, and velocities would be vectors, and a larger number of simultaneous differential equations would be required. For multiple degree of freedom main and internal structures, the equations of motion could be

written just as equations (2-23) and (2-24), but in matrix form. Thus, there would be one simultaneous equation for *each* degree of freedom.

An alternative approach for multiple degree of freedom systems (particularly where the internal structure is complex and a large number of degrees of freedom would be required to adequately represent the dynamics), would be to use the principle of modal superposition under the assumption of linear response (as discussed in section 2.2.3) to approximate the response of the internal structure. By including only those resonant response modes of the main structure and the internal structure which would contribute significantly to the overall response, the complexity of approximating the response of the main structure is greatly reduced. Figure 2-8 depicts a notional complex internal arrangement of discrete masses with many degrees of freedom.

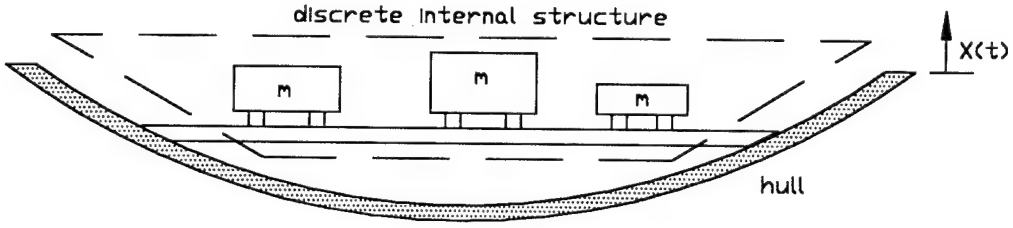

Figure 2-8. Complex internal arrangement of discrete masses with many degrees of freedom.

Using modal superposition, an equivalent mechanical model of the dynamic behavior of the discrete internal structure may be made as shown in figure 2-9. Each mode of resonant response of the discrete internal structure is represented by an equivalent modal mass, modal damping and modal stiffness (mass m_0 represents that portion of the discrete internal structure responding as a rigid body with the main structure). A variation of the dynamic equilibrium equation (2-24) for the dynamic vibration absorber can be written using the principle of modal superposition. The equation of motion for the *n*th mode of the internal structure can be written:

$$m_n\ddot{x}_n + c_n(\dot{x}_n - \dot{X}) + k_n(x_n - X) = 0 \qquad (2\text{-}28)$$

where x_n is the *n*th modal displacement of the internal structure (equivalent to q_n in section 2.2.3) and X is the displacement of the main structure (hull).

The equations of motion for a system made up of an internal structure attached to a large vibrating structure (the hull) can be derived by considering dynamic equilibrium of

the main structure and the superposed modal masses of the internal structure. The forces applied to the main structure by the internal structure can be obtained by modal superposition. Figure 2-10 illustrates the dynamic equilibrium for the main structure.

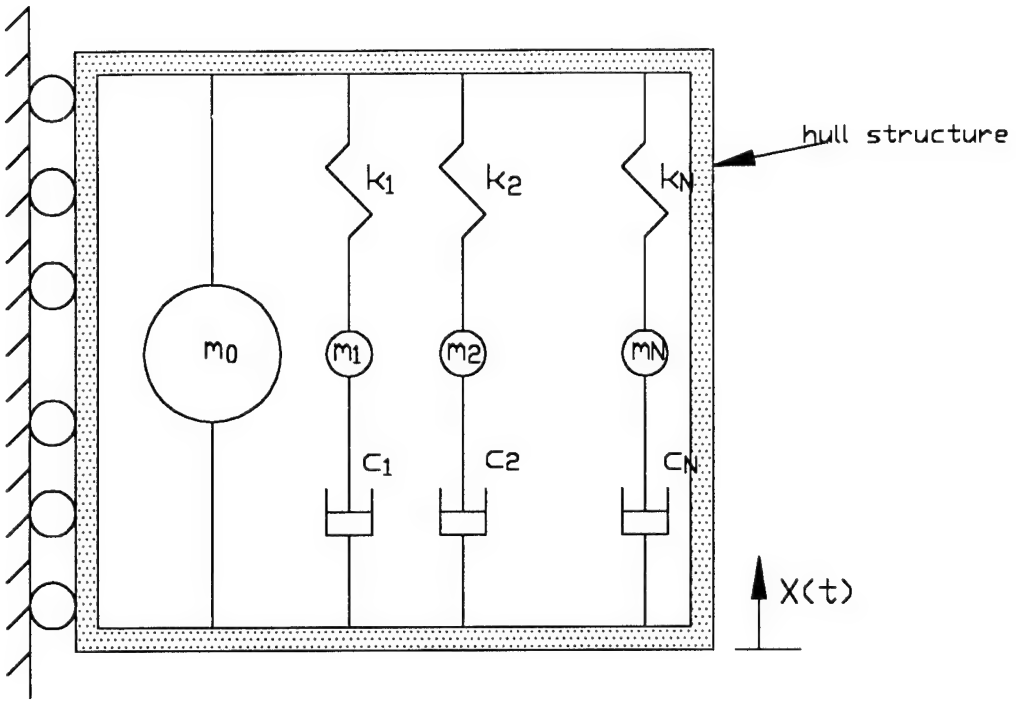

Figure 2-9. Equivalent mechanical model of the dynamic behavior of a discrete internal structure (using modal superposition).

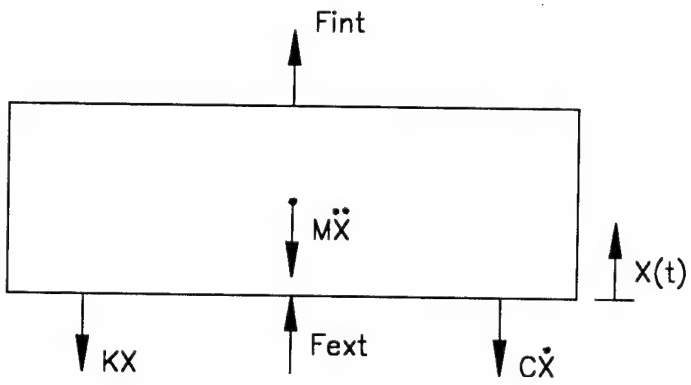

Figure 2-10. Dynamic equilibrium for the main structure.

From dynamic equilibrium, the equation of motion for the main structure can be written:

$$[M\ddot{X} + C\dot{X} + KX] = F_{ext} + F_{int} \qquad (2\text{-}29)$$

where F_{ext} is an external force applied to the main structure, and F_{int} is defined as the force exerted on the main structure by the internal structure. F_{int} can be determined by considering dynamic equilibrium of the internal structure using modal superposition, as shown in figure 2-11. By dynamic equilibrium of the internal structure:

$$F_{int} = -\sum_{n=0}^{N} m_n \ddot{x}_n = \sum_{n=0}^{N} \left[c_n \left(\dot{x}_n - \dot{X} \right) + k_n \left(x_n - X \right) \right] \tag{2-30}$$

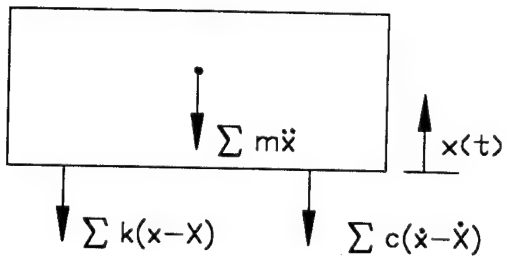

Figure 2-11. Dynamic equilibrium of the internal structure using modal superposition.

It should be noted that the internal structure rigid body case (n = 0) can be taken out of equation (2-30) by noting:

$$\sum_{n=0}^{N} \left[c_n \left(\dot{x}_n - \dot{X} \right) + k_n \left(x_n - X \right) \right] = -\sum_{n=0}^{N} m_n \ddot{x}_n = -m_0 \ddot{X} - \sum_{n=1}^{N} m_n \ddot{x}_n = -m_0 \ddot{X} + \sum_{n=1}^{N} \left[c_n \left(\dot{x}_n - \dot{X} \right) + k_n \left(x_n - X \right) \right] \tag{2-31}$$

With this simplification, the force exerted on the main structure by the internal structure can be written:

$$F_{int} = -m_0 \ddot{X} + \sum_{n=1}^{N} \left[c_n \left(\dot{x}_n - \dot{X} \right) + k_n \left(x_n - X \right) \right] \tag{2-32}$$

Equations (2-29), (2-28), and (2-32) form a set of $N+1$ simultaneous equations (coupled) which can be solved under various conditions for displacements, velocities and accelerations.

It should be noted that, for cases where more than one degree of freedom is important for the main structure (e.g. the main structure moves horizontally as well as vertically), the above method could be extended considering the *modal response* of the internal structure in *each* of the degrees of freedom of the main structure. Thus, the main structure displacement would be represented by a vector **(X),** the internal structure modal displacement would be represented by a vector ($\mathbf{x}_n$), and the forces (F_{int} and F_{ext}) would be represented by vectors.

An application of damping through discrete internal structures will be included in the development of a model for submarine whipping in chapter 3.

2.3.2 Damping through sloshing liquids.

Liquid sloshing has been the focus of considerable attention in the space industry, due primarily to concerns about fuel-rocket interaction forces, and recognition that liquid sloshing resonance can result in significant dissipation of energy and can, therefore, be capitalized upon to suppress vibrations in large structures[16]. Similarly, methods to account for the effects of sloshing liquids on the natural frequencies and damping of offshore platforms have been developed within the marine industry[17]. The occurrence of resonance, effects of nonlinearities, and contribution of devices such as baffles have been the object of numerous other studies. It can be projected that liquids in tanks onboard a whipping ship could undergo sloshing resonance, resulting in the damping of whipping energy. Fundamentally, any onboard liquid with free surface has the potential for absorbing whipping energy through liquid sloshing (liquid without free surface acts only as a rigid mass). Figure 2-12 illustrates a notional liquid storage tank, restrained to move with the whipping hull, and the resulting sloshing (or standing waves) generated due to the existence of the free surface of the liquid in the tank.

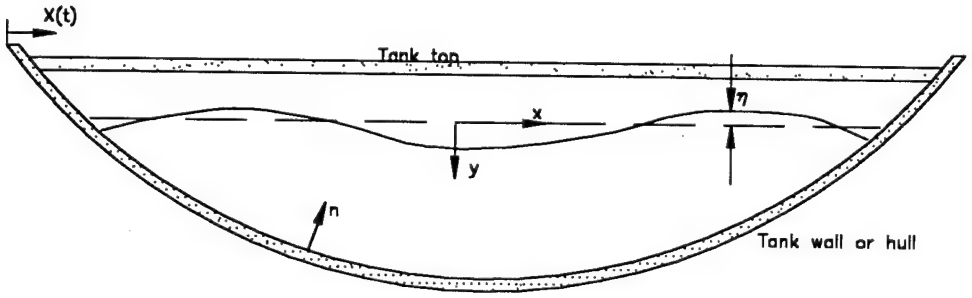

Figure 2-12. Tank with sloshing liquid.

The liquid in a moving tank can be expected to respond in a variety of ways dependent upon many variables (tank geometry, directions of tank motion, amplitudes and frequencies of tank motion, properties of the liquid, etc.). Translational or pitching

---

[16]Welt, F., and Modi, V.J., "Vibration damping through liquid sloshing", *Diagnostics, Vehicle Dynamics and Special Topics: 12th Biennial Conference on Mechanical Vibrations and Noise*, ASME, 1989.
[17]Vandiver, J.K., and Mitome, S., "Effect of liquid storage tanks on the dynamic response of offshore platforms", *Dynamic Analysis of Offshore Structures: Recent Developments*, CML Publications, Southampton, 1982.

motions of a tank lead primarily to *lateral sloshing* (usually antisymmetric liquid mode shapes). Tank motions normal to the equilibrium free surface lead primarily to *vertical sloshing* (usually symmetric liquid mode shapes). Under conditions of abrupt or sudden acceleration, *liquid impact* with tank overheads and opposing bulkheads may provide significant loading on tank boundaries. The high accelerations associated with a whipping ship may require consideration of any or all of these to account for the transfer of whipping energy.

Analysis of liquid sloshing can be carried out by numerous means. Researchers in the field of liquid sloshing have used several principle methods to determine the important dynamic characteristics desired for various applications[18]. In many applications, potential flow models, using linearized and nonlinear free surface conditions, have been developed and used to approximate the fluid motion in various container shapes (Bauer[19], Hutton[20], Welt and Modi[21], for example). In order to properly account for energy transfer and/or dissipation, incorporation of liquid impact loading and viscous effects has been accomplished using equivalent mechanical models in conjunction with potential flow models (Dalzell[22], Vandiver and Mitome[23], Bauer[24], for example).

Potential flow model. Fundamentally, lateral and vertical sloshing can be thought of as the motion of standing waves within a moving rigid container or tank. Under the assumptions of incompressible and irrotational flow, the motion of the liquid in a tank can be approximated well by solving the potential flow problem for the wave motion subject to appropriate boundary conditions (all variables are functions of time). The *velocity potential function* Φ (defined by $\mathbf{v} = \nabla\Phi$ where $\mathbf{v}$ is the fluid velocity vector and ∇ is the vector differential operator) represents solution of the differential equation (Laplace equation)

$$\nabla^2\Phi = 0 \quad \text{(within the fluid domain)} \tag{2-33}$$

subject to the following boundary conditions:

---

[18]Abramson, H.N. (ed.), *The Dynamic Behavior of Liquids in Moving Containers, NASA SP-106*, 1966.
[19]Bauer, H.F., "Theory of the Fluid Oscillations in a Circular Ring Tank Partially Filled with Liquid", *NASA Technical Note D-557*, 1960.
[20]Hutton, R.E., "An Investigation of Resonant, Nonlinear, Non-Planar Free Surface Oscillations of a Fluid", *NASA Technical Note D-1870*, 1963.
[21]Welt and Modi, *op. cit.*
[22]Dalzell, J.F., "Liquid Impact on Tank Bulkheads", *The Dynamic Behavior of Liquids in Moving Containers, NASA SP-106*, H.N. Abramson (ed.), 1966, pp. 353-372.
[23]Vandiver and Mitome, *op. cit.*
[24]Bauer, H.F., "Nonlinear Mechanical Model for the Description of Propellant Sloshing", *AIAA Journal*, Vol. 4, No. 9, 1966, pp. 1662-1668.

$$\frac{\partial \Phi}{\partial n} = V_n \quad \text{(on the wall of the tank)} \tag{2-34a}$$

$$\frac{\partial^2 \Phi}{\partial t^2} + g\frac{\partial \Phi}{\partial y} + 2\nabla\Phi \cdot \nabla\frac{\partial \Phi}{\partial t} + \frac{1}{2}\nabla\Phi \cdot \nabla(\nabla\Phi \cdot \nabla\Phi) = 0$$

$$\text{(at } y = \eta \text{ (on the free surface))} \tag{2-34b}$$

where **n** is the normal vector of the tank wall, $\mathbf{V_n}$ is the velocity of the tank wall normal to its surface, g is the acceleration due to gravity, and η is the free surface elevation. The free surface boundary condition, equation (2-34b), represents the complete nonlinear free surface boundary condition[25]. The linearized free surface boundary condition (linearized about the mean free surface) would be written:

$$\frac{\partial^2 \Phi}{\partial t^2} + g\frac{\partial \Phi}{\partial y} = 0 \quad \text{(at } y = 0\text{)} \tag{2-34c}$$

The fluid velocity vector (**v**) can be obtained from (by definition of the velocity potential):

$$v = \nabla\Phi \tag{2-35}$$

The hydrodynamic pressure (P_h) exerted on the tank wall by the sloshing liquid can be obtained from the unsteady Bernoulli equations:

$$P_h = -\rho\left[\frac{\partial \Phi}{\partial t} + \frac{1}{2}|\nabla\Phi|^2\right] \tag{2-36}$$

where ρ is the liquid density. Finally, the hydrodynamic force exerted on the tank wall by the sloshing liquid can be obtained by integration of the hydrodynamic pressure over the area of the tank wall:

$$F_h = \iint_S (P_h \cdot n)dS \tag{2-37}$$

where **F** is the hydrodynamic force vector (on the tank wall) and S is the surface of the tank wall (below the free surface). Thus, for a specified tank geometry and motion, the hydrodynamic forces exerted by the sloshing liquid on the tank can be approximated using a potential flow model.

Equivalent mechanical model. As mentioned previously, in order to properly account for energy dissipation, viscous effects at the tank wall must be included. While it is difficult to include viscous effects in the potential flow solution, viscous damping may be included in an equivalent mechanical model for the sloshing. In an equivalent

[25]Newman, J.N., *Marine Hydrodynamics*, The MIT Press, Cambridge, MA, 1986, p. 247.

mechanical model, each of the sloshing modes (or modes of standing wave motion) is represented by an equivalent spring-mass-damper as shown in figure 2-13. In typical practice, linear viscous damping is usually assumed for the (modal) dampers in the mechanical model[26], however, nonlinear mechanical modeling techniques do exist[27].

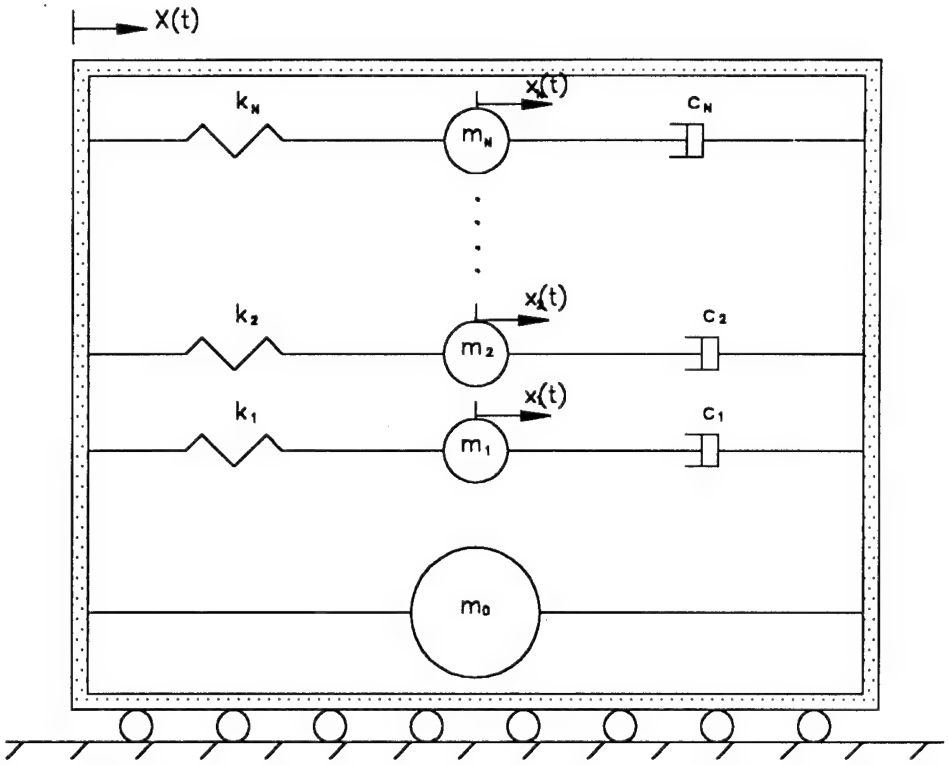

Figure 2-13. Equivalent mechanical model of a tank with sloshing liquid using modal superposition.

In an equivalent mechanical model, the size of the equivalent masses for each of the resonant sloshing modes ($m_1, m_2, \ldots$) may be determined by requiring that the (hydrodynamic) force exerted on the tank wall by the equivalent mass-spring system, for the case of zero damping, be equal to the force calculated from the potential flow theory for each resonant sloshing mode (m_0 is the portion of the liquid in the tank which acts as a rigid body).

$$f_n^h = m_n \ddot{x}_n \Rightarrow m_n = \frac{f_n^h}{\ddot{x}_n} \tag{2-38}$$

[26]Silverman, S., and Abramson, H.N., "Damping of Liquid Motions and Lateral Sloshing", *The Dynamic Behavior of Liquids in Moving Containers, NASA SP-106*, H.N. Abramson (ed.), 1966, pp. 105-144.
[27]Bauer, *op. cit.*

where f_n^h is the hydrodynamic force exerted on the tank wall by the *n*th sloshing mode. The equivalent modal stiffnesses $(k_1, k_2, \ldots)$ may be determined from the natural frequencies (ω_n) calculated from the potential flow theory for each resonant sloshing mode:

$$\omega_n = \sqrt{\frac{k_n}{m_n}} \Rightarrow k_n = \omega_n^2 m_n \tag{2-39}$$

Damping coefficients for each resonant sloshing mode can be determined experimentally for a given tank configuration via a logarithmic decrement method (section 1.2). The modal damping ratio for the *n*th mode (ζ_n) can be determined from the log decrement (δ) measured for each mode by

$$\zeta_n = \frac{\delta}{\sqrt{(2\pi)^2 + \delta^2}} \approx \frac{\delta}{2\pi} \text{ (for small damping)} \tag{2-40}$$

where the log decrement is defined by equation (1-1). The modal damping ratio is the ratio of the modal damping coefficient to the critical modal damping coefficient (c / c_c), where the critical modal damping coefficient represents that value of damping where the motion would not oscillate, but would be non-periodic. The modal damping coefficients $(c_1, c_2, \ldots)$ can be determined from

$$c_n = 2\zeta_n m_n \omega_n \tag{2-41}$$

Referring to figure 2-13, the equation of motion for the *n*th equivalent mass can be written in terms of the displacement, velocity, and the acceleration of the equivalent mass as follows:

$$m_n \ddot{x}_n + c_n(\dot{x}_n - \dot{X}) + k_n(x_n - X) = 0 \tag{2-42}$$

where X is the displacement of the tank, x_n is the displacement of the *n*th sloshing mode (equivalent mass), and velocities and accelerations are represented by superposed dots. The total hydrodynamic force on the wall of the tank can be found by summing the forces contributed by each mode:

$$F_h = -\sum_{n=0}^{\infty} m_n \ddot{x}_n = -m_0 \ddot{X} - \sum_{n=1}^{\infty} m_n \ddot{x}_n \tag{2-43}$$

Similar to the discrete internal structure, *each* of the resonant modes of liquid sloshing can be applied to the main structure (the hull).

As an example, consider the lateral motion of a rigid structure with an integral laterally sloshing tank. The equivalent mechanical model could be as shown in figure

2-14. The equation of motion for each of the equivalent liquid masses (modal masses) is given by equation (2-42), and the total hydrodynamic force on the wall of the tank due to the liquid sloshing is given by equation (2-43). The equation of motion for the main structure can then be found by adding the total hydrodynamic force *into* the equation of motion for the structure without the liquid:

$$\left[M\ddot{X} + C\dot{X} + KX\right] = F_{ext} + F_h \tag{2-44}$$

where F_{ext} is an external force applied to the main structure. The hydrodynamic force (F_h) may be written (following the same principles of modal superposition used for the internal structure):

$$F_h = -\sum_{n=0}^{\infty} m_n \ddot{x}_n = -m_0 \ddot{X} + \sum_{n=1}^{\infty}\left[c_n(\dot{x}_n - \dot{X}) + k_n(x_n - X)\right] \tag{2-45}$$

It can also be noted that m_0, the portion of the liquid which acts as a rigid body, can be found from:

$$M_l = \sum_{n=0}^{\infty} m_n \Rightarrow m_0 = M_l - \sum_{n=1}^{\infty} m_n \tag{2-46}$$

where M_l is the total mass of liquid in the tank.

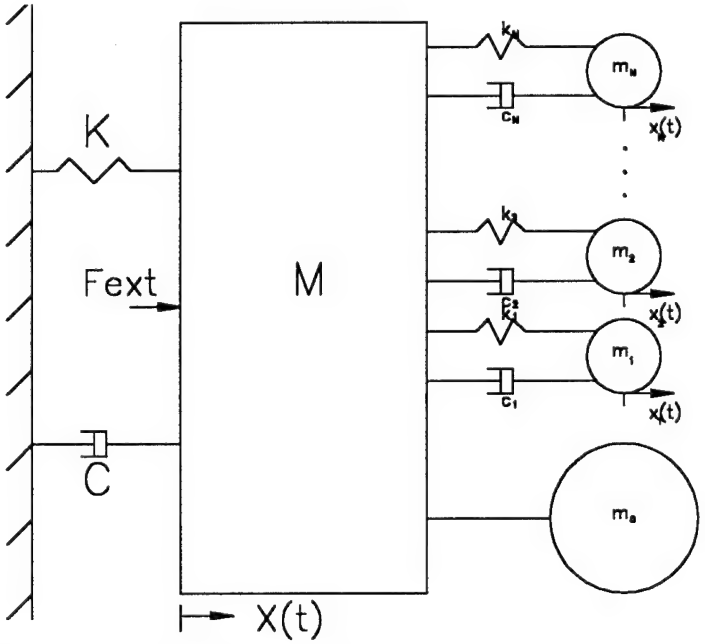

Figure 2-14. Equivalent mechanical model for the lateral motion of a rigid structure with an integral laterally sloshing tank.

In terms of real applications, such as in the whipping of a ship hull, equation (2-45) may be truncated because the equivalent masses m_n and modal displacements x_n grow smaller with *n* (the rate at which they grow smaller depends upon the geometry of the tank). All terms should be included for which the natural frequencies of the tank (ω_n) are less than or equal to the natural flexural frequency of the overall structure (less than the fundamental flexural/whipping natural frequency). If equation (2-45) is truncated to include *N* modes, then equations (2-44), (2-45), and (2-46) form a set of *N+1* simultaneous equations of motion for the *total* dynamic system consisting of the main structure and the sloshing liquid.

It should be noted that, for cases where more than one degree of freedom is important for the main structure (e.g. the main structure moves horizontally as well as vertically), the above method could be extended considering the *modal response* of the sloshing liquid in *each* of the degrees of freedom of the main structure. Thus, the main structure displacement would be represented by a *vector* **(X),** the sloshing liquid modal displacement would be represented by a *vector* ($\mathbf{x}_n$), and the forces (F_h and F_{ext}) would be represented by *vectors*.

An application of liquid sloshing will be included in the development of a model for submarine whipping in chapter 3.

2.4 External (fluid) damping.

The loss of vibrational energy of a whipping ship into the surrounding fluid medium can be accomplished through several general mechanisms. If the ship is sufficiently close to the free surface, or its motion is of sufficient velocity and/or frequency, surface and pressure waves of non-negligible energy can be generated. This form of fluid damping is often referred to as *wave radiation damping*. Additionally, whipping energy can be lost through mechanisms associated with the viscosity of the surrounding fluid. These mechanisms can be lumped under the general heading of *viscous fluid damping*, but include specific mechanisms associated with time-dependent viscous boundary layer shear forces ("skin friction" drag) as well as boundary layer separation ("form" drag).

In general, the dominant hydrodynamic forces on a structure are determined primarily by the characteristics of the fluid flow around the structure. For a whipping ship, the relative fluid flow around the hull would be *generally* oscillatory in nature. For oscillatory flow, the following non-dimensional parameters are often used to characterize the flow:

$$\text{Peak Reynolds' number, } Rn = \frac{U_0 D}{\nu}$$

$$\text{Keulegan-Carpenter number, } KC = \frac{U_0 T}{D}$$

$$\text{Viscous-frequency parameter, } \beta = \frac{Rn}{KC} = \frac{D^2}{\nu T}$$

where U is the characteristic *relative* free stream velocity (U_0 is the amplitude of the characteristic *relative* free stream velocity or maximum *relative* velocity), D is the characteristic dimension of the structure (i.e. the diameter), ν is the kinematic viscosity of the fluid, and T is the characteristic period of oscillation of the *relative* fluid flow. Additionally, the flow can be influenced significantly by the geometry of the structure, free surface effects, sea floor effects, roughness on the surface of the structure, and the orientation of the structure relative to the flow. It may also be shown that for *harmonically* oscillating flow around a fixed circular cylinder, $KC = 2\pi A / D$, where A is the amplitude of the oscillation of the fluid particle displacement. Thus, KC may be thought of as representing an amplitude of motion between a structure and the fluid relative the characteristic dimension of the body.

These parameters, in addition to the other influencing factors listed above, determine the characteristics of the flow, and thus the major components of the hydrodynamic force on the structure. As will be discussed in greater detail subsequently, these characteristic parameters (i.e. the characteristics of the flow) effect the occurrence of boundary layer separation, and thus a major component of viscous fluid forces (as will be discussed subsequently, boundary layer separation forces tend to dominate over boundary layer shear forces for bluff bodies). For fully submerged bodies, if KC is *large* (i.e. U_0 is large and D is small), then boundary layer separation is likely to occur, and the major hydrodynamic forces are likely to be associated with viscous drag effects (the so-called "drag-dominated regime"). If both Rn *and* KC are *large* (i.e. U_0 is large but D is *not* small), then the added forces associated with the inertia of the surrounding fluid (called fluid inertia forces) must also be considered in addition to the drag forces (the so-called "Morison regime"). If KC is *small* (Rn may still be moderately large), then boundary layer separation is *not* likely to occur and the only viscous forces would be due to boundary layer shear. If, in addition to KC being small, the structure is on or near a free surface then radiation of surface waves tends to dominate the hydrodynamic damping (the so-called "diffraction/radiation" regime). It is important to note that, for complex structures such as ships, different portions of the structure may be subject to different

types of hydrodynamic loading (depending upon the *local* characteristics of the structure and the relative fluid flow).

2.4.1 Wave radiation damping.

Fundamentally, waves are radiated whenever a structure moves in a fluid medium. As mentioned above, when KC is small (i.e. when D is large), and the structure is on or near a free surface, then forces associated with wave radiation are generally important. In typical practice, panel or boundary element methods are used to solve the boundary-value problem in analyzing hydrodynamic forces due to incident, diffracted and radiated pressures. Boundary element methods are based upon potential flow theory, which neglects the effects of viscosity. However, there has been some effort in recent years to include some of the effects of viscosity within the boundary element method (as will be discussed subsequently).

Potential flow theory and its application to the hydrodynamics of structures is discussed in great detail in numerous sources (Newman[28], Chakrabarti[29], Faltinsen[30], for example). Under potential flow theory (assuming inviscid, irrotational flow), the fluid velocity within the fluid domain may be represented as the gradient of a scalar potential function

$$v = \nabla\Phi \equiv i\frac{\partial\Phi}{\partial x} + j\frac{\partial\Phi}{\partial y} + k\frac{\partial\Phi}{\partial z} \qquad (2\text{-}47)$$

where **v** is the fluid velocity vector, $\Phi(x,y,z,t)$ is the scalar velocity potential function (written here in terms of Cartesian coordinates), and ∇ is the vector differential operator. The velocity potential must satisfy Laplace's equation

$$\nabla^2\Phi \equiv \frac{\partial^2\Phi}{\partial x^2} + \frac{\partial^2\Phi}{\partial y^2} + \frac{\partial^2\Phi}{\partial z^2} = 0 \qquad (2\text{-}48)$$

within the fluid domain, and satisfy boundary conditions specific to the geometry of the application. For the case of a body of general shape moving near a free surface in a fluid of finite depth (figure 2-15), the velocity potential must satisfy the following boundary conditions:

$$\frac{\partial\Phi}{\partial n} = V \cdot n \quad \text{(on the surface of the body)} \qquad (2\text{-}49a)$$

---

[28]Newman, *op. cit.*

[29]Chakrabarti, S.K., *Hydrodynamics of Offshore Structures*, Springer-Verlag, London, 1987.

[30]Faltinsen, O.M., *Sea Loads on Ships and Offshore Structures*, Cambridge University Press, UK, 1990.

$$\frac{\partial \Phi}{\partial y} = 0 \quad \text{(at y = -h (for finite water depth))} \tag{2-49b}$$

$$\frac{\partial^2 \Phi}{\partial t^2} + g\frac{\partial \Phi}{\partial y} + 2\nabla\Phi \cdot \nabla\frac{\partial \Phi}{\partial t} + \frac{1}{2}\nabla\Phi \cdot \nabla\left(\nabla\Phi \cdot \nabla\Phi\right) = 0$$

$$\text{(at y = } \eta \text{ (on the free surface))} \tag{2-49c}$$

where **n** is the normal vector of the body surface (pointing from the body into the fluid domain), **V** is the velocity vector of the body, g is the acceleration due to gravity, η is the free surface elevation above the mean, and h is the mean depth of the water. The free surface boundary condition, equation (2-49c), represents the complete nonlinear free surface boundary condition[31]. The linearized free surface boundary condition (linearized about the mean free surface) would be written:

$$\frac{\partial^2 \Phi}{\partial t^2} + g\frac{\partial \Phi}{\partial y} = 0 \quad \text{(at y = 0)} \tag{2-49d}$$

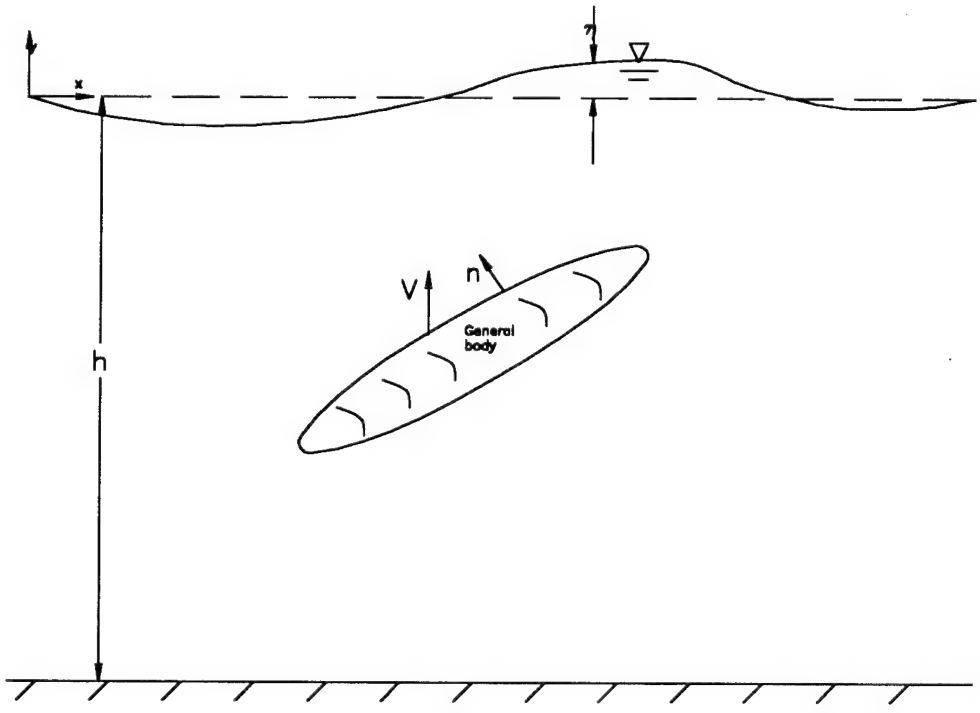

Figure 2-15. Body of general shape moving in fluid with free surface.

[31]Newman, *op. cit.*, p. 247.

Additionally, a radiation condition must be established (as a boundary condition limit at infinity) in order to ensure that radiated waves propagate away from the body. For solution of equation (2-48) in the time domain, initial conditions are also required:

$$\Phi \to 0$$

$$\frac{\partial \Phi}{\partial t} \to 0 \quad (\text{as } t \to -\infty) \tag{2-50}$$

Solution of Laplace's equation (2-48) for the velocity potential, Φ, is obtained by the method of integral equations using Green's theorem which can be written in the general form:

$$\int_{\forall} \left(\Phi \nabla^2 G - G \nabla^2 \Phi\right) d\forall = \int_{S} \left(\Phi \nabla G - G \nabla \Phi\right) \cdot n dS \tag{2-51}$$

where $\forall$ is defined as the volume bound by surface S, where S includes the body surface, the free surface, the bottom surface, and the surface at "infinity" (figure 2-16). An appropriate Green function (G) can be obtained which satisfactorily represents the source potentials and their derivatives for various boundary condition combinations (Wehausen and Laitone[32], Newman[33], for example).

Once the velocity potential function is obtained, the fluid velocity vector in the fluid domain can be found by definition of the potential function as written in equation (2-47). The hydrodynamic pressure exerted on the body by the fluid is obtained from the unsteady Bernoulli equations:

$$P = -\rho \left[\frac{\partial \Phi}{\partial t} + \frac{1}{2} |\nabla \Phi|^2 \right] \tag{2-52}$$

where P is the hydrodynamic pressure (a function of position) and ρ is the fluid density. The hydrodynamic force exerted on the body (or the panel of interest) by the fluid is obtained by integrating the hydrodynamic pressure over the submerged portion of the surface:

$$F = \iint_{S} (P \cdot n) dS \tag{2-53}$$

where **F** is the force vector on the surface or panel, S is the submerged surface of the body or panel, and **n** is the direction normal of the panel surface.

---

[32]Wehausen, J.V., and Laitone, E.V., "Surface Waves", *Encyclopedia of Physics (Vol. 9)*, Springer-Verlag, Berlin, 1960.

[33]Newman, J.N., "Algorithms for the free surface Green function", *Journal of Engineering Mathematics*, 19, 1985, pp. 57-67.

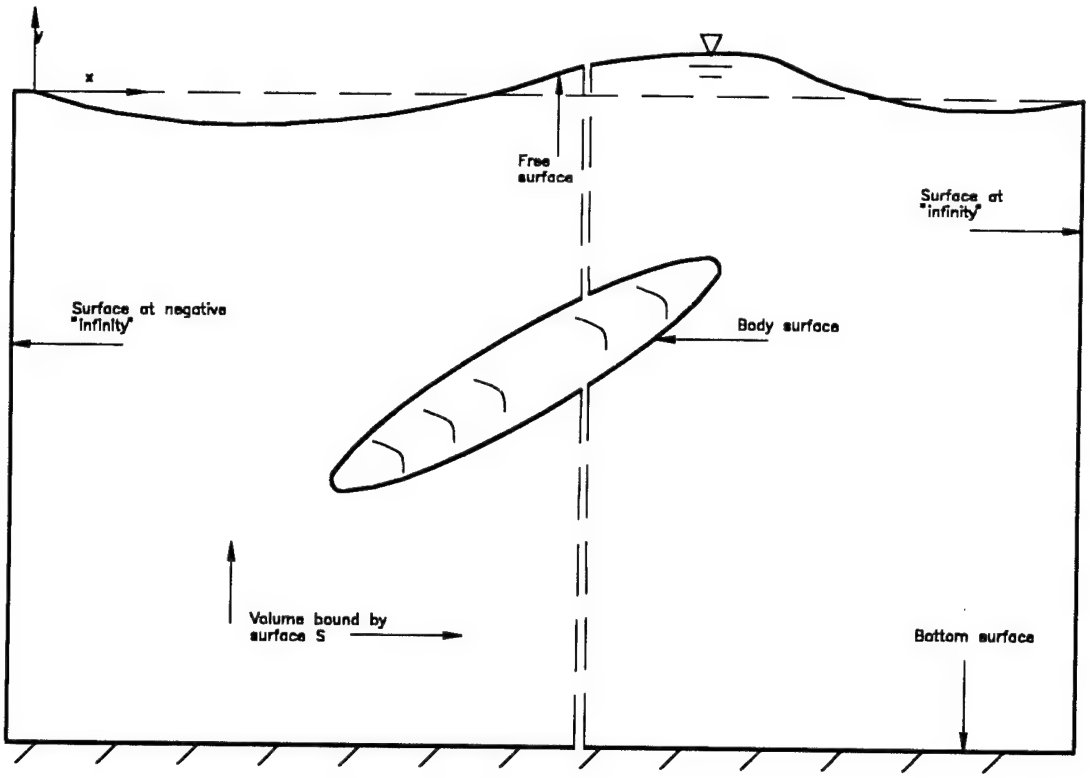

Figure 2-16. Surfaces of integration for Green's theorem.

For slender bodies (where length is much greater than width), application of two-dimensional diffraction/radiation potential theory has proven accurate and useful, particularly at higher frequencies[34]. Several two-dimensional approaches are available in the literature, the most common of which is *strip theory*[35]. In strip theory, the slender body is divided into many thin slices or strips, each of which has approximately constant cross-section, so that two-dimensional potential theory could be applied to determine the approximate hydrodynamic forces on each strip *independently* (figure 2-17). For rigid body hydrodynamics applications, the hydrodynamic forces on each strip could then be integrated along the length of the body to determine the total hydrodynamic force on the body. Alternatively, similar to panel methods, the hydrodynamic forces on each "strip" can be resolved and integrated into the fluid-structure interaction dynamic problem as external loads.

Thus, the motions of a *large* structure on or near a free surface (where viscosity effects can be ignored) could be obtained using the complete potential flow theory

---

[34]Lewis, E.V. (ed.), *Principles of Naval Architecture (Vol. III - Motions in Waves and Controllability)*, Second Revision, SNAME, Jersey City, NJ, 1989.

[35]Salveson, N., Tuck, E.O., and Faltinsen, O., "Ship Motions and Sea Loads", *SNAME Transactions*, Vol. 78, 1970, pp. 250-279.

(linearized or fully nonlinear). It computes the forces exerted on the structure by the incident pressure (the external "loading" force - the bubble pulse for a whipping ship subjected to an underwater explosion bubble), the diffraction pressure (scattering of the incident pressure from the "rigid" structure), and the radiation pressure (wave radiation from the structure as it moves in *each* of its degrees of freedom). Thus, the *total* velocity potential (Φ) at any point in the fluid in the presence of a moving structure (either three-dimensional if panel methods are used, or two-dimensional if strip theory is used) can be written as a superposition of the velocity potentials due to incident, diffracted, and radiated pressures as follows:

$$\Phi = \Phi^{\circ} + \sum_{i=1}^{M} \Phi_i^s + \sum_{i=1}^{M} \sum_{j=1}^{N} \Phi_{ij}^r \qquad (2\text{-}54)$$

where Φ° is the velocity potential due to the incident pressure, Φ_i^s is the velocity potential due to the diffracted or scattered pressure from the *i*th panel (where M is the total number of panels making up the total surface S), and Φ_{ij}^r is the velocity potential due to the radiated pressure caused by motion of the *i*th panel in the *j*th direction (where N is the number of degrees of freedom for each panel) .

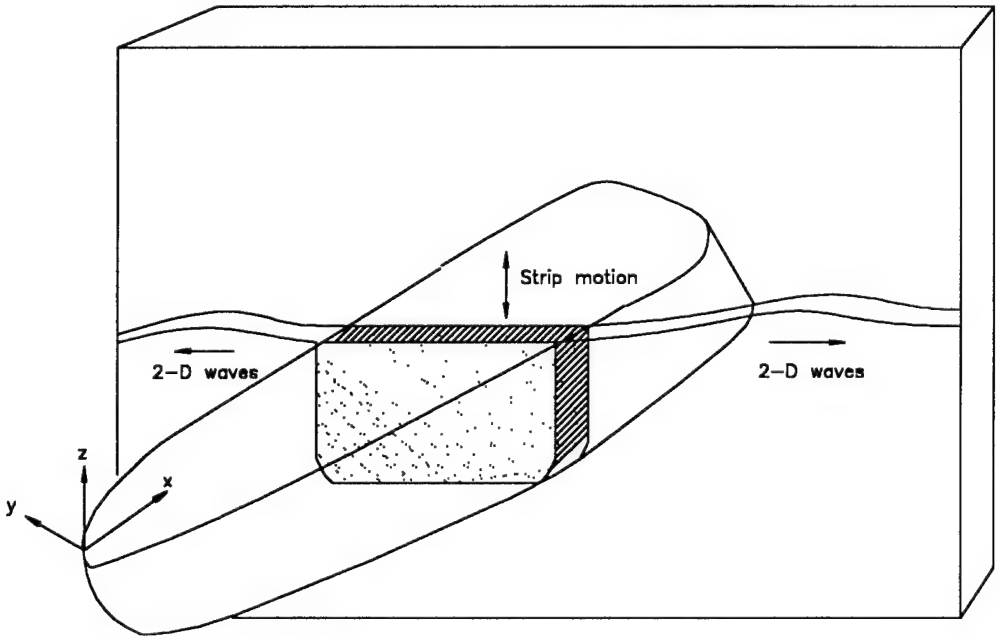

Figure 2-17. Two-dimensional strip theory.

For *most* marine applications, rigid body *translations* are ignored and the solution of the equations of motion is carried out in the frequency domain, assuming harmonic motion of the structure centered around an equilibrium position. The incident and diffracted velocity potentials are computed on the assumption that the structure is *fixed* in its equilibrium position, subjected only to the given external loading (usually wave loading). The radiated velocity potentials are then computed assuming that the structure undergoes one simple harmonic motion at a time (i.e. at each frequency in each degree of freedom) in calm water (see Chakrabarti[36], Faltinsen[37], for example). For assumed simple harmonic motion of the form:

$$x = Xe^{i\omega t} \tag{2-55}$$

where **x** is the displacement vector, **X** is the displacement magnitude vector, and ω is the frequency, the total hydrodynamic force on the structure (calculated with potential flow theory) has the form:

$$F_n = -\omega^2 X_n M_{mn} + i\omega X_n C_{mn} \tag{2-56}$$

in which F_n is the force on the structure in the *n*th degree of freedom, and X_n is the displacement of the structure in the *n*th degree of freedom. M_{mn} is called the added mass matrix (hydrodynamic added mass in the *n*th degree of freedom due to unit displacement in the *m*th degree of freedom), and thus the first term on the right hand side represents the hydrodynamic forces which are *in phase with acceleration*. C_{mn} is called the radiation damping matrix (hydrodynamic damping in the *n*th degree of freedom due to unit displacement in the *m*th degree of freedom), and thus the second term on the right hand side represents the hydrodynamic forces which are *in phase with velocity*.

For applications where simple harmonic motion about a fixed equilibrium position is *not* a reasonable assumption (e.g. when rigid body translations are important), the separate accounting for added mass and radiation damping forces as above is normally not possible (except in the case of *steady* rigid body translation). For cases with *unsteady* rigid body translation in addition to harmonic vibration (e.g. whipping of a submerged submarine subjected to an underwater explosion bubble), the calculation of the *total* hydrodynamic forces must be accomplished in the time-domain. Application of potential flow theory in the time-domain to predict *general* motions of structures is not new and fundamentally straight forward, but has had limited application for complex geometries and loadings because of limited computational resources. Discussions of direct time-

---

[36]Chakrabarti, *op. cit.*
[37]Faltinsen, *op. cit.*

domain solution techniques are presented by various authors for various applications (Beck and Magee[38], Ogilvie[39], for example).

2.4.2 Viscous fluid damping.

As mentioned previously, dynamic energy can be lost into the surrounding fluid medium through forces associated with fluid viscosity. First, viscous shear forces occur within the viscous boundary layer surrounding the moving structure (so-called "skin friction" drag). Second, separation of the boundary layer from the structure leads to additional forces on the moving structure (so-called "form" drag). Together, boundary layer shear forces and boundary layer separation forces constitute the viscous fluid forces.

The extent to which each of these forces is important is a function of the geometry of the body, and the relative fluid motion around the body (characteristic amplitude of relative fluid motion and characteristic frequency). Where geometry and fluid flow around the structure are such that the boundary layer remains attached (e.g. streamlined bodies at low angles of attack), boundary layer shear forces tend to dominate. However, for "bluff" bodies such as circular cylinders and "flat" plates, boundary layer separation readily occurs which tends to produce forces greatly exceeding the boundary layer shear forces. Numerous experiments have been conducted on various geometries giving indication under which conditions each of the forces would be significant, and estimation of the forces.

The largest body of data exists for harmonic transverse oscillation of horizontal cylinders for which two dimensional flow around the body can be assumed. As discussed previously, flow around a two-dimensional body is typically characterized by several non-dimensional parameters, including the Keulegan-Carpenter number and the Reynolds' number (or alternatively the viscous-frequency parameter, β). Anaturk[40] and Anaturk et. al.[41] present regions in the KC - β plane where two dimensional flows possess different characteristics. For example, when $KC < 1$ and $\beta \leq 10^3 - 10^4$ ($Rn \leq 10^3 - 10^4$), the boundary layer flow *typically* remains attached for the case of a smooth circular cylinder.

---

[38]Beck, R.F., and Magee, A.R., "Time-domain Analysis for Predicting Ship Motions", *Dynamics of Marine Vehicles and Structures in Waves*, Elsevier Science Publishers, B.V., 1991, pp. 49-64.

[39]Ogilvie, T.F., "Recent Progress Toward the Understanding and Prediction of Ship Motions", *Proceedings of the Fifth Symposium on Naval Hydrodynamics*, Office of Naval Research, Washington, DC, 1964, pp. 3-128.

[40]Anaturk, A.R., "An experimental investigation to measure hydrodynamic forces at small amplitudes and high frequencies", *Applied Ocean Research*, 13, 4, 1991, pp. 200-208.

[41]Anaturk, A.R., Tromans, P.S., van Hazendonk, H.C., Sluis, C.M., and Otter, A., "Drag forces on cylinders oscillating at small amplitude; a new model", *Journal of Offshore Mechanics and Arctic Engineering*, 114, 1992, pp. 91-103.

As KC and β (or Rn) increase, the turbulence in the boundary layer increases and flow separates.

For the case where the two dimensional flow does not separate, the flow (and resulting forces) can be satisfactorily predicted using an attached laminar boundary layer theory (Newman[42], Stuart[43], Batchelor[44], for example). This theory predicts the drag forces resulting from the combined normal and tangential stresses in the fluid using Navier-Stokes equations.

For a body of *general* shape, the forces associated with separated flow, and the point at which transition to separated flow occurs (i.e. the stability of the boundary layer) is dependent upon many factors. Many attempts have been made to solve separated flow around marine structures numerically (generally limited to two dimensional flow). Examples of various "state-of-the-art" methods include:

(a) Single vortex method (Faltinsen and Sortland[45])

(b) Vortex sheet model (Faltinsen and Pettersen[46])

(c) Discrete vortex method (Sarpkaya[47], Clements[48])

(d) Vortex-in-cell method (Stansby and Dixon[49])

(e) Combination of Chorin's method and vortex-in-cell method (Chorin[50], Smith and Stansby[51])

(f) Navier-Stokes solvers (Lecointe and Piquet[52])

Additionally, attempts have been made to include vortex shedding models in numerical solutions for potential flows and thus combine wave radiation with the effects of viscosity

---

[42]Newman, *op. cit.*

[43]Stuart, J.T., "Double boundary layers in oscillatory viscous flow", *Journal of Fluid Mechanics*, 24, 1966, pp. 673-687.

[44]Batchelor, G.K., *An Introduction to Fluid Dynamics*, Cambridge University Press, London, 1973.

[45]Faltinsen, O.M., and Sortland, B., "Slow-drift eddy making damping of a ship", *Applied Ocean Research*, 9, 1, 1987, pp. 37-46.

[46]Faltinsen, O.M., and Pettersen, B., "Application of a vortex tracking method to separated flow around marine structures", *Journal of Fluids and Structures*, 1, 1987, pp. 217-237.

[47]Sarpkaya, T., "Computational Methods With Vortices - The 1988 Freeman Scholar Lecture", *Journal of Fluids Engineering*, Vol. 111, March 1989, pp. 5-45.

[48]Clements, R.R., and Maull, D.J., "The representation of sheets of vorticity by discrete vortices", *Progress in Aerospace Science*, Vol. 16, No. 2, 1975, pp. 129-146.

[49]Stansby, P.K., and Dixon, A.G., "Simulation of flows around cylinders by a Lagrangian vortex scheme", *Applied Ocean Research*, Vol. 5, No. 3, 1983, pp. 167-178.

[50]Chorin, A.J., "Numerical study of slightly viscous flow", *Journal of Fluid Mechanics*, 57, 1973, pp. 785-796.

[51]Smith, P.A., and Stansby, P.K., "Impulsively started flow around a circular cylinder by the vortex method", *Journal of Fluid Mechanics*, 194, 1988, pp. 45-77.

[52]Lecointe, Y., and Piquet, J. "Compact finite-difference methods for solving incompressible Navier-Stokes equations around oscillatory bodies", *Von Karman Institute for Fluid Dynamics Lecture Series 1985-04, Computational Fluid Dynamics*, 1985.

(Yeung and Wu[53], Wong and Calisal[54], for example). While these methods have documented satisfactory agreement with experiment in some cases, they are generally not considered robust enough (numerical instabilities, etc.) to be applied with complete confidence to *new* problems where there is no guidance from experiments[55]. Thus, numerical methods to characterize separated flow are often used *in conjunction with* experimental methods.

Morison's equations. In practice, when drag forces are important (and wave radiation may be ignored), and two-dimensional oscillatory flow can be assumed, a Morison's equation or modified Morison's equation can be used to predict hydrodynamic forces . Originally proposed by Morison et. al.[56] for the prediction of wave forces on vertical piles which extend from the bottom through the free surface, the Morison equation has been modified to include application to cylinders of varying orientation under various loading conditions, including cases where the cylinders are free to move under the imposed fluid loading.

Morison's equation for a *stationary cylinder in an oscillating flow field* includes the effect of fluid inertia forces and assumes drag forces to be a quadratic function of velocity:

$$F = \rho A C_m \dot{u} + \frac{1}{2}\rho D C_d u|u| \qquad (2\text{-}57)$$

where F is the hydrodynamic force (per unit length of cylinder - similar to "strip theory", the total force on the cylinder can be found by integrating over the length of the cylinder), A is cross sectional area, D is diameter, u is fluid velocity ($\dot{u}$ is fluid acceleration), coefficient C_m is called the inertia coefficient (the first term being proportional to acceleration is equivalent to an inertia force), and coefficient C_d is called the drag coefficient (the second term being proportional to velocity (squared) is equivalent to a drag force). Figure 2-18 illustrates the parameters used in Morison's equation.

Morison's equation for an *oscillating cylinder in a stationary fluid* includes the effect of fluid added mass forces and again assumes drag forces to be a quadratic function of velocity, giving the *reaction* forces on the cylinder:

---

[53]Yeung, R.W., and Wu, C., "Viscosity effects on the radiation hydrodynamics of two-dimensional cylinders", *Proceedings of the 10th International Conference on Offshore Mechanics and Arctic Engineering*, ASME, 1991, pp. 309-316.

[54]Wong, L.H., and Calisal, S.M., "A numerical solution for potential flows including the effects of vortex shedding", *Proceedings of the 11th International Conference on Offshore Mechanics and Arctic Engineering*, ASME, 1992, pp. 363-368.

[55]Faltinsen, *op. cit.*

[56]Morison, J.R., O'Brien, M.P., Johnson, J.W., and Schaaf, S.A., "The force exerted by surface waves on piles", *Petroleum Transactions*, AIME, 189, 1950, pp. 149-157.

$$F' = -\rho A C_A \ddot{x} - \frac{1}{2}\rho D C_d' \dot{x}|\dot{x}| \qquad (2\text{-}58)$$

where $\ddot{x}$ and $\dot{x}$ are the acceleration and velocity of the cylinder, C_A is called the added mass coefficient, and C_d' is the drag coefficient for and *oscillating cylinder in still water*.

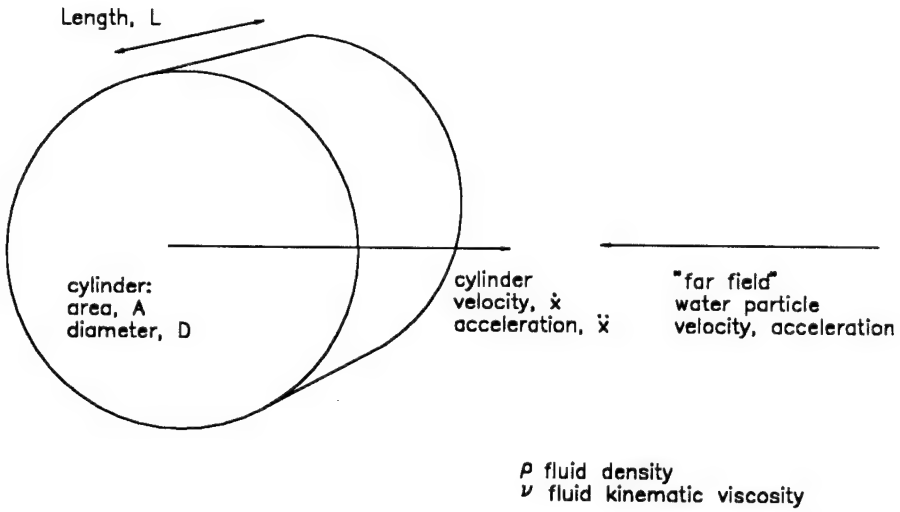

Figure 2-18. Parameters used in Morison's equation.

Coefficients C_m, C_d, C_A, and C_d' are normally experimentally determined for various geometries and loading conditions (usually as functions of KC and β or Rn), and have been determined in a large number of experimental studies (Bearman et. al.[57], Sarpkaya[58], Chakrabarti and Cotter[59], for example).

When a *cylinder is free to move in a moving fluid*, Morison's equation can be written in an extended form by combining equations (2-57) and (2-58):

$$F = \rho A C_m \dot{u} + \frac{1}{2}\rho D C_d u|u| - \rho A C_A \ddot{x} - \frac{1}{2}\rho D C_d' \dot{x}|\dot{x}| \qquad (2\text{-}59)$$

This form is known as the *independent flow fields model*[60] and is obtained as the superposition of the two independent flow fields; a far field due to the water particle motion (i.e. the external loading) and relatively unaffected by the presence and motion of

---

[57]Bearman, P.W., Lin, X.W., and Mackwood, P.R., "Measurement and prediction of response of circular cylinders in oscillating flow", *Proceedings of the 6th International Conference on the Behavior of Offshore Structures (BOSS)*, 1992, pp. 297-307.

[58]Sarpkaya, T., "Force on a cylinder in viscous oscillatory flow at low Keulegan-Carpenter numbers", *Journal of Fluid Mechanics*, Vol. 165, 1986, pp. 61-71.

[59]Chakrabarti, S.K., and Cotter, D.C., "Hydrodynamic coefficients of mooring tower", *Proceedings of the 15th Annual Offshore Technology Conference, OTC 4496*, 1983, pp. 449-458.

[60]Chakrabarti, *op. cit.*, p. 187.

the structure, and a near field resulting from the motion of the structure. Coefficients C_m and C_d may be obtained from experiments where the cylinder is held fixed in oscillating fluid, and coefficients C_A, and C_d^l may be obtained from experiments of an oscillating cylinder in otherwise still fluid. Alternatively, the coefficients could be determined from empirical relations (using KC and Rn, for example):

$$C_m, C_d = f\left(KC_f = \frac{u_0 T}{D}, Rn_f = \frac{u_0 D}{\nu} \right) \tag{2-60}$$

$$C_A, C_d^l = f\left(KC_n = \frac{\dot{x}_0 T^l}{D}, Rn_n = \frac{\ddot{x}_0 D}{\nu} \right) \tag{2-61}$$

where $u_0, \dot{x}_0$ are the amplitudes of water particle and structure velocity, respectively, T, T^l are periods of oscillation of water particle and structure, respectively, and subscripts *f* and *n* refer to the far field and near field, respectively.

An alternative to the independent flow fields model is the *relative velocity model*, in which forces are written in terms of the *relative motion* between the structure and the fluid, in which single coefficients are assumed to apply:

$$F = \rho A C_m (\dot{u} - \ddot{x}) + \rho A \ddot{x} + \frac{1}{2} \rho D C_d (u - \dot{x}) |u - \dot{x}| \tag{2-62}$$

In the relative velocity model, the coefficients may be determined using empirical relations (using KC and Rn, for example):

$$C_m, C_d = f\left(KC_r = \frac{v_{r0} T_r}{D}, Rn_r = \frac{v_{r0} D}{\nu} \right) \tag{2-63}$$

where subscript *r* refers to the relative motion, v_r is the relative velocity between the structure and the fluid (v_{r0} is the amplitude of the relative velocity), and T_r is the combined period of the relative motion. The relative velocity model has seen extensive use in the analysis of hydrodynamic forces on drag dominated offshore structures (Laya et. al.[61], Spidsoe and Karunakaran[62], for example).

Thus, the Morison equation can be used under various conditions to predict the hydrodynamic forces on structures (or portions of structures) where drag forces and fluid

---

[61]Laya, E.J., Conner, M., and Sunder, S.S., "Hydrodynamic forces on flexible offshore structures", *Journal of Engineering Mechanics*, ASCE, March 1984, pp. 433-448.

[62]Spidsoe, N., and Karunkaran, D., "Nonlinear effects of damping to dynamic amplification factors for drag-dominated offshore platforms", *Proceedings of the 11th International Conference on Offshore Mechanics and Arctic Engineering*, ASME, 1992, pp. 231-239.

inertia forces are important. An application of Morison's equation to the development of a model for submarine whipping will be made in chapter 3.

3. MODEL FOR SUBMARINE WHIPPING INCLUDING DAMPING EFFECTS

3.1 Introduction.

In order to gain some quantitative insight into the *relative* amount of damping which could be provided by each of the mechanisms discussed in the previous chapter, it is first necessary to develop a *general* model for submarine whipping, which may include *any or all* of the specific mechanisms. One way of doing this would be to develop a *simplified* model of *each of the mechanisms* based upon the *fundamental principles of mechanics*, some of which were used in the discussion in the previous chapter, and utilize a flexible formulation for the equations of motion which permits inclusion of *selected* mechanisms. Using this approach, any individual mechanism could be evaluated *separately* for its expected effect on total damping.

The equations of motion. The dynamic behavior of any structure is described by the equations of motion, which are simply extensions of Newton's second law of motion. Fundamentally, an equation of motion can be written as a sum of forces which *resist* motion of the structure (i.e. the inertial forces ($F_{inertial}$), the damping or dissipative forces ($F_{damping}$), and the elastic or stiffness forces ($F_{elastic}$)), and forces which *induce* motion (i.e. the external or loading forces ($F_{loading}$)). Thus, an equation of motion may be written in the general form:

$$F_{inertial} + F_{damping} + F_{elastic} = F_{loading} \qquad (3\text{-}1)$$

Inertial forces are those forces through which kinetic energy is stored, and are dependent upon acceleration and a mass coefficient ($F_{inertial}(M, \ddot{x})$). Elastic forces are those forces through which potential energy is stored and are generally dependent upon displacement and some elastic or stiffness coefficient ($F_{elastic}(K, x)$). As discussed previously, damping forces are those forces related to the dissipation of energy, and depend upon the mechanisms through which energy is dissipated, generally dependent upon velocity and some damping coefficient ($F_{damping}(C, \dot{x})$). It should be noted that, in general, these dependencies are neither constant nor linear.

The external loading forces include all forces which are "externally" applied to the structure. These forces may themselves be thought of as being inertial, dissipative, or elastic in nature. Thus, equation (3-1) may be rewritten by redefining the inertial, damping, and elastic terms such that they also include the "external" loading forces. For example, for a system consisting of a structure moving in a fluid, equation (3-1) may be rewritten

$$F^{I}_{inertial} + F^{I}_{damping} + F^{I}_{elastic} = 0 \tag{3-2}$$

where $F^{I}_{inertial}$ represents *all* inertial forces (inertia of the structure and inertia of the surrounding fluid), $F^{I}_{damping}$ represents *all* damping or dissipative forces (energy dissipation within the structure and energy lost into the surrounding fluid), and $F^{I}_{elastic}$ represents *all* elastic forces (structural stiffness and hydrodynamic buoyancy forces).

In general, the terms associated with inertial forces, damping forces, and elastic forces may be written in any order as long as all forces are accounted for (and as long as a proper sign convention is maintained). In keeping with the classification of damping forces discussed in chapter 2, the equations of motion for a whipping ship might therefore be written in the form:

$$F_{hull} + F_{internal} + F_{external} = 0 \tag{3-3}$$

where:

$$\begin{aligned} F_{hull} &= \left\{ F_{inertial} + F_{damping} + F_{elastic} \right\}_{hull} \\ F_{internal} &= \left\{ F_{inertial} + F_{damping} + F_{elastic} \right\}_{internal} \\ F_{external} &= \left\{ F_{inertial} + F_{damping} + F_{elastic} \right\}_{external} \end{aligned} \tag{3-4}$$

where $F_{external}$ would include *all* external forces on the hull. Thus, the dynamics of a whipping ship may be thought of as a (coupled) *superposition* of the dynamics of the hull, any internal components, and the external fluid medium. Equations (3-3) and (3-4) represent *one form* of the complete, coupled, *nonlinear* equations of motion for a whipping ship.

Using this approach to the equations of motion, *each term* may be represented by an *independent* formulation (which may involve specific assumptions of linearity for *that* term), so long as the terms remain coupled via a single solution technique. As an example, the dynamic behavior of a slender ship *hull* (such as a modern submarine) might be calculated based upon a linear simple beam finite element model, while the external (hydrodynamic) forces might be calculated based upon a nonlinear three-dimensional panel method. As will be discussed subsequently, even if the hull itself can be assumed to respond linearly, the nonlinearities associated with the external (hydrodynamic) forces require the solution of the equations of motion in the time-domain. It is the existence of the coupling of the terms within the equations of motion which require the solution of the combined equation by a *single* numerical algorithm.

3.2 Formulation of the dynamic analysis procedure.

In general structural dynamics, the selection of the most appropriate method to solve the equations of motion depends upon the type of loading on the structure, the extent to which the equations of motion can be uncoupled and linearized, and the existence of rigid body motions. Nonlinearities which must be addressed include geometric nonlinearities (large rotations), material nonlinearities (nonlinear material stress-strain relations), nonlinearities associated with the external loading (hydrodynamic nonlinearities), nonlinear boundary conditions, and so on. The extent to which nonlinearities can be "linearized" depends upon the assumptions made in developing the physical model for the motions of the particular structure. For ship whipping, even if material and geometric nonlinearities can be effectively linearized (by assuming linear elastic stress-strain relations and small rotations - reasonable assumptions for the case of *elastic* whipping of a *steel* ship hull), hydrodynamic forces can be expected to be highly non-linear (as discussed in chapter 2), and thus complete linearization of the equations of motion is generally *not* possible. Additionally, for the general dynamic response of a whipping ship subjected to an underwater explosion bubble, it could be expected that there would be a significant potential for rigid body motion. For these reasons, the equations of motion must be solved directly in the time-domain (utilizing a time-stepping numerical algorithm).

Implementation of time-domain analysis procedures for the dynamic response of a structure in a fluid medium is discussed in great detail in a large number of texts and journals articles. Bathe[63], Clough and Penzien[64], and Argyris and Mlejnek[65] provide particularly thorough discussions of the solution of nonlinear equations of motion by direct time integration methods. Direct time integration means that the equations of motion would be solved using a numerical step-by-step procedure. The term "direct" *generally implies* that there is no transformation of the equations into a different form prior to numerical integration, although using the formulation of the equations of motion discussed above, it is feasible to utilize a coordinate transformation, so long as it is conducted at *each time step* (this will be discussed in greater detail later). In essence, instead of trying to satisfy equilibrium at only one distinct time t (as for static equilibrium), direct time integration aims to satisfy dynamic equilibrium at *all* discrete time intervals Δt apart. This implies that, basically, dynamic equilibrium (which includes the effects of inertia, damping

---

[63]Bathe, *op. cit.*

[64]Clough and Penzien, *op. cit.*

[65]Argyris, J., and Mlejnek, J.P., *Dynamics of Structures*, Elsevier Science Publishers, The Netherlands, 1991.

and elastic forces) is sought at discrete time points within the interval of solution. Typically, for direct time integration algorithms, the solution at the "next" required time, $t+\Delta t$, is calculated based upon the solutions at all previous times, and assuming an incremental variation in displacements, velocities, and accelerations. It is the form of the assumption on the variation of displacements, velocities, and accelerations within each time interval that determines the accuracy, stability, and required time of the solution procedure.

For direct time integration methods, the *incremental* equation of motion can be written as an extension of equation (3-2) by subtracting the equilibrium equation at time t from that at time $t+\Delta t$:

$$\left\{F_{\text{inertial}}^{t+\Delta t} - F_{\text{inertial}}^{t}\right\} + \left\{F_{\text{damping}}^{t+\Delta t} - F_{\text{damping}}^{t}\right\} + \left\{F_{\text{elastic}}^{t+\Delta t} - F_{\text{elastic}}^{t}\right\} = 0 \qquad (3\text{-}5)$$

As discussed above, inertial forces are dependent upon acceleration and a mass coefficient ($F_{\text{inertial}}(M,\ddot{x})$), damping forces are dependent upon velocity and some damping coefficient ($F_{\text{damping}}(C,\dot{x})$), and elastic forces are dependent upon displacement and some elastic or stiffness coefficient ($F_{\text{elastic}}(K,x)$). Thus, if coefficients M, C, and K can be related to acceleration, velocity and displacement (respectively), then equation (3-5) contains only three unknowns at time $t+\Delta t$ (the solution at time t would be known) and may be solved if two of the three are known as relations to the third.

The Newmark time integration method. The Newmark integration method[66], which is one of the most reliable direct time integration schemes, and whose stability condition is well known, can be employed quite appropriately for this application (see also Bathe[67], Argyris and Mlejnek[68], and Doyle[69]). In the Newmark method (often referred to as the Newmark β Method), iterative calculation is carried out at each time step and is moved to the next time step after an equilibrium condition is reached.

The basic equations of the Newmark method are derived by assuming Taylor expansions for displacements ($\mathbf{x}$) and velocities ($\dot{\mathbf{x}}$):

$$x_{t+\Delta t} = x_t + \dot{x}_t \Delta t + \ddot{x}_t \frac{\Delta t^2}{2} + \beta(\ddot{x}_{t+\Delta t} - \ddot{x}_t)\Delta t^2 \qquad (3\text{-}6)$$

$$\dot{x}_{t+\Delta t} = \dot{x}_t + \ddot{x}_t \Delta t + \gamma(\ddot{x}_{t+\Delta t} - \ddot{x}_t)\Delta t \qquad (3\text{-}7)$$

---

[66]Newmark, N.M., "A method of computation for structural dynamics," *American Society of Civil Engineers Transactions*, Vol. 127, 1962, pp. 601-630.
[67]Bathe, *op. cit.*
[68]Argyris and Mlejnek, *op. cit.*, pp. 485-488.
[69]Doyle, J.F., *Static and Dynamic Analysis of Structures*, Kluwer Academic Publishers, Boston, 1991, pp. 353-357.

where β and γ are coefficients to evaluate contributions of remainders. Thus, the displacements and velocities are approximated based upon "assumed" accelerations at each time interval (thus requiring an iterative approach), and based upon the solution at the previous time interval. Newmark showed that γ and β are not entirely arbitrary and their selection determines the stability and accuracy of the numerical solution. Newmark found that unless γ is greater than or equal to 0.5, spurious damping is introduced into the equations of motion. Additionally, unless β is greater than or equal to 0.25, there is an incorrect maximum velocity response. Further, with $\gamma = 0.5$ and $\beta = 0.25$, the scheme leads to unconditionally stable solutions.

To implement the Newmark method in the analysis of the dynamics of a structure subject to nonlinear loading forces (such as a whipping submarine), the equations of motion are first put in the form:

$$F_{resisting} = F_{loading} \tag{3-8}$$

where $F_{resisting}$ refers to all those forces associated with the *structure itself* which *resist* motion (i.e. F_{hull} as defined in section 3.1) and $F_{loading}$ refers to all (other) forces which *induce* motion (i.e. $F_{internal} + F_{external}$ as defined in section 3.1). Defining $F_{resisting}$ for a structure as:

$$F_{resisting} = M\ddot{x} + C\dot{x} + Kx \tag{3-9}$$

the equations of motion for a structure can be written in the general form:

$$M\ddot{x} + C\dot{x} + Kx = F_{loading} \tag{3-10}$$

or in *incremental* form:

$$M(\ddot{x}_{t+\Delta t} - \ddot{x}_t) + C(\dot{x}_{t+\Delta t} - \dot{x}_t) + K(x_{t+\Delta t} - x_t) = F_{loading_{t+\Delta t}} - F_{loading_t} \tag{3-11}$$

From equation (3-10), the acceleration required for dynamic equilibrium to exist at time $t+\Delta t$ can be written:

$$\ddot{x}_{t+\Delta t} = M^{-1}\left\{\left\{F_{loading}\right\}_{t+\Delta t} - \left\{C\dot{x}_{t+\Delta t} + Kx_{t+\Delta t}\right\}\right\} \tag{3-12}$$

Because $F_{loading}$ is generally also dependent upon the accelerations (and displacements and velocities by equations (3-6) and (3-7)), it is evident that an iterative procedure must be implemented at each time $t+\Delta t$ in order to obtain equilibrium by equation (3-12).

Newmark[70] proposed a general method for the solution of structural dynamics which may be summarized as follows:

1. Assume initial values of displacement, velocity, and acceleration (i.e. at each node) for time t = 0.
2. For each time step:
   (a) Assume values of acceleration for the current time step.
   (b) Compute displacement and velocity for the current acceleration (from equations (3-6) and (3-7).
   (c) For the current displacement, velocity, and acceleration, compute the loading and resisting forces in accordance with the physical model for the particular application.
   (d) Compute the acceleration required to obtain dynamic equilibrium with these loading and resisting forces (from equation (3-11)).
   (e) Compare the required acceleration with the assumed acceleration for the current time step. If these are the same (i.e. within tolerance), the calculation for this time step is complete. If these are different, repeat the calculation (i.e. perform another iteration through steps (a) - (e)) with a different value of assumed acceleration (the derived acceleration could be used as the new assumed acceleration).
3. Move onto the next time step (t+Δt), assuming the final acceleration for the last time step (t).

It should be briefly noted here that the modeling of internal damping devices such as structures or liquids requires only the addition of *N* equations of motion to the set defined above (for an internal damping device with *N* participating modes of response). Thus, in addition to the requirement for equations (3-12) to be satisfied at each time t+Δt, the following equations must also be satisfied at each time t+Δt:

$$\ddot{x}_n = -\frac{F_{internal}}{m_n} \qquad (3\text{-}13)$$

where subscript n is for each mode of the internal damping device (up to mode N). Thus, if there are *M* degrees of freedom required to represent the displacements of the hull, and *N* (modal) degrees of freedom required to represent the (modal) displacements of the internal device, then a total of *M*+*N* simultaneous equations must be satisfied using the form of equations (3-12) and (3-13).

---

[70]Newmark, *op. cit.*, pp. 606-611.

To implement the Newmark method in the analysis of the dynamics of a structure subject to loading that is *highly nonlinear* (such as a whipping submarine subject to nonlinear hydrodynamic forces), a slight modification to the above method must be made. Because of the highly nonlinear loading forces, the equations of motion must be solved at each time step using an iterative process (such as a Newton-Raphson process) which "guarantees" convergence. Without such an iterative process, the solution may not converge and equilibrium may not be (numerically) obtained.

Suzuki and Yoshida[71] discuss application of the Newmark method with solution at each time step by an iterative Newton-Raphson method. In the case of elastic ship whipping with nonlinear hydrodynamic loading, the specific formulation of the Newton iteration may proceed by using equations (3-6), (3-7) and (3-11), and expressing acceleration and velocity at time t+Δt in terms of displacement at time t+Δt

$$\ddot{x}_{t+\Delta t} = \frac{1}{\beta \Delta t^2}\left(x_{t+\Delta t} - x_t\right) - \frac{1}{\beta \Delta t}\dot{x}_t + \left(1 - \frac{1}{2\beta}\right)\ddot{x}_t \tag{3-14}$$

$$\dot{x}_{t+\Delta t} = \frac{\gamma}{\beta \Delta t}\left(x_{t+\Delta t} - x_t\right) + \left(1 - \frac{\gamma}{\beta}\right)\dot{x}_t + \left(1 - \frac{\gamma}{2\beta}\right)\ddot{x}_t \Delta t \tag{3-15}$$

In order for equilibrium to exist at time t+Δt, equations (3-11), (3-14) and (3-15) must be *simultaneously* satisfied. Residuals (which must vanish for equilibrium to exist) may be defined for equations (3-11), (3-14) and (3-15):

$$F^1_{res} = M\left[\frac{1}{\beta \Delta t^2}\left(x_{t+\Delta t} - x_t\right) - \frac{1}{\beta \Delta t}\dot{x}_t + \left(-\frac{1}{2\beta}\right)\ddot{x}_t\right] + C\left[\frac{\gamma}{\beta \Delta t}\left(x_{t+\Delta t} - x_t\right) + \left(-\frac{\gamma}{\beta}\right)\dot{x}_t + \left(1 - \frac{\gamma}{2\beta}\right)\ddot{x}_t \Delta t\right] + K\left[x_{t+\Delta t} - x_t\right] - F_{loading_{t+\Delta t}} + F_{loading_t} \tag{3-16}$$

$$F^2_{res} = \dot{x}_{t+\Delta t} - \frac{\gamma}{\beta \Delta t}\left(x_{t+\Delta t} - x_t\right) - \left(1 - \frac{\gamma}{\beta}\right)\dot{x}_t - \left(1 - \frac{\gamma}{2\beta}\right)\ddot{x}_t \Delta t \tag{3-17}$$

$$F^3_{res} = \ddot{x}_{t+\Delta t} - \frac{1}{\beta \Delta t^2}\left(x_{t+\Delta t} - x_t\right) + \frac{1}{\beta \Delta t}\dot{x}_t - \left(1 - \frac{1}{2\beta}\right)\ddot{x}_t \tag{3-18}$$

The Newton iteration is carried out such that the unsatisfied equilibrium at iteration *j* is to be satisfied at iteration *j+1*. In other words, all residuals at iteration *j+1* must *simultaneously vanish*. To obtain expressions for residuals at iteration step *j+1*, the

---

[71]Suzuki, H., and Yoshida, K., "Three dimensional nonlinear dynamic analysis method of underwater line structure and its validation", *Proceedings of the 10th International Conference on Offshore Mechanics and Arctic Engineering (OMAE)*, ASME, 1991, pp. 87-94.

residuals at iteration step j may be expanded in linearized Taylor expansion (in matrix form):

$$\begin{bmatrix} F_{res}^1 \\ F_{res}^2 \\ F_{res}^3 \end{bmatrix}_{j+1} \approx \begin{bmatrix} F_{res}^1 \\ F_{res}^2 \\ F_{res}^3 \end{bmatrix}_j + \frac{\partial\left[F_{res}^1, F_{res}^2, F_{res}^3\right]_j}{\partial[x, \dot{x}, \ddot{x}]} \begin{bmatrix} \delta x \\ \delta \dot{x} \\ \delta \ddot{x} \end{bmatrix}$$

$$= \begin{bmatrix} F_{res}^1 \\ F_{res}^2 \\ F_{res}^3 \end{bmatrix}_j + \begin{bmatrix} \left[\frac{1}{\beta\Delta t^2} M + \frac{\gamma}{\beta\Delta t} C + K - \frac{\partial F_{loading}}{\partial x}\right] & \left[-\frac{\partial F_{loading}}{\partial \dot{x}}\right] & \left[-\frac{\partial F_{loading}}{\partial \ddot{x}}\right] \\ \left[-\frac{\gamma}{\beta\Delta t}\right] & [I] & [0] \\ \left[-\frac{1}{\beta\Delta t^2}\right] & [0] & [I] \end{bmatrix}_j \begin{bmatrix} \delta x \\ \delta \dot{x} \\ \delta \ddot{x} \end{bmatrix}$$

(3-19)

where $\delta x = (x_{t+\Delta t_{j+1}} - x_{t+\Delta t_j})$, $\delta \dot{x} = (\dot{x}_{t+\Delta t_{j+1}} - \dot{x}_{t+\Delta t_j})$ and $\delta \ddot{x} = (\ddot{x}_{t+\Delta t_{j+1}} - \ddot{x}_{t+\Delta t_j})$ are displacement, velocity, and acceleration corrections to be made for the $j+1$th iteration at time step $t+\Delta t$. An expression for the displacement correction (δx) may be obtained by substituting the last two equations in (3-19) into the first, giving:

$$\left[\frac{1}{\beta\Delta t} M + \frac{\gamma}{\beta\Delta t} C + K - \frac{1}{\beta\Delta t^2}\left[\frac{\partial F_{loading}}{\partial \ddot{x}}\right] - \frac{\gamma}{\beta\Delta t}\left[\frac{\partial F_{loading}}{\partial \dot{x}}\right] - \left[\frac{\partial F_{loading}}{\partial x}\right]\right]\delta x + F_{res}^1 + \left[\frac{\partial F_{loading}}{\partial \dot{x}}\right] F_{res}^2 + \left[\frac{\partial F_{loading}}{\partial \dot{x}}\right] F_{res}^3 = 0$$

(3-20)

Solving equation (3-20) for δx and substituting this term back into equation (3-19) gives expressions for improved displacement, velocity and acceleration (i.e. displacement, velocity and acceleration for iteration step $j+1$ based upon iteration step j)

$$x_{t+\Delta t}^{j+1} = x_{t+\Delta t}^{j} + \delta x$$

$$\dot{x}_{t+\Delta t}^{j+1} = \dot{x}_{t+\Delta t}^{j} + \frac{\gamma}{\beta\Delta t}\delta x - F_{res}^2$$

$$\ddot{x}_{t+\Delta t}^{j+1} = \ddot{x}_{t+\Delta t}^{j} + \frac{1}{\beta\Delta t^2}\delta x - F_{res}^3 \qquad (3\text{-}21)$$

The Jacobian matrices, $\left[\frac{\partial F_{loading}}{\partial\{x, \dot{x}, \ddot{x}\}}\right]$, may be approximated at each iteration step by numerically differentiating the loading vector.

With these modifications, the calculation of dynamic equilibrium using the Newmark method for the case of highly nonlinear loading could proceed as follows:

1. Assume initial values of displacement, velocity and acceleration (i.e. vectors of nodal values).
2. For each time step:
   (a) Assume initial values of displacement, velocity, and acceleration equal to those of the last time step.
   (b) Calculate the loading forces for the current displacement, velocity, and acceleration using the chosen physical model.
   (c) Calculate the Jacobian matrices (numerically) for the current loading forces.
   (d) Calculate the residuals using equations (3-16) through (3-18).
   (e) Solve for the displacement correction (δx) using equation (3-20).
   (f) Calculate improved values of displacement, velocity, and acceleration using equations (3-21).
   (g) Reiterate through steps (b) through (g) until the residuals are within a specified tolerance (i.e. a vector norm tolerance).
3. Move onto the next time step, assuming the final displacements, velocities, and accelerations of the previous time step.

3.3 Definition of dynamic forces.

3.3.1 Hull structure forces.

As discussed in section 3.1, the forces associated with the dynamics of the hull structure may be represented by an *independent* formulation from that used to represent the internal and external forces. This formulation may involve specific assumptions of linearity which may be applied only to the dynamics of the hull structure.

3.3.1.1 Finite element beam model.

In representing the whipping response of most conventional ships to low frequency bubble pulse loading, it has been found that a simple beam model of the hull structure has provided good results[72]. This idealization is supported by recognizing that most conventional ships (particularly submarines) have length/beam ratios greater than eight. Thus, the low frequency vibrational modes occur as beam-like flexural motions, which are represented well by simple beam theory. It should be noted, however, that nonlinear hull response (i.e. where the assumptions of linear elastic stress-strain relations and small rotations *cannot* be made), makes the utility of the simple beam theory limited. For nonlinear hull response, a fully nonlinear, three-dimensional finite element technique would be more appropriate. Therefore, for this analysis procedure, the assumptions of linear elastic stress-strain relations and small rotations will be made in order to justify the use of the simple beam model.

Because sectional properties vary gradually along the length of the hull, a *finite element* beam model could be used to represent the structural properties of the submarine (figure 3-1). The model consists of a specified number of beam elements (equal to the number of hull *stations* specified on the ship's drawings). Most ships have 19 stations specified, and thus would be modeled with 19 beam elements. A three-dimensional beam model will be used because of the directionality of the loading of the underwater explosion, as well as the lack of complete axial symmetry of submarines (i.e. properties differ in each plane of symmetry).

Most methods for structural finite element analysis develop matrices to represent the stiffness and mass properties of each finite *element*, and then combine element matrices into *global* or *structure* matrices. Modeling of beams using a finite element technique, and assignment of the properties of each finite element is discussed in numerous sources

---

[72]Hicks, *op. cit.*, p. 395.

(Smith[73], Bathe[74], Doyle[75], Hughes[76], for example). An appropriate finite element analysis procedure which could be used to approximate the hull forces associated with submarine hull whipping could be outlined as follows:

1. Define the model (coordinate system, nodes, element types, etc.).
2. Determine each *element*'s stiffness and mass matrices ($\mathbf{k}^e, \mathbf{m}^e$) and transform them to *hull* (or global) coordinates.
3. Assemble the *hull* or *global* stiffness and mass matrices ($\mathbf{K}, \mathbf{M}$) by superposition of the element matrices.
4. Approximate a reasonable *hull* damping matrix ($\mathbf{C}$) by applying appropriate Rayleigh coefficients, as discussed in sections 2.2.3 and 3.3.1.2 ($\mathbf{C} = \alpha\mathbf{M} + \beta\mathbf{K}$).
5. Combine the hull mass, damping, and stiffness matrices to obtain the total hull force as described in section 3.1 ($\mathbf{F}_{hull} = \mathbf{M}\ddot{\mathbf{x}} + \mathbf{C}\dot{\mathbf{x}} + \mathbf{K}\mathbf{x}$).

This procedure will be incorporated into an overall computational algorithm and used for analyses in the next chapter.

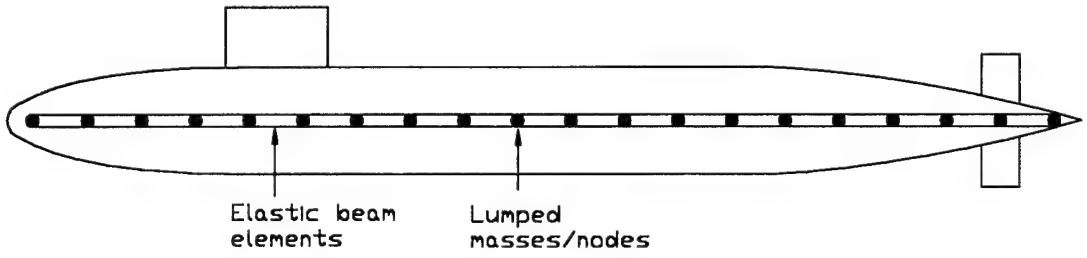

Figure 3-1. Structural model for submarine hull whipping.

Figure 3-2 illustrates a two-dimensional, two-node beam element with vertical translation and rotation as the nodal displacements. It should be noted that because a submarine should be classified as a relatively thick beam (i.e. the cross-sectional dimensions are *not* small compared to the length), the effects of rotary inertia and shear deformation at each element should be accounted for in the finite element model.

---

[73]Smith, *op. cit.*
[74]Bathe, *op. cit.*
[75]Doyle, *op. cit.*
[76]Hughes, O.F., *Ship Structural Design*, SNAME, Jersey City, NJ, 1988.

To be rigorous, a three-dimensional beam element could be used which also considers additional nodal displacements in the horizontal plane as well as torsion and axial displacements (a total of 6 degrees of freedom at each node). Figure 3-3 illustrates a general three-dimensional, two-node beam finite element with 6 degrees of freedom at each node. It should be noted that axial displacements can generally be ignored for submarine whipping due to the lack of axial loading provided by the surrounding fluid. Additionally, torsional displacements may also be ignored, although it could be argued that torsional loading could become important under some conditions in accounting for potential asymmetry associated with the underwater explosion bubble loading on external hull appendages such as the sail and planes. Therefore, axial and torsional degrees of freedom will be omitted for this analysis, although the entire 3-dimensional beam element will be used for illustration in the following discussion.

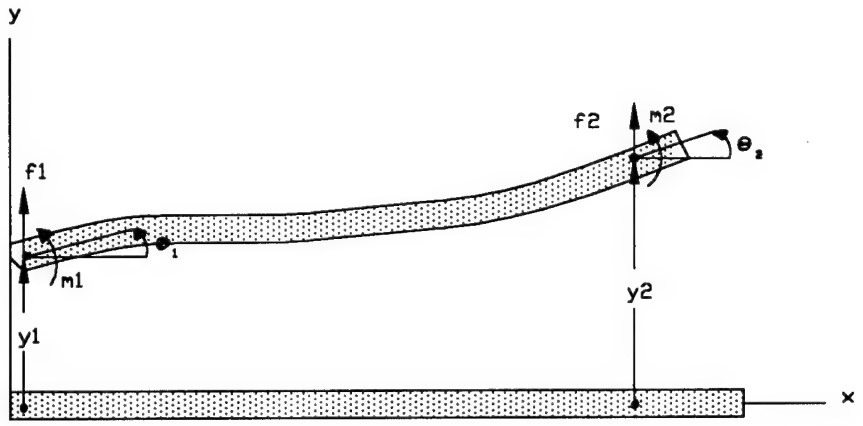

Figure 3-2. Two-dimensional, two-node beam finite element.

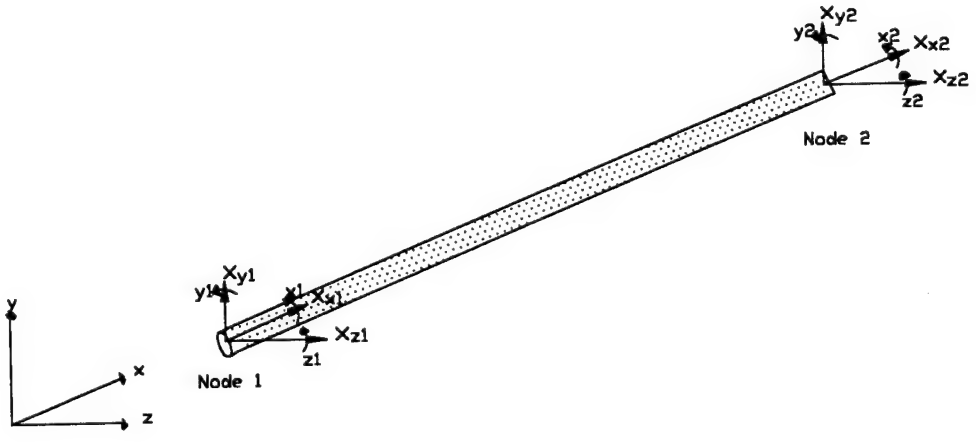

Figure 3-3. General three-dimensional, two-node beam finite element.

In order to simplify the assembly of the *global* equations of motion for the hull, the equations of motion for *each* beam finite element may be written in the partitioned form:

$$\begin{bmatrix} M_{11} & M_{12} \\ M_{21} & M_{22} \end{bmatrix} \begin{Bmatrix} \ddot{x}_1 \\ \ddot{x}_2 \end{Bmatrix} + \begin{bmatrix} C_{11} & C_{12} \\ C_{21} & C_{22} \end{bmatrix} \begin{Bmatrix} \dot{x}_1 \\ \dot{x}_2 \end{Bmatrix} + \begin{bmatrix} K_{11} & K_{12} \\ K_{21} & K_{22} \end{bmatrix} \begin{Bmatrix} x_1 \\ x_2 \end{Bmatrix} = \begin{Bmatrix} f_1 \\ f_2 \end{Bmatrix} \qquad (3\text{-}22)$$

where subscripts 1 and 2 refer to nodes 1 and 2 of the element, and each partition is a 6x6 submatrix or 6 element subvector. For the general three-dimensional beam element, the subvectors for nodal displacement and nodal force would be written in the form:

$$\{x_i\} = \begin{Bmatrix} x_{xi} \\ x_{yi} \\ x_{zi} \\ \theta_{xi} \\ \theta_{yi} \\ \theta_{zi} \end{Bmatrix} ; \quad \{f_i\} = \begin{Bmatrix} f_{xi} \\ f_{yi} \\ f_{zi} \\ m_{xi} \\ m_{yi} \\ m_{zi} \end{Bmatrix} \qquad (3\text{-}23)$$

where subscript *i* refers to the node (1 or 2), x is nodal translation, θ is nodal rotation, f is the (external) force acting on the node, and m is the (external) moment acting on the node. It will be shown subsequently that formulation of submatrices for mass and stiffness can be readily accomplished. However, the definition of element damping matrices as in equation (3-22) is generally not possible, thus a formulation of *global* hull damping will be given in the next section which will approximate the overall energy dissipation within the hull structure.

The stiffness matrix. The derivation of stiffness properties for a finite element is a lengthy process and will not be discussed in detail here. Barltrop and Adams[77] and Hughes[78] provide formulation for the element stiffness matrix of a general three-dimensional, two-noded beam finite element. The element stiffness matrix can be written in a node-oriented partitioned form consistent with equations (3-22) and (3-23). Each partitioned submatrix (6x6) has terms *i,j* which represent the element elastic force in the direction of freedom *i* when a unit displacement is applied to freedom *j* with all other freedoms held at zero displacement. The stiffness submatrices consistent with equation (3-22) can be defined as shown in figure 3-4.

The mass matrix. The simplest method of assigning mass properties of the ship/beam model is to assume that the mass of each *section* is lumped or concentrated at

---

[77]Barltrop, N.D.P., and Adams, A.J., *Dynamics of Fixed Marine Structures*, Butterworth-Heinemann, UK, 1991, Appendix D.

[78]Hughes, *op. cit.*, pp. 212-217.

the nodal points (figure 3-1). This is called the *lumped mass* formulation. In this way, the lumped masses fill the diagonal terms of the element mass matrix (corresponding to the individual nodal degrees of freedom), while the off-diagonal terms are *all* zero. The matrix (or submatrix) elements would therefore equal the *mass* of the node for elements corresponding to translational degrees of freedom, or the *mass moment of inertia* of the node for those elements corresponding to rotational degrees of freedom. The translation of a lumped mass accounts for translational inertia effects, while the rotation of the lumped mass accounts for rotary inertia effects.

The lumped mass formulation has some very appealing properties. Firstly, it is easy to associate a physical model with the matrix (each degree of freedom at each node having its own mass). Secondly, the entire structure mass matrix is diagonal, leading to significantly fewer computations and storage requirements. The finite element mass submatrices as defined in equation (3-22), for a lumped mass beam finite element, could be written as shown in figure 3-5.

$$K_{11} = \begin{bmatrix} a & 0 & 0 & 0 & 0 & 0 \\ 0 & 12b_z & 0 & 0 & 0 & 6b_zL \\ 0 & 0 & 12b_y & 0 & -6b_yL & 0 \\ 0 & 0 & 0 & t & 0 & 0 \\ 0 & 0 & -6b_yL & 0 & (4+\phi_z)b_yL^2 & 0 \\ 0 & 6b_zL & 0 & 0 & 0 & (4+\phi_y)b_zL^2 \end{bmatrix}$$

$$K_{21} = \begin{bmatrix} -a & 0 & 0 & 0 & 0 & 0 \\ 0 & -12b_z & 0 & 0 & 0 & -6b_zL \\ 0 & 0 & -12b_y & 0 & 6b_yL & 0 \\ 0 & 0 & 0 & -t & 0 & 0 \\ 0 & 0 & -6b_yL & 0 & (2-\phi_z)b_yL^2 & 0 \\ 0 & 6b_zL & 0 & 0 & 0 & (2-\phi_y)b_zL^2 \end{bmatrix} = K_{12}^T$$

$$K_{22} = \begin{bmatrix} a & 0 & 0 & 0 & 0 & 0 \\ 0 & 12b_z & 0 & 0 & 0 & -6b_zL \\ 0 & 0 & 12b_y & 0 & 6b_yL & 0 \\ 0 & 0 & 0 & t & 0 & 0 \\ 0 & 0 & 6b_yL & 0 & (4+\phi_z)b_yL^2 & 0 \\ 0 & -6b_zL & 0 & 0 & 0 & (4+\phi_y)b_zL^2 \end{bmatrix}$$

$$a = \frac{AE}{L} \quad \phi_y = \frac{12EI_z}{GA_{sy}L^2} \quad \phi_z = \frac{12EI_y}{GA_{sz}L^2} \quad b_z = \frac{EI_z}{(1+\phi_y)L^3} \quad b_y = \frac{EI_y}{(1+\phi_z)L^3}$$

$$t = \frac{GJ}{L}$$

A is the cross-sectional area of the element, E is Young's Modulus, L is the length of the element, I_z, I_y are the 2nd moments of area of the element cross-section about the z and y axes, G is the shear modulus, J is the polar moment of inertia of the element cross-section (about the x axis), and A_{sy}, A_{sz} are the portions of the cross-sectional area over which the y and z-directed shear forces are assumed to act.

Figure 3-4. Partitioned submatrices for stiffness of a general 3-D beam finite element.

$$M_{11} = \begin{bmatrix} m_1 & 0 & 0 & 0 & 0 & 0 \\ 0 & m_1 & 0 & 0 & 0 & 0 \\ 0 & 0 & m_1 & 0 & 0 & 0 \\ 0 & 0 & 0 & I_{x1} & 0 & 0 \\ 0 & 0 & 0 & 0 & I_{y1} & 0 \\ 0 & 0 & 0 & 0 & 0 & I_{z1} \end{bmatrix} \qquad M_{22} = \begin{bmatrix} m_2 & 0 & 0 & 0 & 0 & 0 \\ 0 & m_2 & 0 & 0 & 0 & 0 \\ 0 & 0 & m_2 & 0 & 0 & 0 \\ 0 & 0 & 0 & I_{x2} & 0 & 0 \\ 0 & 0 & 0 & 0 & I_{y2} & 0 \\ 0 & 0 & 0 & 0 & 0 & I_{z2} \end{bmatrix}$$

$M_{12} = M_{21} = [0]$ (no off-diagonal terms for the lumped mass formulation)

m_i is the mass associated with node i

I_{xi}, I_{yi}, I_{zi} are the mass moments of inertia of node i about axes x,y,z.

Figure 3-5. Partitioned submatrices for mass of a general 3-D beam finite element.

It is also possible to take advantage of the finite element formulation to develop what is called a *consistent mass* formulation for a beam element. In contrast to the lumped mass matrix, the components of the consistent mass matrix cannot be associated with a physical model. More importantly, after assemblage, the global mass matrix will not be diagonal, but will include both diagonal and off-diagonal terms. For this reason, the consistent mass matrix formulation requires considerably more computational effort than the lumped mass formulation. While the consistent mass matrix formulation is generally superior in terms of minimizing errors in calculation of natural frequencies[79], the errors associated with the lumped mass formulation significantly decrease as the number of nodes used to model the beam increases. Additionally, when external loads are being applied directly to the nodes (as will be discussed subsequently), the equations of motion behave better when the inertial forces are likewise lumped at the nodes. For these reasons, the lumped mass matrix formulation will be used in this submarine whipping model.

3.3.1.2 Hull damping model.

Rayleigh damping. As mentioned previously, an approximation for the *global* damping matrix (**C**) associated with the *hull structure* can be made by applying appropriate Rayleigh coefficients to the *global* mass and stiffness matrices derived by superposition of the element mass and stiffness matrices:

[79]Doyle. *op. cit.*, p. 272.

$$\mathbf{C} = \alpha\mathbf{M} + \beta\mathbf{K} \tag{3-24}$$

where **M** and **K** are the *global* mass and stiffness matrices, and coefficients α and β are the two damping proportionality constants. As discussed in section 2.2.3, coefficients α and β can be calculated if two modal damping ratios (ζ_a and ζ_b) associated with two specific modal frequencies (ω_a and ω_b) are known:

$$\begin{Bmatrix}\alpha\\ \beta\end{Bmatrix} = 2\frac{\omega_a\omega_b}{\omega_b^2 - \omega_a^2}\begin{bmatrix}\omega_b & -\omega_a\\ -1/\omega_b & 1/\omega_a\end{bmatrix}\begin{Bmatrix}\zeta_a\\ \zeta_b\end{Bmatrix} \tag{3-25}$$

The downside to the Rayleigh (or proportional) damping matrix formulation is that the contribution of the higher frequency modes of hull flexural response (modal frequencies much greater than ω_b) are effectively eliminated by the high damping imposed by the selection of the particular coefficients (see figure 2-4). In the case of elastic ship whipping, where only the lower few modes of flexural response are generally required to adequately describe the motion of the structure, this limitation can be considered acceptable as long as the higher frequency used for evaluation of the Rayleigh coefficients (ω_b) is set among the higher modes expected to contribute significantly to the whipping response. Thus, the problem becomes one of calculating the modal (natural) frequencies for the lowest modes of hull whipping, applying experimentally determined (or reasonably approximated) modal damping ratios for two of the modes, and calculating the appropriate Rayleigh coefficients using equation (3-25). As discussed in section 2.2.3, the modal (natural) frequencies of a submarine structure can be calculated by solving the generalized eigenproblem for the undamped free vibration of the dynamic system:

$$\mathrm{K}\phi_n = \omega_n^2\mathrm{M}\phi_n \tag{3-26}$$

where ω_n is the natural frequency of vibration of the *n*th mode and ϕ_n is the mode shape vector of the *n*th mode. Data for experimentally determined (hull) modal damping ratios for the fundamental modes of submarine vibrations is lacking in the literature. However, some work has been done in the marine industry to estimate hysteretic and structural modal damping ratios for steel pile platforms for fundamental-mode flexural vibrations in random seas[80], implying that hysteretic damping in thin steel cylindrical structures is typically less than 1% of critical (i.e. $\zeta \le 0.01$) for the fundamental flexural mode. There is also some older data available in the literature for modal damping ratios of steel circular cylinder ship masts based upon modal "bump" testing[81], suggesting that general steel

---

[80]Cook, M.F., and Vandiver, J.K., "Measured and Predicted Dynamic Response of a Single Pile Platform to Random Wave Excitation", *Proceedings of the 14th Offshore Technology Conference, OTC 4285*, 1982, pp. 637-645.

[81]Smith, *op. cit.*

cylinders have (material and structural) modal damping ratios on the order of 2-3 % of critical for the lower flexural modes, although this data seems less reliable because of other unknown damping effects on the mast not considered (air and structural connection to the ship hull). Although submarines are not precisely the same as thin steel pile structures or ship masts, the general hysteretic damping mechanisms are basically the same and thus it would seem reasonable to extend this to data for a similar cylindrical steel structures to a steel submarine. Thus, it would be reasonable to assume (as a first approximation) modal damping ratios (for the *hull*) on the order of 1% for the fundamental flexural modes of a steel submarine.

Thus, once the modal (natural) frequencies of the hull structure have been calculated by equations (3-26), reasonable Rayleigh coefficients could be calculated by equations (3-25) assuming modal damping ratios on the order of 0.01. Finally, the hull damping matrix to be applied in the finite element calculations can be calculated using the global mass and stiffness matrices and equation (3-24).

This process will be incorporated into the computational algorithm and used in analyses in the next chapter.

An alternative approach. "Dry mode" modal superposition. An alternative to developing an explicit damping matrix (**C**) using Rayleigh damping and solving the complete equations of motion, is to use the approximated hull modal damping ratios directly and a modal superposition approach. As discussed in section 3.1, each vector term of the equations of motion may be represented by an *independent* formulation (which may involve specific assumptions of linearity for that term), so long as all the terms remain coupled via a single numerical solution algorithm. Although forces associated with external (fluid) loading may be nonlinear, and the equations of motion must therefore be solved in the time domain, it is still possible to solve for the forces associated with the hull structure using a modal superposition technique. This type of approach has been referred to as "dry mode" modal superposition[82]. In a "dry mode" modal superposition approach, all forces *not* associated with the hull are simply termed "loading" forces and thus carried on the right hand side of the equations of motion.

$$\left\{M\ddot{x} + C\dot{x} + Kx\right\}_{hull} = F_{loading} \qquad (3\text{-}27)$$

Thus, a coordinate transformation (of the generalized coordinates of the ship *hull*) may be conducted, so long as the transformation of the *loading vector* (i.e. $F_{internal}$ and $F_{external}$ as discussed previously) is conducted at *each time interval*.

---

[82]Bishop, R.E.D., and Price, W.G., *Hydroelasticity of Ships*, Cambridge University Press, Cambridge, UK, 1979.

This formulation is consistent with the formulation of the Newmark time integration method presented in section 3.2 (i.e. equation (3-10)). Because the forces associated with the hull are to be modeled using assumptions of linearity (as discussed in the previous section), these forces may be redefined using the principles of modal superpostion outlined in section 2.2.3. The "dry" mode shapes are first found by solving the generalized eigenproblem for the undamped free vibration of the hull structure using equation (3-26). The modal equations of motion (equations (2-12)) are then written from equations (3-27) by applying the modal transformation, equations (2-10) and (2-13). The transformation of the modal force (i.e. Q_n in equations (2-13)) must be performed *at each iteration at each time step* of the direct time integration procedure, since the loading forces ($F_{loading}$) are generally nonlinear and coupled to the generalized displacements, velocities, and accelerations (i.e. are functions of $\mathbf{x}, \dot{\mathbf{x}}, \ddot{\mathbf{x}}$).

While this approach has some appealing qualities in terms of representation of the response of a whipping ship in terms of its fundamental flexural mode shapes, it affords little (if any) computational advantage over rigorous computation using the generalized coordinates in that two transformations must still be made *at each iteration step of each time step*. Thus, the fundamental benefit of modal decomposition is lost due to the requirement of maintaining the complex (i.e. nonlinear) external loading forces in terms of the generalized coordinate system. For this reason, this approach will not be pursued in this analysis and all computation will be carried out in terms of generalized coordinates.

3.3.2 Internal forces.

In order to analyze the potential contribution of discrete internal structures and sloshing liquids on the whipping response of a ship, it is necessary to assume some "reasonable" properties of the internal structure and liquid storage tanks as might be found on a "real" ship. Appropriate models to account for the dynamics of the internal structure and sloshing liquid could be made using simplified geometries and the general models discussed in chapter 2.

3.3.2.1 Model for discrete masses.

The most straight-forward method of quantitatively determining *potential* dynamic effects of internal structures on the whipping response of a ship is to model the internal structure with only a few degrees of freedom (i.e. modes of response), and select properties of the structure (i.e. mass, stiffness, damping) which are realistic and will make the internal structure respond near resonance (response modes *not* near resonance would

contribute little to the overall response). This amounts to finding a maximum effect provided by an internal structure if it were "tuned" to the resonant whipping frequency (or the exciting bubble pulse frequency). By using this approach, a quantitative measure of the damping effects of internal structures could be obtained for various combinations of mass sizes and locations. While mass sizes should represent reasonable ship internal structures, the locations of the masses may influence any of the low frequency flexural modes of the *hull*, and thus a range of potential effects can be predicted. Figure 3-6 illustrates a notional internal structure connected to the hull through some combination of foundation and mounts with known mechanical properties.

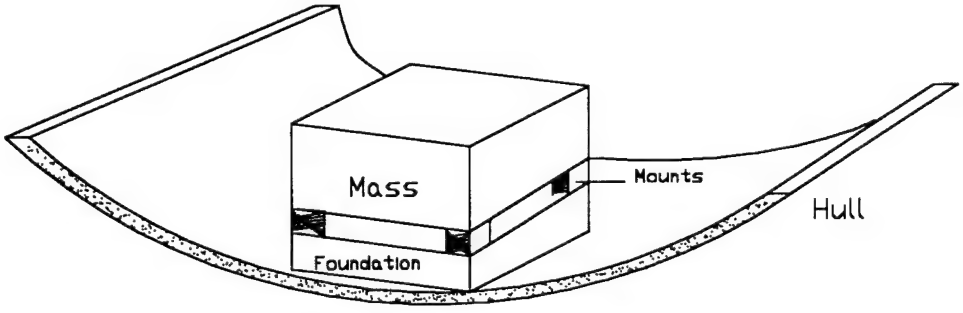

Figure 3-6. Notional internal structure connected to the hull.

The dynamic vibration absorber. For this analysis, a dynamic vibration absorber will be used to model a discrete internal structure. The absorber is considered as a single discrete mass, as discussed in section 2.3.1, and connected to the ship hull at one of the "nodes" defined in section 3.3.1. Ideally, it would be desirable to permit the absorber to respond in all six degrees of freedom (three translational and three rotational). However, in order to reasonably limit the computational and modeling effort, the absorber will be limited to respond only in the vertical or horizontal directions, as shown in figure 3-7. This limitation simplifies the computational algorithm, without unduly restricting the value of the model. The absorber model can be thought of as being representative of a resonant mode of any discrete internal structure.

Using the approach developed in section 2.3.1 for a two degree of freedom dynamic absorber, the equations of motion for the ship hull, as modified for the forces exerted on the hull by the absorber may be written in matrix form:

$$\left[M\ddot{X} + C\dot{X} + KX\right]_{hull} = F_{external} + F_{absorber} \qquad (3\text{-}28)$$

where terms on the left hand side are defined by the finite element model for the ship hull as described in section 3.3.1. Displacements and forces are vectors positioned at the hull nodes, and hull mass, damping, and stiffness are matrices, constructed for the finite element formulation. The vector of forces exerted on the hull structure (i.e. at the nodes) by the absorber ($F_{absorber}$) is written (ignoring damping associated with the absorber):

$$F_{absorber} = \{k(x - X)\} = \{-m\ddot{x}\} \tag{3-29}$$

where X (capital) refers to the *hull* displacement at the node where the absorber acts, and x (small case) is the *absorber* displacement in the direction corresponding to X, as shown in figure 3-7. Thus, for a finite element representation of a ship hull with N degrees of freedom (i.e. N equations), one additional degree of freedom (i.e. one equation) is required for each absorber used.

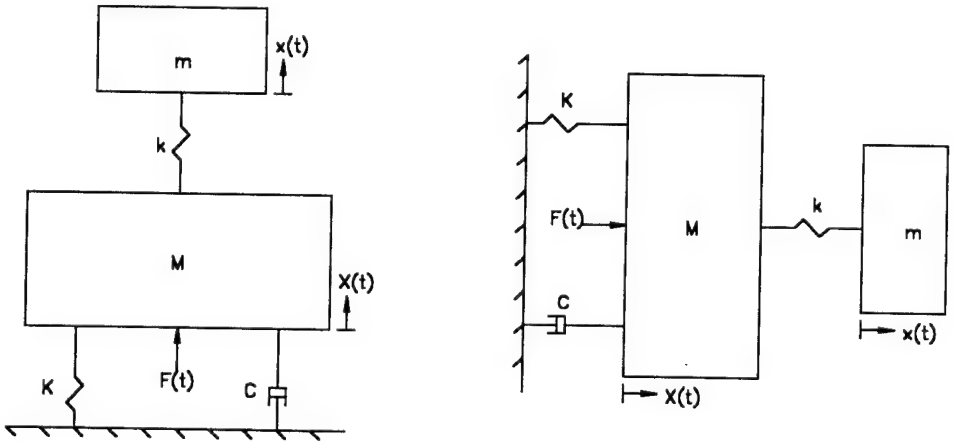

Figure 3-7. Dynamic vibration absorber free to respond in vertical or horizontal directions.

Suppression of dynamic response of the whipping hull. As was discussed in section 2.3.1, the amplitude of motion of a structure could be decreased if the properties of a dynamic vibration absorber were "tuned" to match the resonant response frequency of the main structure. If it is desired to consider decrease in amplitude of one of the flexural modes of hull whipping by application of a dynamic vibration absorber (the lowest flexural mode for example), then the *hull* portion of the two degree of freedom system depicted in figure 3-7 could be represented by the *modal* mass, damping and stiffness for *that whipping mode* (defined by equations (2-13)).

In order to quantify the *potential dynamic effects* of internal structures on the low frequency flexural (whipping) modes of a submarine hull, the following process could be implemented to develop the equations of motion for the forces exerted by the absorber mass (internal structure) on the hull:

1. Calculate the mode shapes and natural flexural frequencies of hull whipping (Ω_n) by solving the finite element eigenproblem as discussed in section 3.3.1. These represent the *dry mode shapes* and natural frequencies of hull whipping. For a submerged submarine, the mass matrix (M) should be modified by adding approximate fluid added mass (M_a) prior to calculating the (modal) natural frequencies since the added mass could have a significant effect on the natural frequencies.
2. Calculate the *modal* mass, damping, and stiffness for the hull whipping mode of interest as discussed in section 2.2.2 (equations (2-13)).
3. Select a "reasonable" absorber mass or mass of an internal structure (m) (this could be done for a range of masses).
4. Calculate the "optimum" absorber stiffness (k), which will "tune" the absorber to the resonant frequency of the hull (or the exciting bubble pulse frequency): $k = m \cdot \Omega_n^2$
5. Solve for the dynamic response of the structure with the internal absorber under specified loading or initial conditions using equations (3-28) and (3-29).

This process will be incorporated into the computational algorithm and used in analyses in the next chapter.

3.3.2.2 Model of liquid sloshing in a rectangular tank.

Similarly to the case of internal structure, a quantitative measure of the potential damping effects provided by internal sloshing liquids may be made by considering the forces exerted on the whipping hull by the modal equivalent mechanical system for the complex internal sloshing liquid. In effect, only those sloshing modes likely to be excited by the whipping of the hull need be considered in the mechanical equivalent system. The sloshing modes not excited may be considered as rigid masses, and thus may be considered as part of the main hull mass.

Using the relations developed in section 2.3.2, the equations of motion for the ship hull, as modified for the forces exerted on the hull by a sloshing liquid may be written in matrix form:

$$\left[M\ddot{X} + C\dot{X} + KX\right]_{hull} = F_{external} + F_{liquid} \tag{3-30}$$

where terms on the left hand side are defined by the finite element model for the hull as described in section 3.3.1. Displacements and forces are vectors positioned at the hull nodes, and hull mass, damping, and stiffness are matrices, constructed for the finite element formulation. The vector of forces exerted on the hull structure (i.e. at the nodes) by the sloshing liquid (F_{liquid}) can be written (ignoring damping in the tank):

$$F_{liquid} = -\sum_{n=0}^{\infty} m_n \ddot{x}_n = -m_0 \ddot{X} + \sum_{n=1}^{\infty} \left[k_n (x_n - X)\right] \tag{3-31}$$

where small case letters refer to the mechanical equivalent dynamic parameters for the liquid, and subscript *n* refers to the mode of sloshing. Additionally, the portion of the liquid which acts as a rigid body (m_0) may be found from equation (2-46):

$$m_0 = M_l - \sum_{n=1}^{\infty} m_n \tag{3-32}$$

where M_l is the total mass of liquid in the tank.

These relations may be simplified if it is assumed that only the fundamental sloshing mode (n = 1) is excited near its resonance (the higher sloshing modes therefore may be considered to act as part of the rigid body mode, m_0). Equation (3-31) and (3-32) may be rewritten and combined:

$$F_{liquid} = -\sum_{n=0}^{1} m_n \ddot{x}_n = -(M_l \ddot{X} - m_l \ddot{X} + m_l \ddot{x}_l) = (m_l - M_l)\ddot{X} + \left[k_l (x_l - X)\right] \tag{3-33}$$

Thus, for a finite element representation of a ship hull with N degrees of freedom (i.e. N equations), one additional degree of freedom (i.e. one equation) is added for each sloshing mode of interest and equations (3-30) and (3-33) form a set of N+1 simultaneous equations.

Lateral sloshing in a rectangular tank. Figure 3-8 illustrates a rectangular tank, containing a liquid with a free surface, which is oscillating laterally. The potential flow solution for the lateral sloshing natural frequencies and hydrodynamic forces are given by Vandiver and Mitome[83] for the case where horizontal displacement of the tank is assumed to be harmonic and of the form:

$$X(t) = Ae^{i\omega t} \tag{3-34}$$

[83]Vandiver and Mitome, *op. cit.*, pp. 26-28.

where A is the amplitude of the harmonic motion of the tank wall. The natural frequencies are given for mode n:

$$\omega_n^2 = g(2n-1)\frac{\pi}{a}\tanh\left(\frac{2n-1}{a}\pi h\right) \tag{3-35}$$

where g is the acceleration due to gravity, a is the width of the rectangular tank, and h is the mean depth of liquid in the tank. The modal masses are given for each mode n:

$$m_n = M_l\left[\frac{8\tanh\left\{(2n-1)\pi\frac{h}{a}\right\}}{\pi^3\frac{h}{a}(2n-1)^3}\right] \tag{3-36}$$

As discussed in section 2.3.2, the modal stiffnesses can be computed from the modal mass and natural frequency by the expression:

$$k_n = \omega_n^2 m_n \tag{3-37}$$

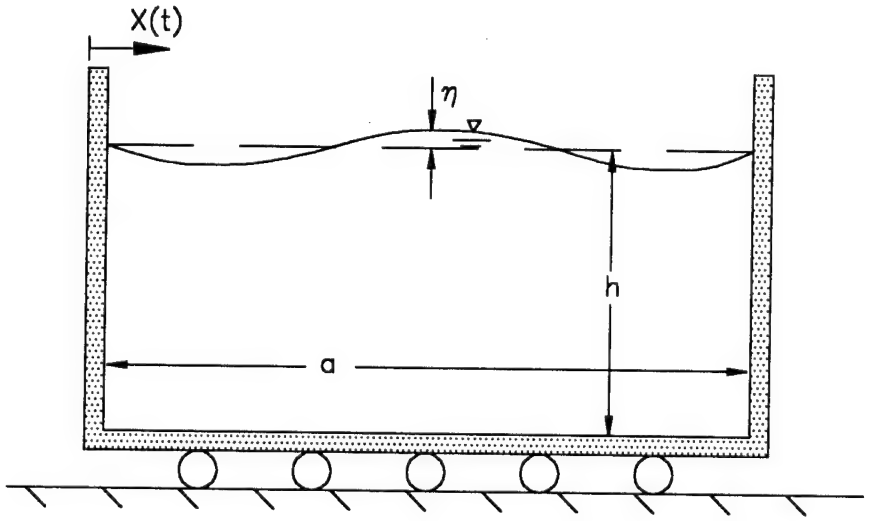

Figure 3-8. Laterally oscillating rectangular tank with standing waves.

Suppression of dynamic response of the whipping hull. Similarly to the application of the dynamic vibration absorber, the motion of the whipping hull could be analyzed by considering any onboard tanks as "liquid slosh" dampers. The main differences between sloshing liquids and dynamic vibration absorbers discussed in the previous section come about because of the numerous sloshing modes which are *not*

excited by the whipping (i.e. the portion of the liquid in the tank which responds as a rigid body with the hull, m_0). Each sloshing mode which responds may be thought of as an individual vibration absorber, but the sloshing modes which do not respond might simply be added to the mass of the hull structure.

Thus, a quantitative feel for the effects of sloshing liquids might be obtained by considering the effects of internal structures or absorbers, but also considering the portion of the liquids which are not excited, but respond as rigid masses. A more thorough discussion of this will be presented in the next chapter.

3.3.3 External (fluid) forces.

3.3.3.1 Representation of the hull surface.

As discussed in section 2.3.1, slender bodies are often represented hydrodynamically using a "strip theory" approach since flow around each strip of the hull tends to be represented well by considering the flow to be two-dimensional (particularly at higher frequencies). Slender submarine hulls, whose length-to-diameter ratios typically range from eight to twelve, would therefore be represented well using the hydrodynamic "strip theory" approach.

For purposes of this analysis, a submarine hull will be represented hydrodynamically using a number of *surface elements* ("strips") as shown in figure 3-9. The centers of pressure of the surface elements will be considered to be located coincident with the beam finite element nodes defined in section 3.3.1.1. Thus, the net forces exerted on each of the hull sections by the surrounding fluid could be considered to act *at the nodes* of the finite element model. The properties of each surface element (i.e. principle dimensions) would be considered constant for the length of *that* surface element.

Because two-dimensional flow is assumed around each surface element, the forces on each surface element (and therefore on each finite element node) will generally be resolved into two Cartesian coordinate components corresponding to the horizontal and vertical directions (normal to the ship axis). Force components on each surface element will be computed and applied to the beam finite element node. In the case where a particular surface element has appendages, additional contributions to the horizontal and vertical forces will be computed for the given appendage geometry.

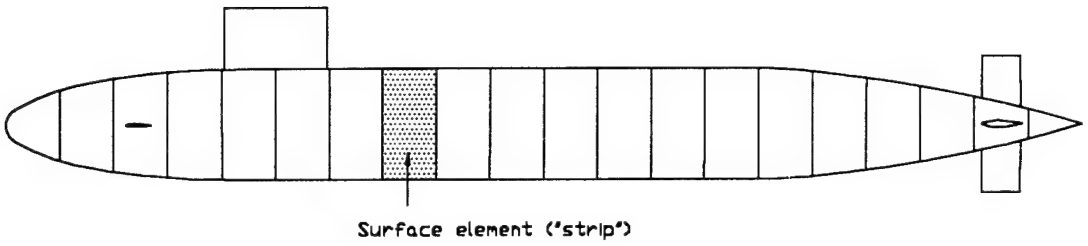

Figure 3-9. Hydrodynamic representation of the submarine hull by surface elements ("strips").

3.3.3.2 Morison relative velocity model.

As discussed in section 2.3.2, when two dimensional, generally oscillating flow can be assumed, and when both fluid inertia and drag forces are important (and wave radiation may be ignored), then a Morison's equation may be used to predict hydrodynamic forces on a body. It will be assumed for this analysis, that the whipping submarine is sufficiently below the free surface such that wave radiation may be ignored. Under this assumption, the hydrodynamic forces on each of the surface elements may be predicted using the Morison relative velocity formulation given by equation (2-62) and corrected by multiplying by the length of the element:

$$F_{hydro} = \left(\rho A C_m (\dot{u} - \ddot{x}) + \rho A \ddot{x} + \frac{1}{2} \rho D C_d (u - \dot{x}) |u - \dot{x}| \right) L \qquad (3\text{-}38)$$

where F_{hydro} is the total hydrodynamic force on the surface element, ρ is the fluid density, A is the cross-sectional area of the surface element (normal to the direction of flow), D is the characteristic diameter of the surface element (normal to the direction of flow), L is the length of the surface element, u is the fluid velocity at the location of the center of pressure of the surface element (i.e. the "free field" fluid velocity caused by the pulsating explosion bubble and considered relatively unaffected by the presence of the hull), and x is the displacement of the center of pressure of the surface element (i.e. the finite element nodal displacement). C_m and C_d are the *relative* motion fluid inertia and drag hydrodynamic coefficients (respectively) and are defined by equation (2-63).

Determination of hydrodynamic coefficients. For the case of the whipping of a submerged submarine, particular care must be taken to select hydrodynamic coefficients for analysis which properly represent both the geometry *and* the conditions of the relative

fluid flow around the surface element. Generally, it would be expected that separation of flow around the hull would occur during submarine whipping motions, particularly around those sections with small characteristic dimensions (or containing components with small characteristic dimensions). Determination of the extent to which separation occurs and the resulting forces generally requires a complex evaluation of the separation and vortex shedding mechanisms. In the "discrete-point" vortex method[84], for example, forces on an isolated sharp edge may be predicted my modeling the separating shear layers which feed the growing vortices. The hydrodynamic coefficients are calculated iteratively over a number of cycles by a Fourier averaging process. This type of evaluation, while perhaps required for completely rigorous solution of the hydrodynamic forces, is beyond the scope of this analysis and will not be considered here.

An initial perspective of the flow fields which could be expected around a whipping submarine, and thus of the criteria necessary for initial selection of hydrodynamic coefficients for analysis, could be attained by considering past experience with ship whipping, and considering typical submarine geometries. As pointed out by Hicks[85], the *fundamental* (i.e. lowest) natural whipping period of most ships is typically between 0.3 and 1.0 seconds (fairly well matched with typical bubble pulse periods). For typical characteristic dimensions (D) of submarine hull sections (ranges might be between 0.1 m for small control surfaces, to 15 meters for an entire hull section), characteristic frequencies (β) would range from 1×10^{4} to 7.5×10^{8} (higher whipping modes would yield even higher β). These characteristic frequencies correspond to very large Reynolds' numbers (Rn) over a large range of Keulegan-Carpenter numbers (KC).

Extensive experimental studies have been conducted in the marine industry in order to obtain values for hydrodynamic coefficients C_m, C_d, C_A, and C_d^l, particularly for smooth horizontal cylinders, as discussed in section 2.3.2. Even with the extensive studies, a great deal of experimental "scatter" exists in the data base, due to such factors as free surface effects, surface roughness, and even the random nature and directionality of the ocean environment (for field tests). For these reasons, a great deal of care must be taken prior to applying coefficient values from the literature to a design or analysis case. Additionally, most experimental studies have been carried out at relatively low frequencies (and therefore low Reynolds' numbers), and thus there is limited data which could be directly applied to submarine whipping without some extrapolation.

---

[84]Graham, J.M.R., "The forces on sharp-edged cylinders in oscillatory flow at low Keulegan-Carpenter numbers". *Journal of Fluid Mechanics*, 97, 1980, pp. 331-346.
[85]Hicks, *op. cit.*, p. 393.

Extensive laboratory research conducted by Sarpkaya[86] showed that, for smooth *circular cylinders* at high Reynolds' numbers (and therefore high β), the value of C_d approaches 0.65 and C_m approaches 1.8 (relatively constant over a wide range of KC). These coefficients should provide good first approximations for inertia and drag coefficients of the *circular* hull sections (surface elements) for high-frequency whipping.

Generally, there may be several sharp-edged portions of a submarine surface (control surfaces and sail) which may induce significant vortex shedding and therefore significant viscous drag on particular hull surface elements. Some accounting must therefore be made for the additional forces exerted on these surface elements. Test data on sharp-edged cylinders in high Reynolds' number oscillatory flow is generally lacking in the literature. Some data is presented by Bearman, et. al.[87] for flat plates in oscillatory flow at Keulegan-Carpenter numbers between 1 and 10 (relatively low) which might be extrapolated to predict that C_d would fall in the range of 4-6 and C_m would fall in the range of around 1.0 for higher Reynolds' number (higher frequency) flows. While these values are probably not experimentally sound, they should at least provide reasonable first order approximations of *additional* viscous forces exerted on certain hull surface elements by sharp-edged control surfaces or sail.

The modeling of hydrodynamic forces on a whipping submarine using equation (3-38) will be included as part of the computational algorithm developed in section 3.4. One analysis application will be made in chapter 4 where whipping response of the submarine is due only to an initial displacements (i.e. free whipping), and therefore no "free field" fluid velocity or acceleration terms (i.e. u and $\dot{u}$) will be included, and the hydrodynamic forces will be due only to the motion of the hull in otherwise still water. Additional analyses will include cases where the submarine is excited by a pulsating explosion bubble, and "free field" fluid motion will be included in the hydrodynamic model.

3.3.3.3 Model of fluid loading from a pulsating explosion bubble.

In analysis cases where it is desirable to couple ship whipping with the loading imposed by the pulsation of an explosion bubble, it is necessary to define a time-varying formulation for the "free field" fluid velocity and acceleration associated with the pulsating

---

[86]Sarpkaya, T., "In-line and transverse forces on cylinders in oscillating flow at high Reynolds' numbers", *Proceedings of the Eight Offshore Technology Conference*, OTC 2533, 1976, pp. 95-108.
[87]Bearman, P.W., Downie, M.J., Graham, J.M.R., and Obasaju, E.D., "Forces on cylinders in viscous oscillatory flow at low Keulegan-Carpenter numbers", *Journal of Fluid Mechanics*, 154, 1985, pp. 344-345.

bubble (i.e. u and $\dot{u}$). Because derivation of equations for bubble dynamics is a lengthy process and not a goal of this analysis, formulation available in the literature will be only briefly summarized. A particularly useful formulation for spherically symmetric, pulsating and migrating explosion bubbles is presented by Wilkerson[88], which is based upon the published theories of Herring[89], Friedman[90], Taylor[91], Cole[92], and Hicks[93]. This formulation includes accounting of effects due to the presence of a free surface and drag forces on the migration of the bubble.

The free field equations of motion for a spherically symmetric, pulsating and migrating explosion bubble are described adequately using inviscid, irrotational fluid flow theory (i.e. potential flow). Figure 3-10 illustrates an appropriate coordinate system which encompasses the explosion bubble, its "image bubble" (to account for the presence of the free surface), and an arbitrary point in the fluid. The fluid velocity potential function (ϕ) resulting from a pulsating and migrating explosion bubble may be written as the superposition of potentials resulting from a simple source and its image (representing pulsation of the spherical bubble) and potentials resulting from a dipole and its image (representing migration of the spherical bubble)

$$\phi = \frac{e_1}{r_1} + \frac{e_2}{r_1^2}\cos\theta_1 - \frac{e_1}{r_2} + \frac{e_2}{r_2^2}\cos\theta_2 \qquad (3\text{-}39)$$

where e_1 and e_2 are the time-dependent strengths of the sources and dipoles (respectively), r_1, r_2 are the radial distances from the center of the bubbles to the arbitrary point in the fluid, and θ_1, θ_2 are the angles from the vertical (as shown in figure 3-10). The first term on the right hand side is the potential due to the source representing the pulsation of the explosion bubble. The second term is the potential due to the dipole representing the migration of the explosion bubble. The last two terms represent the potentials due to the effects of the "image bubble" which accounts for the effect of the free surface (i.e. satisfies the boundary condition at the free surface).

---

[88]Wilkerson, S.A., "Elastic Whipping Response of Ships to an Underwater Explosion Loading", *Master of Science in Engineering Thesis*, George Washington University, 1985.
[89]Herring, C., "Theory of the Pulsations of the Gas Bubble Produced by an Underwater Explosion", *Underwater Explosions Research, Vol. II - The Gas Globe*, Office of Naval Research, 1950.
[90]Friedman, B., "Theory of the Underwater Explosion Bubbles", *Underwater Explosions Research, Vol. II - The Gas Globe*, Office of Naval Research, 1950.
[91]Taylor, G.I., "Vertical Motion of a Spherical Bubble and the Pressure Surrounding It", *Underwater Explosions Research, Vol. II - The Gas Globe*, Office of Naval Research, 1950.
[92]Cole, R.H., *Underwater Explosions*, Princeton University Press, Princeton, NJ, 1948.
[93]Hicks, A.N., "The Theory of Explosion-Induced Ship Whipping", *Naval Construction Research Establishment, NCRE Report R579*, 1972.

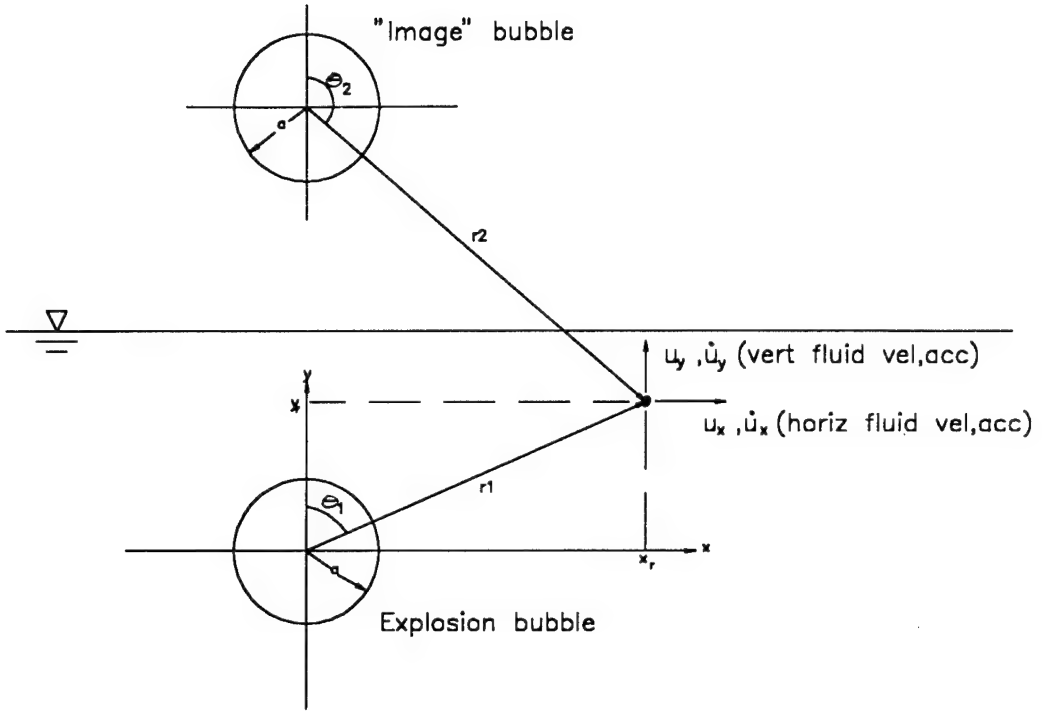

Figure 3-10. Coordinate system for explosion bubble dynamics. Explosion and "image" bubble representation.

The time-dependent source and dipole strengths are those required to maintain continuity of the normal fluid particle velocity at the bubble surface (i.e. the normal fluid particle velocity must equal the rate of change of the bubble radius, $\dot{a}$, corrected for the migration velocity). The required source and dipole strengths are:

$$e_1 = a^2\dot{a}$$

$$e_2 = \frac{a^3}{2}\left(v_m - \frac{a^2\dot{a}}{4d^2}\right) \qquad (3\text{-}40)$$

where v_m is the upward velocity of the (migrating) bubble and d is the depth of the bubble. Using conservation of energy, the differential equations which govern the pulsation and migration of the bubble (i.e. solve for the bubble radius and location) may be derived[94]. The differential equations (in non-dimensionalized form) which describe bubble

[94]Wilkerson, *op. cit.*, pp. 7-24.

pulsation and migration are presented as part of figure 3-11, along with other defined constants and non-dimensionalized variables used in the solution of the bubble dynamics.

The first order differential equations which govern the pulsation and migration of the bubble may be integrated using a time-stepping integration procedure such as a Runge-Kutta method. It is recommended[95] that a variable time-stepping procedure be used because of the rapid changes in radius during the phases of bubble minima. With the calculated bubble radii and positions (with time), the velocity potential may be calculated using equations (3-39) and (3-40), and the "free field" fluid velocity for any arbitrary point in the fluid may be calculated by differentiating the velocity potential (equation (2-47)). Wilkerson[96] derived expressions for fluid velocities and accelerations (horizontal and vertical components) at an arbitrary point in the fluid as functions of position and source and dipole strengths. The resulting expressions (given in Cartesian coordinates of figure 3-10) are given in figure 3-12.

[95]Hicks, *op. cit.*, p. 159.
[96]Wilkerson, *op. cit.*, pp. 25-29.

Differential equations which govern bubble pulsation and migration:

$$\dot{\alpha} = \sigma \qquad \dot{\sigma} = -\frac{3}{2\left\{1-\frac{\beta\alpha}{2\delta}\right\}}\left\{\frac{\sigma^2}{\alpha}\left(1-\frac{2\beta\alpha}{3\delta}\right)-\frac{\hat{\lambda}^2}{6\alpha}+\frac{\zeta}{\alpha\zeta_0}-\frac{(\gamma-1)k}{\alpha^{3\gamma-1}}+\frac{\beta\alpha}{4\delta^2}\left(\frac{\sigma\hat{\lambda}}{3}-\frac{\alpha}{\zeta_0}+\frac{C_D\hat{\lambda}^2}{4}\right)\right\}$$

$$\dot{\zeta} = \lambda \qquad \dot{\lambda} = -3\varepsilon\left\{\frac{1}{\zeta_0}+\frac{\sigma\hat{\lambda}}{\alpha}-\frac{C_D\hat{\lambda}^2}{4\alpha}+\frac{\beta\alpha}{4\delta^2}\left(3\sigma^2+\alpha\dot{\sigma}\right)\right\}$$

Initial Conditions: $\alpha = k^{4/3}\left[1+\frac{4k^4}{3}\right]$ $\zeta = \zeta_0 = -d/L$ $\sigma = 0$ $\lambda = 0$

Non-dimensionalized defined variables:

$\alpha = a/L$ (non-dimensional bubble radius)

$\zeta = y_b/L$ (non-dimensional bubble depth)

$\tau = t/T$ (non-dimensional time)

where: $L \approx 13.6(W/D_0)^{1/3}$ for TNT $\quad T \approx 2.94\left(\frac{W^{1/3}}{D_0^{5/6}}\right)$ for TNT

$k \approx (0.0552)D_0^{0.25}$ for TNT $\quad \gamma \approx 1.25$ for TNT $\quad C_D = 2.25$

$D_0 = d + 33$ d is initial depth of charge W is charge weight of TNT

Control variables: ε (0 for non-migrating; 1 for migrating)

β (0 for no free-surface effect; 1 for free-surface effect)

Figure 3-11. Non-dimensionalized variables and differential equations which describe the pulsation and migration of an underwater explosion bubble.

$$u_x = \frac{e_1 x_r}{\left(y_r^2 + x_r^2\right)^{3/2}} + \frac{3e_2 y_r x_r}{\left(y_r^2 + x_r^2\right)^{5/2}}$$

$$u_y = \frac{e_1 y_r}{\left(y_r^2 + x_r^2\right)^{3/2}} + \frac{3e_2 y_r^2}{\left(y_r^2 + x_r^2\right)^{5/2}} - \frac{e_2}{\left(y_r^2 + x_r^2\right)^{3/2}}$$

$$\dot{u}_x = \frac{\dot{e}_1 x_r}{\left(y_r^2 + x_r^2\right)^{3/2}} + \frac{3\dot{e}_2 y_r x_r}{\left(y_r^2 + x_r^2\right)^{5/2}} + v_m\left[\frac{3e_1 y_r x_r}{\left(y_r^2 + x_r^2\right)^{5/2}} - \left(\frac{3e_2 x_r}{\left(y_r^2 + x_r^2\right)^{5/2}}\right)\left(1 - \frac{5y_r^2}{\left(y_r^2 + x_r^2\right)}\right)\right]$$

$$\dot{u}_y = \frac{\dot{e}_1 y_r}{\left(y_r^2 + x_r^2\right)^{3/2}} + \frac{3\dot{e}_2 y_r^2}{\left(y_r^2 + x_r^2\right)^{5/2}} - \frac{\dot{e}_2}{\left(y_r^2 + x_r^2\right)^{3/2}} - v_m\left[\left(\frac{e_1}{\left(y_r^2 + x_r^2\right)^{3/2}}\right) + \left(\frac{9e_2 y_r}{\left(y_r^2 + x_r^2\right)^{5/2}}\right) - \left(\frac{3e_1 y_r^2}{\left(y_r^2 + x_r^2\right)^{5/2}}\right) - \left(\frac{15e_2 y_r^3}{\left(y_r^2 + x_r^2\right)^{7/2}}\right)\right]$$

where source and dipole strengths may be defined (in non-dimensionalized form):

$$e_1 = L^3\alpha^2\sigma / T \qquad e_2 = -\frac{L^4\alpha^3\lambda}{2T}$$

$$\dot{e}_1 = \frac{L^3}{T^2}\left(\alpha^2\dot{\sigma} + 2\alpha\sigma^2\right) \qquad \dot{e}_2 = -\frac{L^4}{2T^2}\left[\alpha^3\dot{\lambda} + 3\alpha^2\lambda\sigma\right]$$

and: $v_m = -\dot{\zeta}L / T = -\lambda L / T$ (the upward velocity of the bubble)

Figure 3-12. Fluid velocities and accelerations (in relative Cartesian coordinates) for given source and dipole strengths and upward bubble velocity.

3.4 Formulation of the computational algorithm.

In order to integrate each of the desired force components presented in the previous sections, a comprehensive computational algorithm must be developed. The required algorithm must be capable of performing the following:

1. Compute the time histories of the explosion bubble radius and depth by integration of the differential equations governing bubble dynamics using a Runge-Kutta time integration procedure.
2. Compute the "free-field" fluid velocities and accelerations due to the pulsating and migrating explosion bubble. These velocities and accelerations must be calculated at the locations of *each* of the finite element nodes used to model the dynamics of the hull structure at *each iteration at each time step*, and must be resolved into the vertical and horizontal directions defined by the ship coordinate system (a change of coordinates from the bubble coordinate system to the ship coordinate system is required).
3. Compute the external and internal loading on the ship hull using the appropriate models developed in the previous sections.
4. Iteratively determine the hull structure displacements, velocities, and accelerations using the Newmark method (with Newton-Raphson iterations conducted at each time step) as described in section 3.2. Also, iteratively determine displacements, velocities, and accelerations of internal masses as required.

A computational algorithm satisfying the above requirements may be generated using a suitable computer language, separating the algorithm into sections or subroutines appropriate for computation using the chosen language. For this application, the algorithm will be implemented on a personal computer using subroutines written for the MATLAB® computer program. Appendix A presents MATLAB® subroutines written for this analysis, each of which addresses specific portions of the overall algorithm. The subroutines are presented as follows:

a. Subroutine IN.M - Serves as an input file for other subroutines. Data is loaded from formatted batch-type files. Arrays and constants used in other subroutines are generated.

b. Subroutine HULL.M - Calculates global mass and stiffness matrices for the hull structure, solves the generalized eigenproblem to obtain the "dry mode" natural frequencies and mode shapes, calculates an appropriate viscous hull damping matrix for the hull using a Rayleigh damping approach, and calculates vectors for modal mass, damping, and stiffness.

c. Subroutine WETMODE.M - Calculates an approximate fluid added mass matrix for the hull using a Morison equation approach (i.e. strip theory), adds the fluid added mass matrix to the dry hull mass matrix and solves the generalized eigenproblem to obtain the "wet mode" natural frequencies and mode shapes, and calculates vectors for "wet mode" modal mass, damping and stiffness.

d. Subroutine FREEWHIP.M - Calculates nodal point response (displacements, velocities, and accelerations) during free vibration with initial displacements given by scaled mode shape vectors for specified modes. Response is calculated using the Newmark time integration method with iteration conducted at each time step using a Newton-Raphson method. This subroutine is designed primarily to compare damping associated with hull mechanisms (i.e. material hysteretic and structural) and damping associated with external hydrodynamic forces.

e. Subroutine BUBBLE.M - Computes and saves the time histories of the explosion bubble radius and bubble depth by integration of the differential equations governing bubble dynamics. Time histories are computed using a Runge-Kutta integration method with a variable time step. The differential equations governing bubble radius are called from function routines RADFN.M and RFUNC.M. The differential equations governing bubble depth are called from function routines DPTHFN.M and DFUNC.M.

f. Subroutine BUBWHIP.M - Calculates the nodal point response (displacements, velocities, and accelerations) during forced vibration due to a pulsating explosion bubble. Response is calculated using the Newmark time integration method with iteration conducted at each time step using a Newton-Raphson method. Additionally, local axial strains are calculated at specified hull locations using simple beam theory (used for comparison of the computational algorithm with model test data). The free-field fluid velocities and accelerations due to the pulsating explosion bubble are calculated at each iteration when function routine FLUID.M is called from within BUBWHIP.M. This subroutine is designed primarily to provide a comprehensive computation of explosion-induced whipping effects. Additionally, it may be used to quantify damping associated with internal structures and to provide for comparison of the computational algorithm with model test data.

4. ANALYSIS OF WHIPPING OF A SUBMERGED SUBMARINE

4.1 Introduction.

In this chapter, the prediction of the whipping response of a submerged submarine is discussed, including an analysis of specific damping mechanisms. The computational algorithm developed in the previous chapter is utilized to predict the response of a notional 7400 long ton fast attack submarine (SSN). Additionally, the computational algorithm is used to predict the response of the U.S. Navy test platform "Red Snapper", subjected to specified explosive charge weight/standoff combinations for comparison with model test data. The latter analysis is presented in non-specific response units due to security concerns with the actual test data used for comparison.

General characteristics of the notional submarine (SSN) are given in Table 4-1. From these general characteristics, specific characteristics (beam element data, hull section data, etc.) are formulated and provided as input via subroutine IN.M. The "dry" mode natural frequencies and mode shapes are calculated using subroutine HULL.M, and the "wet" mode natural frequencies and mode shapes are calculated using subroutine WETMODE.M (i.e. the effects of fluid added mass are included). Table 4-2 gives both "dry mode" and "wet mode" natural frequencies computed for the first 12 displacement modes. It should be noted that this represents the first 6 displacement modes in *each plane* (i.e. horizontal and vertical), of which the first 2 are considered *rigid body modes* (corresponding to zero natural frequencies), and the remaining 4 modes are considered as the *fundamental flexural modes*. The horizontal "wet" mode shapes are plotted (as normalized nodal displacements) and shown in figure 4-1 (rigid body mode shapes) and figure 4-2 (fundamental flexural mode shapes).

Table 4-1. General characteristics of the notional SSN.

Length (ft)	350
Displacement/weight (long tons)	7440
Maximum beam/diameter (ft)	35
Hull material	HY-80 steel
Number of hull sections/beam elements	20/19
Appendages	Sail, bow planes, stern planes, rudder

Table 4-2. Rigid body and fundamental flexural "dry" mode and "wet" mode natural frequencies for notional SSN.

Mode	"Dry mode" natural frequency, ω (hz, rad/sec)	"Wet mode" natural frequency, ω (hz, rad/sec)
1 Rigid body	0	0
2 Rigid body	0	0
3 Rigid body	0	0
4 Rigid body	0	0
5 Flexural (V)	1.984, 12.466	1.370, 8.608
6 Flexural (H)	1.984, 12.466	1.373, 8.627
7 Flexural (V)	4.498, 28.262	3.060, 19.227
8 Flexural (H)	4.498, 28.262	3.074, 19.315
9 Flexural (V)	7.054, 44.322	4.827, 30.329
10Flexural (H)	7.054, 44.322	4.863, 30.555
11Flexural (V)	9.802, 61.588	6.907, 43.398
12Flexural (H)	9.802, 61.588	6.922, 43.492

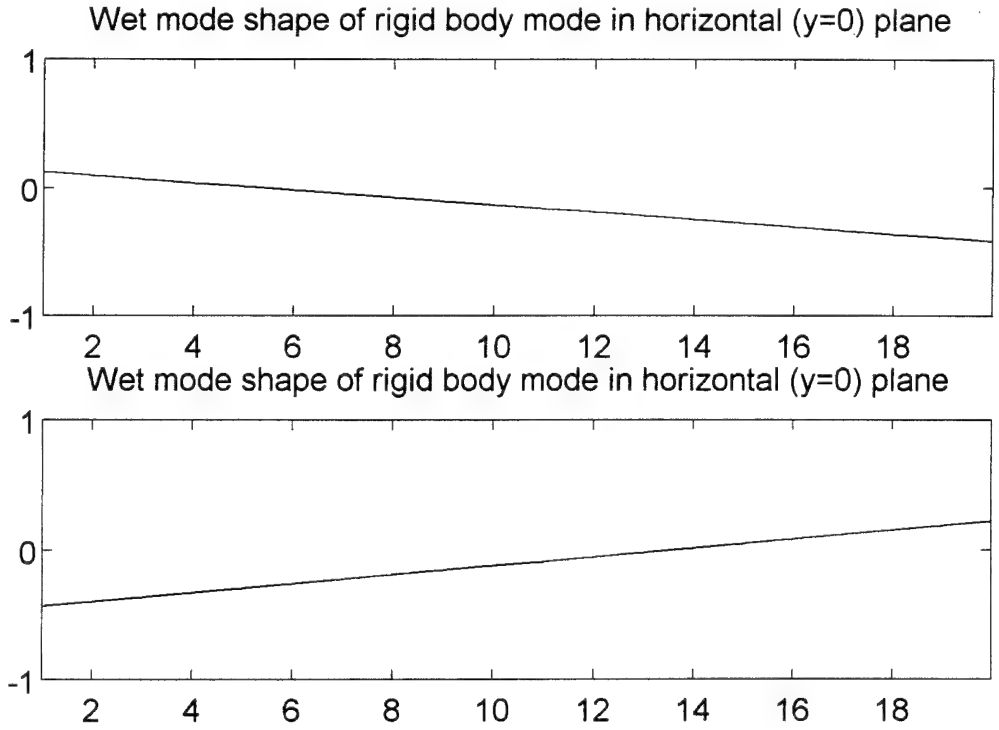

Figure 4-1. Horizontal rigid body "wet" mode shapes for notional SSN.

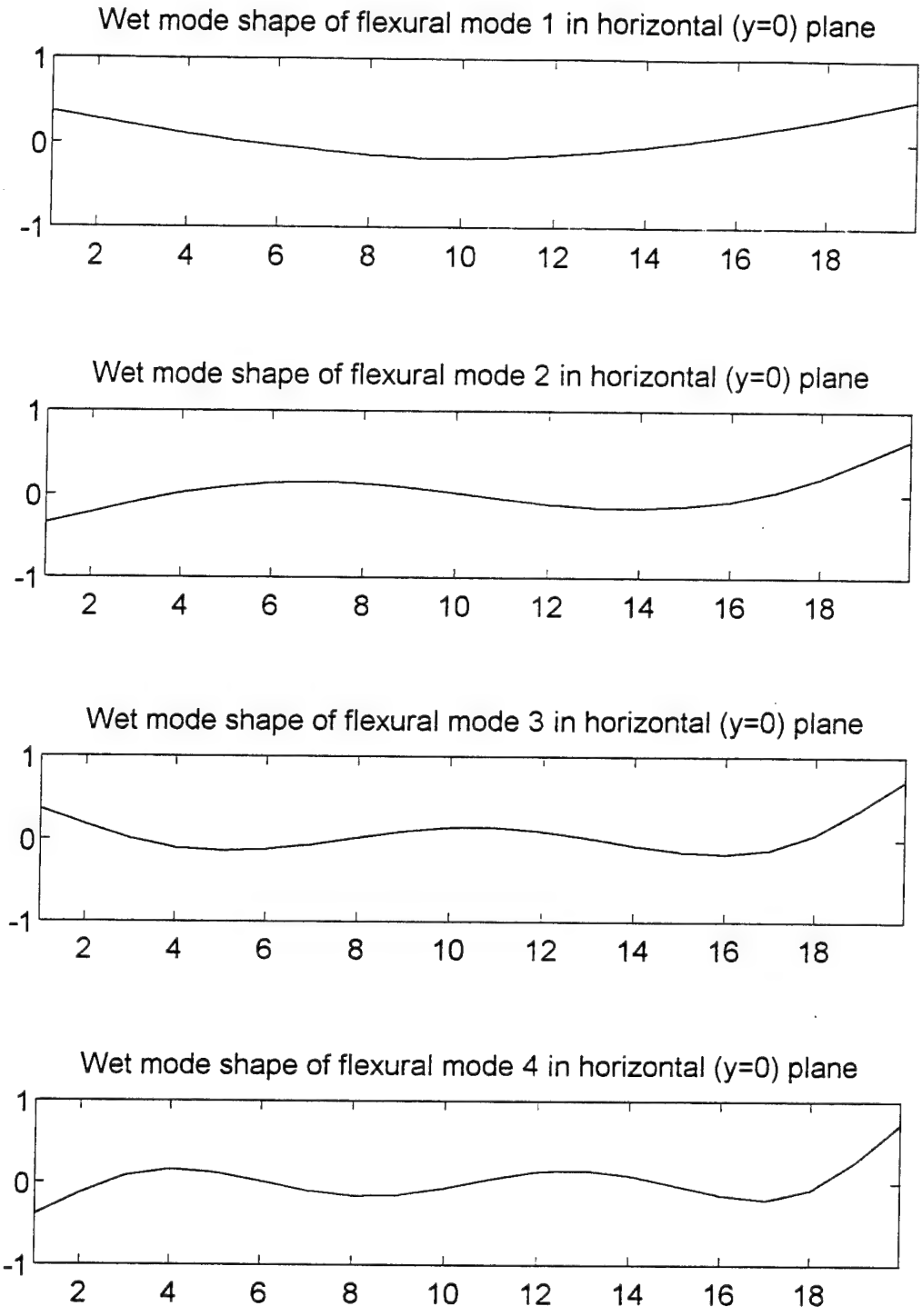

Figure 4-2. Horizontal fundamental flexural "wet" mode shapes for notional SSN.

4.2 Prediction of "dry" whipping response. Hull damping.

The "dry" whipping response of the SSN is computed for given initial conditions using subroutine FREEWHIP.M (with fluid density set to zero in Morison's equation). For free "dry" whipping (as well as free "wet" whipping discussed subsequently), initial nodal point displacements are specified as scaled horizontal mode shape vectors, and time histories of nodal point displacements, velocities, and accelerations are computed based upon these initial displacements. Thus, initial loading on the hull structure is due only to internal forces due to structural stiffness.

For this analysis, initial displacements are set to the first and second horizontal fundamental flexural mode shapes (scaled by 2% of the total ship length). Appendix B presents plots of horizontal displacements, velocities, and accelerations for nodes 7, 10, and 20 for initial displacements (a) scaled from the 1st horizontal fundamental flexural mode shape (i.e. mode 6 in Table 4-2), and (b) scaled from the 2nd horizontal fundamental flexural mode shape (i.e. mode 8 in Table 4-2).

As discussed in chapter 3, it has been assumed that the inherent *hull damping* (i.e. due to material hysteresis and structural damping) would reasonably follow experimental data for steel cylindrical marine structures and ship masts. Thus, it was assumed that modal damping ratios on the order of 1% for hull damping would be sufficient and Rayleigh coefficients could be calculated on this basis. Thus, reductions in free response amplitude with time (damping) seen in graphs presented in Appendix B are merely manifestation of this initial assumption, and no further conclusions may be drawn concerning the validity of this initial assumption.

However, an approximate graphical check could be performed to verify that damping in the case of "dry" whipping is indeed represented computationally by the assumed 1% modal damping. Indeed, measurement of amplitude log decrements (recall equation (1-1)) and calculation of modal damping ratios (recall equation (2-40)) for both mode 1 horizontal flexure (represented by node 10 displacement) and mode 2 horizontal flexure (represented by node 7 displacement), show that graphically determined modal damping ratios are approximately 1%.

4.3 Prediction of "wet" whipping response. Hydrodynamic damping.

The "wet" whipping response of the SSN is computed for the same given initial conditions as the "dry" mode analysis, also using subroutine FREEWHIP.M (with inclusion of hydrodynamic forces by Morison's equation). Appendix C presents plots of horizontal displacements, velocities, and accelerations for nodes 7, 10, and 20 for initial displacements (a) scaled from the 1st horizontal fundamental flexural mode shape, and (b) scaled from the 2nd horizontal fundamental flexural mode shape.

Figure 4-3 shows comparisons between nodal point displacements for "wet" and "dry" cases for initial displacements scaled from mode 1 and mode 2 flexural mode shapes. Even though modal damping cannot be directly applied to the *nonlinear* hydrodynamic damping forces, a calculated "equivalent" modal damping might still serve as a measure of hydrodynamic damping in comparison to the "dry" case. As was done for "dry" whipping, a graphical approximation of "equivalent" modal damping ratios can be made for mode 1 horizontal flexure and mode 2 horizontal flexure (represented by node 10 and node 7 displacements, respectively). As expected, the inclusion of external hydrodynamic forces (represented by Morison's equation) provide for increased modal damping ratios for both flexural modes. Both mode 1 and mode 2 flexure are characterized by "equivalent" modal damping ratios of approximately 2.2%.

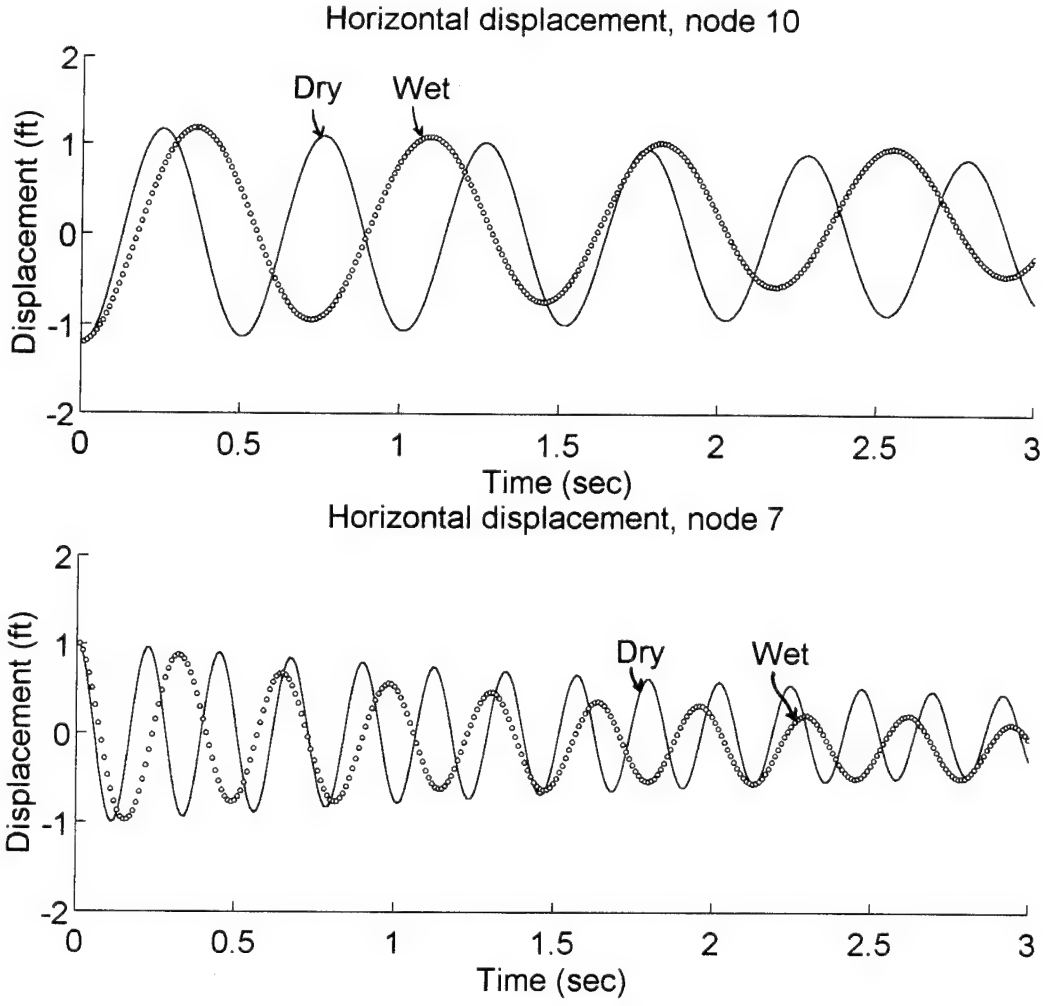

Figure 4-3. Comparison between nodal point displacements for "dry" and "wet" hull flexure. Top: mode 1 flexure, represented by node 10 displacement. Bottom: mode 2 flexure, represented by node 7 displacement.

4.4 Prediction of whipping response due to explosion bubble pulse loading.

The previous sections presented analysis based upon an assumption of initial displacements set to flexural mode shapes (i.e. free whipping), aimed only at providing some quantitative measure of hydrodynamic damping. As discussed in chapter 1, the main concern with submarine whipping involves the quasi-periodic bubble pulse loading resulting from near to intermediate stand-off explosions. It is this quasi-periodic bubble pulse loading which can reinforce the free vibration and magnify the whipping response, particularly when the period of the bubble pulse is in the vicinity of one of the natural periods of hull flexure. Indeed, if the overall dissipative forces (damping forces) are low, whipping response magnitudes (and therefore resulting hull damage) could be quite substantial.

To see potential dynamic effects associated with matched bubble pulse (i.e. bubble pulse frequency matched to ship's flexural frequency), explosive charge characteristics (charge weight, depth, etc.) must first be defined. Using the formulation for bubble pulsation and migration discussed in chapter 3, and the known "wet" natural frequencies of hull flexure (Table 4-2), explosive charge characteristics could be iteratively determined. Table 4-3 specifies explosive charge characteristics used in this analysis to match bubble pulse frequency with 1st and 2nd horizontal flexural mode natural frequencies (i.e. modes 6 and 8 in Table 4-2). A charge depth of 100 feet was selected, as deeper depths require unrealistically large charges to match the 1st fundamental flexural frequency (1.37 Hz). Ship location relative to the charge was chosen to promote excitation of the mode (both frequency and shape) of interest.

Figure 4-4 shows plots of bubble radius, depth, and migration velocity for the explosive charge weight/depth combination selected to excite mode 2 horizontal whipping of the SSN. It can be seen from the plot of radius vs. time that the bubble period is *not* constant with time, but increases as the bubble migrates toward the surface. This is an important phenomenon, which limits the ability of the pulsating bubble to excite a particular flexural natural frequency for a prolonged period of time (thus, the bubble pulse could only be considered to be quasi-periodic in nature).

The whipping response of the SSN is predicted for the cases when excited by explosion bubble pulse characterized by charges specified in Table 4-3. Subroutine BUBBLE.M predicts explosion bubble radius and depth time histories for each of the charge weight/depth combinations selected. Subroutine BUBWHIP.M predicts the nodal point response of the SSN, initially at rest and subject to the incident bubble pulse loading. Appendix D presents plots of displacements, velocities, and accelerations for nodes 7, 10, and 20 for the charges designed to excite horizontal modes 1 and 2 flexural whipping.

Table 4-3. Charge characteristics selected to excite mode 1 and mode 2 horizontal flexural whipping for SSN.

	First horizontal flexural mode	Second horizontal flexural mode
Charge weight (lb TNT)	1000	85
Charge depth (ft)	100	100
Bubble pulse frequency (Hz)	1.35	3.05
Depth of ship (ft)	70	80
Charge location along length of ship (ft)	157.5 (node 10)	105.0 (node 7)
Charge standoff from ship centerline (ft)	33.5	15
Charge depth below ship centerline (ft)	30	20

Because of the swiftness with which the (large) bubble migrates to the surface from its initial depth for the larger/lower frequency charge (mode 1 whipping), the calculated response time period was limited to the first 2.5 seconds. Despite the short time of excitation (only 3 flexure/bubble periods), it can be easily observed that the quasi-periodic bubble pulse does indeed magnify the whipping response. For the smaller/higher frequency charge (mode 2 whipping), the magnification effect can be more easily observed over a larger number of whipping cycles.

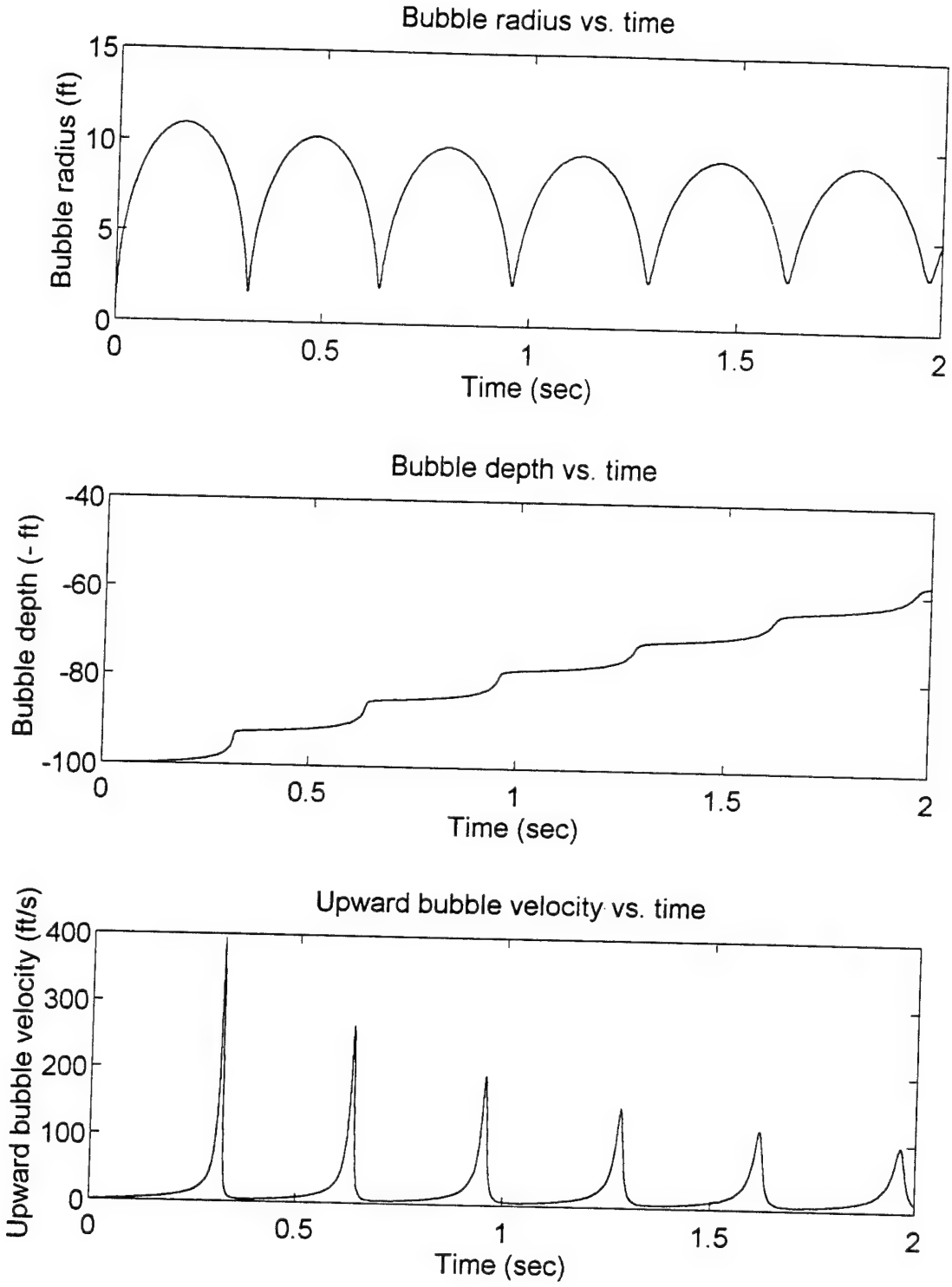

Figure 4-4. Plots of bubble radius, depth, and migration velocity for the explosive charge weight/depth combination selected to excite mode 2 horizontal whipping of the SSN.

4.5 Damping from discrete internal structures and sloshing liquids.

Discrete internal structures. As discussed in chapters 2 and 3, whipping energy can be transferred to internal structures within the hull, particularly when the internal structure is "tuned" to the bubble pulse frequency (and one of the natural frequencies of hull flexure). Using the model developed in chapter 3 (which models the internal structure as a discrete mass or dynamic vibration absorber), a brief analysis is conducted to gain some insight into potential dynamic effects of these internal structures on the whipping response of a hull.

The analysis discussed in the previous section is extended to include "tuned" vibration absorbers (internal masses on springs) where each absorber is "tuned" to the matched bubble pulse/whipping frequency. The effects of a "tuned" internal absorber are predicted for the case of the bubble pulse matched to the 2nd horizontal flexural frequency. The internal absorber is located at node 7 (i.e. "attached" to node 7) and free to move in the horizontal direction only, as discussed in section 3.3. Thus, the effect of the absorber is on the 2nd horizontal whipping mode.

The effect of a 200 long ton internal mass, "tuned" to the 2nd horizontal whipping mode and "attached" to the hull at node 7, is considered. Appendix E presents plots of horizontal displacements, velocities, and accelerations for nodes 7, 10, and 20, as well as horizontal displacement, velocity, and acceleration of the absorber mass. Figure 4-5 plots horizontal displacement of node 7, with and without the 200 ton internal mass.

Several interesting phenomenon are evident from the plot and should be briefly noted. First, the presence of the absorber has a significant overall effect on reducing the magnitude of response. While no specific measure of "damping" can be made, there is obviously significant energy transferred into the absorber. Second, the ability of the absorber to "absorb" whipping energy is very sensitive to the frequency of excitation. As discussed in the previous section, the bubble period (and therefore the frequency of whipping excitation) is *not constant*, but rather increases as the bubble migrates toward the surface. By "tuning" the internal absorber to the 2nd horizontal flexural frequency, the absorber is not then truly tuned to the excitation frequency (recall that matching bubble period to hull flexural frequency was accomplished by *iteration* of *average bubble periods* - over the 3 seconds of bubble pulsation). Thus, the usual "internal absorber effect" (i.e. reducing vibration amplitude of the main structure to *zero*) would not occur. Figure 4-6 plots the horizontal displacement of node 7 and the horizontal displacement of the absorber mass. Because the oscillation of node 7 and the oscillation of the absorber mass occur at *slightly* different frequencies, a sharp (but temporary) reduction in node 7 amplitude can be seen around 2.5 seconds, when the absorber shifts from a lag angle to a

lead angle (i.e. the node and the mass are temporarily 180° out of phase). What *can* be deduced from this is that internal structures do have potential for significant absorption of hull whipping energy, even though bubble pulse frequencies are not truly constant.

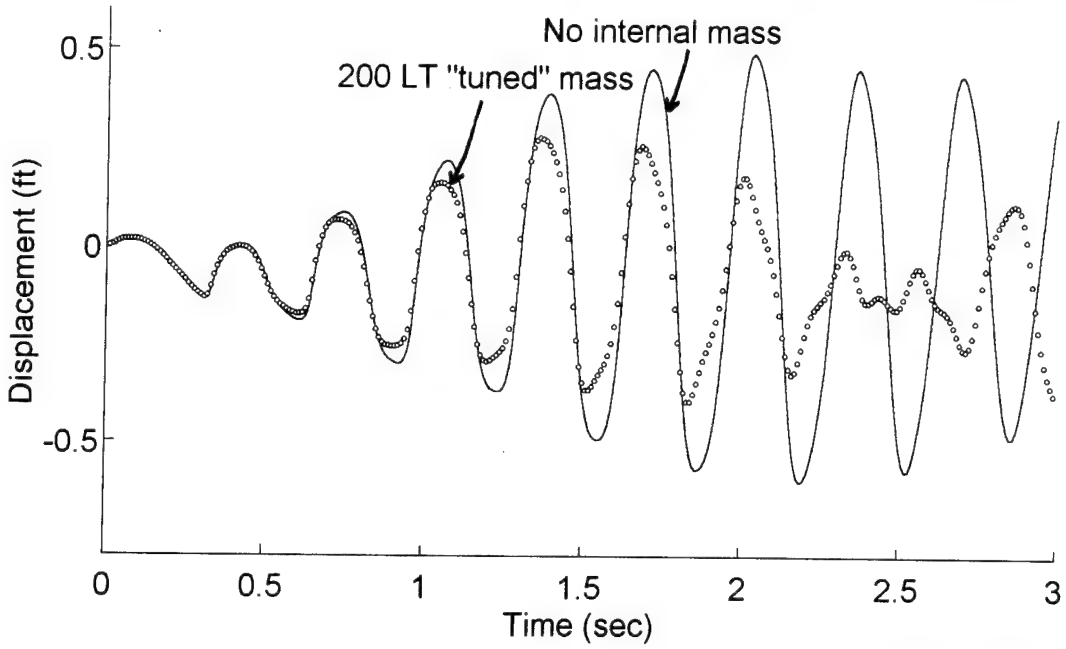

Figure 4-5. Horizontal displacement of node 7, with and without internal absorber.

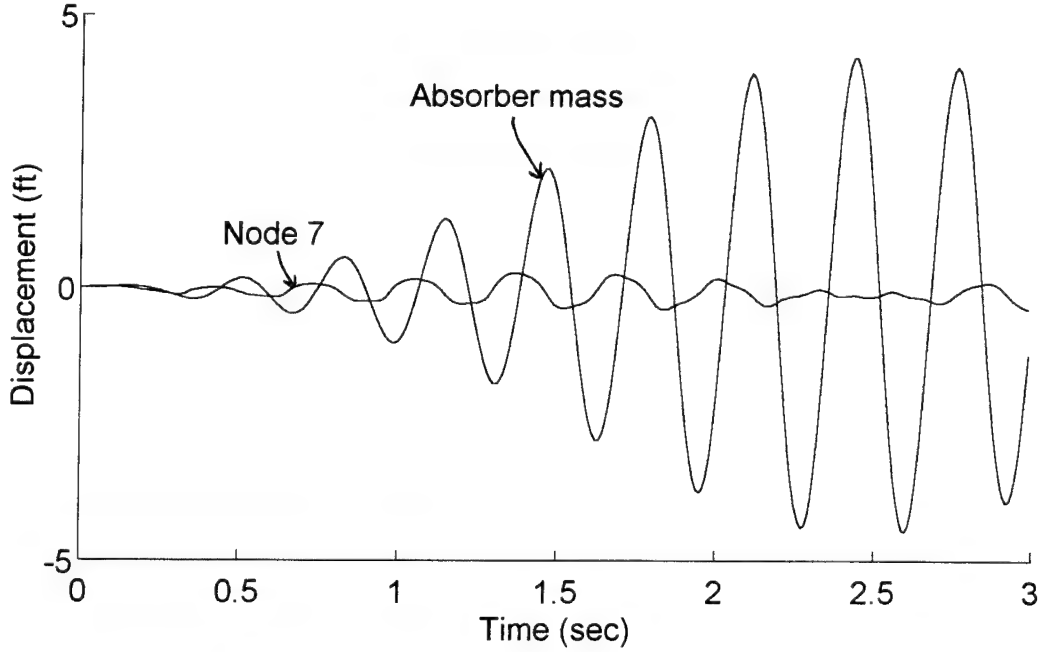

Figure 4-6. Horizontal displacement of node 7 and 200 LT absorber mass.

Liquid sloshing. As discussed in chapters 2 and 3, the fundamental mechanism by which energy is "transferred" to internal liquids through the mechanism of sloshing can be thought of much in the same way as that by which it is transferred to internal structures. In fact, liquid sloshing may be modeled quite accurately using a mechanical equivalent system approach, where each sloshing mode is considered to have its own modal mass, damping and stiffness, each responding as its own dynamic system (i.e. its own dynamic absorber). Using the formulation for natural sloshing frequency, modal mass, and modal stiffness presented in chapter 3 for lateral sloshing in a rectangular tank, the discussion of damping through liquid sloshing follows quite nicely behind that of the discrete internal structure. Recalling equations (3-35) through (3-37), it is clear that the natural frequency, modal mass, and modal stiffness of each mode of sloshing are dependent only upon the mode number (n), the total mass of liquid in the tank (M_l), and the geometry of the tank (i.e. tank depth and width).

Using the standard rectangular tank formulations, it is a trivial procedure to generate plots of natural frequency vs. sloshing mode and sloshing modal mass vs. sloshing mode. When this is done over a wide range of possible tank configurations, it quickly becomes clear that liquid sloshing could *not* become a *significant* contributor to the dissipation or absorption of hull whipping energy. Figure 4-7 plots both natural sloshing frequency (ω_n) and sloshing modal mass (m_n) for a 20' x 20' x 20' rectangular tank (a total liquid weight of 228.5 long tons). Two interesting things may be noted for this *very large tank* (much larger than any single, unbaffled tank on any submarine). First, the only sloshing modal mass of any substance (i.e. which *might* effect hull whipping) is that of the first/fundamental sloshing mode (i.e. 60 long ton). Second, the natural frequency of this fundamental sloshing mode is only 2.24 rad/sec (0.35 Hz), well below any natural flexural frequency. As other tanks are considered, it is found that the fundamental sloshing modes (of all reasonable tank sizes) fall well below 1 Hz. While higher sloshing modes may have natural sloshing frequencies in the range of hull whipping frequencies, the modal masses of these modes are significantly smaller than would contribute to any noticeable reduction in whipping response. Appendix F presents plots of natural sloshing frequency vs. sloshing mode and sloshing modal mass vs. sloshing mode for several representative rectangular tank geometries.

From this basic analysis of natural sloshing frequencies and sloshing modal masses, it can be justifiably deduced that liquid sloshing would have little impact on the whipping response of most ships. Because the significant sloshing modal masses have natural frequencies well below hull flexural frequencies, it can also be deduced that the major

effect of liquids with free surface would only be toward the addition of total ship mass (i.e. the significant sloshing modes would act only as rigid bodies).

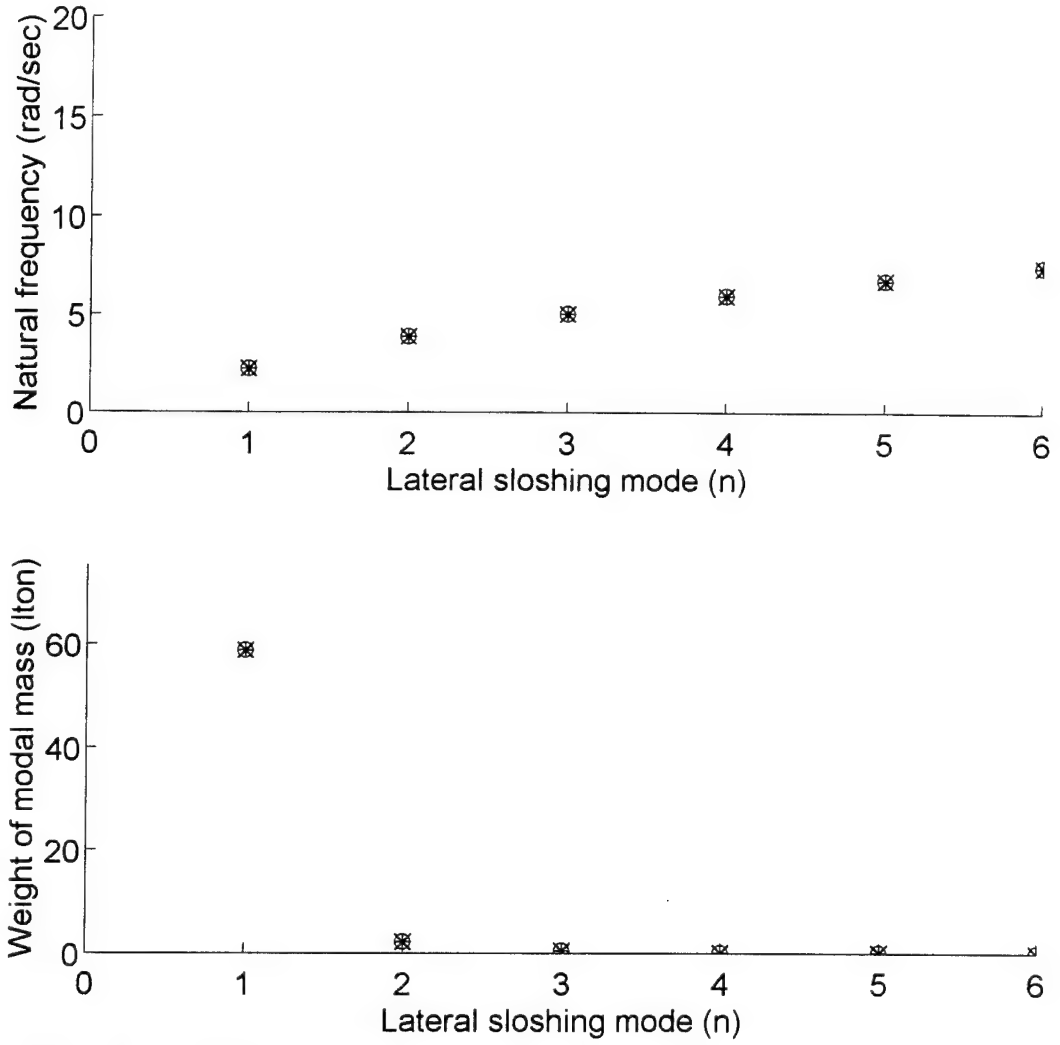

Figure 4-7. Natural sloshing frequency and sloshing modal mass vs. mode number for lateral sloshing of a (20' x 20' x 20') rectangular tank.

4.6 Comparison of computational algorithm with the "Red Snapper" model test.

The computational algorithm for submarine whipping developed in chapter 3, and applied to the whipping of a notional SSN in the previous sections, is used to predict the response of the U.S. Navy test platform "Red Snapper". Thus, some "verification" of the computational algorithm is made with actual model test data. Due to the security concerns with the actual test data used for comparison, the following is presented in non-specific response units (i.e. the y-axes are unlabeled).

The "Red Snapper" model is on the order of 1/4 the size of the notional SSN discussed previously (geometrically), and thus natural frequencies of hull flexure are much higher than the notional SSN. Whipping response was measured in terms of local axial strains (at specific beam element locations) and horizontal and vertical velocities (at specific node locations). For comparative purposes, subroutine BUBWHIP.M includes a scheme for calculating local axial strains at specified finite beam elements. This scheme is based upon simple beam theory an provides local axial strains at port and starboard extreme fibers, as well as crown and keel extreme fibers for the specified elements (see subroutine BUBWHIP.M in Appendix A).

Three specific model tests, which were conducted on the "Red Snapper" model, are used for comparison. One test was designed such that the explosion bubble pulse would excite mode 1 horizontal whipping. A second test was designed such that the bubble pulse would excite mode 1 whipping in both horizontal and vertical planes. A third test was designed such that the bubble pulse would excite mode 2 horizontal whipping. The design of the bubble pulse to match the flexural frequencies and mode shapes was carried out in a manner similar to that discussed in section 4.4. In all cases, there where no internal structures or liquids, and thus all forces were either hydrodynamic or structural in nature.

General comparisons. Figure 4-8 shows starboard-side fiber strain histories for elements 6 and 9 for Test 1 (horizontal mode 1 whipping), and strains calculated using the computational algorithm. In general, it appears that calculated strains match well with measured through the 2nd bubble period, but then over predict strains. Figure 4-9 shows horizontal velocity histories for nodes 10 and 20 for Test 1, and velocities calculated using the computational algorithm. Calculated velocities for this test are only slightly under predicted.

Comparisons between measured and calculated strains and velocities for Test 2 (mode 1 horizontal and vertical whipping) and Test 3 (mode 2 horizontal whipping) are presented in Appendix G. In general, the computational algorithm slightly under predicts and predicts slightly early for both strains and velocities for Test 2. For Test 3, the computational algorithm predicts quite well through the first two bubble periods, but then grossly over predicts both strains and velocities.

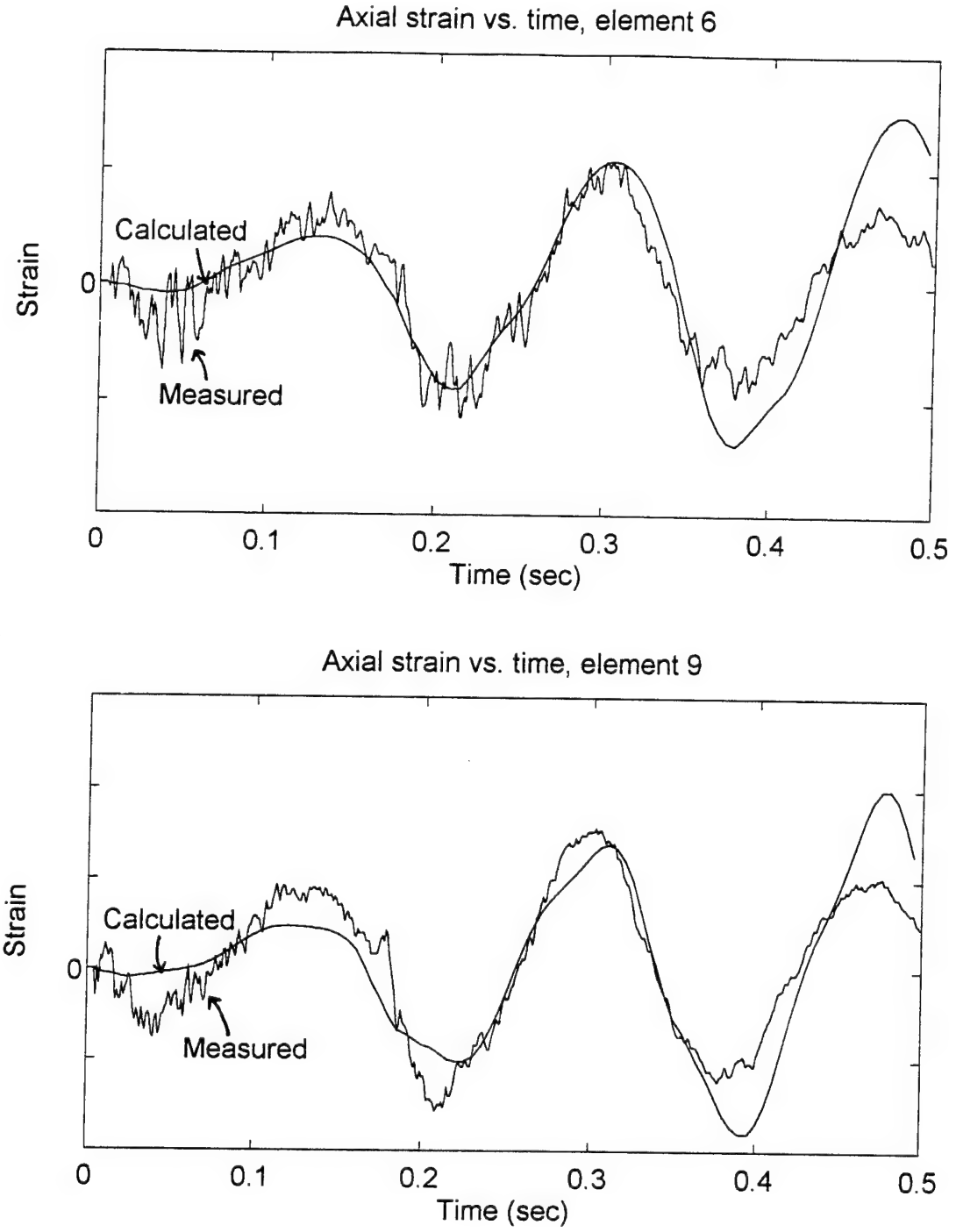

Figure 4-8. Starboard-side fiber strain histories for elements 6 and 9 for Test 1 of the "Red Snapper" model test (horizontal mode 1 whipping), and strains calculated using the computational algorithm

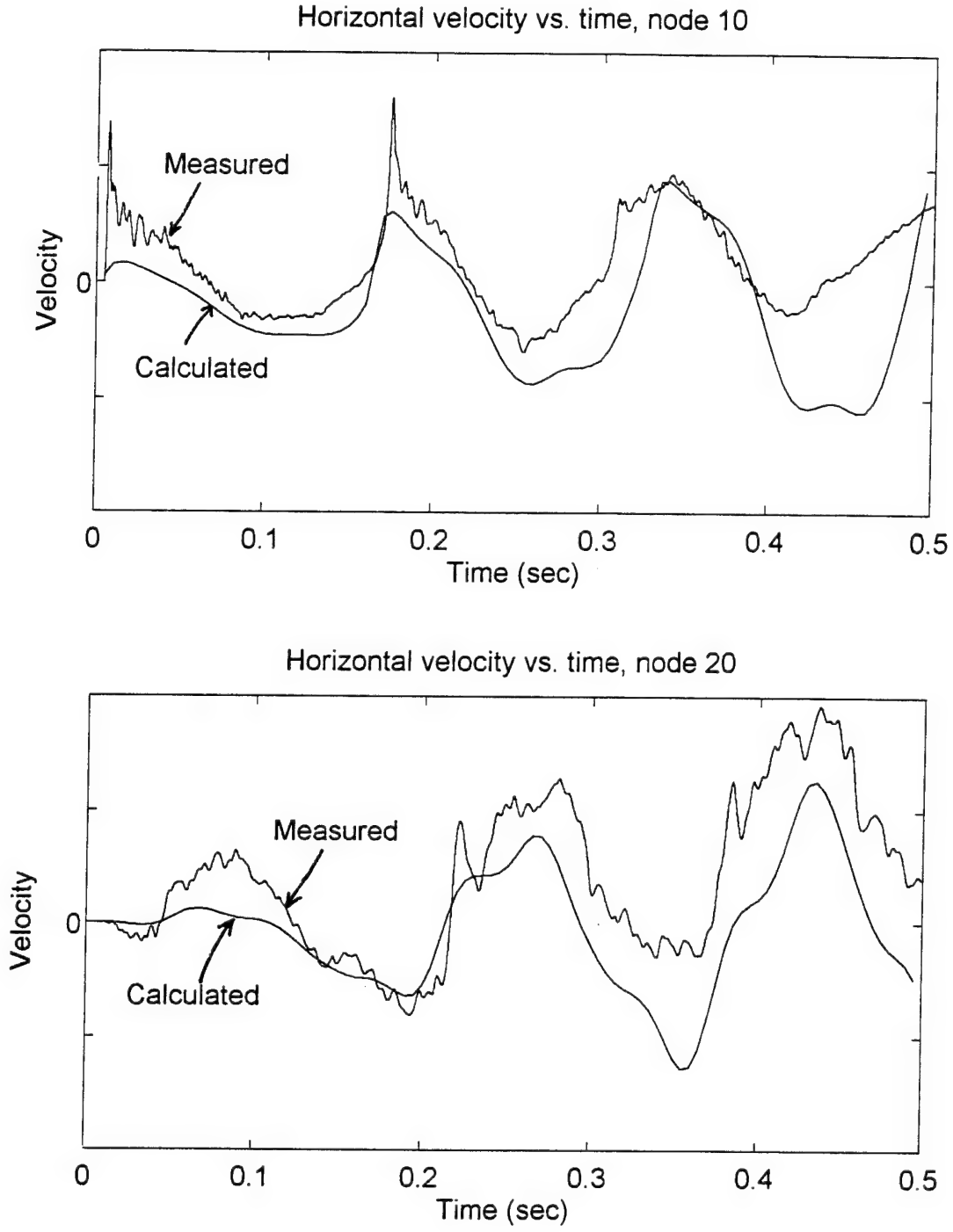

Figure 4-9. Horizontal velocity histories for nodes 10 and 20 for Test 1 of the "Red Snapper" model test (horizontal mode 1 whipping), and velocities calculated using the computational algorithm

Discussion of general comparison. There are several possible explanations for the failure of the computational algorithm to properly predict strains and velocities for the "Red Snapper" tests.

a. The bubble model used for formulation of equations governing bubble dynamics has been known to be inaccurate past the 2nd bubble period[97]. Although no satisfactory purely physical model exists for long-time bubble dynamics (some more restrictive empirical relations are available), this particular bubble model has proven to be fairly accurate through the 2nd bubble period. The reasons for the inaccuracy past the 2nd bubble period lie in the inability of the model to properly account for dissipation of bubble energy during bubble pulsation and migration. Thus, the model believes that the bubble maintains more of its original energy throughout the longer time history. This translates into greater bubble radii and greater velocities being modeled in the computational algorithm (resulting in over predicting hydrodynamic loading past the 2nd bubble period). Thus, some explanation for overproduction of response past the 2nd bubble period exists.

b. The use of the hydrodynamic "line-structure" model in the computational algorithm (i.e. hydrodynamic loading being applied at the nodes along the ship centerline, vice on the outer hull of the ship), leads to inaccuracies in hydrodynamic loading. This is particularly important when the explosive charge is close aboard. In this case, the actual hydrodynamic loading is more appropriately seen *directly on the outer hull*, while the computational algorithm believes the loading to be applied at the ship's centerline (i.e. calculated "free-field" fluid velocities and accelerations). Thus, an error is introduced due to the unaccounted-for distance between the centerline and the outer hull of the ship. For large ships, subjected to charges with large standoffs, this geometric inaccuracy is less important. But, for smaller ships subjected to near-standoff charges, this inaccuracy could lead to significant error.

c. There is a general inability of Morison's equation to adequately account for the *transient-type* vortex shedding and convection (viscous drag forces), which is undoubtedly important in this application. The original Morison's equation was designed to account for hydrodynamic loading for the relatively low-frequency wave loading on pile structures in regular sea waves (i.e. quasi-steady). There is no adequate data in the literature to support extension of the Morison formulation to transient-type analyses. This is particularly important in the justification and selection of the coefficients used in Morison's equation. As discussed in chapter 3, coefficients for the computational algorithm were merely extrapolated from low frequency data. Additionally, this data was itself obtained

[97]Misovec, A., "Comments on SITE meeting of 5/10/94", (Unpublished meeting minutes), 1994, pp. 1-2.

by Fourier time-averaging of measured forces (i.e. quasi-steady). For transient-type analyses, such as submarine whipping, a more complex approach would probably be appropriate to properly account for the transient vortex shedding and convection.

5. CONCLUSIONS

An analytical approach has been presented which predicts the elastic whipping response of a submerged submarine to the pulsating bubble of a nearby underwater explosion. The approach presented concentrates on mechanisms associated with energy dissipation (damping), and includes specific mechanisms associated with hull damping (material and structural), internal damping (internal structures and sloshing liquids), and external damping (hydrodynamic damping forces in conjunction with traditional inertial loading forces). The formulation utilizes a numerical time-domain solution technique to directly solve the nonlinear equations of motion.

While the *general* mechanisms associated with damping are reasonably well understood, application of this understanding to complex high-frequency, non-harmonic vibration problems (such as ship whipping due to explosion bubble pulse loading) has not been met with much success. For this reason, the approach has been designed to utilize a robust solution technique (the time-domain solution), and incorporate physically-based models where possible.

Modal damping ratios for material and structural damping were assumed to be on the order of 1 % of critical for fundamental flexural modes, based upon data available from steel marine structures. Thus, results for "dry" whipping only reflect this initial assumption. With this initial assumption for material and structural damping, "equivalent" modal damping ratios for mode 1 and mode 2 whipping (the first two fundamental flexural modes) for the case where hydrodynamic damping effects are included (via Morison's equation), are computed to be on the order of 2.2 %.

The effects of internal structures and sloshing liquids on whipping response is approximated using a 200 long ton "tuned" mass damper, located to effect mode 2 whipping. The effects, illustrated in figure 4-5, are significant only when bubble pulse frequencies are *precisely* equal to the "tuned" frequency of the internal structure. The effects of internal sloshing liquids are shown to be negligible because of the low natural fundamental sloshing frequency associated with larger liquid tanks.

Several of the selected modeling techniques are shown by comparison with actual test data to be questionable. Firstly, the representation of hydrodynamic forces solely by a Morison's equation approach fails to fully account for the expected vortex shedding and convection forces during the transient vibration. The selection procedure (or more appropriately, the calculation procedure) of hydrodynamic coefficients appropriate for ship whipping must be better understood and implemented. Mere extrapolation of known data based upon harmonic, low frequency motion of small scale cylinders and flat plates is

probably inaccurate. A more robust model for hydrodynamic forces, coupling numerical simulation with experimental verification should be developed.

A second modeling technique of questionable success is the bubble pulsation and migration equations used to produce the free-field fluid velocities and accelerations. Because the model does not account for proper dissipation of energy by the pulsating explosion bubble, it is believed that the model over predicts fluid loading after the 2nd bubble period. A more robust model for fluid loading from the pulsation of the explosion bubble, again, coupling numerical simulation with experimental verification should be more successful.

Finally, the general nature of the line-structure model for the ship structural and hydrodynamic interaction (i.e. the fluid-structure interaction) introduces geometric errors, particularly when the explosion is close aboard. A more robust, 3-dimensional fluid-structure interaction solution would be more precise for the solution process.

Even with several questionable physical models for particular aspects of the whipping model, comparison with test data shows that the model provides reasonable results, particularly in early-time response. It is believed that the general approach of solving the equations of motion directly in the time domain was reasonable and necessary. It is in the modeling of each individual component of the forces on the whipping ship where future work should be concentrated.

REFERENCES (Listed alphabetically)

Abramson, H.N. (ed.), *The Dynamic Behavior of Liquids in Moving Containers, NASA SP-106*, 1966.

Anaturk, A.R., "An experimental investigation to measure hydrodynamic forces at small amplitudes and high frequencies", *Applied Ocean Research*, 13,4, 1991, pp. 200-208.

Anaturk, A.R., Tromans, P.S., vanHazendonk, H.C., Sluis, C.M., and Otter, A., "Drag forces on cylinders oscillating at small amplitude; a new model", *Journal of Offshore Mechanics and Arctic Engineering*, 114, 1992, pp. 91-103.

Argyris, J., and Mlejnek, J.P., *Dynamics of Structures*, Elsevier Science Publishers, The Netherlands, 1991.

Barltrop, N.D.P., and Adams, A.J., *Dynamics of Fixed Marine Structures*, Third edition, Butterworth/Heinemann, 1991.

Batchelor, G.K., *An Introduction to Fluid Dynamics*, Cambridge University Press, London, 1973.

Bathe, K.J., and Gracewski, S., "On nonlinear dynamic analysis using substructuring and mode superposition", *Computers and Structures*, Vol. 13, 1981, pp. 699-707.

Bathe, K.J., *Finite Element Procedures in Engineering Analysis*, Prentice-Hall, Englewood Cliffs, NJ, 1982.

Bauer, H.F., "Theory of the fluid oscillations in a circular ring tank partially filled with liquid", *NASA Technical Note D-557*, 1960.

Bauer, H.F., "Nonlinear mechanical model for the description of propellant sloshing", *AIAA Journal*, Vol. 4, No. 9, 1966.

Bearman, P.W., Downie, M.J., Graham, J.M.R., and Obasaju, E.D., "Forces on cylinders in viscous oscillatory flow at low Keulegan-Carpenter numbers", *Journal of Fluid Mechanics*, 154, 1985, pp. 344-345.

Bearman, P.W., Lin, X.W., and Mackwood, P.R., "Measurement and prediction of response of circular cylinders in oscillating flow", *Proceedings of the 6th International Conference on the Behavior of Offshore Structures (BOSS)*, 1992, pp. 297-307.

Bishop, R.E.D., and Price, W.G., *Hydroelasticity of Ships*, Cambridge University Press, Cambridge, UK, 1979.

Chakrabarti, S.K., and Cotter, D.C., "Hydrodynamic coefficients of mooring tower", *Proceedings of the 15th Annual Offshore Technology Conference, OTC 4496*, 1983, pp. 449-458.

Chakrabarti, S.K., *Hydrodynamics of Offshore Structures*, Springer-Verlag, London, 1987.

Chakrabarti, S.K., *Nonlinear Methods in Offshore Engineering*, Elsevier, New York, 1990.

Chorin, A.J., "Numerical study of slightly viscous flow", *Journal of Fluid Mechanics*, 57, 1973, pp. 785-796.

Clements, R.R., and Maull, D.J., "The representation of sheets of vorticity by discrete vortices", *Progress in Aerospace Science*", Vol. 116, No. 2, 1975, pp. 129-1456.

Clough, R.W., and Penzien, J., *Dynamics of Structures* (Second edition), McGraw-Hill, New York, 1993.

Cole, R.H., *Underwater Explosions*, Princeton University Press, Princeton, NJ, 1948.

Cook, M.F., and Vandiver, J.K., "Measured and Predicted Dynamic Response of a Single Pile Platform to Random Wave Excitation", *Proceedings of the 14th Offshore Technology Conference, OTC 4285*, 1982, pp. 637-645.

Dalzell, J.F., "Liquid impact on tank bulkheads", *The Dynamic Behavior of Liquids in Moving Containers, NASA SP-106*, H.N. Abramson (ed.), 1966.

Den Hartog, J.P., *Mechanical Vibrations* (4th edition), McGraw-Hill, New York, 1956.

Doyle, J.F., *Static and Dynamic Analysis of Structures*, Kluwer Academic Publishers, Boston, 1991.

Faltinsen, O.M, and Pettersen, B., "Application of a vortex tracking method to separated flow around marine structures", *Journal of Fluids and Structures*, 1, 1987, pp. 217-237.

Faltinsen, O.M., and Sortland, B., "Slow-drift eddy making damping of a ship", *Applied Ocean Research*, 9,1, 1987, pp. 37-46.

Faltinsen, O.M., *Sea Loads on Ships and Offshore Structures*, Cambridge University Press, UK, 1990.

Fine, N., *In-Fluid Damping of Submarine Hull Vibrations* (unpublished report), Engineering Technology Center, Groton, CT, 1994.

Friedman, B., "Theory of the Underwater Explosion Bubbles", *Underwater Explosions Research, Vol. II, The Gas Globe,* Office of Naval Research, 1950.

Graham, J.M.R., "The forces on sharp-edged cylinders in oscillatory flow at low Keulegan-Carpenter numbers", *Journal of Fluid Mechanics*, 97, 1980, pp. 331-346.

Herring, C., "Theory of the Pulsations of the Gas Bubble Produced by an Underwater Explosion", *Underwater Explosions Research, Vol. II, The Gas Globe,* Office of Naval Research, 1950.

Hicks, A.N., "The Theory of Explosion-Induced Ship Whipping", *Naval Construction Research Establishment, NCRE Report R579*, 1972.

Hicks, A.N., "Explosion Induced Hull Whipping", *Advances in Marine Structures,* Admiralty Research Establishment, Dunfermline, Scotland, UK, 1986.

Hughes, O.F., *Ship Structural Design,* SNAME, Jersey City, NJ, 1988.

Hunt, J.B., *Dynamic Vibration Absorbers*, Mechanical Engineering Publications, London, 1979.

Hutton, R.E., "An investigation of resonant, nonlinear non-planar free surface oscillations of a fluid", *NASA Technical Note D-1870*, 1963.

Kaliske, M., Jagusch, J., Gebbeken, N., and Rothert, H., "Damping models in finite element computations", *Structural Dynamics - Proceedings of the 2nd European Conference on Structural Dynamics (Vol. I)*, Rotterdam, 1993.

Korenev and Reznikov, *Dynamic Vibration Absorbers,* John Wiley and Sons, NY, 1993.

Laya, E.J., Conner, M., and Sunder, S.S., "Hydrodynamic forces on flexible offshore structures", *Journal of Engineering Mechanics*, ASCE, March 1984, pp. 433-448.

Lazan, B.J., *Damping of Materials and Members in Structural Mechanics,* Pergamon Press, New York, 1968.

Lecointe, Y., and Piquet, J., "Compact finite-difference methods for solving incompressible Navier-Stokes equations around oscillatory bodies", *Von Karman Institute for Fluid Dynamics Lecture Series 1985-04, Computational Fluid Dynamics*, 1985.

Lewis, E.V. (Ed), *Principles of Naval Architecture,* SNAME, Jersey City, NJ, 1988.

MATLAB® High-Performance Numeric Computation and Visualization Software - User's Guide and Reference Manual, The Mathworks, Inc., Natick, MA, 1993.

McClintock, F.A., and Argon, A.S., *Mechanical Behavior of Materials*, Techbooks, Fairfax, VA, 1965.

Misovec, A., "Comments on SITE meeting of 5/10/94", (Unpublished meeting minutes), 1994, pp. 1-2.

Morison, J.R., O'Brien, M.P., Johnson, J.W., and Schaaf, S.A., "The force exerted by surface waves on piles", *Petroleum Transactions*, AIME, 189, 1950, pp. 149-157.

Nashif, A.D., Jones, D.I.G., and Henderson, J.P., *Vibration Damping,* John Wiley and Sons, NY, 1985.

Newman, J.N., "Algorithms for the free surface Green function", *Journal of Engineering Mathematics*, 19, 1985- pp. 57-67.

Newman, J.N., *Marine Hydrodynamics*, The MIT Press, Cambridge, MA, 1986.

Newmark, N.M., "A method of computation for structural dynamics", *American Society of Civil Engineers Transactions*, Vol. 127, 1962, pp. 1406-1435.

Rao, S., *Mechanical Vibrations,* Addison-Wesley Publishing Co. , Reading, MA, 1990.

Ross, C.T.F., *Advanced Applied Stress Analysis*, John Wiley and Sons, New York, 1987.

Salveson, N., Tuck, E.O., and Faltinsen, O.M., "Ship motions and sea loads", *SNAME Transactions*, Vol. 78, 1970, pp. 250-279.

Sarpkaya, T., "In-line and transverse forces on cylinders in oscillating flow at high Reynolds' numbers", *Proceedings of the 8th Offshore Technology Conference*, OTC 2533, 1976, pp. 95-108.

Sarpkaya, T., "Force on a cylinder in viscous oscillatory flow at low Keulegan-Carpenter numbers", *Journal of Fluid Mechanics*, Vol. 165, 1986, pp. 61-71.

Sarpkaya, T., "Computational methods with vortices - The 1988 Freeman Scholar Lecture", *Journal of Fluids Engineering*, Vol. 111, March 1989, pp. 5-45.

Silverman, S., and Abramson, H.N., "Damping of liquid motions an lateral sloshing", *The Dynamic Behavior of Liquids in Moving Containers, NASA SP-106*, H.N. Abramson (ed.), 1966.

Smith, J.W., *Vibration of Structures - Applications in Civil Engineering Design,* Chapman and Hall, London, 1988.

Smith, P.A., and Stansby, P.K., "Impulsively started flow around a circular cylinder by the vortex method", *Journal of Fluid Mechanics*, 194, 1988, pp. 45-77.

Spidsoe, N., and Karunkaran, D., "Nonlinear effects of damping to dynamic amplification factors for drag-dominated offshore platforms", *Proceedings of the 11th International Conference on Offshore Mechanics and Arctic Engineering*, ASME, 1992, pp. 231-239.

Stansby, P.K., and Dixon, A.G., "Simulation of flows around cylinders by a Lagrangian vortex scheme", *Applied Ocean Research*, Vol. 5, No. 3, 1983, pp. 167-178.

Stuart, J.T., "Double boundary layers in oscillatory viscous flow", *Journal of Fluid Mechanics*, 24, 1966, pp. 673-687.

Suzuki, H., and Yoshida, K., "Three-dimensional nonlinear dynamic analysis method of underwater line structure and its validation", *Proceedings of the 10th International Conference on Offshore Mechanics and Arctic Engineering*, ASME, 1991, pp. 87-94.

Taylor, G.I., "Vertical Motion of a Spherical Bubble and the Pressure Surrounding It", *Underwater Explosions Research, Vol. II, The Gas Globe*, Office of Naval Research, 1950.

Taylor, R.E., and Duncan, P.E., "Fluid-induced inertia and damping in vibrating offshore structures", *Dynamic Analysis of Offshore Structures: Recent Developments*, CML Publications, Southampton, UK, 1982.

Vandiver, J.K., and Mitome, S., "Effect of liquid storage tanks on the dynamic response of offshore platforms", *Dynamic Analysis of Offshore Structures: Recent Developments*, CML Publications, Southampton, 1982.

Wehausen, J.V., and Laitone, E.V., "Surface waves", *Encyclopedia of Physics (Vol. 9)*, Springer-Verlag, Berlin, 1960.

Welt, F., and Modi, V.J., "Vibration damping through liquid sloshing", *Diagnostics, Vehicle Dynamics and Special Topics: 12th Biennial Conference on Mechanical Vibrations and Noise*, ASME, 1989.

Wilkerson, S.A., "Elastic Whipping Response of Ships to an Underwater Explosion Loading", *Master of Science in Engineering Thesis*, George Washington University, 1985.

Wilson, J.F. (ed.), *Dynamics of Offshore Structures*, John Wiley and Sons, New York, 1984.

Wong, L.H., and Calisal, S.M. "A numerical solution for potential flows including the effects of vortex shedding", *Proceedings of the 11th International Conference on Offshore Mechanics and Arctic Engineering*, ASME, 1992, pp. 363-368.

Yeung, R.W., and Wu, C., "Viscosity effects on the radiation hydrodynamics of two-dimensional cylinders", *Proceedings of the 10th International Conference on Offshore Mechanics and Arctic Engineering*, ASME, 1991, pp. 309-316.

APPENDIX A

MATLAB® ROUTINES

```
% Subroutine IN.M
%
% This matlab subroutine is written as an INPUT FILE for all other MATLAB
% subroutines. Data is loaded from formatted batch-type input files using
% the MATLAB "load" command, and arrays and constants are generated for
% the other MATLAB subroutines.
%
% MISCELLANEOUS/DEFAULT VALUES
%
% Number of hull stations or finite beam elements
NE=19;
% Number of hull sections or finite beam nodes
NNODES=20;
% Number of degrees of freedom (4 DOF at each node)
NDOF=4*NNODES;
%
%
% PROPERTIES OF EACH FINITE BEAM ELEMENT
load element.dat
%
% Element number
e=element(1,:);
% Cross-sectional area of element (in2)
Ae=element(2,:);
% Length of element (ft)
Le=element(3,:);
% Area effective in y-directed shear (in2)
Asy=element(4,:);
% Area effective in z-directed shear (in2)
Asz=element(5,:);
% Second moment of area about y-axis (in2ft2)
Iay=element(6,:);
% Second moment of area about z-axis (in2ft2)
Iaz=element(7,:);
% Y-distance from the neutral axis to the outer fiber of the crown (ft)
Yc=element(8,:);
% Y-distance from the neutral axis to the outer fiber of the keel (ft)
Yk=element(9,:);
% Z-distance from the centerline to the outer fiber of the port hull (ft)
Zp=element(10,:);
% Z-distance from the centerline to the outer fiber of the stbd hull (ft)
Zs=element(11,:);
%
%
% PROPERTIES OF EACH HULL SECTION (NODE)
load node.dat
%
% Node number
nnode=node(1,:);
% Length of each hull section (ft)
Lh=node(2,:);
% Weight of hull section (i.e. in air) (lton)
wh=node(3,:);
% mass of hull section (lbf-sec2/ft=slug)
```

```
mh=wh*2240./32.174;
% Buoyancy of hull section (displacement of salt water) (lton)
bh=node(4,:);
% Weight moment of inertia of hull section about y-axis (lton-ft2)
Imyh=node(5,:);
% Mass moment of inertia of hull section about y-axis (slug-ft2)
Imy=Imyh*2240./32.174;
% Weight moment of inertia of hull section about z-axis (lton-ft2)
Imzh=node(6,:);
% Mass moment of inertia of hull section about z-axis (slug-ft2)
Imz=Imzh*2240./32.174;
% Maximum section beam of main hull perp. to motion in z direction (ft)
Bz=node(7,:);
% Maximum section beam of main hull perp. to motion in y direction (ft)
By=node(8,:);
% Cross-sectional area of Appended hull (appended portion of each section)
% perp. to motion in y direction (ft2)
Aapy=node(9,:);
% Cross-sectional area of Appended hull (appended portion of each section)
% perp. to motion in z direction (ft2)
Aapz=node(10,:);
% Width of Appended hull perp. to motion in y direction (ft)
Dapy=node(11,:);
% Width of Appended hull perp. to motion in z direction (ft)
Dapz=node(12,:);
% Length of Appended hull perp. to motion in y direction (ft)
Lapy=node(13,:);
% Length of Appended hull perp. to motion in z direction (ft)
Lapz=node(14,:);
%
% Hydrodynamic coefficients (non-dimensional)
%
% Added mass, inertia, and drag coefficients for each main hull section
% for motion in vertical (y) and horizontal (z) directions
Ca1y=node(15,:);
Ca1z=node(16,:);
Cm1y=node(17,:);
Cm1z=node(18,:);
Cd1y=node(19,:);
Cd1z=node(20,:);
% Added mass, inertia, and drag coefficients for appended hull sections
% (appended portion of each hull section) for motion in y and z directions
Ca2y=node(21,:);
Ca2z=node(22,:);
Cm2y=node(23,:);
Cm2z=node(24,:);
Cd2y=node(25,:);
Cd2z=node(26,:);
%
%
% MISCELLANEOUS INPUT
load misc.dat
%
% Acceleration due to gravity (ft/sec2)
```

```
g=misc(1);
% Density of salt water (lbf-sec2/ft4=slugs/ft3)
rho=misc(2);
% Young's modulus for steel (lbf/in2)
E=misc(3);
% Poisson ratio for steel (non-dimensional)
Nu=misc(4);
% Yield stress for steel (lbf/in2)
Sigy=misc(5);
% Shear modulus for steel (lbf/in2)
G=misc(6);
% Assumed material (hysteresis) modal viscous damping coefficients for
% all low frequency (fundamental) flexural "dry" modes (non-dimensional)
damp=misc(7);
% Whipping mode to scale as initial condition for use in FREEWHIP.M
MODE=misc(8);
% Switch to determine whether or not "wet" whipping is used in FREEWHIP.M
WET=misc(9);
% Node numbers to plot displacements,velocities,accelerations
NODE1=misc(10);
NODE2=misc(11);
NODE3=misc(12);
NODE4=misc(13);
% Element numbers to plot strains
ELEMENT1=misc(14);
ELEMENT2=misc(15);
ELEMENT3=misc(16);
%
% Input parameters for Newmark time integration algorithms
%
% time step (sec)
dt=misc(17);
% gamma parameter (non-dimensional)
gammap=misc(18);
% beta parameter (non-dimensional)
betap=misc(19);
% time limit (sec)
tmax=misc(20);
% vector norm tolerance
tol=misc(21);
%
% Input for internal vibration absorbers
%
% "Reasonable" weight of an absorber or internal structure (lton)
wa=misc(22);
% mass of absorber or internal structure (slug)
ma=wa*2240/32.174;
% Node number where absorber is "attached" to the hull
nabs=misc(23);
%
% Input for internal sloshing tank
%
% "Reasonable" weight of liquid in a (large) internal tank (lton)
wl=misc(24);
```

```
% mass of liquid (slug)
Ml=wl*2240./32.174;
% "Reasonable" aspect ratio of tank depth/width (h/a) (non-dimensional)
ha=misc(25);
% Node number where tank is "attached" to the hull
ntank=misc(26);
%
% Input for explosion bubble dynamics
%
% Initial depth of charge (ft)
Dchg=misc(27);
% Charge weight of TNT (lb)
Wchg=misc(28);
% Initial location of charge relative to ship hull (in hull coordinate system)
xchg=misc(29);
ychg=misc(30);
zchg=misc(31);
% Initial depth of the ship (ft)
Dship=misc(32);
```

```
% SUBROUTINE HULL.M
%
% This subroutine performs the following:
%       1. Calculates the global mass and stiffness matrices (K and M)
%              for the 3-D beam finite element formulation (ignoring axial
%              and torsional effects).
%       2. Solves the generalized eigenvalue problem to obtain the
%              "dry mode" eigenvalues (natural freqs squared) and
%              corresponding eigenvectors ("dry mode" shapes).
%       3. Calculates the Rayleigh coefficients for critical hull
%              (structural and hull hysteresis) damping defined by
%              the 1st and 3rd lowest fundamental flexural modes.
%       4. Calculates the equivalent viscous hull damping matrix for the
%              calculated Rayleigh coefficients.
%       5. Calculates vectors for modal mass, modal damping, and
%              modal stiffness (for N modes) corresponding to the "dry
%              mode" shape vectors.  These are used for optimization
%              of internal absorber and liquid sloshing dampers (tanks)
%              in other subroutines.
%       6. Provides for validation against the "exact" solution given by
%              Rao (chapter 8) for a continuous uniform free-free beam.
%              The natural frequencies of the finite element solution
%              can be compared to the natural frequencies of the
%              "exact" solution.  This may be disabled after validation
%              by placing % before each calculation.
%
% (1)
% Formulate the global (hull) stiffness and mass matrices (K and M).
%
% Initialize K and M
K=zeros(NDOF);
M=zeros(NDOF);
%
% Determine the global stiffness matrix (lbf/ft for translation or or lbf-ft for rotation)
%
% Determine the element stiffness matrices (KE)
%
% Step through each of the 19 elastic beam elements
for e=1:NE
        %
        Py=(12*E*Iaz(e))/(G*Asy(e)*Le(e)^2);
        Pz=(12*E*Iay(e))/(G*Asz(e)*Le(e)^2);
        bz=E*Iaz(e)/((1+Py)*Le(e)^3);
        by=E*Iay(e)/((1+Pz)*Le(e)^3);
        K11=[12*bz 0 0 6*bz*Le(e); 0 12*by -6*by*Le(e) 0;
                0 -6*by*Le(e) (4+Pz)*by*Le(e)^2 0; 6*bz*Le(e) 0 0 (4+Py)*bz*Le(e)^2];
        K21=[-12*bz 0 0 -6*bz*Le(e); 0 -12*by 6*by*Le(e) 0;
                0 -6*by*Le(e) (2-Pz)*by*Le(e)^2 0; 6*bz*Le(e) 0 0 (2-Py)*bz*Le(e)^2];
        K12=K21';
        K22=[12*bz 0 0 -6*bz*Le(e); 0 12*by 6*by*Le(e) 0;
                0 6*by*Le(e) (4+Pz)*by*Le(e)^2 0; -6*bz*Le(e) 0 0 (4+Py)*bz*Le(e)^2];

        KE=[K11 K12; K21 K22];
        %
```

```
            % Transform element stiffness matrices into their
            % global coordinate matrices
            for ie=1:8
                    for je=1:8
                            i=ie+4*(e-1);
                            j=je+4*(e-1);
                            K(i,j)=K(i,j)+KE(ie,je);
                    end
            end
    end
    %
    % Once each of the elastic beam elements has been considered and added.
    % the global (hull) stiffness matrix is K.
    %
    % Determine the global mass matrix (lbf-sec2/ft=slug for translation or  slug-ft2 for rotation)
    %
    % Step through each of the 20 nodes
    %
    for n=1:NNODES
            % Step through each of the 4 dof at each node and define the NODE mass matrix
                    MN(1,1)=mh(n);
                    MN(2,2)=mh(n);
                    MN(3,3)=Imy(n);
                    MN(4,4)=Imz(n);
            % Transform node mass matrices for each node into their global  coordinate matrices
                    for in=1:4
                            for jn=1:4
                                    i=in+4*(n-1);
                                    j=jn+4*(n-1);
                                    M(i,j)=M(i,j)+MN(in,jn);
                            end
                    end
    end
    %
    % Once each of the nodes has been considered, the global
    % mass matrix is M
    %
    % (2)
    % Solve the eigenvalue problem to obtain the "dry mode" natural frequencies  (square roots of
    % eigenvalues) and corresponding "dry mode" shape vectors  (eigenvectors).
    %
    % *** It should be noted that because the hull has 4 rigid body modes,
    %    the lowest 4 eigenvalues will be zero (zero natural frequency).
    %    These correspond to the lowest 4 eigenvectors which are the
    %    RIGID BODY mode shapes.  Thus, the lowest FLEXURAL mode
    %    would be mode n=5.
    %
    % "Phi1" is a (NxN) matrix whose columns are "dry mode" shape vectors.
    % "W1" is a diagonal (NxN) matrix whose diagonal elements are (square of  the natural frequencies).
    %  (Note: W is NOT necessarily defined in ascending order).
    %
    [Phi1,W1]=eig(K,M);
    %
    % Define a VECTOR of natural frequencies:
```

```
for r=1:NDOF
        w1(r)=sqrt(W1(r,r));
end
%
% Sort natural frequencies and define a vector of natural frequencies given  in ascending order:
[w2.i]=sort(w1);
% where "i" is a vector of indices such that w2=w1(i).
%
% Sort the matrix of eigenvectors (mode shapes) as columns in an order corresponding to ascending
% natural frequencies  (defined by index vector "i"):
for r=1:NDOF
        s=i(r);
        Phi2(:,r)=Phi1(:,s);
end
%
% Plot the 2 rigid body mode shapes and the first 4 flexural mode shapes corresponding to motion in the
% horizontal plane (for example):
% Step through the first 12 modes:
%for m=1:12
%       phi=Phi2(:,m);
%       for n=1:NNODES
%               nd(n)=n;
%               ny=1+4*(n-1);
%               nz=2+4*(n-1);
%               phiy(n)=phi(ny);
%               phiz(n)=phi(nz);
%       end
%       % For rigid body modes (m<=4):
%       if m<=4
%               figure(1)
%               if m<=2,  rbm=1;
%               elseif m<=4,  rbm=2;
%               end
%               if phiz(1)~=0
%                       subplot(2,1,rbm), plot(nd,phiz)
%                       axis([1 NNODES -1.0 1.0])
%                       title('Dry mode shape of rigid body mode in horizontal (y=0) plane')
%               end
%       % For flexural modes (m>4):
%       else
%               figure(2)
%               mcount=(m-4);
%               if mcount<=2
%                       flexmode=1;
%               elseif mcount<=4
%                       flexmode=2;
%               elseif mcount<=6
%                       flexmode=3;
%               else,   flexmode=4;
%               end
%               if phiz(1)~=0
%                       subplot(4,1.flexmode), plot(nd,phiz)
%                       axis([1 NNODES -1.0 1.0])
%                       title(['Dry mode shape of flexural mode ',int2str(flexmode),' in ...
```

```
%                           ...horizontal (y=0) plane'])
%                   end
%         end
% end
% Print "dry" mode shapes
%         figure(1)
%         set(gcf,'PaperPosition',[1.0, 4.5, 6.5, 4.0])
%         print
%         figure(2)
%         set(gcf,'PaperPosition',[1.0, 2.0, 6.5, 8.5])
%         print
%
%
% (3)
% Calculate the Rayleigh coefficients defined by the natural frequencies  of the 1st and 3rd flexural modes
% (1st and 2nd flexural mode for one of  the planes of motion - horizontal or vertical).  Ignoring the 4
% rigid body modes, these would be correspond to modes n=5 and n=7.
%
% Define the "dry mode" natural frequencies for modes 5 and 7:
w5=w2(5);
w7=w2(7);
%
% Find the Rayleigh coefficients using equation (3-16):
w57=[w7 -w5; -1/w7 1/w5];
damping=[damp; damp];
pre=2*(w5*w7)/(w7^2-w5^2);
coeff=pre*w57*damping;
alpha=coeff(1);
beta=coeff(2);
%
%
% (4)
% Calculate the equivalent viscous damping matrix for hull damping using the calculated Rayleigh
% coefficients:
%
C=alpha*M+beta*K;
%
%
% (5)
% Define the "dry" mode shape vectors and natural frequencies  and calculate vectors for modal mass
% (Mn), modal damping (Cn), and modal stiffness (Kn) corresponding to the "dry mode" mode
% shape vectors:
%
for n=1:NDOF
        phin=Phi2(:,n);
        phint=phin';
        Phi(:,n)=phin;          % "dry" mode shape vectors
        Mn(n)=phint*M*phin;     % modal mass vector
        Cn(n)=phint*C*phin;     % modal damping vector
        Kn(n)=phint*K*phin;     % modal stiffness vector
        w(n)=w2(n);             % "dry" natural frequencies
end
%
% (6)
```

```
% Validation of a sample finite element formulation (uniform beam) against the "exact" solution, for a
% defined axisymmetric (about x-axis) beam arrangement.
%
% The "exact" solution is given by Rao (Chapter 8) for a uniform, continuous
% free-free beam with axisymmetry about the x-axis. This "exact" solution
% does not include shear effects, so the approximate solution should
% provide natural frequencies which are slightly lower than the "exact".
%
% Natural frequencies for the "exact" solution for the first 3 transverse flexural modes (modes 1,2,3):
%
%       Bnl1=4.73;
%       Bnl2=7.85;
%       Bnl3=11.0;
%       rho=mh(1)/Lh(1);
%       Sqroot=sqrt((E*Iay(1))/(rho*(Lh(1)*NE)^4));
%       omega1=(Bnl1^2)*Sqroot;
%       omega2=(Bnl2^2)*Sqroot;
%       omega3=(Bnl3^2)*Sqroot;
%
% Compare "exact" solution to the (approximate) numerical solution.
% For approximate solution, rigid body modes are ignored and the 1st, 2nd
% and 3rd flexural modes for transverse displacement (in each plane (y=0,z=0))
% are considered. It should be noted that because of axisymmetry, natural
% frequencies and mode shapes in each plane should be the same
% (i.e. repeated eigenvalues).
%
%               w1=w(5);
%               w2=w(7);
%               w3=w(9);
% Compare
%       omega1
%       w1
%       omega2
%       w2
%       omega3
%       w3
```

```
% SUBROUTINE WETMODE.M  (called as a MATLAB function)
%
% This subroutine performs the following:
%       1.  Calculates the fluid added mass matrix for the submarine
%               using a Morison equation approach (i.e. strip theory). This
%               approach includes added mass effects in the translational
%               degrees of freedom only (rotational fluid added mass effects
%               are not included).
%       2.  Adds the fluid added mass matrix to the hull mass matrix (subroutine
%               HULL.M) and solves the generalized eigenvalue problem to obtain
%               the "wet mode" eigenvalues (natural frequencies squared) and
%               corresponding "wet mode" eigenvectors ("wet mode" shapes).
%       3.  Calculates vectors for "wet" modal mass, modal damping, and modal
%               stiffness (for N modes) corresponding to the "wet mode" shape
%               vectors.  These are used for optimization of internal absorber
%               and liquid sloshing dampers (tanks) in other subroutines.
%
%
% (1)
% Calculate the fluid added mass matrix (lbf-sec2/ft=slug for translation).
%
% Initialize the fluid added mass matrix
Ma=zeros(NDOF);
%
% Step through each of the 20 hull sections (nodes) and define the NODE  fluid added mass matrices:
for n=1:NNODES
        % Calculate the fluid added mass associated with the main hull (Ma1)
        % and the appended hull (Ma2)
        %
        % Step through each of the 4 dof at each node and define the NODE
        % fluid added mass matrices for the main hull and appended hull
                MNa1(1,1)=rho*(pi*By(n)^2/4)*Ca1y(n)*Lh(n);
                MNa2(1,1)=rho*Aapy(n)*Ca2y(n)*Lapy(n);
                MNa1(2,2)=rho*(pi*Bz(n)^2/4)*Ca1z(n)*Lh(n);
                MNa2(2,2)=rho*Aapz(n)*Ca2z(n)*Lapz(n);
                MNa1(3,3)=0;
                MNa2(3,3)=0;
                MNa1(4,4)=0;
                MNa2(4,4)=0;
        % Transform NODE fluid added matrices into their global coordinate matrices
                for in=1:4
                        for jn=1:4
                                i=in+4*(n-1);
                                j=jn+4*(n-1);
                                Ma(i,j)=Ma(i,j)+MNa1(in,jn)+MNa2(in,jn);
                        end
                end
end
%
% Once each of the nodes has been considered, the global fluid added mass matrix is Ma
%
% (2)
% Add the fluid added mass matrix to the hull mass matrix and solve the generalized eigenvalue
% problem to obtain the "wet mode" eigenvalues (natural frequencies squared) and corresponding
```

```
% "wet mode" eigenvectors ("wet mode" shapes).
%
% Total mass matrix (Mt):
Mt=M+Ma;
%
% "Phi1" is a (NxN) matrix whose columns are "wet mode" shape vectors.
% "W1" is a diagonal (NxN) matrix whose diagonal elements are (square of  the "wet" natural
% frequencies). (Note: W is NOT necessarily defined in ascending order).
%
[Phi1,W1]=eig(K,Mt);
%
% Define a VECTOR of natural frequencies:
for r=1:NDOF
        w1(r)=sqrt(W1(r,r));
end
%
% Sort natural frequencies and define a vector of "wet" natural frequencies given in ascending order:
[w2,i]=sort(w1);
% where "i" is a vector of indices such that w2=w1(i).
%
% Sort the matrix of eigenvectors ("wet" mode shapes) as columns in an order corresponding to ascending
% "wet" natural frequencies (defined by index vector "i"):
for r=1:NDOF
        s=i(r);
        Phi2(:,r)=Phi1(:,s);
end
%
% Plot the 2 rigid body "wet" mode shapes and the first 4 flexural "wet" mode shapes corresponding to
% motion in the horizontal plane (for example):
% Step through the first 12 modes:
%for m=1:12
%       phi=Phi2(:,m);
%       for n=1:NNODES
%               nd(n)=n;
%               ny=1+4*(n-1);
%               nz=2+4*(n-1);
%               phiy(n)=phi(ny);
%               phiz(n)=phi(nz);
%       end
%       % For rigid body modes (m<=4):
%
%       if m<=4
%               figure(1)
%               if m<=2, rbm=1;
%               elseif m<=4, rbm=2;
%               end
%               if any(phiz)~=0
%                       subplot(2,1,rbm), plot(nd,phiz)
%                       axis([1 NNODES -1.0 1.0])
%                       title('Wet mode shape of rigid body mode in horizontal (y=0) plane')
%               end
%       % For flexural modes (m>4):
%       else
%               figure(2)
```

```
%                mcount=(m-4);
%                if mcount<=2
%                        flexmode=1;
%                elseif mcount<=4
%                        flexmode=2;
%                elseif mcount<=6
%                        flexmode=3;
%                else
%                        flexmode=4;
%                end
%                if phiz(1)~=0
%                        subplot(4,1,flexmode), plot(nd,phiz)
%                        axis([1 NNODES -1.0 1.0])
%                        title(['Wet mode shape of flexural mode ',int2str(flexmode),' in ...
%                        ...horizontal (y=0) plane'])
%                end
%        end
% end
% Print wet mode shapes
%        figure(1)
%        set(gcf,'PaperPosition',[1.0, 4.5, 6.5, 4.0])
%        print
%        figure(2)
%        set(gcf,'PaperPosition',[1.0, 2.0, 6.5, 8.5])
%        print
%
% (3)
% Define the "wet" mode shape vectors and natural frequencies  the first and calculate vectors for "wet"
% modal mass (Mnw), modal damping (Cnw), and modal stiffness (Knw)  corresponding to the "wet"
% mode shape vectors using equations (2-13):
%
for n=1:NDOF
        phin=Phi2(:,n);
        phint=phin';
        Phiw(:,n)=phin;                 % "wet" mode shape vectors
        Mnw(n)=phint*Mt*phin;           % "wet" modal mass vector
        Cnw(n)=phint*C*phin;            % "wet" modal damping vector
        Knw(n)=phint*K*phin;            % "wet" modal stiffness vector
        ww(n)=w2(n);                    % "wet" natural frequencies
end
%
%
%
```

```
% FREEWHIP.M
%
% This subroutine performs the following:
%       Calculates the response (nodal point displacements, velocities,
%               and accelerations) of the submarine during a
%               free vibration with initial displacements given by a
%               scaled mode shape vector for selected mode shapes.
%       Response is calculated using the Newmark time integration
%               method, with iteration conducted at each time step using a
%               Newton-Raphson method.
% Utilize the following:
%       - K,C,M,Phi calculated in HULL.M
%       - Hydrodynamic coefficients provided in IN.M
%       - Parameters for Newmark algorithm provided in IN.M
%
% Define nodes to use for response calculations
N(1)=NODE1;
N(2)=NODE2;
N(3)=NODE3;
N(4)=NODE4;
% Define elements to use for axial strain calculations
El1=ELEMENT1;
El2=ELEMENT2;
El3=ELEMENT3;
%
% Set initial and final times for Newmark integration, and limit on number
% of Newton-Raphson iterations at each time step
t=0;
tf=tmax;
jlimit=50;
%
% Initialize the loading forces on the hull
% Loading forces related to displacement
        Fdisp=zeros(1,NDOF)';
% Loading forces related to velocity
        Fvel=zeros(1,NDOF)';
% Loading forces related to acceleration
        Facc=zeros(1,NDOF)';
% Calculate (constant) static forces (i.e. hydrostatic/buoyancy and weight)
Fgrav=zeros(1,NDOF)';
Fhs=zeros(1,NDOF)';
for n=1:NNODES
        ny=(n-1)*4+1;
        % Hydrostatic/buoyancy force (lbf)
        Fhs(ny)=bh(n)*2240;
        % Static force of gravity/weight (lbf)
        Fgrav(ny)=-wh(n)*2240;
end
% Total loading forces
Floadt=Fdisp+Fvel+Facc+Fhs+Fgrav;
%
% Define initial conditions (displacements/velocities/accelerations)
% given by a scaled mode shape vector (for free whipping)
if MODE==1,  xt=(0.02)*sum(Lh)*Phi(:,6);
```

```
else,       xt=(0.02)*sum(Lh)*Phi(:,8);
end
%
xdt=zeros(1,NDOF)';
Minv=inv(M);
xddt=(Minv*(Floadt-C*xdt-K*xt));
%
% Perform the Newmark time integration
%
% Step through time
%
% Define constants to be used in Newton-Raphson iterations
c1=(1/(betap*dt^2));
c2=(1/(betap*dt));
c3=(1/(2*betap));
c4=(gammap/(betap*dt));
c5=gammap/betap;
c6=(1-gammap/(2*betap));
c7=(1/(2*betap)-1);
%
dx=zeros(1,NDOF)';
%
for i=1:300;
        t=t+dt
        % Set initial displacments,velocities,accelerations, and loading forces for
        % the current time step (equal to the final for the last time step)
        xj=xt;
        xdj=xdt;
        xddj=xddt;
        Floadj=Floadt;
        %
        % Perform Newton-Raphson iterations at current time step
        for j=1:jlimit
                %
                % Calculate loading forces for the current iteration
                for n=1:NNODES
                % Loading forces related to velocity
                        ny=4*(n-1)+1;
                        nz=4*(n-1)+2;
                        Fvel(ny)=-0.5*rho*By(n)*Cd1y(n)*xdj(ny)*abs(xdj(ny))*...
                        ...Lh(n)-0.5*rho*Dapy(n)*Cd2y(n)*xdj(ny)*abs(xdj(ny))*Lapy(n);
                        Fvel(nz)=-0.5*rho*Bz(n)*Cd1z(n)*xdj(nz)*abs(xdj(nz))*...
                        ...Lh(n)-0.5*rho*Dapz(n)*Cd2z(n)*xdj(nz)*abs(xdj(nz))*Lapz(n);
                % Loading forces related to acceleration
                        Facc(ny)=-rho*(pi*By(n)^2/4)*Ca1y(n)*Lh(n)*...
                        ...xddj(ny)-rho*Aapy(n)*Ca2y(n)*Lapy(n)*xddj(ny);
                        Facc(nz)=-rho*(pi*Bz(n)^2/4)*Ca1z(n)*Lh(n)*...
                        ...xddj(nz)-rho*Aapz(n)*Ca2z(n)*Lapz(n)*xddj(nz);
                end
                %
                % Total loading force for the current iteration
                Floadj=Fdisp+Fvel+Facc+Fhs+Fgrav;
                %
                % Calculate Jacobian matrices for each of the loading forces
```

```
% (square diagonal matrices for this formulation)
dFdxdj1=zeros(1,NDOF)';
dFdxddj1=zeros(1,NDOF)';
dFdxj=zeros(NDOF);
dFdxdj=zeros(NDOF);
dFdxddj=zeros(NDOF);
dxdj=zeros(1,NDOF)';
dxddj=zeros(1,NDOF)';
for n=1:NNODES
        ny=4*(n-1)+1;
        nz=4*(n-1)+2;
        dxdj(ny)=0.01;
        dxdj(nz)=0.01;
        dxddj(ny)=0.01;
        dxddj(nz)=0.01;
        dFdxdj1(ny)=...
        ...(-0.5*rho*By(n)*Cd1y(n)*(xdj(ny)+dxdj(ny))*abs(xdj(ny)+dxdj(ny))*...
        ...Lh(n)-
0.5*rho*Dapy(n)*Cd2y(n)*(xdj(ny)+dxdj(ny))*abs(xdj(ny)+dxdj(ny))*...
        ...Lapy(n)-Fvel(ny))/dxdj(ny);
        dFdxdj1(nz)=...
        ...(-.5*rho*Bz(n)*Cd1z(n)*(xdj(nz)+dxdj(nz))*abs(xdj(nz)+dxdj(nz))*...
        ...Lh(n)-
0.5*rho*Dapz(n)*Cd2z(n)*(xdj(nz)+dxdj(nz))*abs(xdj(nz)+dxdj(nz))*...
        ...Lapz(n)-Fvel(nz))/dxdj(nz);
        dFdxddj1(ny)=(-rho*(pi*By(n)^2/4)*Ca1y(n)*Lh(n)*...
        ...(xddj(ny)+dxddj(ny))-rho*Aapy(n)*Ca2y(n)*Lapy(n)*...
        ...(xddj(ny)+dxddj(ny))-Facc(ny))/dxddj(ny);
        dFdxddj1(nz)=(-rho*(pi*Bz(n)^2/4)*Ca1z(n)*Lh(n)*...
        ...(xddj(nz)+dxddj(nz))-rho*Aapz(n)*Ca2z(n)*Lapz(n)*...
        ...(xddj(nz)+dxddj(nz))-Facc(nz))/dxddj(nz);
end
for n=1:NDOF
        dFdxdj(n,n)=dFdxdj1(n);
        dFdxddj(n,n)=dFdxddj1(n);
end
%
% Calculate residuals
f1j=M*(c1*(xj-xt)-c2*xdt-c3*xddt)+C*(c4*(xj-xt)-c5*xdt+c6*xddt*dt)+...
...K*(xj-xt)-Floadj+Floadt;
f2j=xdj-c4*(xj-xt)+(c5-1)*xdt-c6*dt*xddt;
f3j=xddj-c1*(xj-xt)+c2*xdt+c7*xddt;
%
% Solve for the displacement correction (dx)
%
A1=(c1*M+c4*C+K-c1*dFdxddj-c4*dFdxdj-dFdxj);
A1inv=inv(A1);
A2=-f1j-dFdxdj*f2j-dFdxddj*f3j;
dx=(A1inv*A2);
%
% Calculate the next iteration's displacements, velocities, and accelerations
%
xj=xj+dx;
xdj=xdj+(c4*dx)-f2j;
```

```
                xddj=xddj+(c1*dx)-f3j;
                %
                % Check to see if all Norms of residuals are less than tolerance for
                % the current iteration
                % (If so, go to the next time step)
                Normf1j=norm(f1j);
                Normf2j=norm(f2j);
                Normf3j=norm(f3j);
                if Normf1j<=tol & Normf2j<=tol & Normf3j<=tol
                        %
                        % Save current time, displacements, velocities,
                        % and accelerations (at specified nodes) for later plotting
                        time(i)=t;
                        % Displacements/velocities/accelerations
                        for n=1:4
                                Dh(n)=(N(n)-1)*4+2;
                        end
                        X1(i)=xj(Dh(1));
                        Xd1(i)=xdj(Dh(1));
                        Xdd1(i)=xddj(Dh(1));
                        X2(i)=xj(Dh(2));
                        Xd2(i)=xdj(Dh(2));
                        Xdd2(i)=xddj(Dh(2));
                        X3(i)=xj(Dh(3));
                        Xd3(i)=xdj(Dh(3));
                        Xdd3(i)=xddj(Dh(3));
                        X4(i)=xj(Dh(4));
                        Xd4(i)=xdj(Dh(4));
                        Xdd4(i)=xddj(Dh(4));
                        %
                        Dh19=(19-1)*4+2;
                        Dh18=(18-1)*4+2;
                        Fvel18(i)=Fvel(Dh18);
                        Facc18(i)=Facc(Dh18);
                        Fload18(i)=Floadj(Dh18);
                        Fvel19(i)=Fvel(Dh19);
                        Facc19(i)=Facc(Dh19);
                        Fload19(i)=Floadj(Dh19);
                        %
                        % Save the current time step displacements, velocities, and
                        % accelerations, and forces for use in the next time step
                        xt=xj;
                        xdt=xdj;
                        xddt=xddj;
                        Floadt=Floadj;
                        break, end
                end
        if j==jlimit, break, end
        end
if j==jlimit, break, end
if t>=tf, break, end
end
```

```
% Subroutine BUBBLE.M
%
% This subroutine performs the following:
%       1. Computes the time histories of the explosion bubble radius (rad)
%               and bubble depth (depth) by integration of the differential
%               equations governing bubble dynamics.
%               Computation is carried out for specified bubble initial conditions
%               (i.e. initial depth of the charge (Dchg) and weight of the
%               charge (Wchg)).
%
%
function[TM,BR,BD,BRD,BDD,BRDD,BDDD,DEL,btime,brad,bdpth,bvel,L1,T1]=...
...bubble(Dchg,Wchg,tmax)
%
% Define constants
%
% Drag coeff. for bubble
Cd=2.25;
% Initial bubble head (ft)
D0=Dchg+33;
% Adiabatic gas exponent for TNT
g1=1.25;
% Constant for TNT
k1=(0.0552)*D0^0.25;
% Length scale constant
L1=13.67*(Wchg/D0)^(1/3);
% Time scale constant
T1=2.94*(Wchg^(1/3)/D0^(5/6));
% Misc. constants
c1=33/L1;
c2=D0/L1;
c3=(g1-1)*k1;
c4=3*g1+1;
%
% Define initial and final conditions
%
% Non-dim. bubble radius
x0=k1^(4/3)*(1+(4*k1^4)/3);
% Non-dim. bubble depth
y0=c2;
% Rate of change of bubble radius
xd0=0;
% Rate of change of bubble depth
yd0=0;
% Non-dim. start time (i.e. 0 seconds)
T0=0.0;
% Non-dim. end time (i.e. tmax seconds)
Tf=tmax/T1;
% Non-dimensional time step
dT=(5.0*x0^4)/Tf;
% Integration time step parameter
tsp=10.;
%
% Perform Runge-Kutta time iteration
```

```
%
T=T0;
x=x0;
y=y0;
xd=xd0;
yd=yd0;
%
M=3000;  % defined maximum number of time steps (for control)
%
for m=1:M
        % Call the differential eqn. for bubble radius
        [x,xd]=radfn(dT,x,xd,y,yd,c1,c2,c3,c4,Cd);
        xdd=-1.5/(1-x/(2*(y-c1)))*((xd^2/x)*(1-2*x/(3*(y-c1)))-yd^2/(6*x)+y/(x*c2)-c3/(x^c4)+...
        ...(x/(4*(y-c1)^2))*(xd*yd/3-x/c2+Cd*yd^2/4));
        % Call the differential eqn. for bubble depth
        [y,yd]=dpthfn(dT,x,xd,y,yd,xdd,c1,c2,c3,c4,Cd);
        ydd=-3*(1/c2+xd*yd/x-(Cd*yd^2)/(4*x)+(x/(4*(y-c1)^2))*(3*xd^2+x*xdd));
        %
        % Save the current bubble characteristics for plotting and later use
        %
        TM(m)=T;  % non-dim. time
        BR(m)=x;  % non-dim. bubble radius
        BD(m)=y;  % non-dim. bubble depth
        BRD(m)=xd;  % non-dim. rate of change of bubble radius
        BDD(m)=yd;  % non-dim. rate of change of bubble depth (bubble velocity)
        BRDD(m)=xdd;
        BDDD(m)=ydd;
        DEL(m)=(y-c1);  % non-dim. suface pressure
        %
        btime(m)=T*T1;  % dimensional time
        brad(m)=x*L1;  % dimensional bubble radius
        bdpth(m)=(y-c1)*L1;  % dimensional bubble depth
        bvel(m)=yd*L1/T1;  % dimensional bubble velocity
        %
        % Go to next time increment
        x3=x^3;
        x3d=3.0*(x^2)*xd;
        x3dd=3.0*x*(x*xdd+2.0*xd^2);
        dT=2.0/(abs(x3dd)*3.0*tsp);
                if dT<0.001, dT=0.001;
                elseif dT>0.025, dT=0.025;
                end
        T=T+dT;
                if T>Tf, break
                end
end
%
% Plot the results
%
figure(1)
subplot(3,1,1), plot(btime,brad)
title('Bubble radius vs. time')
xlabel('Time (sec)')
ylabel('Bubble radius (ft)')
```

```
subplot(3,1,2), plot(btime,-bdpth)
title('Bubble depth vs. time')
xlabel('Time (sec)')
ylabel('Bubble depth (- ft)')
subplot(3,1,3), plot(btime,-bvel)
title('Upward bubble velocity vs. time')
xlabel('Time (sec)')
ylabel('Upward bubble velocity (ft/s)')
set(gcf,'PaperPosition',[1.0, 2.0, 6.5, 8.5])
% print
```

```
% RADFN.M
%
% Function M-file for calculation of the bubble radius
% (i.e. contains the bubble radius governing equation for use in BUBBLE.M)
%
function [x,xd]=radfn(dT,x,xd,y,yd,c1,c2,c3,c4,Cd)
ak1=dT*rfunc(x,xd,y,yd,c1,c2,c3,c4,Cd);
ak2=dT*rfunc(x+dT*xd/2.0,xd+ak1/2.0,y,yd,c1,c2,c3,c4,Cd);
ak3=dT*rfunc(x+dT*xd/2.0+dT*ak1/4.0,xd+ak2/2.0,y,yd,c1,c2,c3,c4,Cd);
ak4=dT*rfunc(x+dT*xd+dT*ak2/2.0,xd+ak3,y,yd,c1,c2,c3,c4,Cd);
x=x+dT*xd+dT*(ak1+ak2+ak3)/6.0;
xd=xd+(ak1+2.0*ak2+2.0*ak3+ak4)/6.0;
```

```
% RFUNC.M
%
function ak=rfunc(x,xd,y,yd,c1,c2,c3,c4,Cd)
ak=-1.5/(1-x/(2*(y-c1)))*((xd^2/x)*(1-2*x/(3*(y-c1)))-yd^2/(6*x)+y/(x*c2)-c3/(x^c4)+(x/(4*(y-
c1)^2))*(xd*yd/3-x/c2+Cd*yd^2/4));
```

```
% DPTHFN.M
%
% Function M-file for calculation of the bubble depth
% (i.e. contains the bubble depth governing equation for use in BUBBLE.M)
%
function [y,yd]=dpthfn(dT,x,xd,y,yd,xdd,c1,c2,c3,c4,Cd)
ak1=dT*dfunc(x,xd,y,yd,xdd,c1,c2,c3,c4,Cd);
ak2=dT*dfunc(x,xd,y+dT*yd/2.0,yd+ak1/2.0,xdd,c1,c2,c3,c4,Cd);
ak3=dT*dfunc(x,xd,y+dT*yd/2.0+dT*ak1/4.0,yd+ak2/2.0,xdd,c1,c2,c3,c4,Cd);
ak4=dT*dfunc(x,xd,y+dT*yd+dT*ak2/2.0,yd+ak3,xdd,c1,c2,c3,c4,Cd);
y=y+dT*yd+dT*(ak1+ak2+ak3)/6.0;
yd=yd+(ak1+2.0*ak2+2.0*ak3+ak4)/6.0;
```

```
% DFUNC.M
%
%
%
function ak=dfunc(x,xd,y,yd,xdd,c1,c2,c3,c4,Cd)
ak=-3*(1/c2+xd*yd/x-(Cd*yd^2)/(4*x)+(x/(4*(y-c1)^2))*(3*xd^2+x*xdd));
```

```
% BUBWHIP.M
%
%
% This subroutine performs the following:
%       1. Calculates the response (nodal point displacements, velocities, accelerations)
%               of the submarine during a vibration with initial displacements of zero
%               and subjected to fluid loading produced by a pulsating explosion bubble.
%               Response is calculated using the Newmark time integration algorithm,
%               with iteration conducted at each time step using a Newton-Raphson method.
%       2. Calculates the local axial strains at specified hull locations using simple
%               beam theory (used for comparison with model test data).
%
%
% Utilize the following:
% -K,C,M calculated in HULL.M
% -Hydrodynamic coefficients provided in IN.M
% -Parameters for Newmark algorithm provided in IN.M
% -Bubble characteristics (radius, depth, etc.) calculated in BUBBLE.M
%
% Define nodes to use for response calculations
N(1)=NODE1;
N(2)=NODE2;
N(3)=NODE3;
N(4)=NODE4;
% Define hull elements to use for axial strain calculations
El1=ELEMENT1;
El2=ELEMENT2;
El3=ELEMENT3;
%
% Define the horizontal (hull) degree of freedom where internal structure/absorber acts
nnabs=(nabs-1)*4+2;
%
% Define parameters for internal structure/absorber
ka=ma*(ww(8)^2);
mabs=zeros(1,NDOF)';
kabs=zeros(1,NDOF)';
mabs(nnabs)=ma;
kabs(nnabs)=ka;
%
% Set the initial and final times (sec) for Newmark integration, and limit
% on the number of Newton-Raphson iterations
t=0;
tf=tmax;
jlimit=40;
%
% Initialize the loading forces on the hull
% Loading forces related to displacement
        Fdisp=zeros(1,NDOF)';
% Loading forces related to velocity
        Fvel=zeros(1,NDOF)';
% Loading forces related to acceleration
        Facc=zeros(1,NDOF)';
% Calculate (constant) static forces (i.e. hydrostatic/buoyancy and weight)
Fgrav=zeros(1,NDOF)';
```

```
Fhs=zeros(1,NDOF)';
for n=1:NNODES
        ny=(n-1)*4+1;
        % Hydrostatic/buoyancy force (lbf)
        Fhs(ny)=bh(n)*2240;
        % Static force of gravity/weight (lbf)
        Fgrav(ny)=-wh(n)*2240;
end
% Total initial loading forces
Floadt=Fdisp+Fvel+Facc+Fhs+Fgrav;
%
% Define initial conditions (displacements/velocities/accelerations)
% Hull
xt=zeros(1,NDOF)';
xdt=zeros(1,NDOF)';
xddt=zeros(1,NDOF)';
% Internal absorber
xat=0;
xadt=0;
xaddt=0;
%
% Perform the Newmark time integration
%
% Step through time
%
% Define constants to be used in Newton-Raphson iterations
c1=(1/(betap*dt^2));
c2=(1/(betap*dt));
c3=(1/(2*betap));
c4=(gammap/(betap*dt));
c5=gammap/betap;
c6=(1-gammap/(2*betap));
c7=(1/(2*betap)-1);
%
dx=zeros(1,NDOF)';
%
for i=1:199;
        t=t+dt
        %
        % Set initial displacments,velocities,accelerations, and loading forces for
        % the current time step (equal to the final for the last time step)
        xj=xt;
        xdj=xdt;
        xddj=xddt;
        Floadj=Floadt;
        xaj=xat;
        xadj=xadt;
        xadds=xaddt;
        %
        % Perform Newton-Raphson iterations at current time step
        for j=1:jlimit
                %
                xaddj=xadds;
                % Calculate current iteration absorber displacement/velocity
```

```
        xaj=xat+xadt*dt+xaddt*(dt^2/2)+betap*(xaddj-xaddt)*dt^2;
        xadj=xadt+xaddt*dt+gammap*(xaddj-xaddt)*dt;
        %
        % Calculate the loading forces for the current iteration
        %
        % Call function "fluid" to provide free field fluid velocities and
        % accelerations at each node (at the current iteration node location)

[uy,uz,uyd,uzd]=fluid(xj,xchg,ychg,zchg,Dship,t,TM,BR,BD,BRD,BDD,BRDD,BDDD,...
...DEL,L1,T1,btime,bdpth,NDOF,NNODES,Lh);
        %
        for n=1:NNODES
                ny=4*(n-1)+1;
                nz=4*(n-1)+2;
        % Loading forces related to displacement
                Fdisp(nz)=kabs(nz)*(xaj-xj(nz));
        % Loading forces related to velocity
                Fvel(ny)=0.5*rho*By(n)*Cd1y(n)*(uy(n)-xdj(ny))*...
                ...abs(uy(n)-xdj(ny))*Lh(n)+0.5*rho*Dapy(n)*Cd2y(n)*(uy(n)-
                ...xdj(ny))*abs(uy(n)-xdj(ny))*Lapy(n);
                Fvel(nz)=0.5*rho*Bz(n)*Cd1z(n)*(uz(n)-xdj(nz))*...
                ...abs(uz(n)-xdj(nz))*Lh(n)+0.5*rho*Dapz(n)*Cd2z(n)*(uz(n)-
                ...xdj(nz))*abs(uz(n)-xdj(nz))*Lapz(n);
        % Loading forces related to acceleration
                Facc(ny)=rho*(pi*By(n)^2/4)*Cm1y(n)*Lh(n)*(uyd(n)-
                ...xddj(ny))+rho*Aapy(n)*Cm2y(n)*Lapy(n)*(uyd(n)-
        ...xddj(ny))+rho*(pi*By(n)^2/4)*Lh(n)*xddj(ny)+rho*Aapy(n)*Lapy(n)*xddj(ny);
                Facc(nz)=rho*(pi*Bz(n)^2/4)*Cm1z(n)*Lh(n)*(uzd(n)-
                ...xddj(nz))+rho*Aapz(n)*Cm2z(n)*Lapz(n)*(uzd(n)-
        ...xddj(nz))+rho*(pi*Bz(n)^2/4)*Lh(n)*xddj(nz)+rho*Aapz(n)*Lapz(n)*xddj(nz);
        end
        %
        % Total loading force for the current iteration
        Floadj=Fdisp+Fvel+Facc+Fhs+Fgrav;
        %
        % Calculate Jacobian matrices for each of the loading forces
        % (square diagonal matrices for this formulation)
        %
        dFdxj1=zeros(1,NDOF)';
        dFdxdj1=zeros(1,NDOF)';
        dFdxddj1=zeros(1,NDOF)';
        dFdxj=zeros(NDOF);
        dFdxdj=zeros(NDOF);
        dFdxddj=zeros(NDOF);
        dxj=zeros(1,NDOF)';
        dxdj=zeros(1,NDOF)';
        dxddj=zeros(1,NDOF)';
        for n=1:NNODES
                ny=4*(n-1)+1;
                nz=4*(n-1)+2;
                dxj(nz)=0.01;
                dxdj(ny)=0.01;
                dxdj(nz)=0.01;
                dxddj(ny)=0.01;
```

```
                dxddj(nz)=0.01;
                dFdxj1(nz)=(kabs(nz)*(xaj-(xj(nz)+dxj(nz)))-Fdisp(nz))/dxj(nz);
                dFdxdj1(ny)=(0.5*rho*By(n)*Cd1y(n)*(uy(n)-(xdj(ny)+dxdj(ny)))*abs(uy(n)-
                ...(xdj(ny)+dxdj(ny)))*Lh(n)+0.5*rho*Dapy(n)*Cd2y(n)*(uy(n)-
                ...(xdj(ny)+dxdj(ny)))*abs(uy(n)-(xdj(ny)+dxdj(ny)))*Lapy(n)-
                ...Fvel(ny))/dxdj(ny);
                dFdxdj1(nz)=(0.5*rho*Bz(n)*Cd1z(n)*(uz(n)-(xdj(nz)+dxdj(nz)))*abs(uz(n)-
                ...(xdj(nz)+dxdj(nz)))*Lh(n)+0.5*rho*Dapz(n)*Cd2z(n)*(uz(n)-
                ...(xdj(nz)+dxdj(nz)))*abs(uz(n)-(xdj(nz)+dxdj(nz)))*Lapz(n)-
                ...Fvel(nz))/dxdj(nz);
                dFdxddj1(ny)=(rho*(pi*By(n)^2/4)*Cm1y(n)*Lh(n)*(uyd(n)-
                ...(xddj(ny)+dxddj(ny)))+rho*Aapy(n)*Cm2y(n)*Lapy(n)*(uyd(n)-
...(xddj(ny)+dxddj(ny)))+rho*(pi*By(n)^2/4)*Lh(n)*(xddj(ny)+dxddj(ny))+rho*Aapy(n)*...
                ...Lapy(n)*(xddj(ny)+dxddj(ny))-Facc(ny))/dxddj(ny);
                dFdxddj1(nz)=(rho*(pi*Bz(n)^2/4)*Cm1z(n)*Lh(n)*(uzd(n)-
                ...(xddj(nz)+dxddj(nz)))+rho*Aapz(n)*Cm2z(n)*Lapz(n)*(uzd(n)-
...(xddj(nz)+dxddj(nz)))+rho*(pi*Bz(n)^2/4)*Lh(n)*(xddj(nz)+dxddj(nz))+rho*Aapz(n)*...
                ...Lapz(n)*(xddj(nz)+dxddj(nz))-Facc(nz))/dxddj(nz);
        end
        for n=1:NDOF
                dFdxj(n,n)=dFdxj1(n);
                dFdxdj(n,n)=dFdxdj1(n);
                dFdxddj(n,n)=dFdxddj1(n);
        end
        %
        % Calculate residuals
        f1j=M*(c1*(xj-xt)-c2*xdt-c3*xddt)+C*(c4*(xj-xt)-c5*xdt+c6*xddt*dt)+...
        ...K*(xj-xt)-Floadj+Floadt;
        f2j=xdj-c4*(xj-xt)+(c5-1)*xdt-c6*dt*xddt;
        f3j=xddj-c1*(xj-xt)+c2*xdt+c7*xddt;
        %
        % Solve for the displacement correction (dx)
        %
        A1=(c1*M+c4*C+K-c1*dFdxddj-c4*dFdxdj-dFdxj);
        A1inv=inv(A1);
        A2=-f1j-dFdxdj*f2j-dFdxddj*f3j;
        dx=(A1inv*A2);
        %
        % Calculate the next iteration's displacements, velocities, and accelerations
        %
        xj=xj+dx;
        xdj=xdj+(c4*dx)-f2j;
        xddj=xddj+(c1*dx)-f3j;
        %
        % Required acceleration of absorber
        if any(mabs)~=0,  xadds=-Fdisp(nnabs)/mabs(nnabs);
        else,  xadds=0;
        end
        %
        % Check to see if all Norms of residuals are less than tolerance for
        % the current iteration
        % (If so, go to the next time step)
        Normf1j=norm(f1j);
        Normf2j=norm(f2j);
```

```
Normf3j=norm(f3j);
Normabs=norm(xadds-xaddj);
if Normf1j<=tol & Normf2j<=tol & Normf3j<=tol & Normabs<=tol
        %
        % Calculate axial stress at specified hull stations
        % (using simple beam theory)
        %
        qy=zeros(1,NE)';
        qz=zeros(1,NE)';
        Vy=zeros(1,NE)';
        Vz=zeros(1,NE)';
        My1=zeros(1,NE)';
        Mz1=zeros(1,NE)';
        My=zeros(1,NE)';
        Mz=zeros(1,NE)';
        for e=1:NE
                % Net vertical or horizontal force at element e
                ey=(e-1)*4+1;
                ez=(e-1)*4+2;
                qy(e)=Floadj(ey)-M(ey,ey)*xddj(ey);
                qz(e)=Floadj(ez)-M(ez,ez)*xddj(ez);
                %
                % Vertical or horizontal shear force at element e
                Vy(e)=sum(qy);
                Vz(e)=sum(qz);
                %
                % Vertical or horizontal bending moment at element e
                My1(e)=Vy(e)*Le(e);
                Mz1(e)=Vz(e)*Le(e);
                My(e)=sum(My1);   % BM about z-axis
                Mz(e)=sum(Mz1);           % BM about y-axis
                %
                % Axial stress at crown of element e (positive is tension)
                sigc(e)=-My(e)*Yc(e)/Iaz(e);
                % Axial stress at keel of element e
                sigk(e)=My(e)*Yk(e)/Iaz(e);
                % Axial stress at port-side fiber (port=pos z) (positive is tension)
                sigp(e)=-Mz(e)*Zp(e)/Iay(e);
                % Axial stress at stbd-side fiber
                sigs(e)=Mz(e)*Zs(e)/Iay(e);
                %
                % Axial strains
                EPSc(e)=sigc(e)/E;
                EPSk(e)=sigk(e)/E;
                EPSp(e)=sigp(e)/E;
                EPSs(e)=sigs(e)/E;
                %
        end
        % Save current time, displacements and velocities
        % (at specified nodes) and axial strains
        % (at specified elements) for later plotting... also save
        % current horizontal fluid velocity and acceleration, and
        % (at nodes 10 and 20) and all calculated horizontal forces
        % (at nodes 10 and 20) for later plotting.
```

```
time(i)=t;
% Vertical/horizontal displacements/velocities
% at specified nodes
for n=1:4
        Dv(n)=(N(n)-1)*4+1;
        Dh(n)=(N(n)-1)*4+2;
end
xv1(i)=xj(Dv(1));
xh1(i)=xj(Dh(1));
xdv1(i)=xdj(Dv(1));
xdh1(i)=xdj(Dh(1));
xv2(i)=xj(Dv(2));
xh2(i)=xj(Dh(2));
xdv2(i)=xdj(Dv(2));
xdh2(i)=xdj(Dh(2));
xv3(i)=xj(Dv(3));
xh3(i)=xj(Dh(3));
xdv3(i)=xdj(Dv(3));
xdh3(i)=xdj(Dh(3));
xv4(i)=xj(Dv(4));
xh4(i)=xj(Dh(4));
xdv4(i)=xdj(Dv(4));
xdh4(i)=xdj(Dh(4));
%
xabs(i)=xaj;
xdabs(i)=xadj;
xddabs(i)=xaddj;
%
% Horizontal hull/fluid motions and
% external forces
xddh2(i)=xddj(Dh(2));
xddh3(i)=xddj(Dh(3));
uh3(i)=uz(N(3));
udh3(i)=uzd(N(3));
Fvelh3(i)=Fvel(Dh(3));
Facch3(i)=Facc(Dh(3));
Floadh3(i)=Floadj(Dh(3));
%
xddh4(i)=xddj(Dh(4));
uh4(i)=uz(N(4));
udh4(i)=uzd(N(4));
Fvelh4(i)=Fvel(Dh(4));
Facch4(i)=Facc(Dh(4));
Floadh4(i)=Floadj(Dh(4));
%
% Axial strains (keel, crown, port, stbd) at
% at specified elements
straink1(i)=EPSk(El1);
strainc1(i)=EPSc(El1);
strainp1(i)=EPSp(El1);
strains1(i)=EPSs(El1);
straink2(i)=EPSk(El2);
strainc2(i)=EPSc(El2);
strainp2(i)=EPSp(El2);
```

```
                    strains2(i)=EPSs(El2);
                    straink3(i)=EPSk(El3);
                    strainc3(i)=EPSc(El3);
                    strainp3(i)=EPSp(El3);
                    strains3(i)=EPSs(El3);
                    %
                    % Save the current time step displacements, velocities, and
                    % accelerations, and forces for use in the next time step
                    xt=xj;
                    xdt=xdj;
                    xddt=xddj;
                    Floadt=Floadj;
                    xat=xaj;
                    xadt=xadj;
                    xaddt=xaddj;
                    break, end
                end
            if j==jlimit, break, end
            end
    if j==jlimit, break, end
    if t>=tf, break, end
    end
    %
```

```
% FLUID.M
%
% Calculates the free field fluid velocities and accelerations (at each node)
%
function[uy,uz,uyd,uzd]=fluidvel(xj,xchg,ychg,zchg,Dship,t,TM,BR,BD,BRD,BDD...
....,BRDD,BDDD,DEL,L1,T1,btime,bdpth,NDOF,NNODES,Lh)
%
% Non-dimensional bubble parameters
TI=t/T1;
a=interp1(TM,BR,TI);
s=interp1(TM,BRD,TI);
sd=interp1(TM,BRDD,TI);
l=interp1(TM,BDD,TI);
ld=interp1(TM,BDDD,TI);
d=interp1(TM,DEL,TI);
% Source strengths
e1=(L1^3)*(a^2)*s/T1;
e2=-(L1^4/(2*T1))*(a^3*l);
e1d=(L1^3/T1^2)*(a^2*sd+2*a*s^2);
e2d=-(L1^4/(2*T1^2))*(a^3*ld+3*a^2*l*s);
% Vertical bubble velocity
vm=-l*L1/T1;
% Bubble depth
ti=t;
bdepth=interp1(btime,bdpth,ti);
%
for n=1:NNODES
        ny=(n-1)*4+1;
        nz=(n-1)*4+2;
        xnode=(n-1)*Lh(n);
        ynode=xj(ny);
        znode=xj(nz);
        % vr and hr (vertical and horiz relative distance) and angle of flow
        vr=bdepth-Dship+ynode;
        hr=((xnode-xchg)^2+(znode-zchg)^2)^0.5;
        theta=atan((xnode-xchg)/(znode-zchg));
        %
        % Free-field fluid velocities/accelerations (vertical and horizontal)
        % Horizontal and vertical free-field fluid velocities and accelerations
        dis=(vr^2+hr^2)^0.5;
        uh=(e1*hr/dis^3)+(3*e2*vr*hr/dis^5);
        uv=(e1*vr/dis^3)+(3*e2*vr^2/dis^5)-(e2/dis^3);
        uhd=(e1d*hr/dis^3)+(3*e2d*hr*vr/dis^5)+...
        ...vm*(3*e1*hr*vr/dis^5-(3*e2*hr/dis^5)*(1-(5*vr^2/dis^2)));
        uvd=(e1d*vr/dis^3+3*e2d*vr^2/dis^5-e2d/dis^3)-...
        ...vm*(e1/dis^3-3*e1*vr^2/dis^5+9*e2*vr/dis^5-15*e2*vr^3/dis^7);
        %
        % Y and Z directed free-field fluid velocities and accelerations
        uy(n)=uv;
        uz(n)=uh*cos(theta);
        uyd(n)=uvd;
        uzd(n)=uhd*cos(theta);
end
```

APPENDIX B

"DRY" WHIPPING RESPONSE AT SPECIFIED NODES

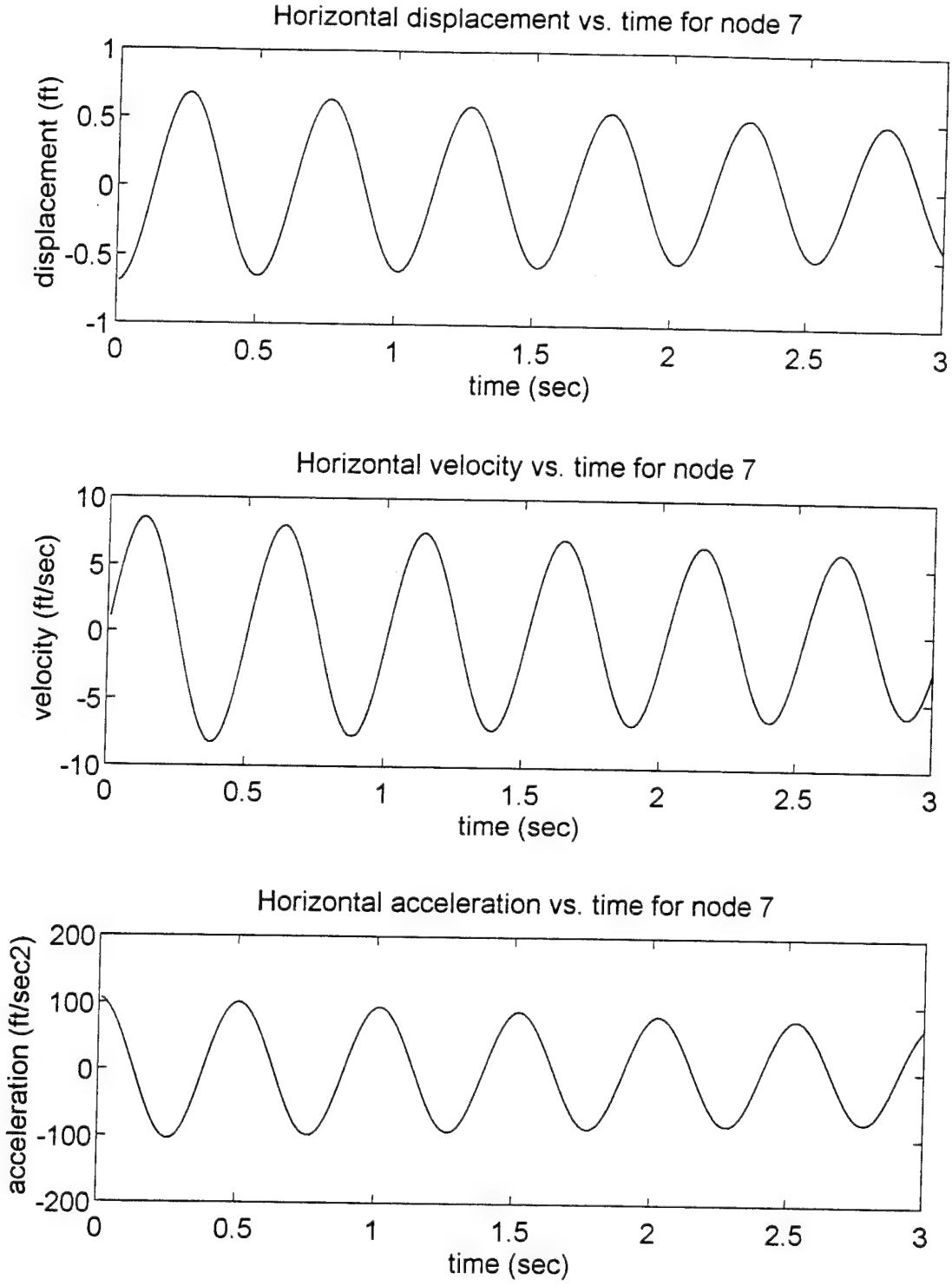

Figure B-1. Horizontal response at node 7, given initial displacments equal to a scaled horizontal mode shape vector for mode 1 flexure.

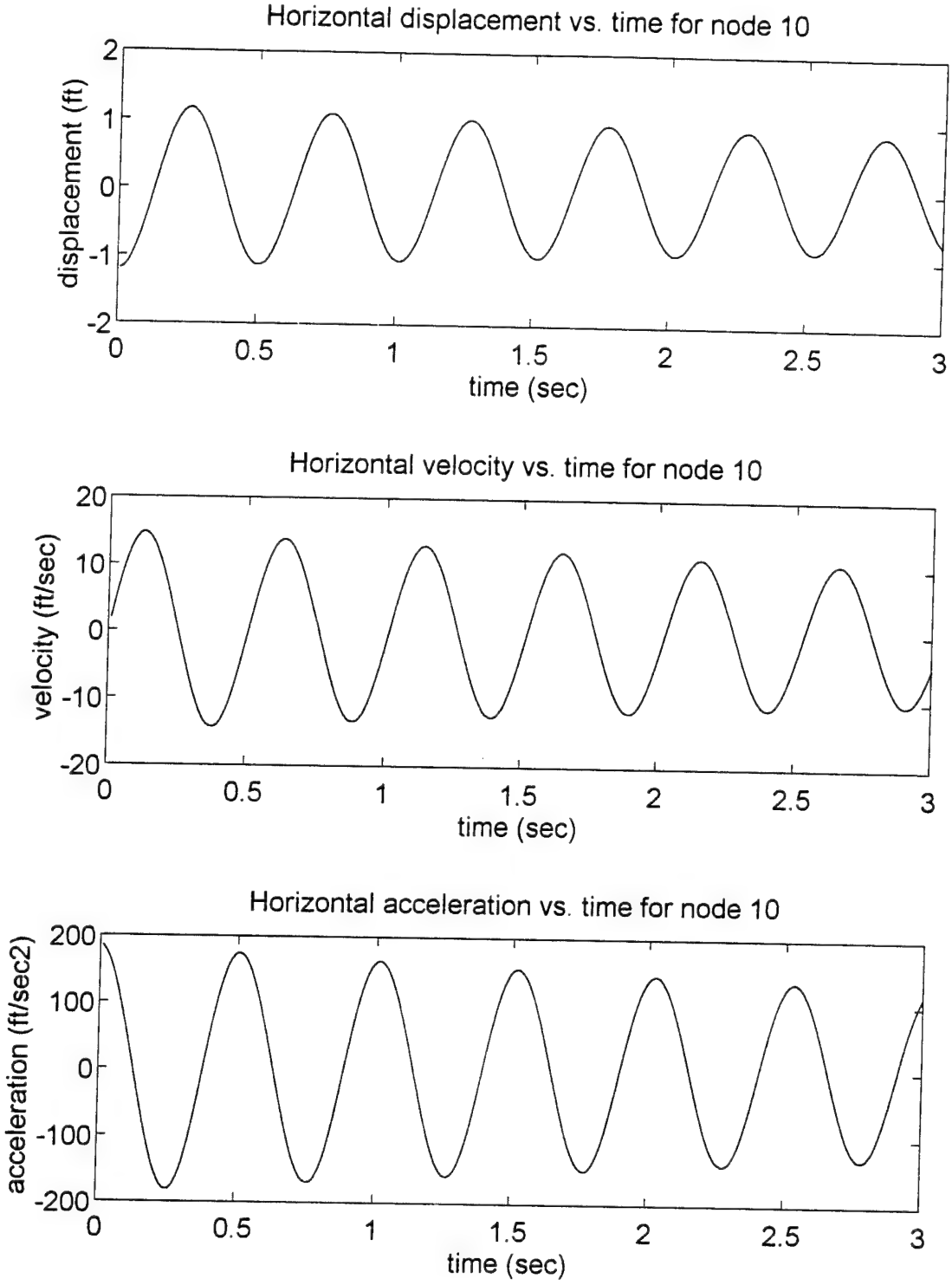

Figure B-2. Horizontal response at node 10, given initial displacments equal to a scaled horizontal mode shape vector for mode 1 flexure.

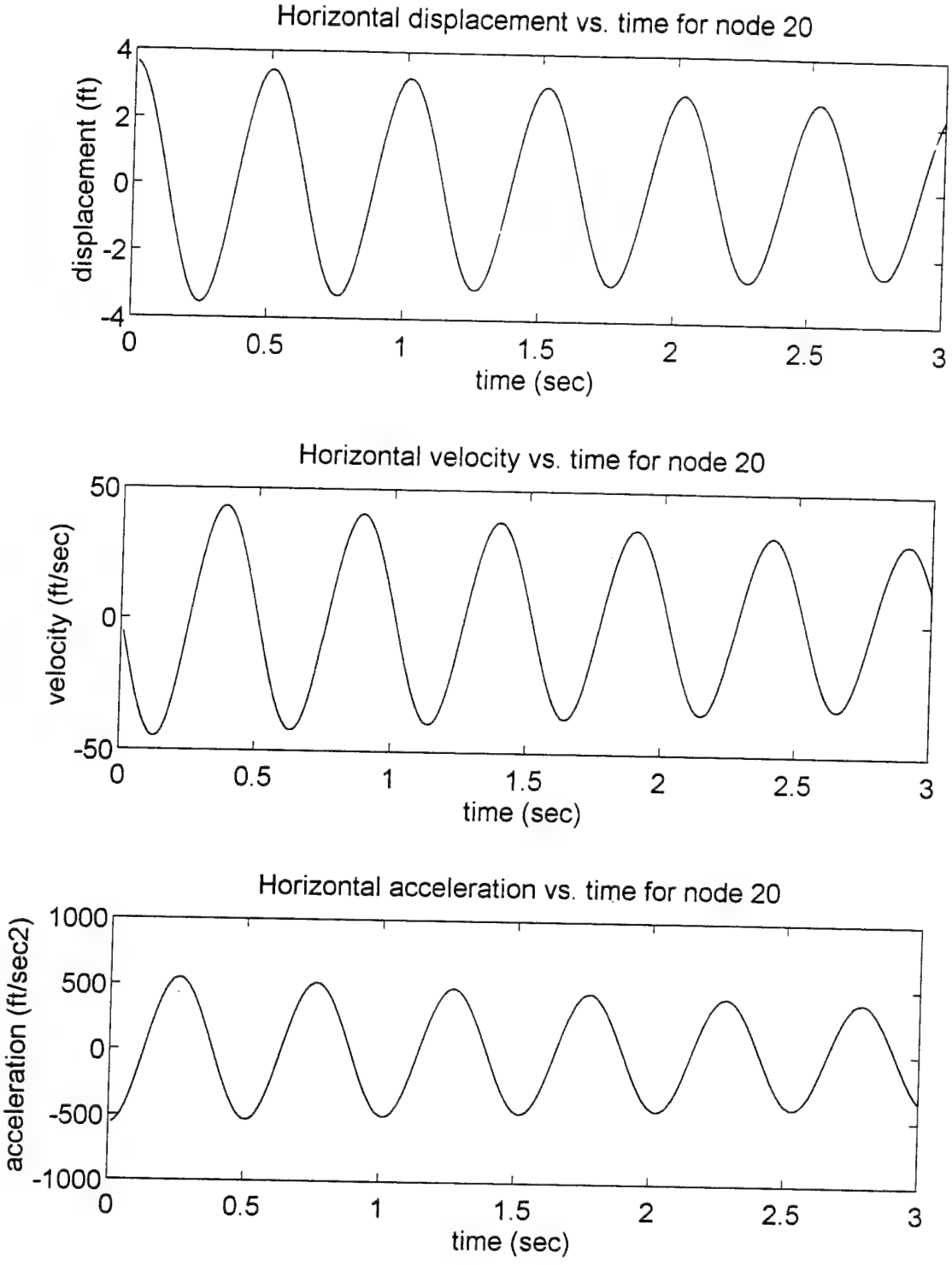

Figure B-3. Horizontal response at node 20, given initial displacments equal to a scaled horizontal mode shape vector for mode 1 flexure.

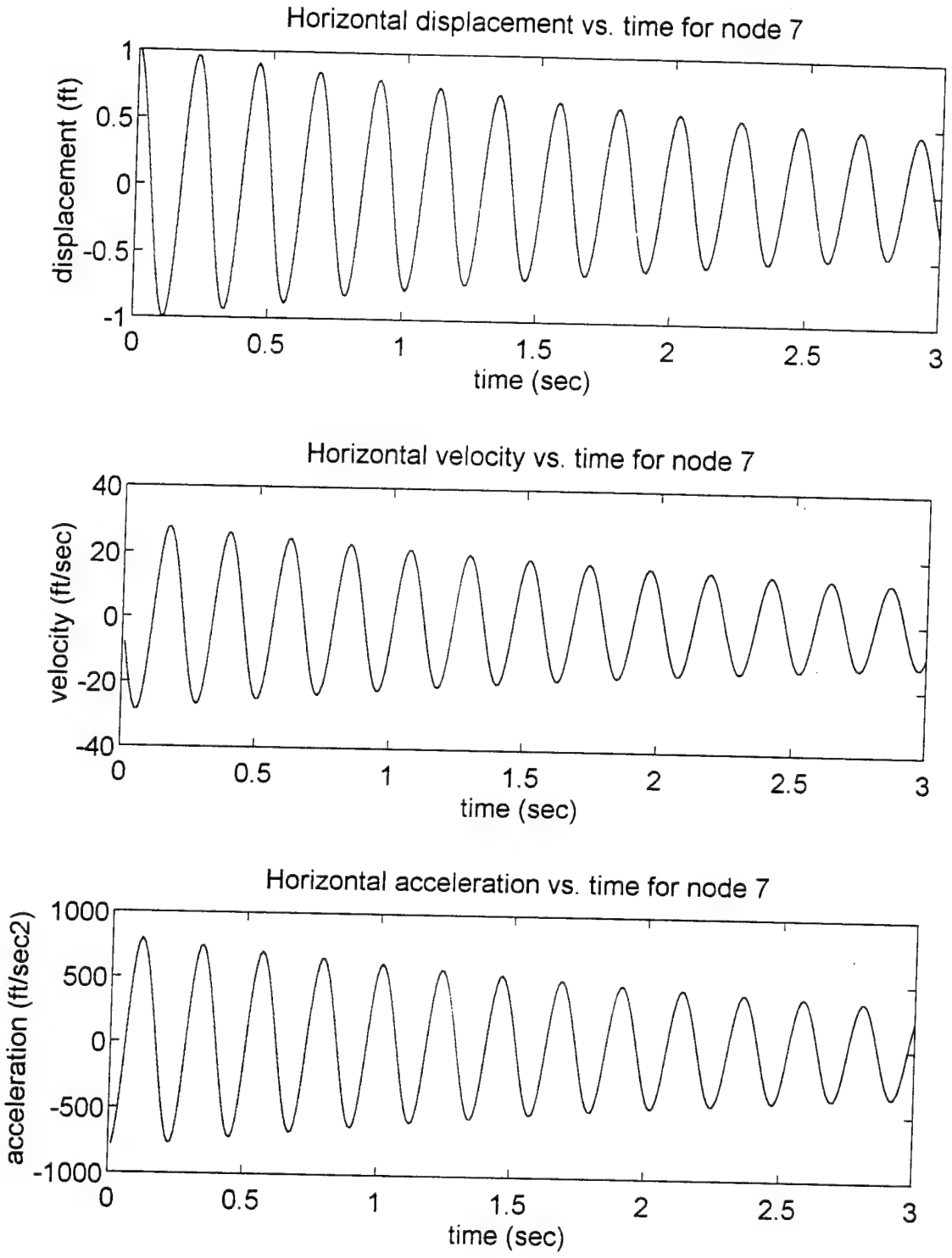

Figure B-4. Horizontal response at node 7, given initial displacments equal to a scaled horizontal mode shape vector for mode 2 flexure.

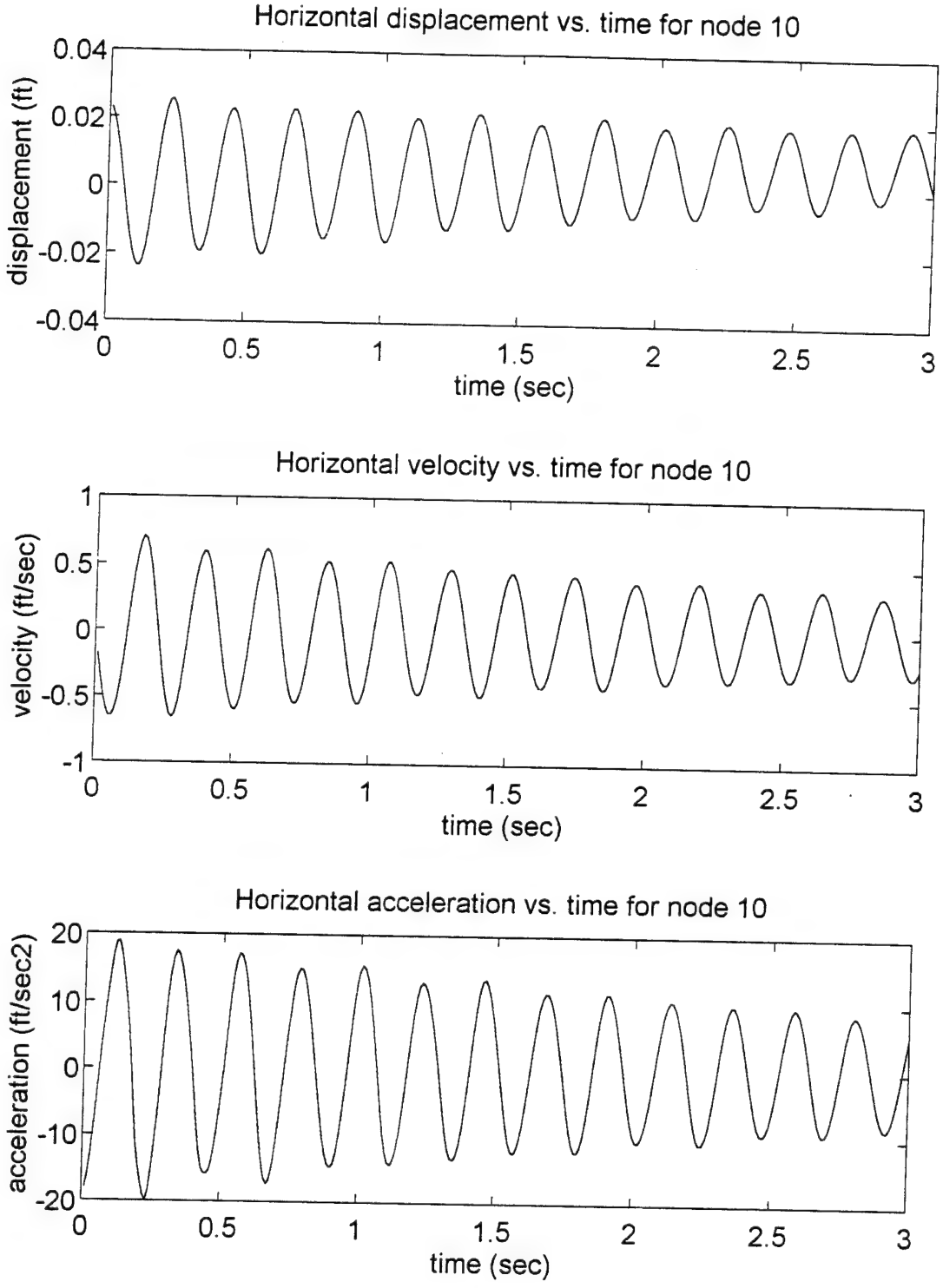

Figure B-5. Horizontal response at node 10, given initial displacments equal to a scaled horizontal mode shape vector for mode 2 flexure.

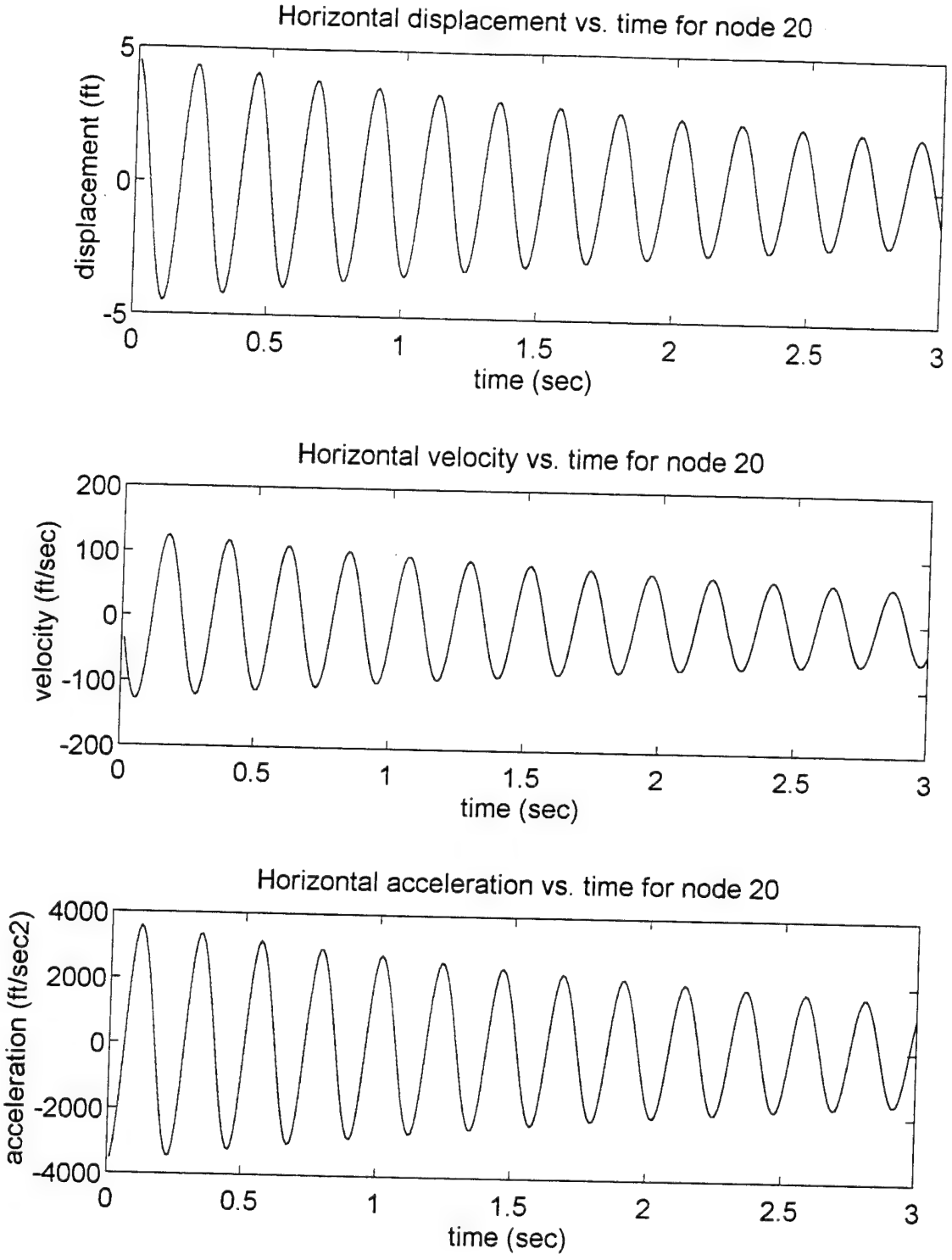

Figure B-6. Horizontal response at node 20, given initial displacments equal to a scaled horizontal mode shape vector for mode 2 flexure.

APPENDIX C

"WET" WHIPPING RESPONSE AT SPECIFIED NODES

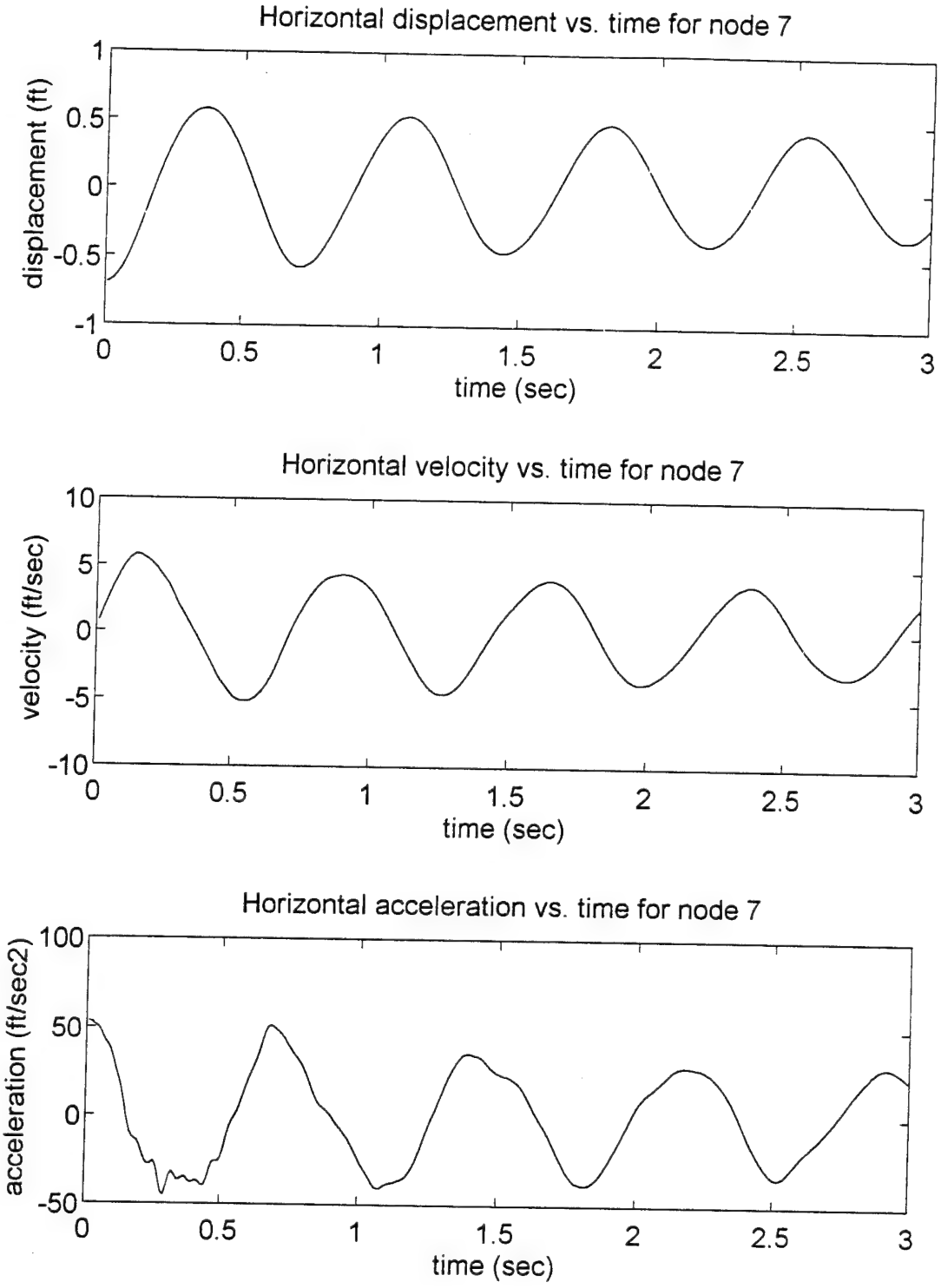

Figure C-1. Horizontal response at node 7, given initial displacments equal to a scaled horizontal mode shape vector for mode 1 flexure.

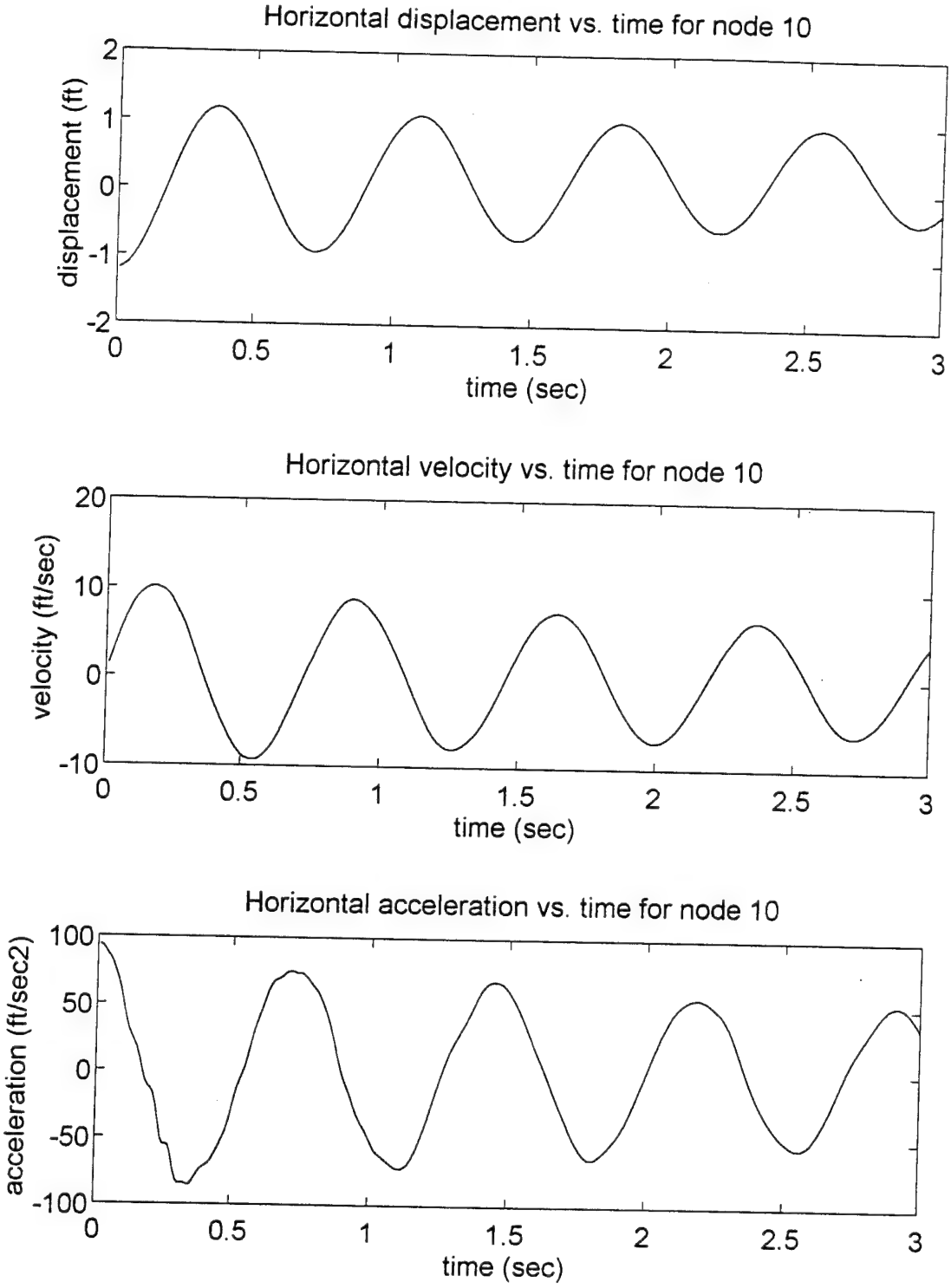

Figure C-2. Horizontal response at node 10, given initial displacments equal to a scaled horizontal mode shape vector for mode 1 flexure.

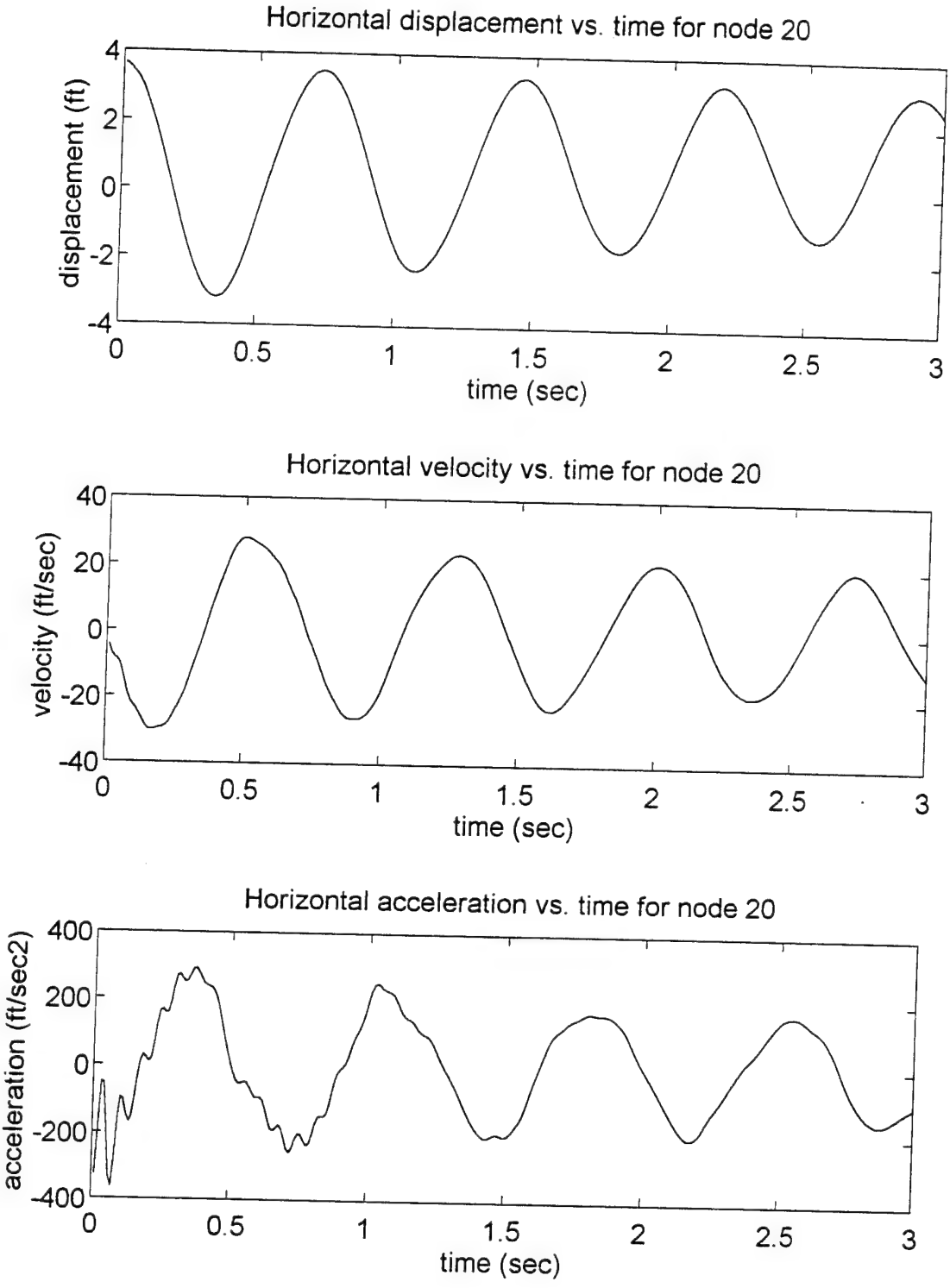

Figure C-3. Horizontal response at node 20, given initial displacments equal to a scaled horizontal mode shape vector for mode 1 flexure.

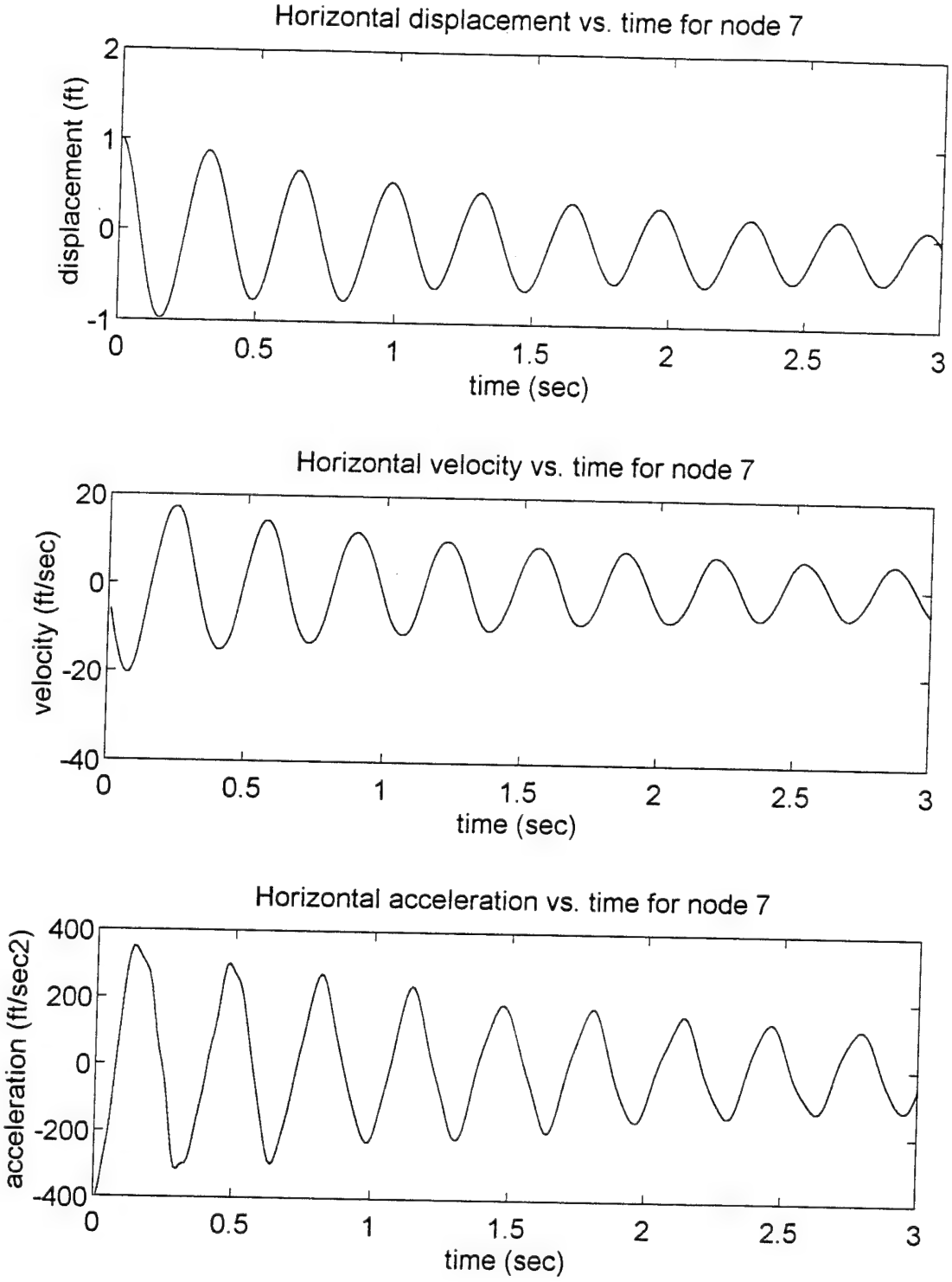

Figure C-4. Horizontal response at node 7, given initial displacments equal to a scaled horizontal mode shape vector for mode 2 flexure.

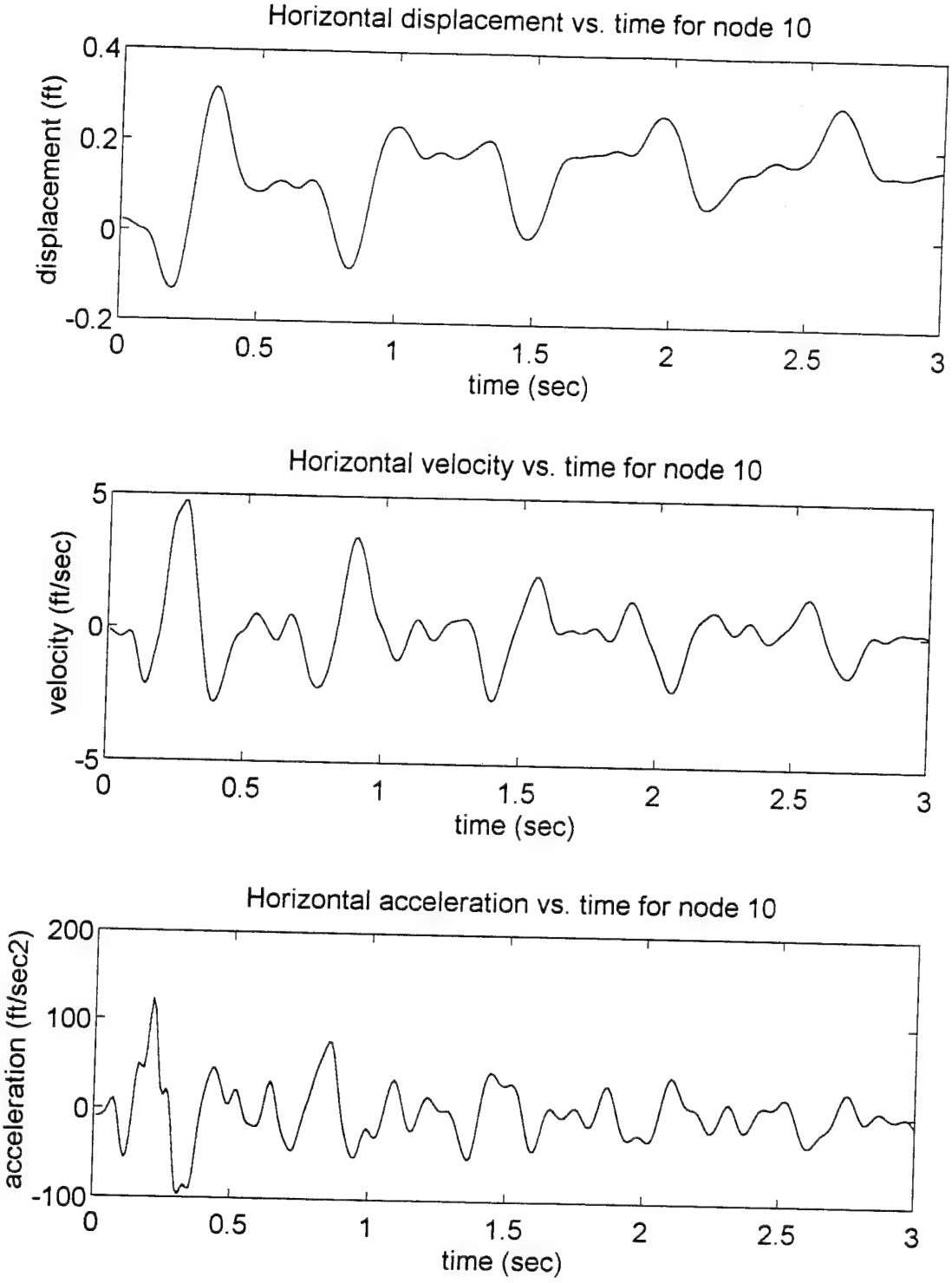

Figure C-5. Horizontal response at node 10, given initial displacments equal to a scaled horizontal mode shape vector for mode 2 flexure.

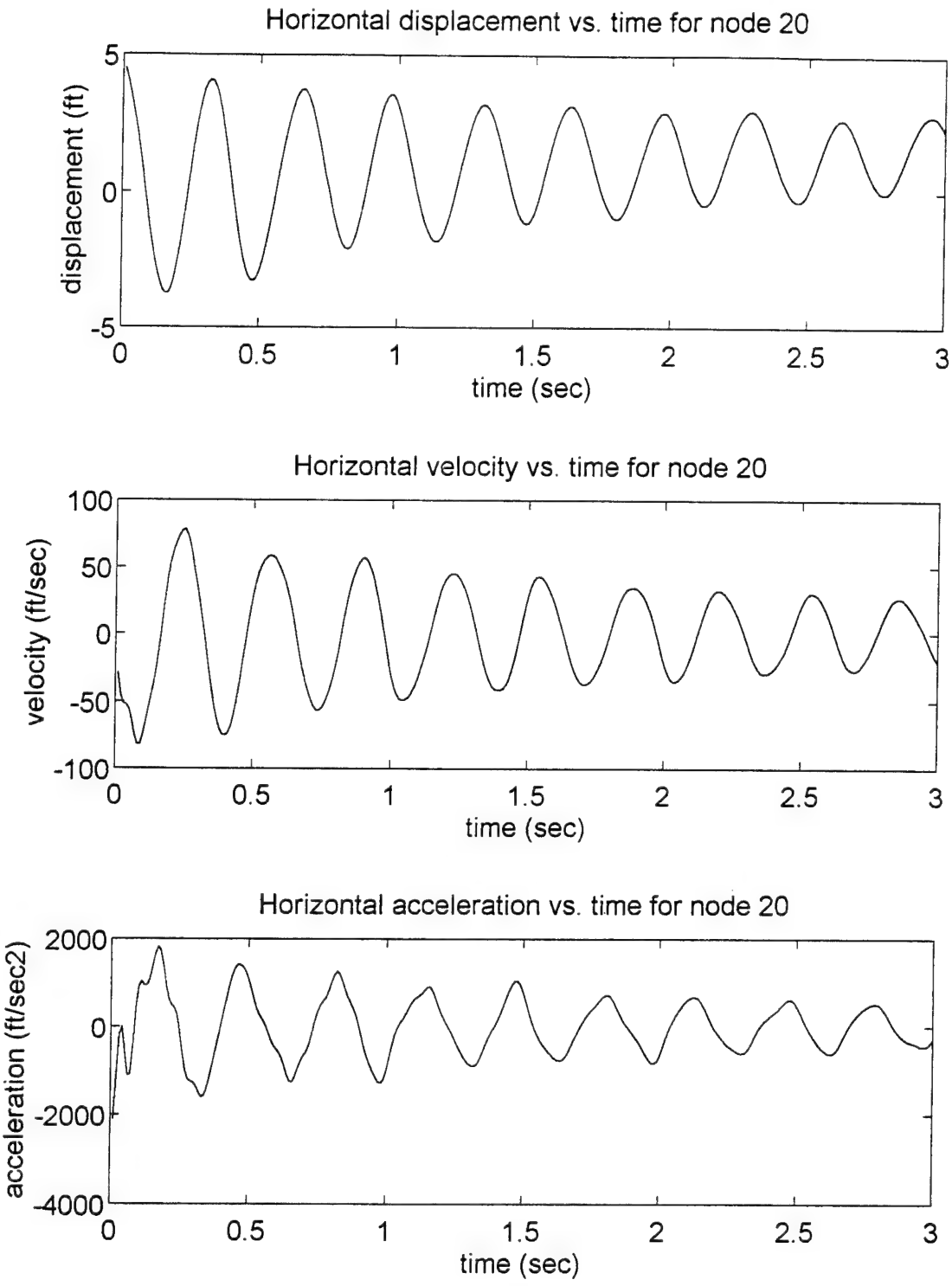

Figure C-6. Horizontal response at node 20, given initial displacments equal to a scaled horizontal mode shape vector for mode 2 flexure.

APPENDIX D

WHIPPING RESPONSE FOR HULL SUBJECTED TO CHARGE DESIGNED TO EXCITE HORIZONTAL MODES 1 AND 2 FLEXURAL WHIPPING

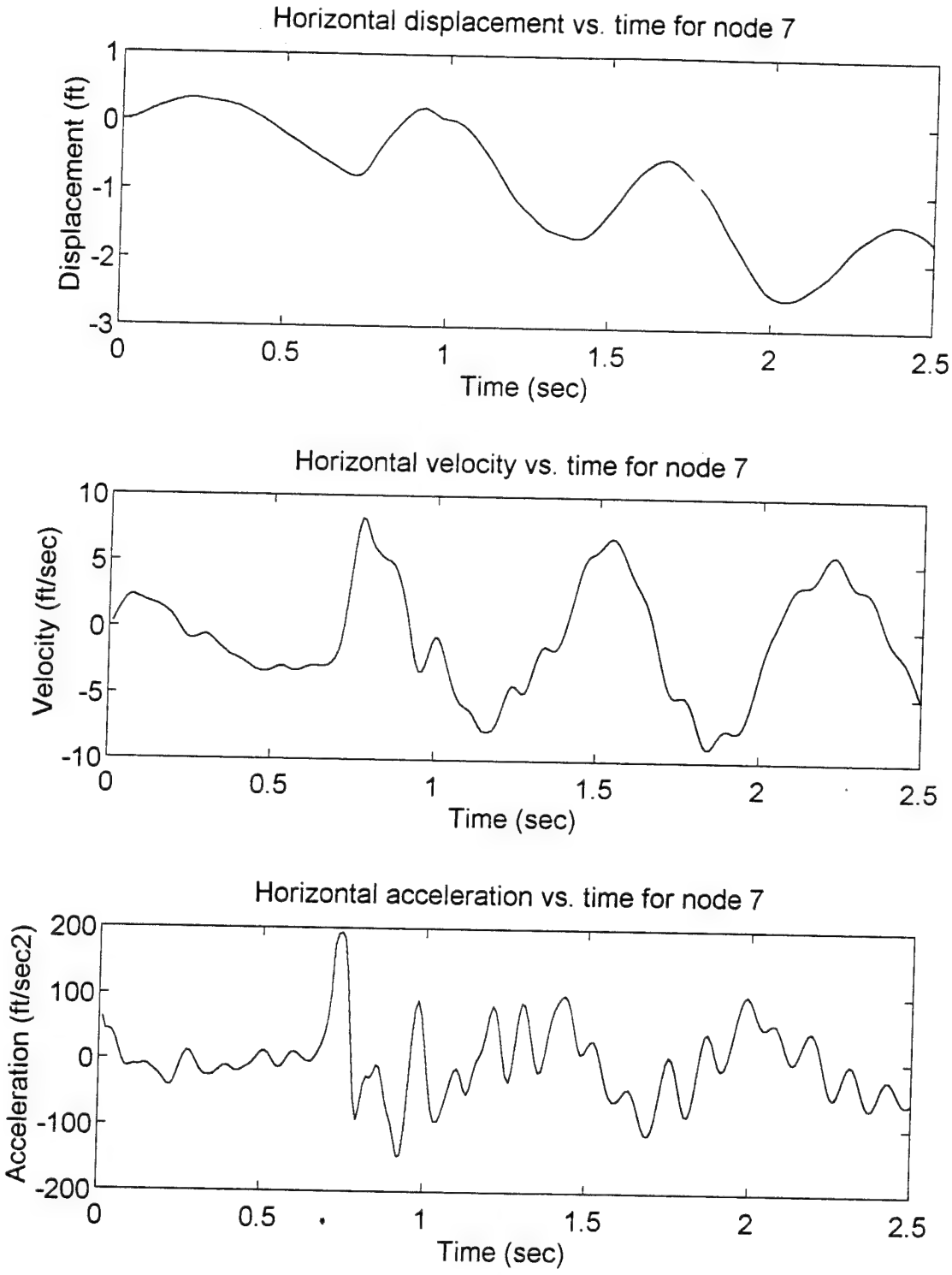

Figure D-1. Horizontal response at node 7, for hull subject to bubble pulse designed to excite horizontal mode 1 flexural whipping.

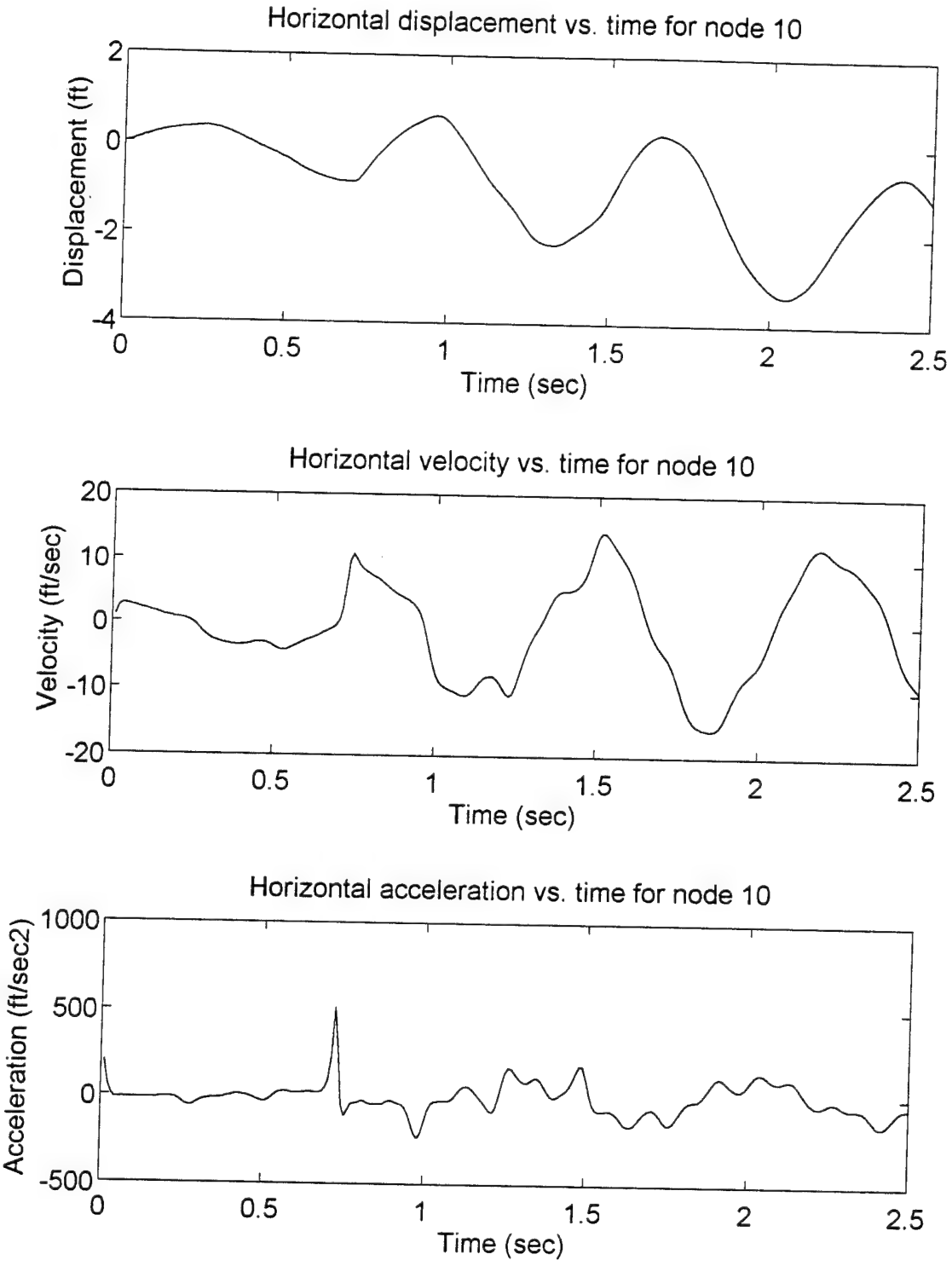

Figure D-2. Horizontal response at node 10, for hull subject to bubble pulse designed to excite horizontal mode 1 flexural whipping.

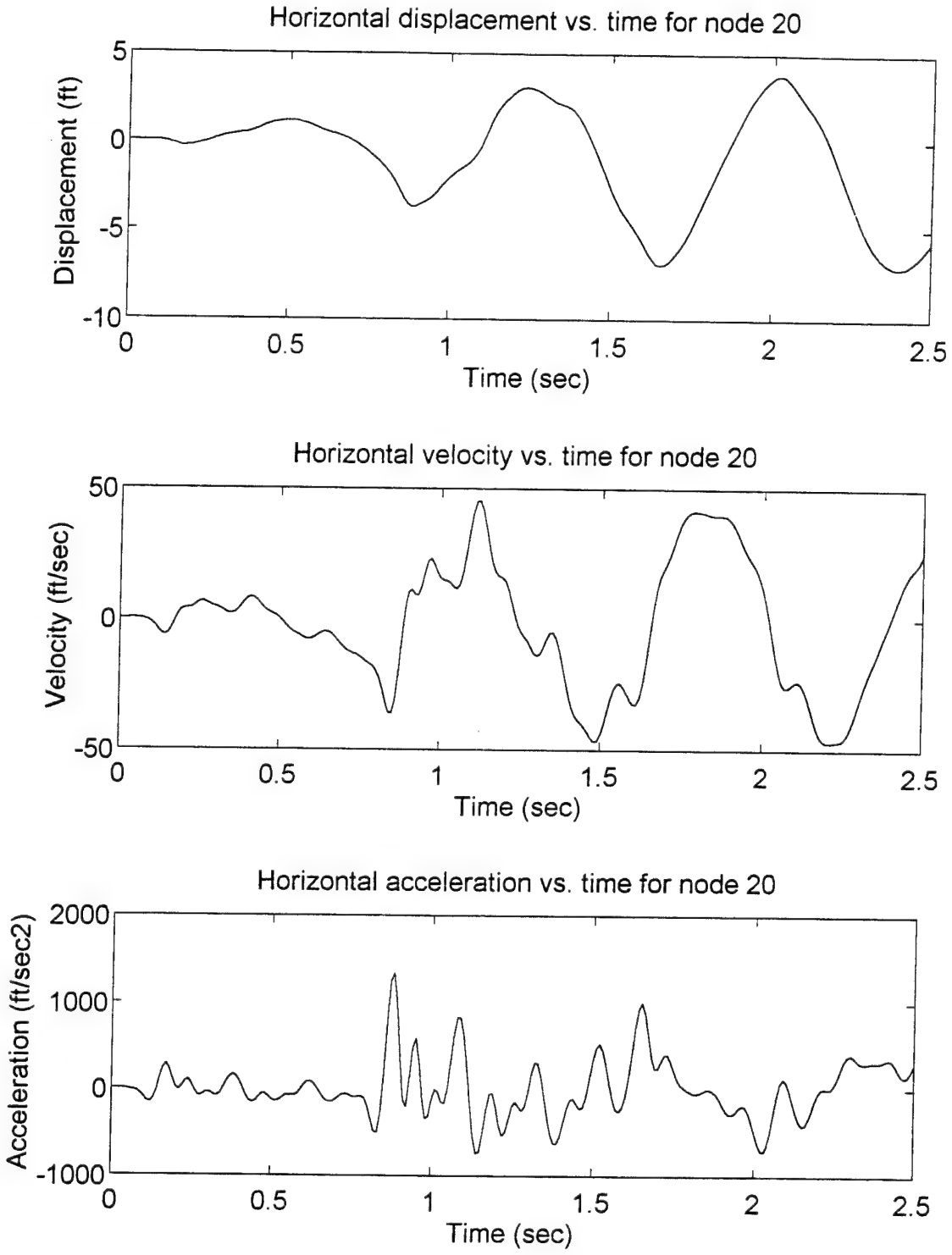

Figure D-3. Horizontal response at node 20, for hull subject to bubble pulse designed to excite horizontal mode 1 flexural whipping.

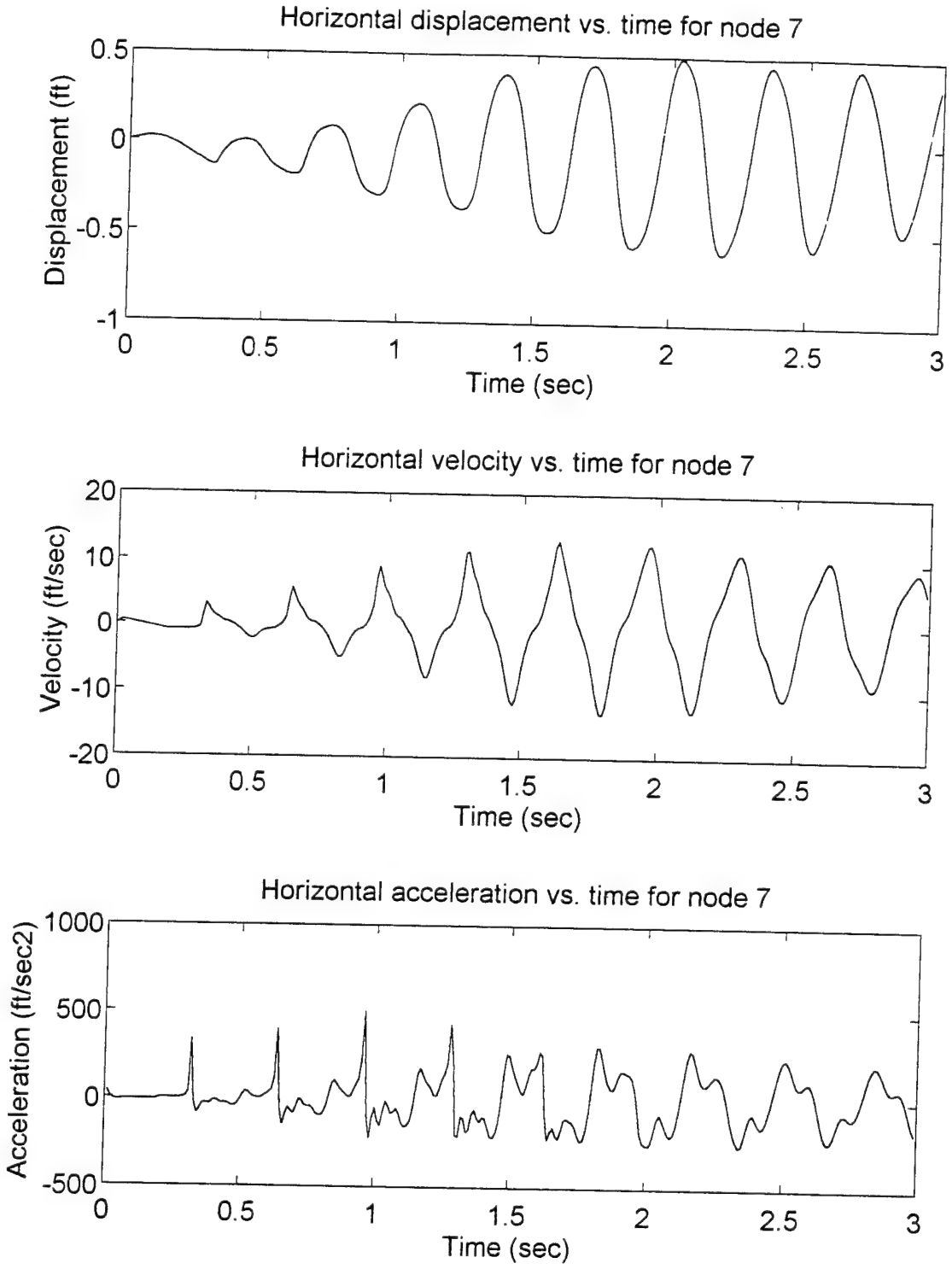

Figure D-4. Horizontal response at node 7, for hull subject to bubble pulse designed to excite horizontal mode 2 flexural whipping.

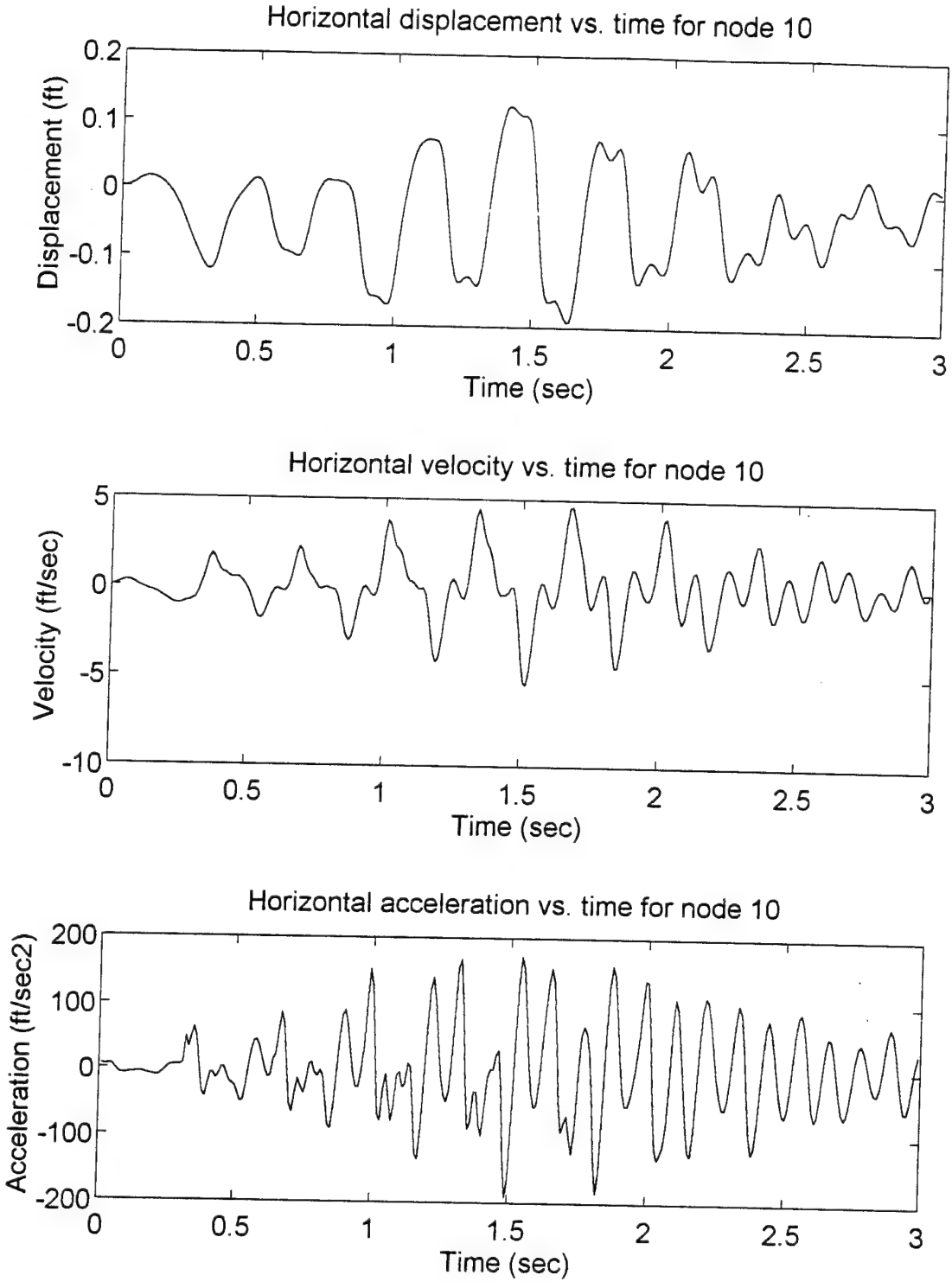

Figure D-5. Horizontal response at node 10, for hull subject to bubble pulse designed to excite horizontal mode 2 flexural whipping.

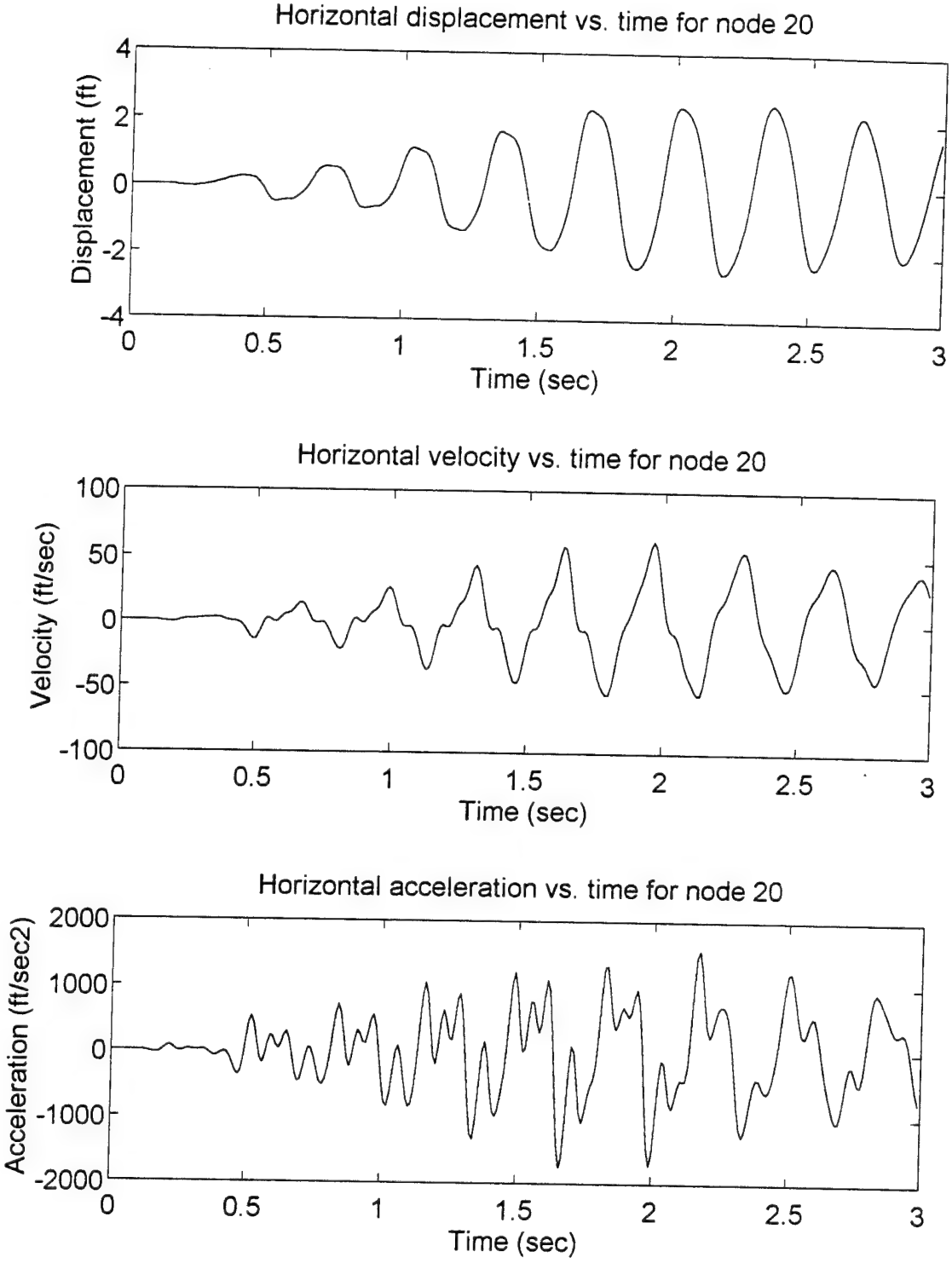

Figure D-6. Horizontal response at node 20, for hull subject to bubble pulse designed to excite horizontal mode 2 flexural whipping.

APPENDIX E

WHIPPING RESPONSE FOR HULL SUBJECTED TO CHARGE DESIGNED TO EXCITE HORIZONTAL MODE 2 FLEXURAL WHIPPING AND INCLUDING INTERNAL MASS/ABSORBER

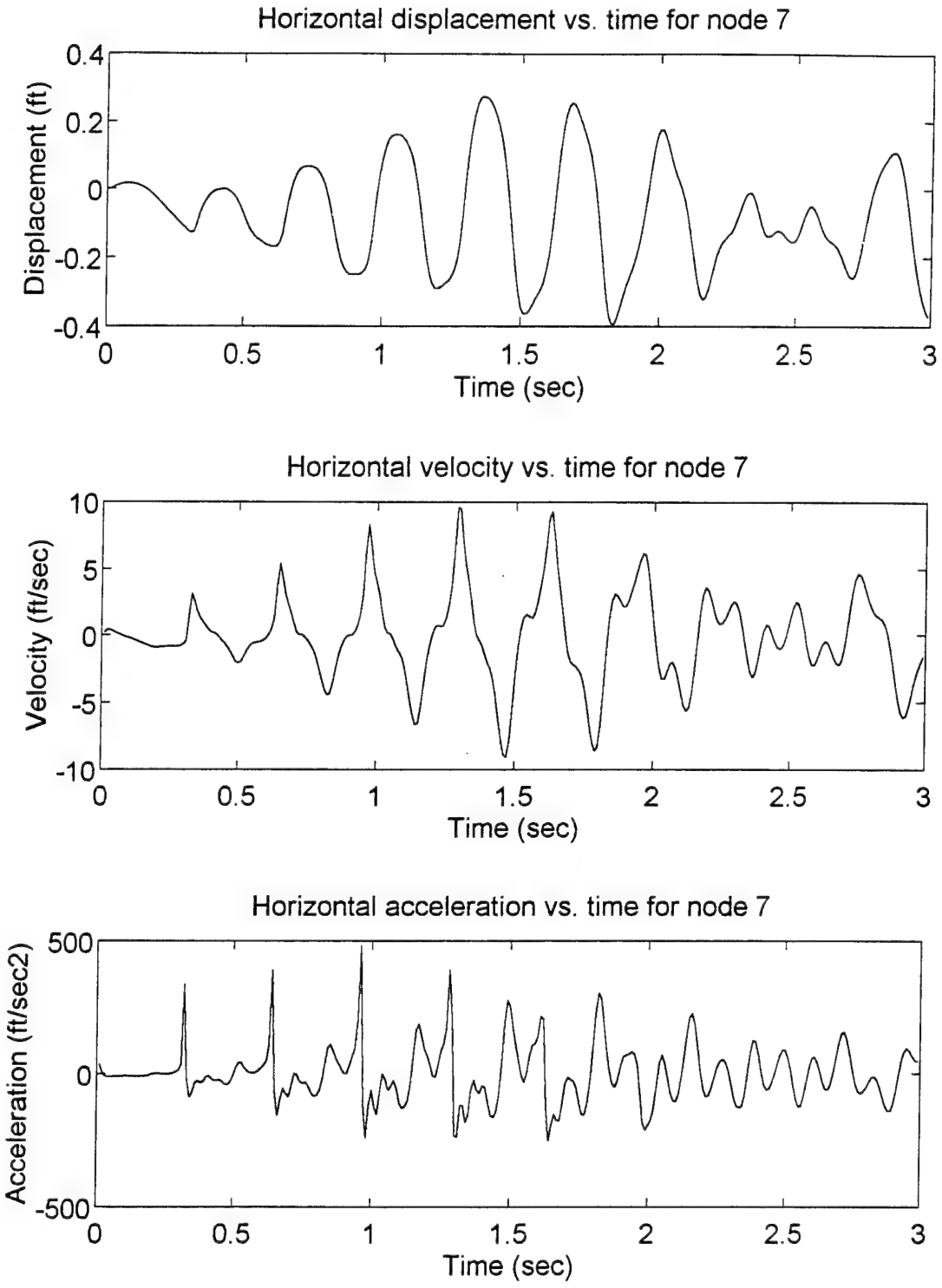

Figure E-1. Horizontal response at node 7, for hull subject to bubble pulse designed to excite horizontal mode flexural whipping and including 200 LT "tuned" mass damper at node 7.

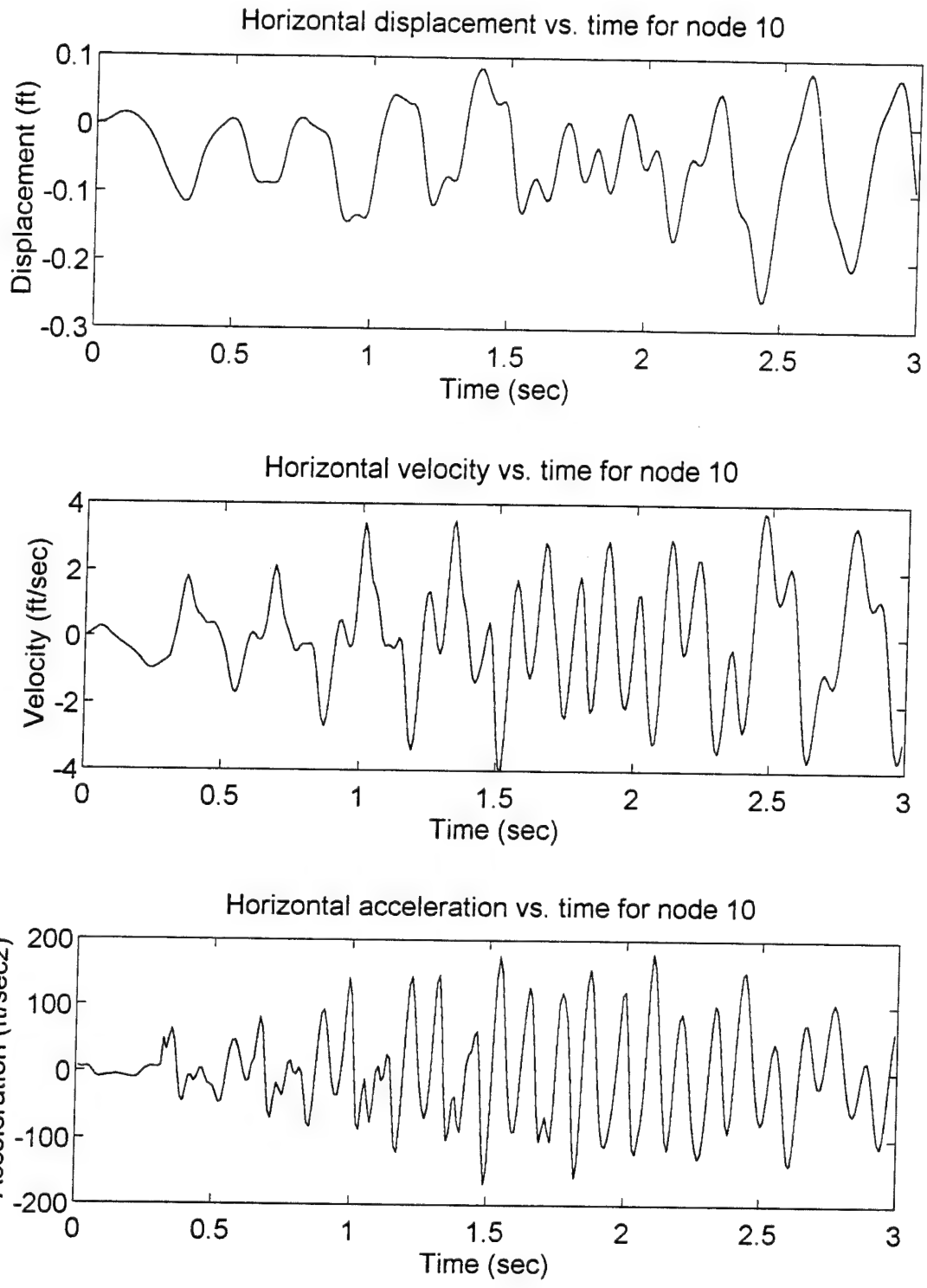

Figure E-2. Horizontal response at node 10, for hull subject to bubble pulse designed to excite horizontal mode flexural whipping and including 200 LT "tuned" mass damper at node 7.

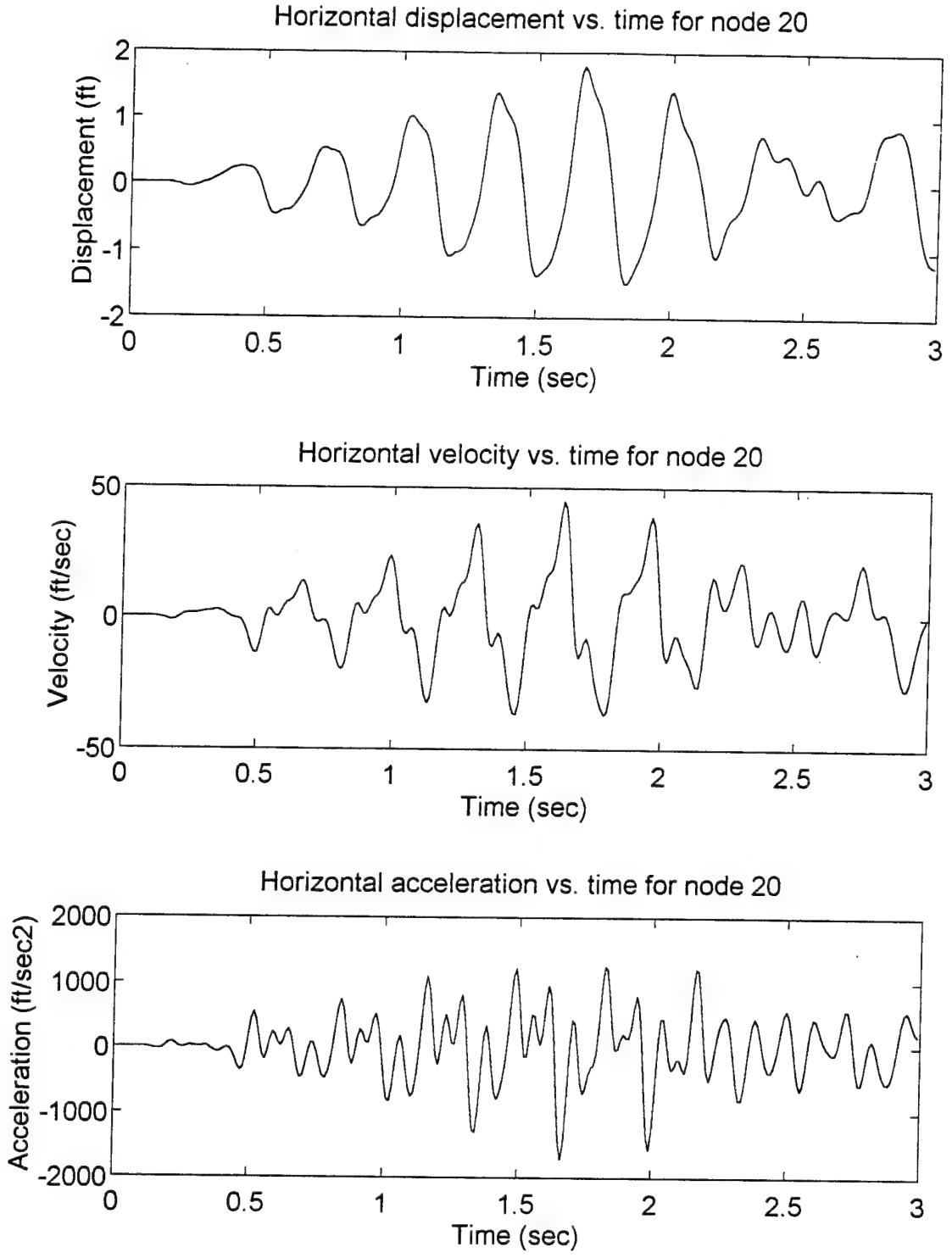

Figure E-3. Horizontal response at node 20, for hull subject to bubble pulse designed to excite horizontal mode flexural whipping and including 200 LT "tuned" mass damper at node 7.

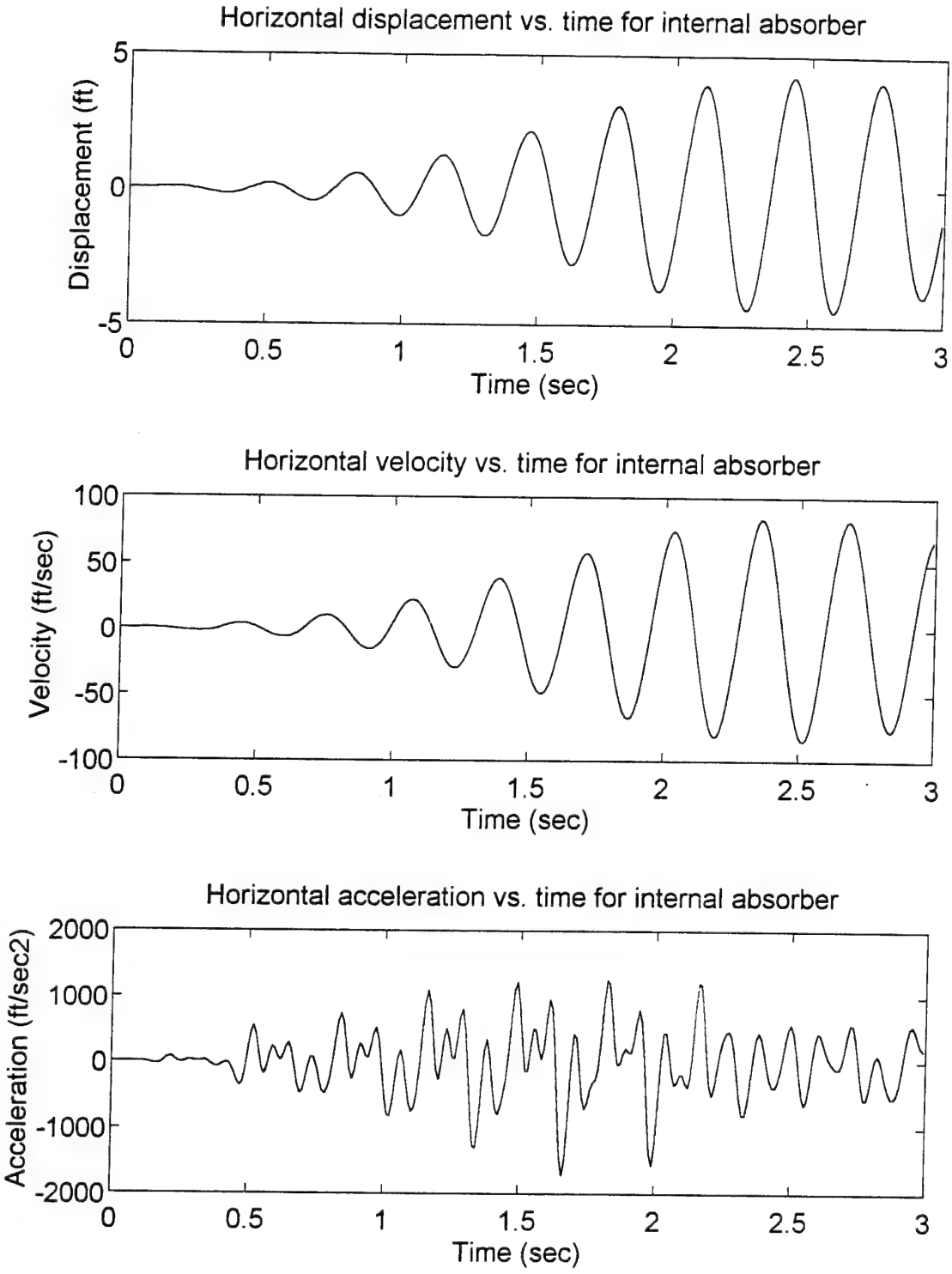

Figure E-4. Horizontal response of 200 LT "tuned" mass located at node 7.

APPENDIX F

NATURAL SLOSHING FREQUENCIES AND SLOSHING MODAL MASS FOR LATERAL SLOSHING OF RECTANGULAR TANKS

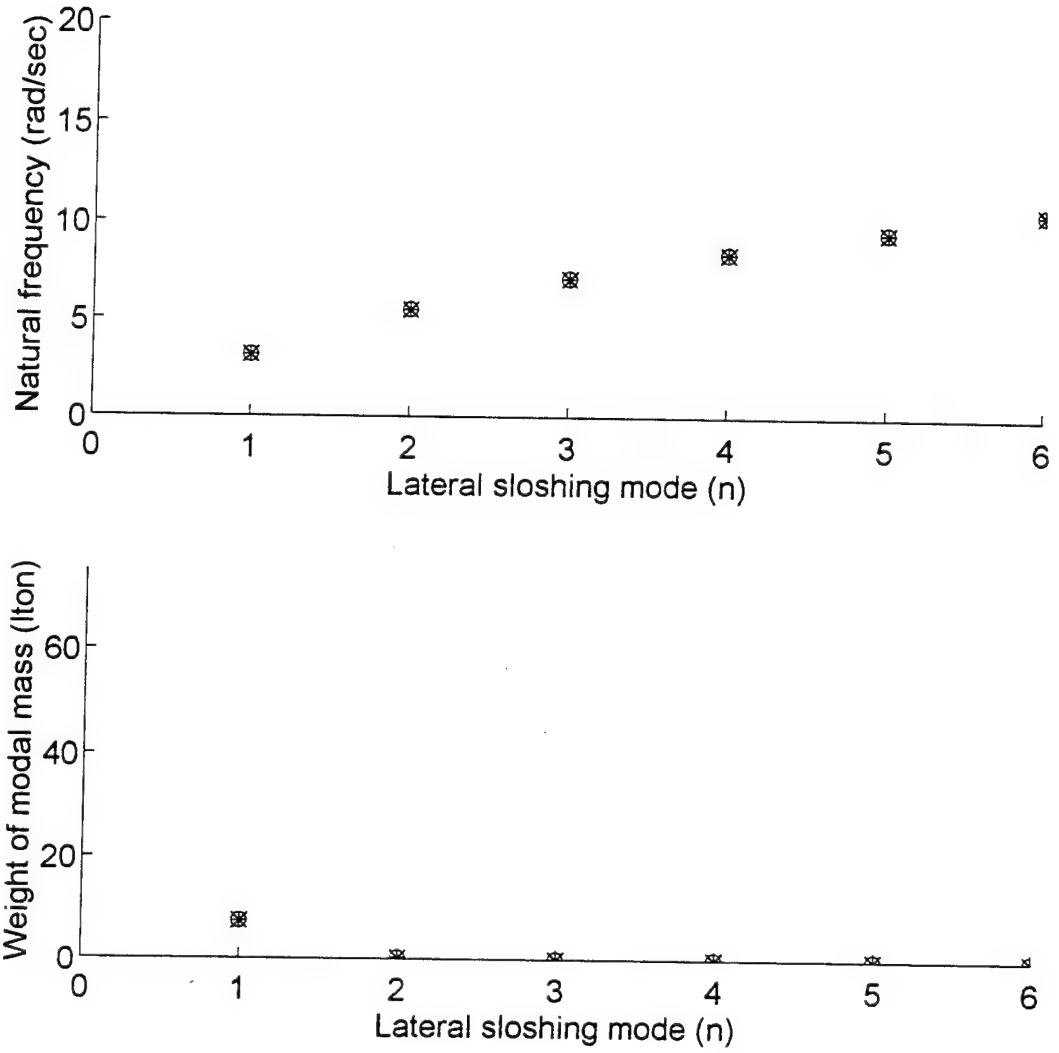

Figure F-1. Natural sloshing frequency and sloshing modal mass for lateral sloshing of a (10'h x 10'w x 10'l) rectangular tank.

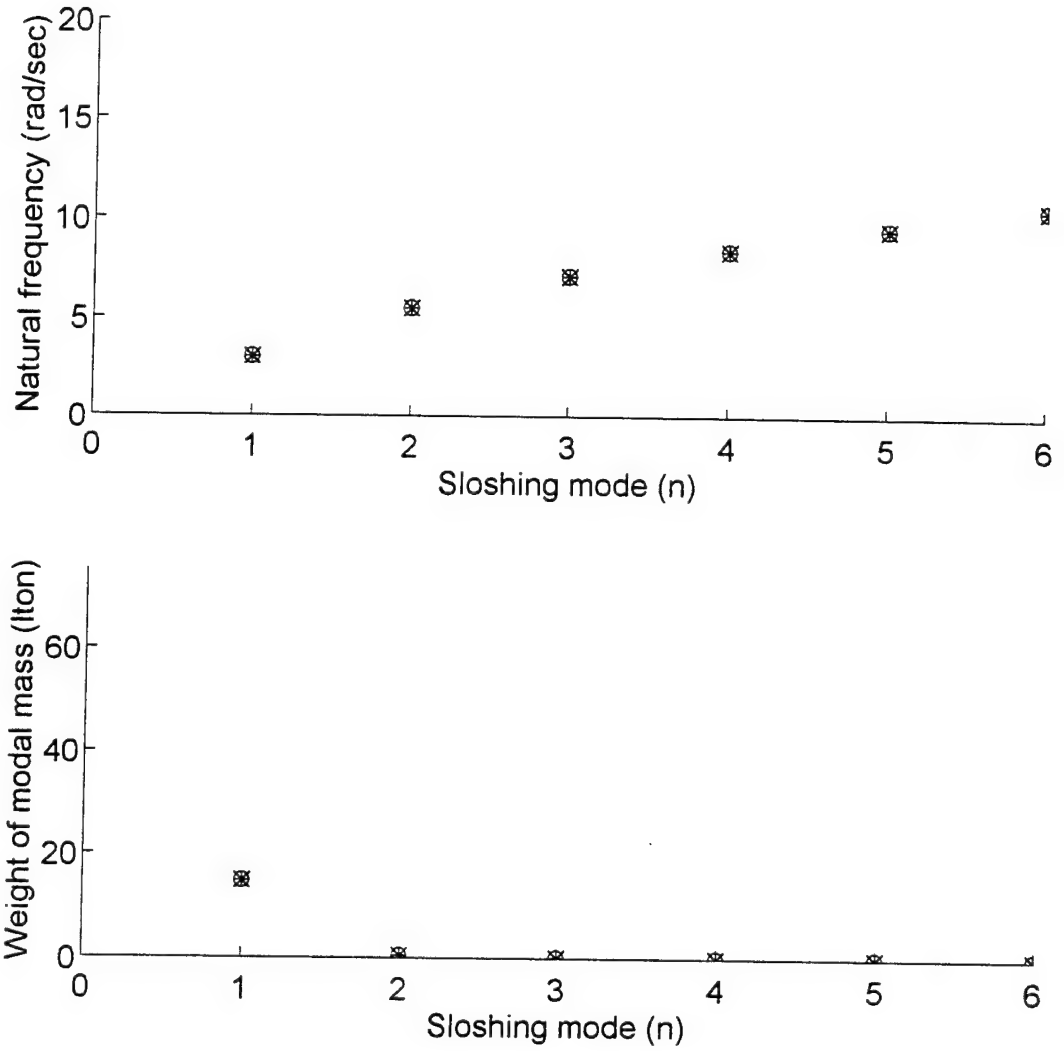

Figure F-2. Natural sloshing frequency and sloshing modal mass for lateral sloshing of a (20'h x 10'w x 20'l) rectangular tank.

APPENDIX G

STRAIN AND VELOCITY HISTORIES (MEASURED AND CALCULATED) FOR THE "RED SNAPPER" MODEL TESTS

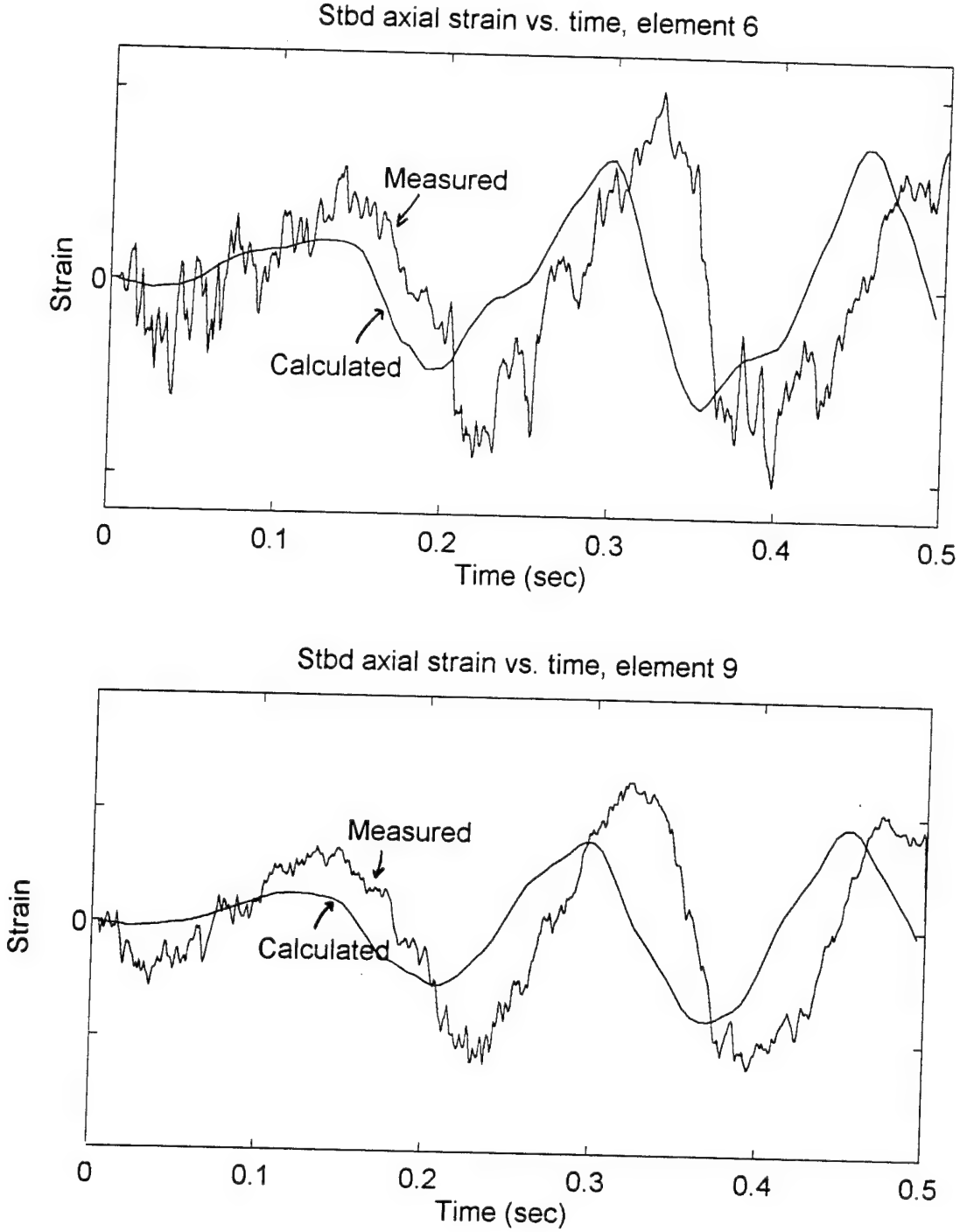

Figure G-1. Starboard-side fiber strain histories for elements 6 and 9 for Test 2 of the "Red Snapper" model test (horizontal and vertical mode 1 whipping), and strains calculated using the computational algorithm.

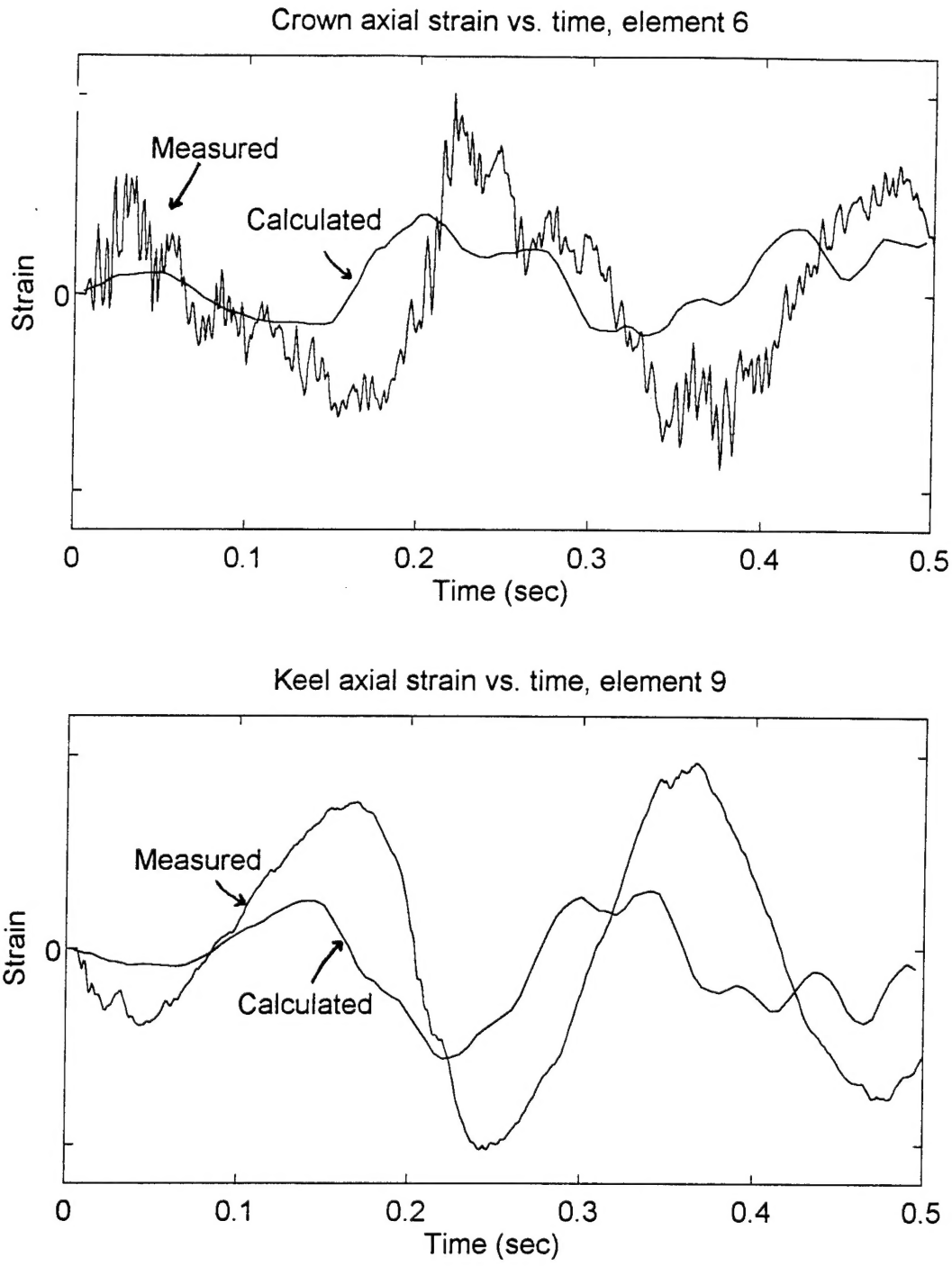

Figure G-2. Crown and keel fiber strain histories for elements 6 and 9 (respectively) for Test 2 of the "Red Snapper" model test (horizontal and vertical mode 1 whipping), and strains calculated using the computational algorithm.

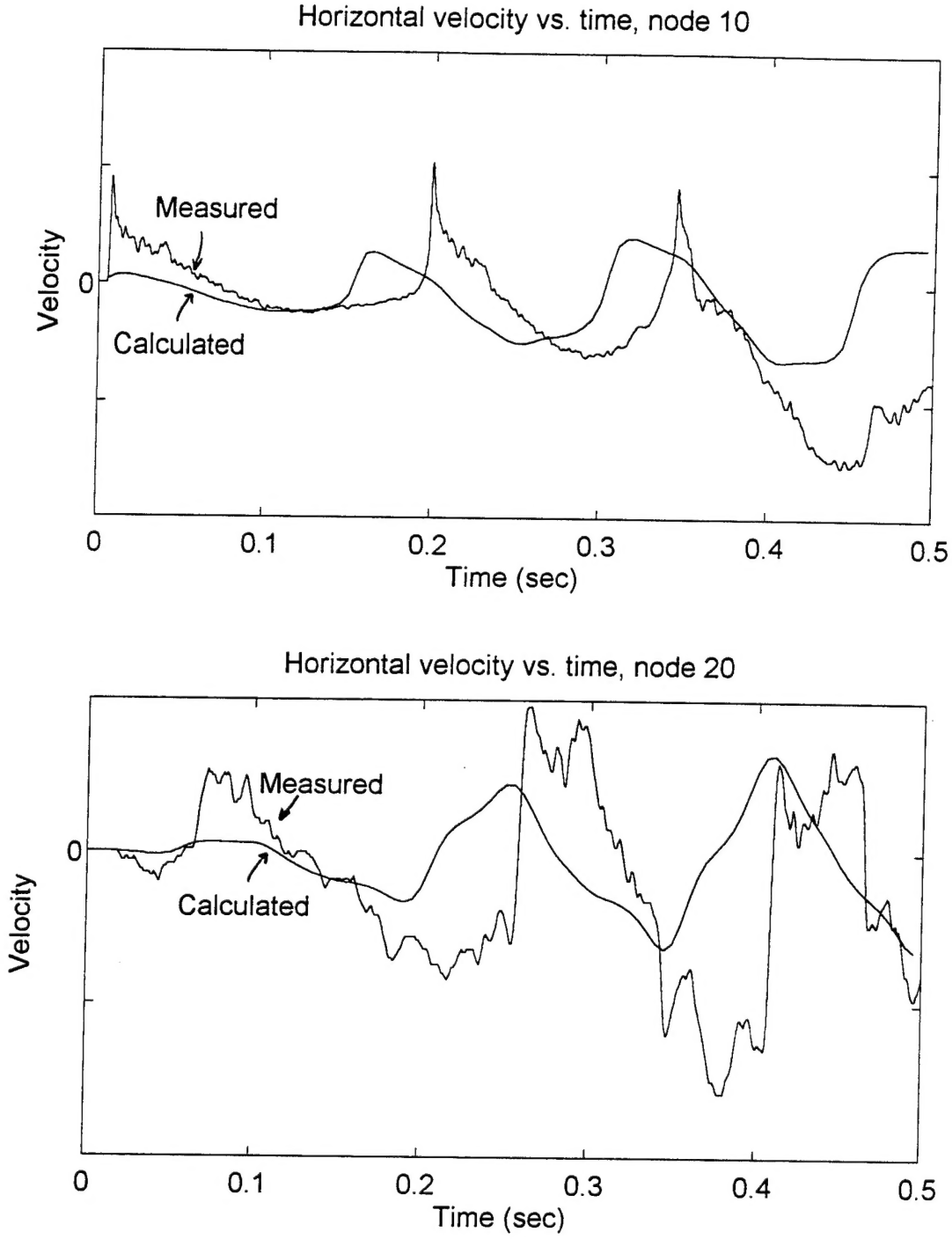

Figure G-3. Horizontal velocity histories for nodes 10 and 20 for Test 2 of the "Red Snapper" model test (horizontal and vertical mode 1 whipping), and velocities calculated using the computational algorithm.

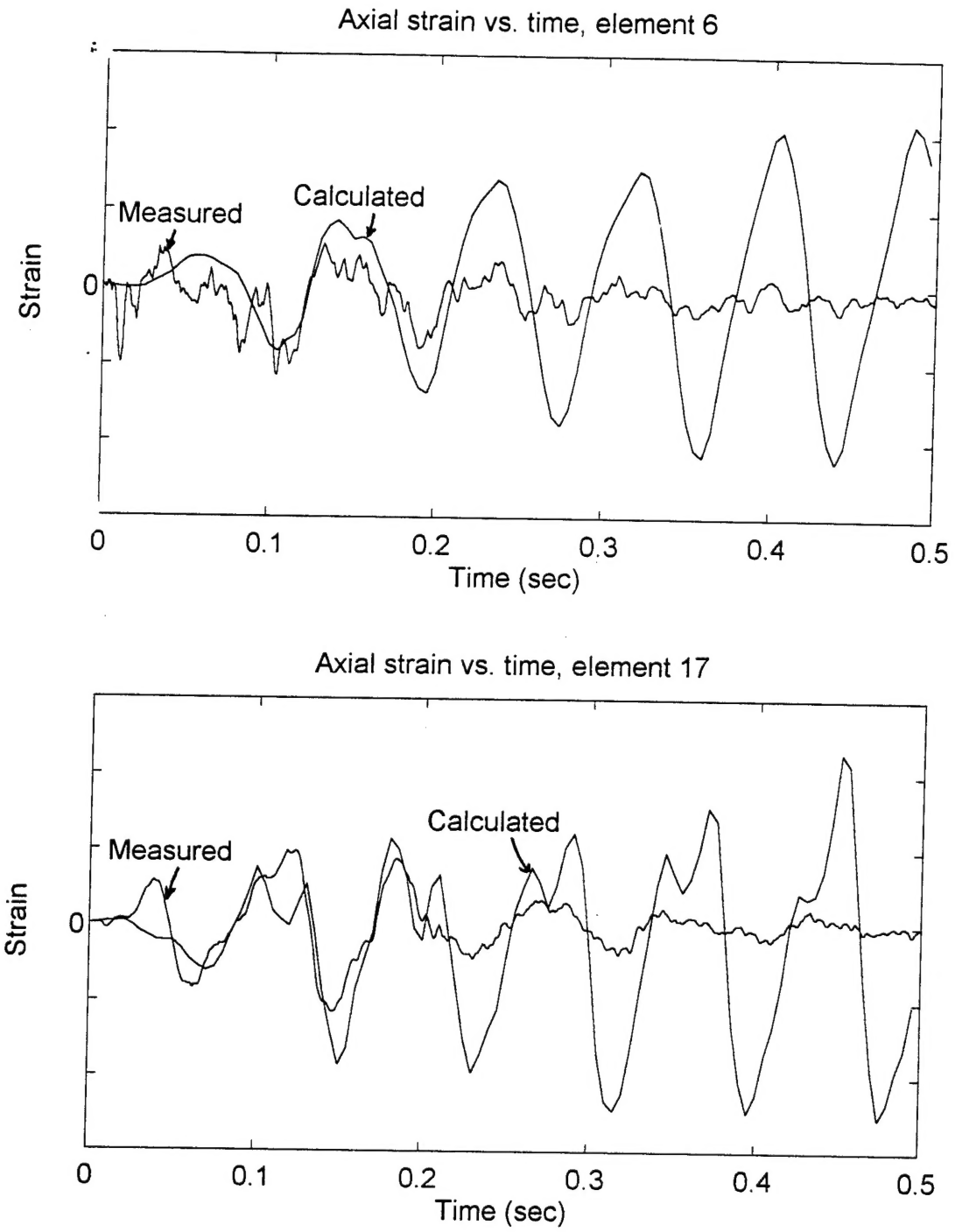

Figure G-4. Starboard-side fiber strain histories for elements 6 and 17 for Test 3 of the "Red Snapper" model test (horizontal mode 2 whipping), and strains calculated using the computational algorithm.

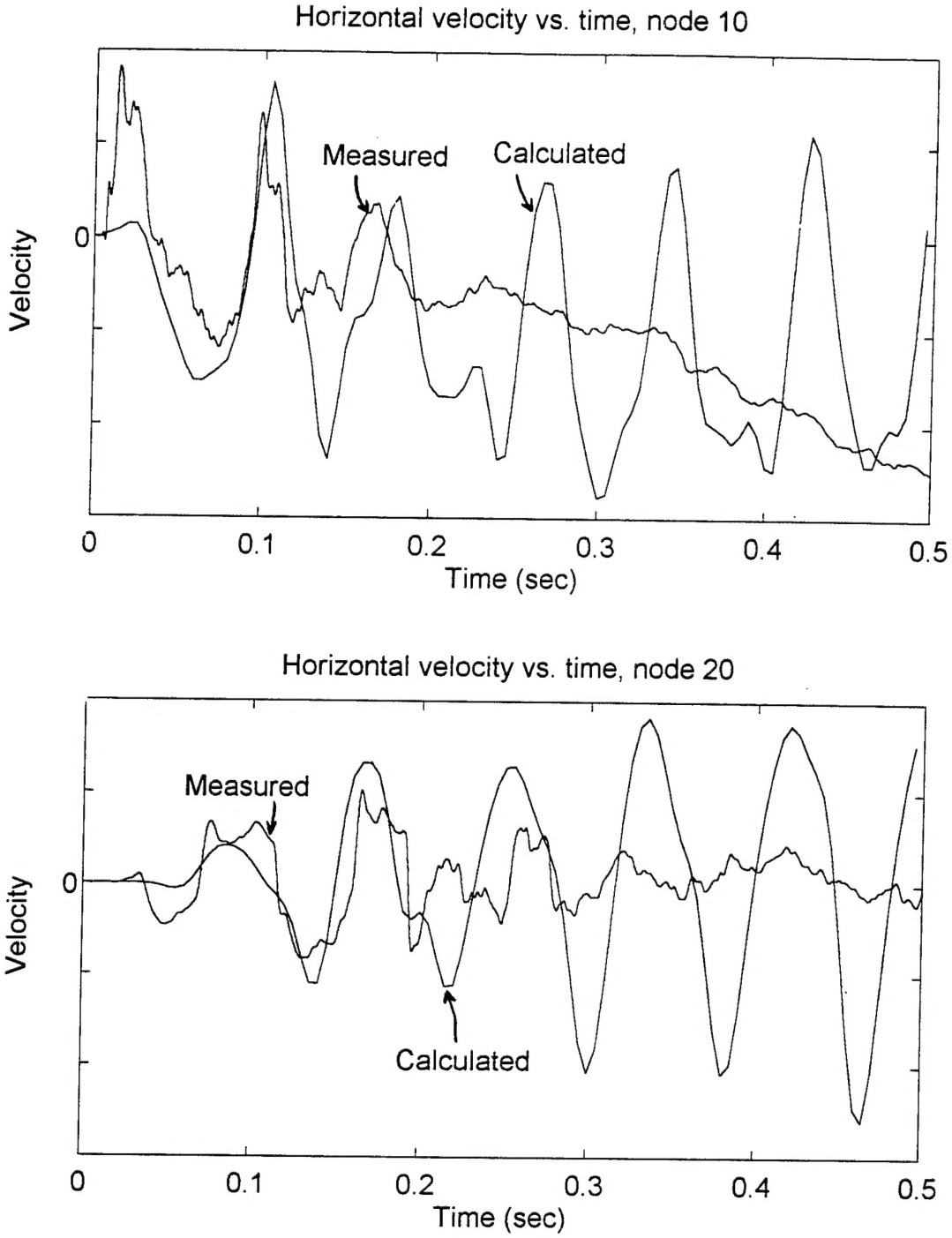

Figure G-5. Horizontal velocity histories for nodes 10 and 20 for Test 3 of the "Red Snapper" model test (horizontal mode 2 whipping), and velocities calculated using the computational algorithm.